Re-evaluating the Role of SARM1 as a Transcriptional Regulator Using Improved Genome-Edited Mouse Models

Thesis submitted to the University of Dublin for the degree of Doctor of Philosophy

2022

Ciara G. Doran B.A. (Mod.)

Declaration

I declare that this thesis has not been submitted as an exercise for a degree at this or any other university and it is entirely my own work.

I agree to deposit this thesis in the University's open access institutional repository or allow the Library to do so on my behalf, subject to Irish Copyright Legislation and Trinity College Library conditions of use and acknowledgement.

I consent to the examiner retaining a copy of the thesis beyond the examining period, should they so wish (EU GDPR May 2018).

RNA sequencing data mapping was performed by Dr Karsten Hokamp (School of Genetics and Microbiology, Trinity College Dublin). Differential gene expression analysis and sequence deviation density analysis was performed by Dr Fiona Roche (School of Genetics and Microbiology, Trinity College Dublin). Genome-edited mice were generated by Dr Claire Fergus and Dr Vincent Kelly of the TBSI transgenics facility. Confirmation of loss of SARM1 protein and protection from axon degeneration in the CRISPR/Cas9 SARM1-deficient mice was performed by Dr Ryoichi Sugisawa. Work carried out by the aforementioned authors is duly noted in the thesis text and acknowledged in figures.

Abstract

SARM1 is an ancient and highly conserved protein, initially described as having functions in innate immunity. In the last decade, our understanding of SARM1 structure and function expanded rapidly. The majority of research studies now focus on the role of SARM1 as an executioner of axon degeneration, leaving non-neuronal roles for SARM1 less well-characterised. Specifically, how and where SARM1 contributes to immune responses remains to be clarified. Murine SARM1 has been reported to regulate the expression of chemokines in both neurons and macrophages. However, the mechanism by which and extent to which SARM1 contributes to transcriptional regulation are not yet fully understood.

Our laboratory previously reported that *Ccl5* induction is impaired in macrophages from C57BL/6 congenic 129 ES cell-derived *Sarm1*$^{-/-}$ mice, or B6 congenic *Sarm1*$^{-/-}$, relative to wild type controls. Here, using RNA sequencing I identify additional differentially expressed genes in the B6 congenic *Sarm1*$^{-/-}$ mice. However, these results were confounded by the presence of passenger genes in the genome of the B6 congenic *Sarm1*$^{-/-}$ mouse, derived from the 129 donor strain of mice used in their generation. To re-evaluate the transcriptional role of SARM1 in the absence of these passenger genes, three novel SARM1-deficient mice were generated by CRISPR/Cas9.

In contrast to results in the B6 congenic *Sarm1*$^{-/-}$ mouse, macrophages from the new SARM1-knockout mice showed similar transcription of all genes measured, including *Ccl5*, compared to wild type littermate controls. Hence I clarified that the differential gene expression previously observed in macrophages from B6 congenic *Sarm1*$^{-/-}$ mice is an artefact resulting from the presence of passenger genes, and is unrelated to the absence of SARM1. This adds to the body of literature implicating passenger genes in congenic mice as the legitimate cause of a phenotype previously ascribed to the targeted gene. Since the generation of these B6 congenic *Sarm1*$^{-/-}$ mice 15 years ago, they have been heavily relied on for the study of SARM1 function. The extent to which the passenger genes present in the genome of these mice may have influenced previous studies, and by extension, misinformed our understanding of SARM1 function has yet to be fully understood. The novel CRISPR/Cas9 SARM1-knockout mice described in thesis provide an improved model in which to further explore the roles for SARM1 and to re-evaluate SARM1 functions previously described in B6 congenic *Sarm1*$^{-/-}$ mice.

Additionally our laboratory has generated, to our knowledge, the first mouse expressing epitope-tagged SARM1 endogenously. Difficulty in detecting SARM1 protein expression outside of the neurons has been reported, and has led to some speculation that SARM1 expression may be limited to the nervous system. Using the mouse expressing epitope-tagged SARM1, I confirmed that SARM1 is abundantly expressed in the brain, where its roles are numerous and varied. SARM1 expression was not confined to the nervous system, as I showed that SARM1 expression is detectable in macrophages from this mouse.

Overall, this work clarifies that murine SARM1 does not function as a transcriptional regulator of *Ccl5* expression in macrophages, though SARM1 expression is detectable in this cell type. This thesis cautions against the use of model animals in which the genome is contaminated by confounding passenger genes, and proposes CRISPR/Cas9 genome-edited animals as a more suitable alternative. Finally, newly generated SARM1-knockout and epitope-tagged mice are described and suggested as an improved new model to explore SARM1 function.

Acknowledgements

Firstly I would like to thank my supervisor, Professor Andrew Bowie, for his invaluable guidance, support, and encouragement throughout my PhD. His positive outlook and passion for research has fostered an enthusiastic and supportive lab environment, and he has been a great team leader.

To all the past and current members of the Bowie lab, I extend my sincere gratitude for the helpful discussions and the many laughs we shared. A special thanks goes to my fellow SARM1 researchers, Dr Michael Carty and Dr Ryoichi Sugisawa, who both regularly shared their extensive knowledge and advice with me. I would also like to thank especially Dr Lili Gu for her assistance with the bacterial infections.

I owe a great deal of thanks to my collaborators who contributed to the paper published in my final year, Dr Fiona Roche and Dr Karsten Hokamp from the School of Genetics and Microbiology, and Dr Claire Fergus and Dr Vincent Kelly from the TBSI transgenics facility. I appreciate their advice, insights, and generosity with their time.

I am extremely thankful to have Katie Shanahan as both a colleague and a friend. Her presence made the early mornings and late nights in the tissue culture room enjoyable rather than daunting, and she was always quick to share insights and helpful suggestions. There's no one I'd rather genotype 800 mice with.

I'm tremendously grateful to my parents, Anne and Michael, and to my sisters, Kim, Shona, and Michaela, for their unwavering support and belief throughout my life. I could not have done any of this without you. I'm extremely grateful to my Gran, who brought me to see Trinity College as a child and has encouraged me every step of the way to where I am now. I'd also like to thank Andrew Bathe, who supported me throughout this PhD and was always ready with a cup of tea to cheer me up after a long day of writing.

This work was funded by Science Foundation Ireland under the grant number 16/IA/4376, and supplemental funding was provided for the final six months by the HEA COVID extension fund.

Table of Contents

List of Figures

List of Tables

List of Abbreviations

3-AP	3-acetylpyridine
3-APMN	3-AP mononucleotide
aa	Amino acid
AAV	Adeno-associated virus
ADPR	Adenosine diphosphate ribose
AIM2	Absent in melanoma 2
ALR	AIM2-like receptors
ALS	Amyotrophic lateral sclerosis
AMP	Antimicrobial peptide
AP-1	Activator protein 1
APS	Ammonium persulfate
ARM	Armadillo
ATP	Adenosine triphosphate
BCA	Bicinchoninic acid
bp	Base pair
BSA	Bovine serum albumin
cADPR	Cyclic adenosine diphosphate ribose
CCCP	Carbonylcyanide m-chlorophenylhydrazone
CCL5	C-C motif chemokine ligand 5
cDNA	Complementary deoxyribonucleic acid
ChIP	Chromatin immunoprecipitation
cM	Centimorgan
CNS	Central nervous system
CRISPR/Cas9	Clustered regularly interspaced short palindromic repeats/CRISPR-associated 9
crRNA	CRISPR RNA
Cryo-EM	Cryo-electron microscopy
DAMP	Damage associated molecular pattern
DCV	Drosophila C virus
DEG	Differentially expressed gene
DIV	Days *in vitro*

DLK	Dual leucine zipper kinase
DMEM	Dulbecco's minimum essential medium
DMSO	Dimethyl sulfoxide
DNA	Deoxyribonucleic acid
dNTPs	deoxynucleoside triphosphates
DRG	Dorsal root ganglion
DSB	Double stranded break
DTT	Dithiothreitol
EGTA	Ethylene glycol-bis(2-aminoethylether)-N,N,N',N'-tetraacetic acid
ELISA	Enzyme-linked immunosorbent assay
ERK	Extracellular signal-regulated kinase
EV	Empty vector
FCS	Fetal calf serum
GAPDH	Glyceraldehyde-3-Phosphate Dehydrogenase
GFP	Green fluorescent protein
gRNA	Guide RNA
GSDMD	Gasdermin D
GWAS	Genome wide association study
H3	Histone 3
HEK	Human embryonic kidney
Het	Heterozygote
Hom	Homozygote
HPLC	High performance liquid chromatography
HRP	Horseradish peroxidase
HSP	Hereditary spastic paraplegia
IB	Immunoblot
iBMDM	Immortalised BMDM
IFN	Interferon
IGV	Integrative genomics viewer
IL	Interleukin
ILC	Innate lymphoid cell
Indel	Insertion/deletion
IP	Immunoprecipitation
iPSC	Induced pluripotent stem cell
IRF	Interferon regulatory factor

ISG	Interferon stimulated gene
JNK	c-Jun N-terminal kinase
Kb	Kilobase
LACV	La Crosse Virus
LCA9	Leber congenital amaurosis type
LDH	Lactate dehydrogenase
LPS	Lipopolysaccharide
LT	Lethal toxin
MAL	MyD88-adaptor-like
MAPK	Mitogen-activated protein kinase
Mb	Megabase
M-CSF	Macrophage colony stimulating factor
MFB	Medial forebrain bundle
MGI	Mouse Genome Informatics
MGV	Multiple genome viewer
miRNA	MicroRNA
MLKL	Mixed-lineage kinase domain like
MLS	Mitochondrial localisation sequence
M-MLV	Moloney Murine Leukemia Virus
MOI	Multiplicity of infection
MPLA	Monophosphoryl Lipid A
mRNA	Messenger RNA
MyD88	Myeloid differentiation factor 88
NaAD	Nicotinic acid adenine dinucleotide
NAD^+	Nicotinamide adenine dinucleotide
Nam	Nicotinamide
NAMPT	Nicotinamide phosphoribosyltransferase
NF-κB	Nuclear factor kappa B
NLR	NOD-like receptor
NLS	Nuclear localisation sequence
NMNAT	Nicotinamide mononucleotide adenylyl transferase
NO	Nitric oxide
NOD	Nucleotide oligomerisation domain
PAM	Protospacer adjacent motif
PAMP	Pathogen associated molecular pattern

PARP1	Poly(ADP-Ribose) Polymerase 1
PBMC	Peripheral blood mononuclear cell
pBMDM	Primary BMDM
PBS	Phosphate buffered saline
PCR	Polymerase chain reaction
Pen/strep	Penicillin-streptomycin
PGN	Peptidoglycan
PMSF	Phenylmethylsulfonyl fluoride
PNS	Peripheral nervous system
poly(I:C)	Polyinosinic:polycytidylic acid
Pre-mRNA	Pre-messenger RNA
PRR	Pattern recognition receptor
qRT-PCR	Quantitative real time PCR
RBP	RNA-binding protein
RGC	Retinal ganglion cell
RIN	RNA integrity number
RIPA	Radioimmunoprecipitation assay buffer
RIPK1	Receptor-interacting serine/threonine protein kinase 1
RNA	Ribonucleic acid
RNAi	RNA interference
RNP	Ribonucleoprotein
RPMI	Roswell Park Memorial Institute Medium
RQ	Relative quantification
RT	Reverse transcription
S724	SARM1 724 amino acid isoform
SAG	Sensitive to apoptosis gene
SAM	Sterile alpha motif
SARM1	Sterile α- and armadillo motif-containing protein
SD	Standard deviation
SDS	Sodium dodecylsulfate
SDS-PAGE	SDS-polyacrilamide gel electrophoresis
SEM	Standard error of the mean
sgRNA	Single guide RNA
siRNA	Small interfering RNA
SKO	SARM1-knockout

SMGP	Sanger Mouse Genomes Project
SMP	Skimmed milk power
SNP	Single nucleotide polymorphism
SOD1	Superoxide dismutase 1
Strep	Streptavidin
TAE	Tris-acetate-EDTA buffer
TBSI	Trinity Biomedical Sciences Institute
TDP-43	TAR DNA-binding protein 43 kDa
TEMED	Tetramethylethylenediamine
TIR	Toll/IL-1 receptor
TLR	Toll-like receptor
TMB	3, 3', 5, 5' Tetramethylbenzidine
TNF	Tumor necrosis factor
TPM	Transcripts per million
TRAM	TRIF-related adaptor molecule
TRIF	TIR-domain-containing adaptor protein inducing IFNβ
TUNEL	Terminal deoxynucleotidyl transferase dUTP nick end labelling
UBE4B	Ubiquitin conjugation factor E4B
UPS	Ubiquitin-proteasome system
UTR	Untranslated region
UXT	Ubiquitously expressed transcript
VAD	Vacor adenine dinucleotide
VMN	Vacor mononucleotide
VSV	Vesicular Stomatitis Virus
WNV	West Nile Virus
WT	Wild type
XAF1	XIAP Associated Factor 1
XIAP	X-linked inhibitor of apoptosis

Chapter 1 Introduction

1.1 Innate Immunity

Each day, the human body is exposed to millions of potentially pathogenic microbes. The skin, gut, and lung are all exposed to the environment, and have an average combined surface area of around 110 m^2 [1-3], which is vulnerable to infection through contact, inhalation, and ingestion of pathogens respectively. To avoid pathogenic infection, we rely upon the immune system to detect invading pathogens and coordinate an appropriate response. The mammalian immune system comprises two branches; the innate and adaptive. The innate immune system is the host's first line of defence against invading pathogens, and is evolutionarily conserved throughout the animal kingdom. Until the end of the twentieth century it was considered that the innate immune system was non-specific, and served only to control the pathogenic challenge until a more refined adaptive immune response could be mounted [4], characterised by recognition of specific epitopes, clonal expansion, and subsequent memory formation.

For some time now, however, it has been appreciated that this model is overly simplistic and neglects to take into account that innate immune cells recognise microbe-specific signatures, known as pathogen-associated molecular patterns (PAMPs), and mount a response appropriate to the specific class of threat, albeit in a non-clonal fashion [5]. This recognition is achieved through germline-encoded pattern recognition receptors (PRRs) which are expressed on the surface of and within innate immune cells, as well as the barrier cells which form the interface between the host and its external environment. Recognition of PAMPs by host PRRs facilitates discrimination of non-self from self, as PAMPs are highly conserved molecules among microbes but not expressed by the host. PRRs can also sense damage associated molecular patterns (DAMPs), which are endogenous host molecules. DAMPs are released from cells upon stress or damage, and due to this inappropriate localisation are recognised by the immune system as a danger or stress signal [6]. Detection of a pathogen by phagocytic innate immune cells, such as macrophages and neutrophils, can result in phagocytosis, whereby the microbe is engulfed by the immune cell and degraded. Following recognition of their cognate ligand many PRRs initiate a

signalling cascade, the result of which is recruitment of transcription factors and transcriptional machinery to the promoters of a set of genes. This leads to the expression of the appropriate inflammatory mediators including pro-inflammatory cytokines, chemokines, type I interferons, and antimicrobial peptides (AMPs) [7]. Pro-inflammatory cytokines induce the rapid inflammation which characterises the innate immune response. Chemokines cause the recruitment of other immune effector cells to the infected area, where they can be activated by PRR recognition of PAMPs and by the local cytokine milieu. Type I interferons are key contributors to the antiviral response, which drive an anti-viral state in both virus-infected cells and uninfected bystander cells through induction of genes which interfere with the viral replication cycle. In addition, the induction of interferon-stimulated genes (ISGs) by type I interferons can promote and enhance the antiviral activities of both innate and adaptive immune cells. Thus, through the production of cytokines, chemokines, and type I interferons, innate immune cells can thereby control or eliminate the pathogen and critically, shape the adaptive immune response. A number of different families of PRRs have been characterised, and are classified based on structure, ligand-type, and subcellular localisation.

1.2 TLRs

Toll-like receptors (TLRs) are one such family of PRRs which are widely expressed and well-characterised. There are ten human TLRs and twelve functional mouse TLRs. TLR1-TLR10 are conserved between human and mouse, though murine TLR10 is non-functional. Murine TLR11-TLR13 are species-specific and are not found in humans. Common among members of the TLR family is the Toll/interleukin-1 (IL-1) receptor (TIR) domain, which can be found on the cytoplasmic face each of the TLRs, and on each of the five adaptor proteins described below [8]. The TLRs can be classified into two groups, extracellular and intracellular, based on their localisation. TLR1, TLR2, TLR4, TLR5, TLR6 and mTLR11 are largely expressed on the cell surface, whereas TLR3, TLR7, TLR8, and TLR9 are primarily intracellular and are found in endosomal or lysosomal compartments, and in the endoplasmic reticulum. Following TLR recognition of PAMPs or DAMPs, signals are conveyed by the adaptor proteins from the receptor to downstream kinases. These adaptors are myeloid differentiation primary-response gene 88 (MyD88), MyD88-adaptor-like (MAL, also known as TIRAP), TIR-domain-containing adaptor

protein inducing IFNβ (TRIF), TRIF-related adaptor molecule (TRAM), and sterile α- and armadillo motif-containing protein (SARM1).

MyD88 is used by all TLRs to transduce signals (through recruitment by MAL in the case of TLR2, TLR4, and TLR9), with the exception of TLR3. MyD88 transduces the signal to pathways which can result in the activation of the transcription factor nuclear factor kappa-light-chain-enhancer of activated B cells (NF-κB), as well as activator protein 1 (AP-1), interferon regulatory factor 3 (IRF3), and IRF7. TLR3 signals exclusively through TRIF, resulting in the activation of IRFs and NF-κB [9]. TLR4 is unique among the TLRs as it can signal through MyD88 [9] and TRIF [10], through the adaptors Mal and TRAM respectively. Once activated, transcription factors can then translocate to the nucleus, where they each regulate the transcription of a specific set of immune genes, which may include cytokines, chemokines, and/or interferons. This is summarised in Figure 1.1. Thus, different TLRs employing different adaptors allows for activation of diverse combinations of transcription factors, leading to induction of different sets of genes as appropriate to the ligand present. SARM1 is the notable outlier among the TIR adaptor proteins; rather than transduce signals it plays an inhibitory role in humans. Additionally, like MyD88 [11] and MAL [12], SARM1 has roles which extend beyond TLR- signalling.

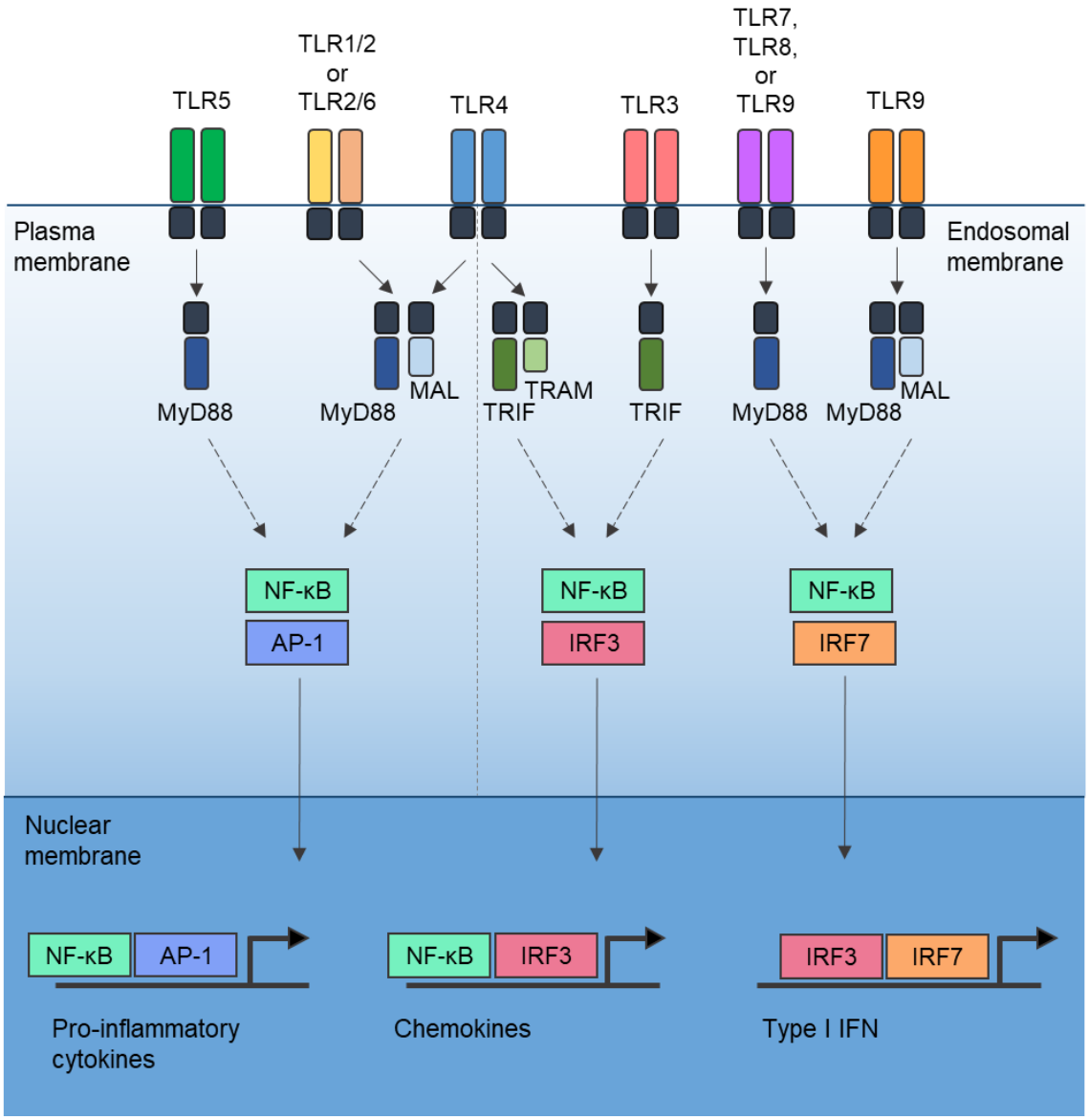

Figure 1.1 An overview of TLR signalling

Upon recognition of their cognate ligand, TLRs recruit TIR domain-containing adaptor proteins, inducing a signalling cascade (denoted by dashed line arrows) which culminates in the activation of transcription factors, including NF-κB, AP-1, IRF3, and IRF7. These transcription factors can then translocate to the nucleus, where they are recruited to the promoter of immune genes to induce their expression. This results in the production of cytokines, chemokines, and/or interferons as appropriate to the detected threat. AP-1, activator protein 1; IFN, interferon; IRF, IFN regulatory factor; MyD88, myeloid differentiation primary-response gene 88; MAL, MyD88 adaptor-like protein; NF-κB, nuclear factor-κB; TLR, Toll-like receptor; TRAM, TRIF-related adaptor molecule.

1.3 SARM1 across species

Though SARM1 is the most recently identified of the TIR adaptor proteins, it is the most evolutionarily conserved, being the only family member to have a clear orthologue in *Caenorhabditis elegans* [13]. Figure 1.2 compares the protein domains in SARM1 orthologues. SARM1 was discovered in 2001 as a protein in *Drosophila melanogaster* which contained armadillo repeats, two sterile α motif (SAM) domains, and had orthologues in mouse and human [14]. Soon after this it was reported that SARM1 contained a TIR domain [8], an exciting development which predicted a role for SARM1 in TLR-signalling. In fact in *C. elegans* the SARM1 orthologue, *tir-1*, is one of only two genes encoding a protein which contains a TIR domain, the other being *tol-1*, a TLR homologue [15]. This suggested a crucial role for this protein in innate immunity in the worm.

1.3.1 SARM1 in C. elegans

Studies soon confirmed this prediction, with tir-1-deficient worms displaying reduced resistance to bacterial and fungal infection as a result of the loss of antimicrobial peptide expression [16]. Surprisingly however, this was independent of the *C. elegans* TLR system. Similarly, Liberati *et al.* found that, in contrast to mutations in the worm TLR, *tol-1*, silencing of *tir-1* by RNA interference (RNAi) in *C. elegans* diminished activation of p38 mitogen-activated protein kinase (MAPK), and rendered the nematodes sensitive to killing by bacterial pathogens [17]. Adding to the body of evidence supporting a non-TLR role for SARM1, the authors of that study also found that overexpression of human SARM1 did not activate either NF-κB- or IRF3-dependent reporter gene expression [17]. Further evidence for a key role for the SARM1 orthologue in innate immunity came from Kurz *et al*., who showed that following RNAi of *tir-1*, nematodes showed reduced survival upon infection with *Pseudomonas aeruginosa*. This was attributed to loss of induction of the glycoprotein pgp-5, which required p38 MAPK signalling downstream of tir-1 for expression [18].

Interestingly, tir-1 has also been shown to mediate a non-apoptotic form of cell death during nematode development [19], and activates the p38 MAPK pathway leading to cell death in response to anoxic stress [20]. These results hinted at a novel, non-TLR role for SARM1, which is functionally distinct from the other TIR-containing adaptor proteins.

1.3.2 SARM1 in D. melanogaster

Like the *C. elegans* tir-1, the *D. melanogaster* SARM1 orthologue, Ect4 has roles in both immune defence and cell death. Surprisingly, it has been reported that Ect4 negatively regulates bacteria-induced AMP production in the airway epithelium [21], and the authors speculate that this functions to dampen the immune response after infection. This is in contrast to the *C. elegans* tir-1, which positively regulates AMP expression. A protective role for Ect4 has been described in the reponse to viral infection. Knockdown of *D. melanogaster Ect4* renders the flies more susceptible to Drosophila C virus (DCV)-induced mortality, due to increased accumulation of virus compared to WT flies [22]. Ect4 levels were demonstrated to be suppressed by a microRNA (miRNA) miRNA-956, whose expression is downregulated upon DCV infection, relieving the suppression of Ect4 [22]. It is not clear if Ect4 has a direct role in the induction of cell death. The authors of that study suggested that Ect4 may also be acting as a negative regulator of immune signalling in this context, protecting from mortality by preventing pathological signalling and restoring immune homeostasis [22]. Ect4 has a reported role in the elimination of unfit cells in developing tissues. These "loser" cells are removed by induction of a cell death pathway requiring the Toll receptors, which activates the NF-κB orthologue Rel through a signalling axis involving Ect4 [23]. Thus in *D. melanogaster*, like in *C. elegans*, the SARM1 orthologue participates in regulation of the immune response and cell death, implying the existence of roles for mammalian SARM1 outside of the TLR system.

1.3.3 Mammalian SARM1

In mice, the SARM1 protein is encoded by the *Sarm1* gene and is 724 amino acids in length. SARM1 consists of armadillo (ARM) repeats followed by two SAM domains which are fused to the C-terminal TIR domain (see Figure 1.2). An N-terminal mitochondrial localisation sequence targets SARM1 to the mitochondria [24] where it is frequently reported to reside [25-27], though some studies report that a cytoplasmic pool of SARM1

also exists [28, 29]. The SAM domains allow SARM1 to oligomerise, and the TIR mediates SARM1 function (this will be described in detail in Section 1.4). A recent and surprising finding is that mammalian SARM1 has intrinsic NADase activity located in the TIR domain [30, 31], like many of the bacterial TIR proteins [32]. This is another property which distinguishes SARM1 from other mammalian TIR family members, and is also conserved across species [33]. In conditions of oxidative stress SARM1 is activated by phosphorylation of serine at residue 548 [31]. A second isoform of murine SARM1 has been reported which is 764 amino acids in length, and is a splice variant with an extended region between the second SAM domain and the TIR domain (see Figure 1.2). Our lab previously reported that the 724 amino acid isoform predominates, and the 764 amino acid isoform is barely detectable in macrophages [34]. This is in agreement with the observed ratio of SARM1 isoforms in T cells [35].

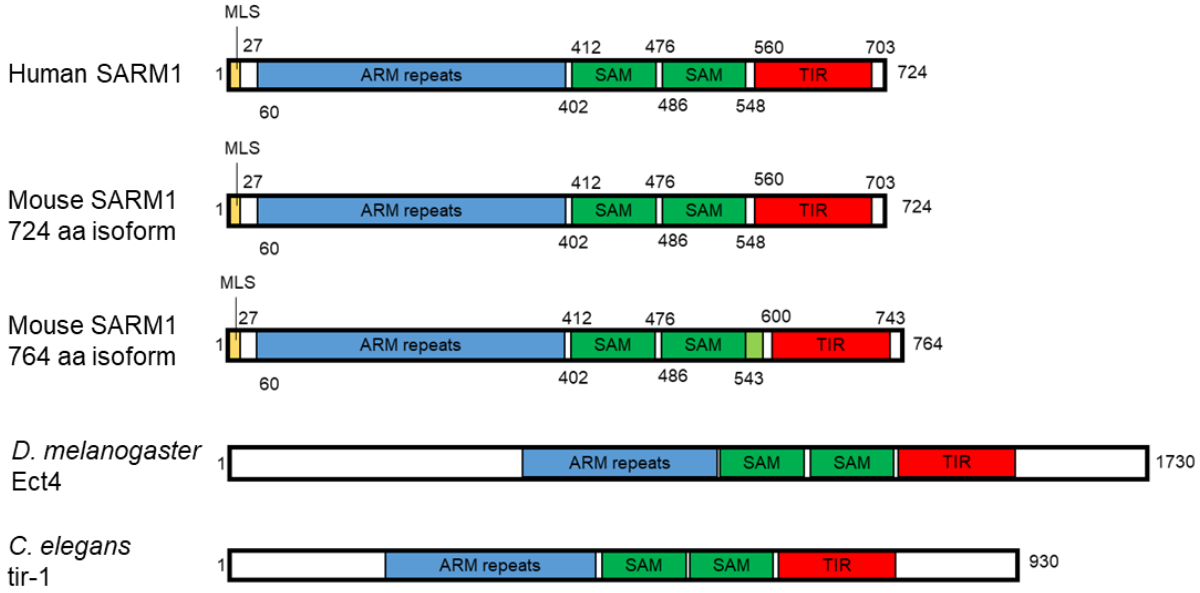

Figure 1.2 SARM1 is conserved across species

A comparison of the domains of human and mouse SARM1 to those of *D. melanogaster* Ect4 and *C. elegans* tir-1. ARM, armadillo; SAM, sterile α motif; TIR, toll/interleukin-1 receptor; MLS, mitochondrial localisation sequence; aa, amino acid. Numbers indicate the residue at which domains or sequences begin and end.

In addition to varying structurally from the other TIR adaptors, mammalian SARM1 is functionally distinct. The first report of SARM1 regulating TLR signalling was published by our lab in 2006. Rather than transducing signals following TLR-stimulation, SARM1 was observed to negatively regulate TRIF-dependent signalling in human peripheral blood mononuclear cells (PBMCs) [36]. SARM1 was shown to physically interact with TRIF, and knockdown of endogenous SARM1 with small interfering RNA (siRNA) led to enhanced TRIF-dependent gene induction [36]. Further studies have since corroborated and added to this, and demonstrated human SARM1 antagonising both TRIF- and MyD88-dependent signalling [37]. This negative regulatory role is functionally conserved among many species, including amphioxus [38], horseshoe crabs [39] and pigs [40], and is likely to be mediated by homotypic TIR-TIR interactions. The BB loop is a sequence of approximately 14 amino acids between the second strand and second helix of a TIR domain, which represents a significant portion of the exposed surface area of the domain [41] and plays an important role in mediating TIR-TIR interactions [42]. Glycine at residue 601 in the BB loop of the SARM1 TIR domain has been identified as a critical residue for SARM1 negative regulation of TRIF-dependent signalling [43]. Remarkably, however, despite sequence and structural similarity between human and mouse SARM1 (see Figure 1.2), *Sarm1*$^{-/-}$ mice do not display enhanced TLR-signalling [25, 26, 34, 44]. One exception to this is in the context of *Burkholderia pseudomallei* infection. Murine macrophage infection with *B. pseudomallei* resulted in increased SARM1 expression, which inhibited TRIF signalling and consequentially reduced IFNβ production [45]. Rather, murine SARM1 has reported roles in regulating gene induction in a TLR-independent manner, which will be discussed in depth in Chapter 3. Briefly, following treatment with both TLR-dependent and –independent stimuli, macrophages from *Sarm1*$^{-/-}$ mice exhibit dramatically less transcription and subsequent secretion of the chemokine C-C motif chemokine ligand 5 (CCL5) than wild type (WT) controls [34]. Additionally, as is observed in *C. elegans* and *D. melanogaster*, mammalian SARM1 also has a regulatory role in numerous forms of cell death and degeneration, and this will be explored in Sections 1.4 and 1.5.

Thus SARM1 exhibits remarkable evolutionary conservation, with roles in regulating immune defence and cell death across a range of species from lower organisms such as *C. elegans* through to mouse and human.

1.4 SARM1 as the executioner of axon degeneration

Although the focus of this project is examining the role of SARM1 in macrophages, SARM1 is now best recognised for its role in inducing the degeneration of axons which have been separated from the neuron cell body or otherwise injured or insulted. In the past decade, tremendous effort has been devoted to understanding what drives this axon degeneration and how we can modulate it for therapeutic benefit.

1.4.1 Axon degeneration

Neurons are the primary cell type of the central nervous system (CNS) and peripheral nervous system (PNS), where they carry out the essential function of signal transmission. They transmit information between different areas of the brain and throughout the body's nervous system using electrical impulses and chemical signals in the form of neurotransmitters. In order to perform this role neurons have evolved an exceptional architecture, comprising the cell body, or soma, and extended processes called dendrites and axons. Dendrites are branched extensions which receive and integrate signals from an upstream source. The axon extends from the cell body, and transmits signals to the dendrites of neighbouring neurons or downstream targets. Axons are typically longer than dendrites, and human peripheral axons can be up to a meter in length. Given their essential role, maintenance of axon integrity is critical to neuronal function. However there are many circumstances in which fully formed axons may be destroyed through a process termed axon degeneration. Axon degeneration is a common feature of numerous neurodegenerative diseases of the CNS, including amyotrophic lateral sclerosis (ALS) [46] and Parkinson's disease [47]. It is also induced by the chemotherapeutic agents paclitaxel and vincristine, which causes painful peripheral neuropathy and limits the usefulness of these drugs [48]. In addition, axon degeneration underlies diabetic peripheral neuropathy [49]. Therefore there is considerable interest in understanding the events which trigger axon degeneration, and identifying potential therapeutic targets.

1.4.2 Wallerian degeneration and the Wld^S mouse

Wallerian degeneration is the prototypical example of axon degeneration, and is often studied as a representative model. It is the process through which the distal axon segment

degenerates following physical injury to an axon [50]. Following transection, the degenerating axon develops focal beads or swellings [51], the microtubules depolymerise and the mitochondria swell [52], and the cytoskeleton fragments [51]. Similar morphological characteristics are observed in axon degeneration induced by pathological conditions. Wallerian degeneration was initially considered to be a passive wasting process, however our understanding was revolutionised upon identification of a naturally occurring mutant mouse, Wld^S, in which Wallerian degeneration is significantly delayed [53]. Remarkably, following axotomy, axons from the Wld^S mouse remain intact for tenfold longer time than those from WT controls [53]. This raised the possibility of the existence of a cellular programme which actively induces axon degradation. This delayed axon degeneration was not exclusive to Wallerian degeneration; axons from Wld^S mice also exhibited delayed degeneration induced by the chemotherapeutic agents vincristine [54] and paclitaxel [55], as well as a range of neurodegenerative disorders [56-58] and spinal injury [59]. Thus there was substantial interest in elucidating the mechanism through which Wallerian degeneration and other forms of axon degeneration occur and how it is delayed by the *Wld*^{S} gene.

1.4.3 dSarm/SARM1 is identified as a key mediator of axon degeneration

The axoprotective effect of the Wld^S protein is not exclusive to mouse; the *Wld*^{S} gene also substantially delays injury-induced axon degeneration in *Drosophila melanogaster* [60]. Thus, the protective phenotype associated with the Wld^S protein is conserved across species, and *D. melanogaster* is a suitable model in which to examine the mechanism through which Wallerian degeneration is induced. The *Wld*^{S} gene was known to be a gain of function mutation [61], and Osterloh *et al.* reasoned that if there were an active self-destruct programme mediating Wallerian degeneration, then a loss of function mutation should exist which would mimic the axoprotective Wld^S phenotype [29]. An F_2 forward genetic screen was performed to identify if such mutants exist. Three mutant lines were identified in which transected axons exhibited long-term survival. Whereas control axons from WT *Drosophila* had degenerated 7 days after axotomy, axons from these mutant *Drosophila* remained intact for the animal's entire lifespan [29]. A single gene which was affected in each of the three mutants was identified through next-generation sequencing: *ect4*, the *Drosophila* orthologue of *Sarm1*, which is henceforth referred to as *dsarm*. Each of the mutants contained a premature stop codon in the *dsarm* gene, indicating that they are

loss-of-function dSarm mutants. Expression of full-length *dsarm* cDNA in the mutant animals was sufficient to restore normal axon degeneration following axotomy [29]. This indicated that Wallerian degeneration is in fact an active process, and that dSarm is a member of the signalling pathway which mediates axon degeneration. The authors then investigated if murine SARM1 would be required for Wallerian degeneration *in vivo* using a sciatic nerve legion model. While substantial axon degeneration was observed in the *Sarm1*$^{+/-}$ control mice within three days of the injury, the majority of axons in *Sarm1*$^{-/-}$ animals remained intact for at least 14 days post-injury [29]. Thus, dSarm/SARM1 is a key effector of the axon degeneration pathway, which is ancient and conserved.

1.4.4 SARM1 mediated axon degeneration in disease and pathology

Studies have since shown that the role of SARM1 in inducing axon destruction is not unique to Wallerian degeneration. SARM1-deficiency also alleviates axon degeneration induced by mitochondrial insults, including the complex I inhibitor rotenone [62], the oxidative phosphorylation uncoupler carbonylcyanide m-chlorophenylhydrazone (CCCP) [62], the reactive oxygen species inducer paraquat [62], the ATP synthase inhibitor oligomycin [63], and the complex III inhibitor antimycin [63]. In addition, *Sarm1*$^{-/-}$ mice are protected from the peripheral neuropathy resulting from axon degeneration induced by the chemotherapeutic agents paclitaxel [64], vincristine [65], and bortezomib [66]. Importantly, it was reported that SARM1 loss was also prevented the hyper-algaesia associated with vincristine-induced peripheral neuropathy [65]. Additionally, SARM1-deletion was protective in a high fat diet-induced peripheral neuropathy [64], which is a model of metabolic syndrome-induced peripheral neuropathy. Thus, understanding the mechanism through which SARM1 executes axon degeneration is crucial for the development of therapeutics to treat chemotherapy and metabolic syndrome-induced peripheral neuropathy.

Axon damage and degeneration is recognised to be an early manifestation of neurodegenerative disease pathology [67] and through retrograde degeneration this can lead to the degeneration of the soma in many cases [68]. Keen interest existed in identifying if SARM1 could therefore be a therapeutic target in the context of neurodegenerative disease. A number of genome wide association studies (GWAS) have linked the human SARM1 locus to sporadic ALS, an adult-onset motor neuron disorder [69, 70]. The effect

of SARM1-deficiency has been investigated in the context of ALS using two different mouse models of the disease, with conflicting results observed. Mice which overexpress an ALS-associated mutant of the human protein superoxide dismutase 1 (SOD1) develop axon degeneration, which is unaffected by loss of SARM1 or by co-expression of Wld^S protein [71]. However, SARM1 deletion was axoprotective in mice expressing an ALS-associated mutant of the human TAR DNA-binding protein 43 kDa (TDP-43) [72], aggregates of which are found in axons in almost all cases of ALS [73]. The authors of that study speculated that the lack of efficacy of SARM1 in preventing axon degeneration in the SOD1 mutant mouse model may be due to the aggressive nature of the model, which exhibits rapid disease onset and progression, and that *Sarm1* deletion may be more beneficial in less extreme models which better recapitulate early ALS disease states.

A recent study examined the requirement for SARM1 in a number of mouse models of Parkinson's disease, the most common neurodegenerative movement disorder. *Sarm1*$^{-/-}$ mice were protected from axon degeneration in the medial forebrain bundle (MFB) lesioning model, in which axons of the MFB specifically are chemically severed *via* induction of lesions by targeted injection of 6-hydroxydopamine [74]. This was associated with improved functional capacity in the brains of these mice, as preservation of synaptic ability to maintain stored reserves of dopamine and its metabolites was observed. This was associated with rescue from behavioural phenotypes. However SARM1-deletion had no effect on a model of Parkinson's disease exhibiting "dying back" form of neurodegeneration, or in a model in which alpha-synuclein is overexpressed [74]. Similar to ALS, SARM1 may therefore only be required in certain models of Parkinson's disease. Thus targeting SARM1 therapeutically may be beneficial in corresponding cases of these neurodegenerative diseases.

In addition to some models of neurodegenerative disorders, *Sarm1*$^{-/-}$ mice show attenuated surrogate markers of axon degeneration and reduced functional deficits following traumatic brain injury [75]. Atrophy of the corpus callosum, one of the central white matter tracts of the brain, is widely observed across patients with moderate-severe brain injury [76]. These white matter tracts are composed mainly of myelinated axons. WT mice exhibit significant corpus callosum atrophy after a concussive model of traumatic brain injury due to axon degeneration, and this is attenuated by the genetic deletion of *Sarm1* [77]. This is associated with reduced neuroinflammation, and improved motor learning and sleep behaviours

relative to WT. Thus, *Sarm1* inactivation can be axoprotective and result in improved outcome following traumatic brain injury. Inhibitors of SARM1 which recapitulate the protection conferred by *Sarm1* deletion could therefore be beneficial as a traumatic brain injury treatment.

There are clearly myriad conditions and pathologies in which SARM1 deletion is advantageous as it ameliorates the pathological outcomes associated with axon degeneration, and development of SARM1 inhibitors is viewed as an attractive therapeutic strategy. There are however contexts in which SARM1-induced axon degeneration is beneficial. Recently, it was demonstrated that SARM1 is protective in a mouse model of ulcerative colitis [78]. SARM1-mediated axon degeneration in the enteric nervous system resulted in reduced secretion of norepinephrine, a neurotransmitter that drives inflammatory interleukin 17 (IL-17) secretion from T_H17 cells and type 3 innate lymphoid cells (ILC3s) causing local inflammation in the colon. In addition, in the context of rabies infection, SARM1-mediated axonal degeneration diminishes the spread of the virus [79]. Thus SARM1 inhibition could have a deleterious effect in such contexts. This would be an important consideration when recommending SARM1 inhibitors therapeutically.

1.4.5 NAD$^+$ metabolism and axon degeneration

The significance of nicotinamide adenine dinucleotide (NAD^+) metabolism in regulating axon degeneration was initially made clear when the protein responsible for the *Wld^S* phenotype was identified. The Wld^S protein comprises an N-terminal fragment of the ubiquitin ligase ubiquitin conjugation factor E4B (UBE4B) lacking catalytic activity connected by an 18aa linker to full length nicotinamide mononucleotide adenylyltransferase 1 (NMNAT1), which retains its catalytic activity [61]. NMNAT1 catalyses the synthesis of NAD^+, and it is this enzymatic activity which is responsible for the phenotype of delayed axon degeneration in *Wld^S* mice [80]. NMNAT1 is normally localised to the nuclear compartment [81] as a result of a nuclear localisation sequence. In contrast, Wld^S protein expression is not restricted to the nucleus, and this is likely a result of the N-terminal UBE4B sequence altering the protein conformation. The axoprotective phenotype observed in Wld^S mice can be mimicked by overexpression of two of the three NMNAT proteins: NMNAT2 [82] which is predominantly Golgi-associated, and NMNAT3 [83] which is predominantly localised to the mitochondria. Overexpression of a

mutant form of NMNAT1 which localises to the cytoplasm can also delay Wallerian degeneration [84], though overexpression of the WT nuclear-localised form cannot [85]. NMNAT2 is the most highly expressed NMNAT isoform in neurons [86], and downregulation of its activity has been demonstrated to be sufficient to induce axon degeneration in uninjured axons [82]. NMNAT2 has a short half-life, and requires constant replenishment to prevent Wallerian degeneration of uninjured axons [82]. Axotomy blocks the transport of NMNAT2 from the soma to the axon, and this leads to rapid local depletion of NMNAT2 levels and axon degeneration. NMNAT2 is therefore considered an axon survival factor. Wld^S functions as a non-labile substitute, which can compensate for NMNAT2 loss after axon injury to prevent induction of axon degeneration [82]. Congruent with this, NAD^+ levels decrease in degenerating axons, and local supplementation of exogenous NAD^+ efficiently prevents the degeneration of transected axons [87]. Overall, these observations suggest that non-nuclear localisation of NMNAT NAD^+ biosynthetic activity contributes to delayed axon degeneration.

1.4.6 SARM1 activation causes NAD^+ depletion

An important step in understanding the mechanism though which axon degeneration occurs was the 2015 discovery by Gerdts *et al.* that activation of SARM1 depletes NAD^+ in transected axons [88]. Prior to this discovery it was known that SARM1 was an essential mediator of axon degeneration, but the mechanism through which this occurs had remained elusive. The group had previously demonstrated that intact SAM and TIR domains are required for SARM1's prodegenerative function [89]. In this study, the group observed that a SARM1 mutant containing only these domains causes axon degeneration even in the absence of axonal insult or injury *in vivo* [89], indicating the N-terminal ARM domain is autoinhibitory. The SAM domains were shown to be necessary and sufficient for SARM1 multimerisation, and the TIR domain was implicated as the effector domain [89]. Thus the authors speculated that multimerisation of the SARM1 TIR domain alone could induce axon degeneration and that these TIR domains could signal to downstream effectors upon dimerization, as is observed in TLR-signalling. Indeed, pharmacologically forced dimerization of the SARM1 TIR domain rapidly induced axon fragmentation, which was associated with dissipation of the mitochondrial membrane potential and calcium accumulation [88]. These are indicators of energetic failure, and this prompted the authors to examine bioenergetics events which occur after SARM1 activation. The specific focus

was on NAD^+ levels, given the established link between axon degeneration and NAD^+ depletion. Thus, NAD^+ levels were measured by high performance liquid chromatography (HPLC) in axons from WT and *Sarm1*$^{-/-}$ axons shortly after transection, when they remained morphologically intact. In WT axons NAD^+ levels and consequently adenosine triphosphate (ATP) levels decreased post-axotomy [88]. This was SARM1-dependent, as NAD^+ levels remained stable in axons from *Sarm1*$^{-/-}$ neurons. Forced dimerization of the SARM1 TIR domain was sufficient to decrease the abundance of NAD^+ in uninjured axons [88]. In this study, Gerdts *et al.* also demonstrate that rapid NAD^+ loss is sufficient to induce rapid axon destruction, even in *Sarm1*$^{-/-}$ neurons [88]. These observations showed that SARM1 is an essential component of the axon degeneration pathway, and that its activation results in local catastrophic NAD^+ depletion which causes axon loss.

At this stage, it was accepted that SARM1 is the central executioner of an axon degeneration programme, however how this pathway culminated in NAD^+ depletion was unknown. Substantial interest arose in identifying the NADase enzyme which responded to SARM1 activation. Two known NAD-depleting enzymes, poly(ADP-ribose) polymerase 1 (PARP1) and CD38 [88, 90], were eliminated as candidates. Essuman *et al.* hypothesised that upon activation, dimerised SARM1 TIR domains may act as a scaffold and physically interact with and activate the responsible NADase [30]. To address this hypothesis, human Strep-tagged SARM1 TIR domain was expressed in HEK293T cells. The cells were lysed and the SARM1-TIR protein complexes were purified. The complexes were incubated with a known concentration of NAD^+ and HPLC was used to measure any changes in NAD^+ concentration over a period of 30 minutes. NAD^+ abundance decreased dramatically within 5 minutes when incubated with the SARM1- TIR protein complexes, but not in the control lysates from HEK293Ts which did not express SARM1, or which expressed previously identified non-functional SARM1 mutants [30]. This enzyme activity also demonstrated substrate specificity, as the NAD^+ analogue nicotinic acid adenine dinucleotide (NaAD) was not degraded by the SARM1-TIR protein complexes in this *in vitro* assay [30]. Gel electrophoresis followed by protein staining was employed to identify the associated proteins in the SARM1-TIR protein complexes. However, while there was a strong band corresponding to SARM1-TIR, there were not many additional proteins in the complex, and those which were present were observed at a similar abundance in the non-functional mutant SARM1-TIR complexes [30]. While this indicated that it was unlikely that a SARM1- associated NADase protein was represented by one of the bands, the group

used mass spectrometry to identify the proteins present in both the WT and non-functional mutant SARM1-TIR complexes. Surprisingly, no known NAD^+ consuming enzymes were among the proteins identified in these complexes [30]. Additionally, there were no unique or significantly enriched proteins in the WT SARM1-TIR complexes compared to the inactive mutant SARM1-TIR complexes. As these analyses did not identify any SARM1-associated NAD^+ consuming enzymes, the authors posited that SARM1 TIR domain itself may be enzymatically active.

1.4.7 SARM1 possesses intrinsic NADase activity

To explore the possibility of SARM1 possessing intrinsic NADase activity, Essuman *et al.* expressed human SARM1-TIR in *Escherischia coli* and examined the NAD^+ levels compared to bacteria expressing empty vector or inactive mutant SARM1-TIR. NAD^+ concentration was measured by HPLC and found to be remarkably low in the bacteria which expressed WT SARM1 compared to the controls [30]. The bacterially expressed SARM1-TIR was then purified and incubated with NAD^+ *in vitro.* In agreement with the NADase activity observed with SARM1-TIR purified from mammalian cells, the bacterially expressed human SARM1-TIR rapidly decreased the concentration of NAD^+ *in vitro* [30]. Consistent with the evolutionary conservation of SARM1's role in axon degeneration, this NADase activity is conserved across species; bacterially expressed SARM1-TIR from mouse, zebrafish, and *Drosophila* all degraded NAD^+ *in vitro* [30]. For further confirmation that SARM1-TIR possesses NADase activity independent of any other bacterial or mammalian protein, the authors used a cell-free protein expression system to synthesise the human SARM1-TIR. This SARM1-TIR could rapidly cleave NAD^+ [30]. Thus, the group had definitively demonstrated that SARM1 possesses intrinsic NADase activity, which is responsible for the NAD^+ depletion observed in axon degeneration. This was also the first demonstration of a TIR domain possessing enzymatic activity. Using HPLC, Essuman *et al.* then identified the NAD^+ cleavage products generated by SARM1-TIR enzymatic activity. Surprisingly in addition to the major products nicotinamide (Nam) and ADP-ribose (ADPR), cyclic ADPR (cADPR) was identified as a minor product [30]. This was observed in human, mouse, and zebrafish SARM1. Curiously, while the same cleavage products were observed following *Drosophila* dSarm1-TIR cleavage of NAD^+, the ratio of cADPR to ADPR was reversed, with ADPR representing only a minor product [30]. Thus SARM1-TIR possesses both NADase and cyclase activity, the products of which

are shown in Figure 1.3. Fascinatingly, it has since been demonstrated TIR domain-containing proteins from a range of bacteria and archaea possess intrinsic NADase activity, with a subset of these also generating cADPR like SARM1 [91]. This is consistent with a phylogenetic analysis which showed that SARM1 clusters more closely with bacterial TIR-domain containing proteins that with other vertebrate TIR-containing adaptor proteins [92], and suggests that NAD^+ depletion is the primordial function of the TIR domain.

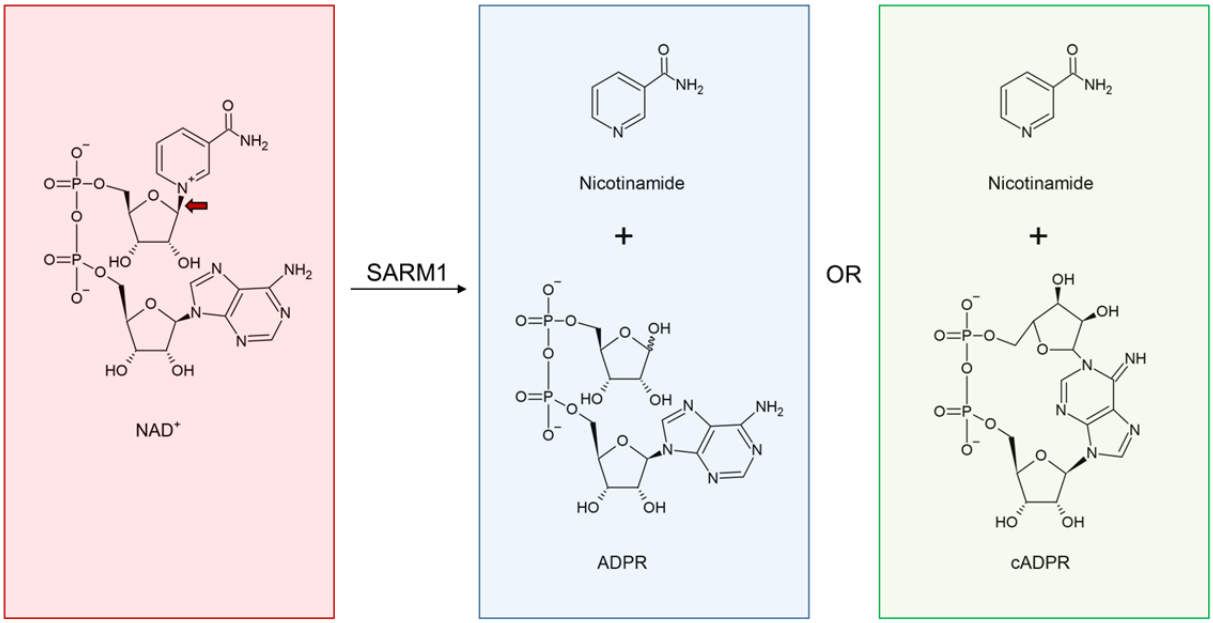

Figure 1.3 The cleavage of NAD^+ by SARM1

Activated SARM1 can catalyse the cleavage of NAD^+ into nicotinamide and ADPR or into nicotinamide and cADPR. NAD^+, nicotinamide adenine dinucleotide; ADPR, adenosine diphosphate ribose; cADPR, cyclic adenosine diphosphate ribose. The point at which SARM1 cleaves NAD^+ is indicated by a red arrow. Adapted from Hopkins *et al.*, 2021 [93].

Essuman *et al.* sought to identify putative residues in the SARM1-TIR domain which contribute to its catalytic activity. Using domain prediction analysis, the group identified protein homologues of the SARM1-TIR domain. In addition to finding other TIR domains to be homologous, the group identified a number of nucleotide hydrolases and nucleotide transferases [30]. This was in line with an earlier bioinformatics-based report that some TIR domains showed structural similarity to these two groups of enzymes [94]. Using the

crystal structures of two of the enzymes in which the catalytic residues were already identified or proposed, the SARM1-TIR domain was modelled. Importantly, glutamic acid E642 in the SARM1-TIR domain aligned with the known catalytic glutamic acids in these enzymes on which it was modelled [95, 96]. Indeed, in other NADases glutamic acid residues are known to be key catalytic residues [97]. Mutation of this residue to an alanine (E642A) disrupted the enzymatic activity of SARM1-TIR; purified SARM1-TIR E642A synthesised in the cell-free translation system failed to cleave NAD^+ *in vitro* [30]. Critically, where expression of WT SARM1 in murine *Sarm1*$^{-/-}$ dorsal root ganglion (DRG) neurons could promote NAD^+ depletion and axon degeneration post-axotomy, expression of SARM1-E642A could not. Similarly, the enzymatically disabled SARM1 could not induce axon degeneration in response to vincristine administration, which is observed in neurons expressing WT SARM1 [30]. Thus, SARM1 NADase activity is required for injury-induced axon degeneration. In addition, this NADase activity has been demonstrated to have a crucial role in disease-related axon degeneration. Recently, SARM1 variants with constitutively hyperactive NADase activity have been identified as enriched in patients with ALS and the related motor neuron disease, hereditary spastic paraplegia (HSP) [98]. Mice infected with a virus expressing the constitutively active variant most frequently observed in ALS patients developed axon loss, motor dysfunction and sustained inflammation [99]. Thus induction of SARM1 NADase activity is the point at which a variety of diverse stimuli and insults converge to induce in axon degeneration. Targeted inhibition of this NADase activity may therefore have therapeutic potential.

1.4.8 SARM1 structural biology and regulation

In order to design effective therapeutics targeting SARM1, it is vital that the mechanism by which SARM1 NADase activity is triggered is well characterised. In recent years, colossal efforts have been devoted to determining the how this activity is stringently controlled. Under conditions of oxidative stress, it was reported that c-Jun N-terminal kinase (JNK) phosphorylates SARM1 at serine S548 to induce NADase activity [31]. Mutation of this residue or treatment with a JNK inhibitor resulted in decreased SARM1 activity [31]. Phosphorylation of SARM1 S548 was also observed in rat model of ischaemia/reperfusion injury [100]. Local overexpression of a SARM1 S548A mutant in the rat brain by lentiviral transduction resulted in reduced ischaemia/reperfusion-induced brain injury compared to both overexpression of WT SARM1 and remarkably,

untransduced controls [100]. However, how phosphorylation of this residue in the SAM domain activates SARM1 to induce axon degeneration remains unknown. Kwong *et al.* developed cell-permeant NMN-mimetic inhibitors of CD38, an enzyme which like SARM1 cleaves NAD^+ and generates cADPR [101]. Curiously one of these inhibitors, CZ-48, could elevate cADPR levels in cells which did not express CD38 [101]. A number of years later the same group identified SARM1 as the cADPR-producing enzyme which is activated by CZ-48, and demonstrated that endogenous NMN itself also activates SARM1 to cleave NAD^+ and produce cADPR [102]. This is consonant with loss of NMNAT activity being pro-degenerative in axons; as a substrate of NMNATs, NMN concentration increases in their absence.

Studies into the structure of SARM1 and how this relates to its function have greatly added to our understanding of SARM1 activity. Horsefield *et al.* determined the crystal structure of the human SARM1 TIR domain, and found that it bore close similarity to the TIR domains from plant immune receptors which trigger localised death, including the NLR RUN1 [103]. In fact, SARM1 TIR showed more similarity to plant TIRs than to the bacterial TIRs that SARM1 was previously predicted to cluster closely with by phylogenetic analysis [92]. The catalytic site of SARM1 TIR was determined, and could be superimposed onto that of two structurally similar enzymes [103]. This revealed a common catalytic glutamic acid residue, confirming the previous report by Essuman *et al.* that glutamic acid E642 mediated human SARM1 enzyme activity [30]. The authors then solved the crystal structure for human SARM1 SAM domains, which suggested a double-layered ring arrangement comprising eight monomers of the tandem SAM domains [103]. A SARM1 mutant in which SAM domains could not oligomerise was unable to cleave NAD^+ and could not induce axon degeneration. In a remarkable parallel, plant TIR domains were also found to cleave NAD^+ and this activity was also dependent on self-association [103]. Simultaneously, Wan *et al.* similarly reported NADase activity in self-associating plant TIR domains, and described a putative catalytic glutamic acid conserved in plant TIRs, bacterial TIRs and SARM1 [104]. Soon after, an additional study was published providing structural evidence that the SAM domains of SARM1 form an octameric ring, and predicting that SARM1 itself adopted an octameric conformation when inactive, with the TIR domains held apart until the point of activation [105].

Four groups independently determined cryo-electron microscopy (cryo-EM) structures of near full length SARM1 in quick succession, and this contributed greatly to the understanding of SARM1 structure and activation. First Bratkowski *et al*. published the structure of near full-length, autoinhibited SARM1 and revealed that it exists as an autoinhibited pre-assembled octamer [106] as was previously observed in the crystal structure of the SAM domains in isolation [103, 105]. Existing in a preassembled octamer allows SARM1 to rapidly transition from being inactive to active upon insult or injury. The autoinhibited SARM1 octamer consists of double-layered ring of the two SAM domains, with the ARM domains assembled at the perimeter of the rings and interacting with the TIR domains of another SARM1 monomer, ensuring TIR domains remain spatially separated from each other [106] (see Figure 1.4). Disruption of this "ARM-TIR lock" by mutation of critical residues in the ARM domain are sufficient to enzymatically activate SARM1 NADase activity, and drive axon fragmentation [106]. NMN treatment could not further stimulate the enzymatic activity of constitutively active SARM1 lacking the autoinhibitory ARM domain, suggesting that an intact ARM-TIR lock is necessary for NMN activation of SARM1 [106]. The group further attempted to solve the cryo-EM structure of active SARM1 lacking the auto-inhibitory ARM domain. The SAM domains adapted a similar conformation, however the TIR domains could not be resolved in the final map, indicating that they may be dynamic [106]. Similarly, the structure of near full length SARM1 in complex with NMN could not be resolved to determine the conformational change of the TIR domains [106].

Adding to this Jiang *et al.* published a similar cryo-EM structure, but surprisingly found that while no EM density corresponding to NAD^+ was present in the active site of the TIR domain, NAD^+ occupied an allosteric binding site in the ARM domain [107]. The group demonstrated that NAD^+ occupation of this site maintains SARM1 in an inhibited state, and disruption of this site caused constitutive SARM1 activation and axonal degradation [107]. Further evidence of NAD^+ inhibition of SARM1 activity was provided by measurement of SARM1 NADase activity over a NAD^+ concentration gradient. When plotted, these measurements exhibited a bell-shaped curve; while increasing NAD^+ at low concentrations resulted in enhanced NADase activity, increasing NAD^+ at higher concentrations had an inhibitory effect, which was only observed when the SARM1 ARM domain was intact [107]. Sporny *et al.* independently determined a similar cryo-EM structure, and confirmed that binding of NAD^+ to an allosteric binding site in the ARM

domain maintained SARM1 self-inhibition. Finally, using cryo-EM, peptide screening, and site-directed mutagenesis, Shen *et al.* determined the interactions across multiple domain interfaces, both inter- and intra-subunit, which are required to keep SARM1 inactive [108]. Thus, the elucidation of the cryo-EM structure of SARM1 illuminated some critical regulatory elements.

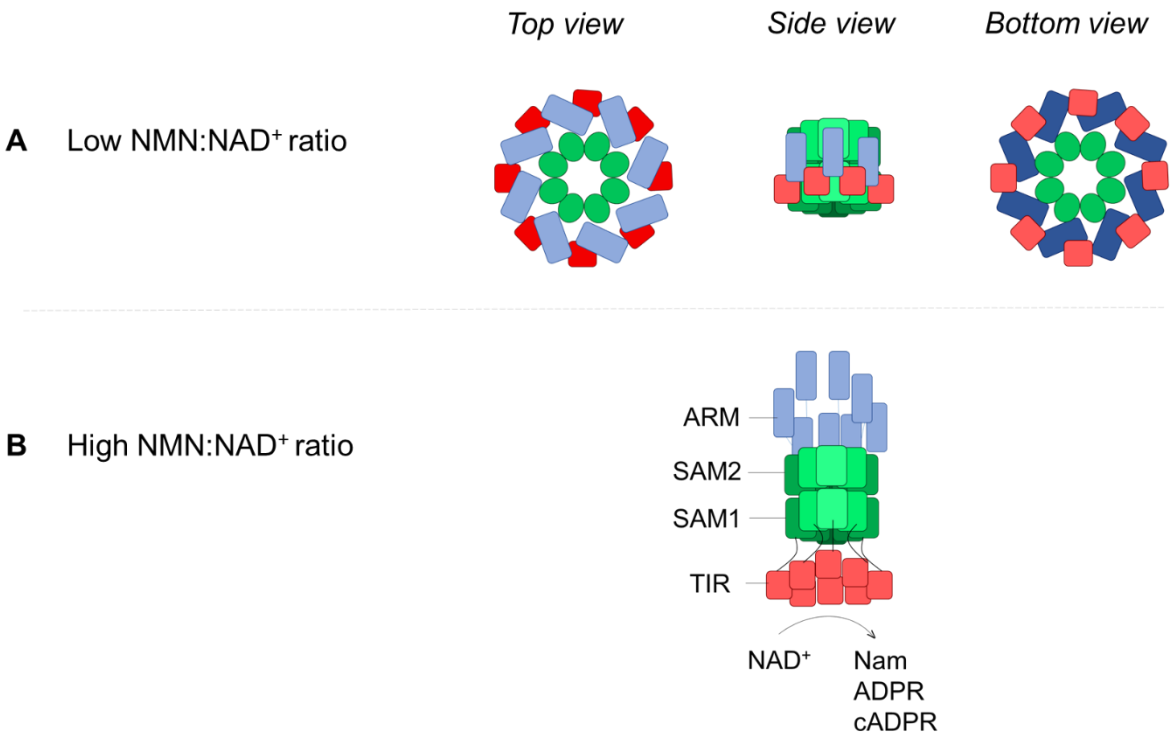

Figure 1.4 SARM1 NADase activity is activated by an increase in the local NMN:NAD$^+$ ratio

In the context of a low NMN:NAD$^+$ ratio, NAD$^+$ binds to the SARM1 allosteric binding site, precluding binding of the less abundant NMN. This maintains SARM1 in an inactive state, with the TIR domains kept spatially separated by interaction with the ARM domain. Upon increasing the NMN:NAD$^+$ratio, NMN can bind the SARM1 allosteric binding site, inducing a conformational change which breaks the ARM-TIR lock and allows homotypic interactions between TIR domains. This facilitates the activation of SARM1 enzymatic activity, causing the cleavage of NAD$^+$, producing Nam, ADPR, and cADPR. NMN, nicotinamide mononucleotide; NAD$^+$, nicotinamide adenine dinucleotide; ARM, armadillo repeats; SAM, sterile α motif domain; TIR, toll/interleukin-1 receptor; Nam, nicotinamide; ADPR, adenosine diphosphate-ribose; cADPR, cyclic ADPR.

1.4.9 SARM1 is a metabolic sensor of the NMN:NAD$^+$ ratio

A notable advancement in our understanding of SARM1 regulation came from a recent report by Figley *et al.* which described SARM1 as a metabolic sensor. Strikingly in this report, a cryo-EM structure of the ARM domain alone was presented in which NMN occupied the same allosteric binding site as NAD$^+$ [109]. In fact, in dSarm1 ARM (which was used instead of human SARM1 for technical reasons), NMN bound to this site with far greater affinity than NAD$^+$ [109]. NMN binding to this site resulted in conformational alteration of the ARM domain, which is predicted to break the inhibitory ARM-TIR lock and free the TIR domains to interact, thereby activating the NADase activity [109], as summarised in Figure 1.4. This suggests a model in which NAD$^+$ and NMN compete for this binding site to maintain SARM1 in an inactive state or switch SARM1 to an active state respectively. Testing this model, Figley *et al.* measured SARM1-induced cADPR production following metabolic manipulations which independently alter NAD$^+$ or NMN levels in neurons *in vitro*. Interestingly, rather than the absolute levels of NMN determining SARM1 activation, it was the NMN:NAD$^+$ ratio which controlled the SARM1 switch to an active state [109]. Thus, both an increase in NMN and a decrease in NAD$^+$ can trigger SARM1 activation. Mutations in this binding site abolished SARM1 activity in response not only to NMN, but also axotomy [109], suggesting that the default state of SARM1 in the absence of either metabolite is inactive. This supports a model in which NAD$^+$ inhibits SARM1 through competition with NMN for binding; rather than inhibiting through active stabilisation of the auto-inhibited state, NAD$^+$ blocks NMN from binding and activating SARM1. This discovery of the allosteric binding site revealed that SARM1 acts as a sensor of the metabolic environment, and was significant in furthering the understanding of the events leading to activation of SARM1 in axon degeneration, and in informing the design of inhibitors.

The current model is that SARM1 senses an alteration in the homeostatic ratio of NMN:NAD$^+$, which triggers the SARM1 NADase activity to deplete NAD$^+$ and induce axon degeneration (Figure 1.5). While the specific basal NMN:NAD$^+$ ratio in the axon is not known, in DRG neurons and in the murine sciatic nerve, NAD$^+$ levels are orders of magnitude higher than NMN [110, 111], and this maintains SARM1 in an autoinhibited state. This ratio can be perturbed by depletion of NMNAT2 or reduction of its activity.

Axotomy precludes transport of newly synthesised NMNAT2 from the soma to the axon, and due to its labile nature, NMNAT2 in the distal axon segment becomes depleted [82]. NMNAT2 depletion can also be induced by mitochondrial toxins, including CCCP and rotenone, through reduced synthesis and reduced axonal transport [112, 113]. In response to axonal stress, dual leucine zipper kinase (DLK) signalling provokes transcriptional changes in the soma, and predisposes axons to SARM1-dependent axon degeneration by reducing NMNAT2 levels [114]. Similarly, the chemotherapeutic agents vincristine and bortezomib decrease axonal NMNAT2 levels by distinct mechanisms. Vincristine interferes with microtubule dynamics, resulting in reduced axonal transport and therefore reduced NMNAT2 in the axon [66]. In contrast, bortezomib depletes NMNAT2 in a transcriptionally-dependent manner involving the apoptotic executioner caspase, caspase 3 [66]. Thus, each of these axonal insults or injuries result in accumulation of NMNAT2's substrate NMN and depletion of its product NAD^+, thereby activating SARM1 and inducing axon degeneration. The presence of Wld^S protein protects axons from degeneration induced by transection, chemotherapeutic, and mitochondrial poison by acting as a stable replacement of NMNAT2 and maintaining a homeostatic NMN:NAD^+ ratio. This is summarised in Figure 1.5.

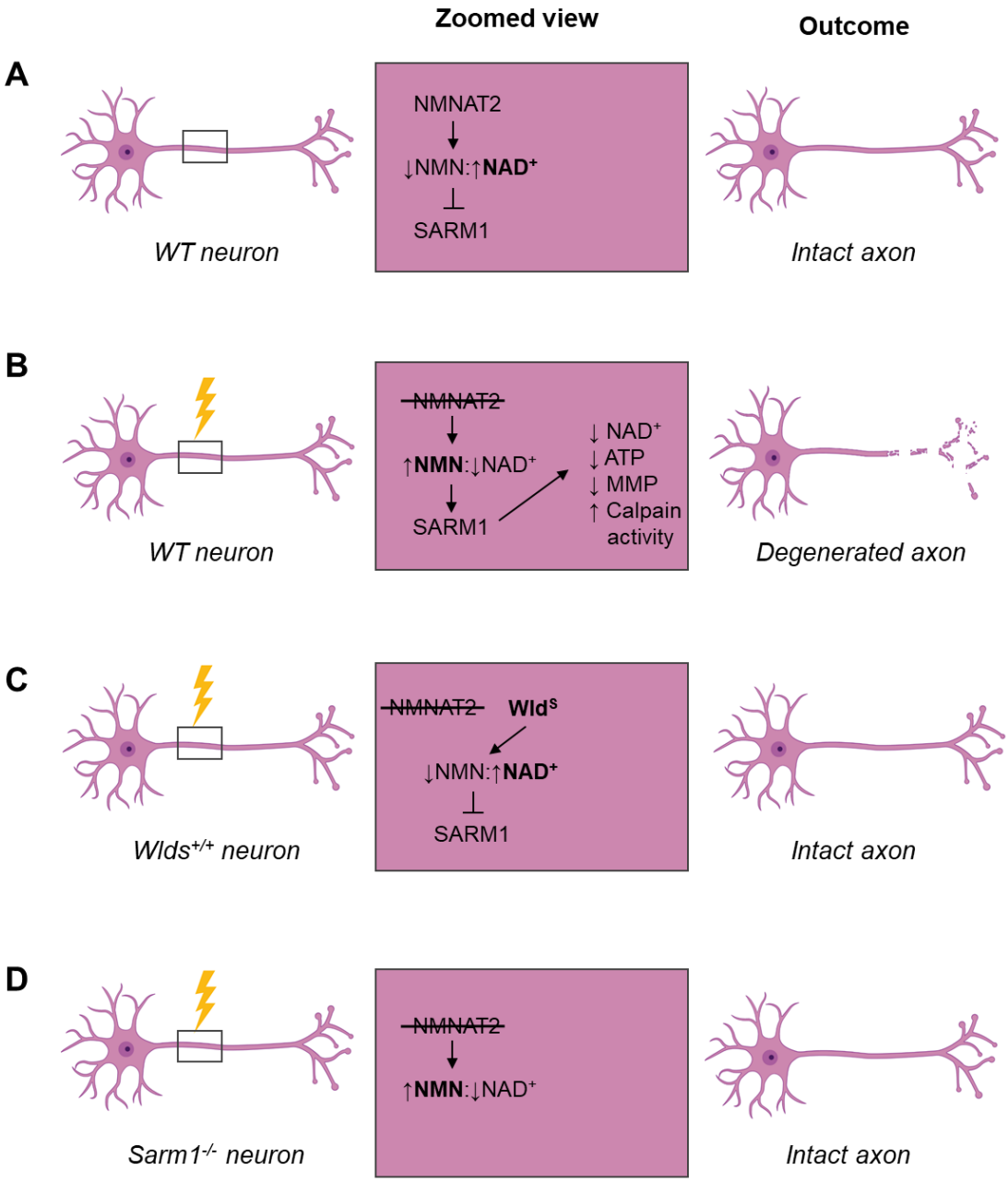

Figure 1.5 SARM1 senses increases in the NMN:NAD$^+$ ratio and induces axon degeneration

(A)WT neurons with intact NMNAT2 have a low NMN:NAD$^+$ ratio which maintains SARM1 in an autoinhibited state. (B) Upon axonal insult or injury in WT neurons, NMNAT2 is rapidly depleted, augmenting the NMN:NAD$^+$ ratio. This induces a conformational change in SARM1 which results in activation of the NADase activity. This culminates in axon degeneration. (C and D) Expression of the Wld^S protein or deletion of the *Sarm1* gene protects injured/insulted axons from degeneration. Expression of the stable Wld^S (C) replaces the labile NMNAT2 in maintaining a low NMN:NAD$^+$ ratio, maintaining SARM1 in an inactive state. In the absence of SARM1 (D) axon degeneration does not proceed following axon insult or injury. WT, wild type; NMN, nicotinamide mononucleotide; NAD$^+$, nicotinamide adenine dinucleotide; ATP, adenosine triphosphate; MMP, mitochondrial membrane potential.

1.4.10 Axon degeneration pathways downstream of SARM1 activation

The order of events downstream of SARM1 activation and NADase activity has been difficult to discern due to the asynchronous nature of axon degeneration. A recent publication by Ko *et al.* sought to gain understanding of the temporal relationship between events downstream of SARM1 activation by employing live imaging at the single axon level [115]. This study also investigated if mammalian SARM1 would have any NADase-independent roles in the major proximal events in injured axons, as an NADase-independent role was described for Drosophila dSarm1 in the inhibition of axonal organelle trafficking in bystander neurons adjacent to injured axons [116]. Three of the major events downstream of SARM1, mitochondrial stalling, mitochondrial depolarisation, and calcium influx were examined in *Sarm1*$^{-/-}$ DRG neurons expressing green fluorescent protein (GFP) as a negative control, WT SARM1, or catalytically inactive SARM1 E642A. After axotomy, mitochondrial movement was unimpaired in DRG neurons from *Sarm1*$^{-/-}$ mice expressing GFP [115]. Expression of WT SARM1 resulted in a substantial reduction in motile mitochondria post-axotomy, and this was not observed in DRG neurons expressing SARM1 E642A. Thus, the NADase activity of SARM1 is required for the stalling of mitochondrial movement in injured axons [115]. SARM1 NADase activity was also observed to be required for the loss of mitochondrial membrane potential observed after axon injury, indicating that the SARM1-induced NAD^+ depletion influences mitochondrial bioenergetics either directly or indirectly [115]. The authors also found that enzymatically intact SARM1 is required for late calcium influx [115], which is responsible for the disrupted calcium homeostasis observed hours after axon injury.

The role of calcium in axon degeneration is unclear. Previous imaging studies of Wallerian degeneration *in vitro* in zebrafish demonstrate that there are two distinct waves of calcium influx. The initial transient wave is triggered at the injury site upon axotomy, and is not blocked by expression of Wld^S, indicating it may be unrelated to SARM1 NADase activity [117]. Chelating calcium to prevent this wave has no impact on axon fragmentation [117]. The second wave of calcium influx immediately precedes axon fragmentation [117, 118]. Calcium chelation prior only to the second wave could inhibit axon fragmentation [117], and SARM1 deletion could prevent this second wave from occurring [118]. The SARM1 product cADPR is a calcium mobilising agent. It can modulate calcium release from intracellular stores through ryanodine receptor channels [119], and activate the calcium-

permeable non-specific cation channel TRPM2, which is predominantly on the plasma membrane [120]. Ko *et al.* manipulated both intracellular and extracellular calcium and induced axotomy, and found that intracellular calcium flux had no clear role in axon degeneration [115]. In contrast however, another group reported that in the context of paclitaxel induced axon degeneration, cADPR produced by SARM1 was required for calcium flux from both intra- and extra-cellular stores, and genetic or pharmacological interference with cADPR signalling could prevent axon degeneration [121]. Thus, the magnitude of SARM1 activation or the context of the activator may determine if SARM1-mediated calcium influx from intracellular stores is a determinant of axon degeneration. In agreement with studies in zebrafish [117, 118], Ko *et al*. found that prevention of late extracellular calcium efflux could block axon fragmentation [115]. However, this did not block the loss of mitochondrial membrane potential and mobility, suggesting that calcium influx may trigger the fragmentation of axons which are already metabolically dead.

Using live cell imaging at the single axon level, the authors delineated the sequence of events leading from injury-induced SARM1 activation [115]. SARM1 activation depletes NAD^+, which is followed by loss of ATP due to impaired glycolysis and oxidative phosphorylation. The authors believe the ATP loss causes the loss of mitochondrial motility, which immediately proceeds it. The halted mitochondria lose membrane potential, likely due to the absence of ATP. This is followed by calcium influx, which the authors speculate may be related to the impact of the loss of ATP on numerous ionic pumps [115]. Phosphatidylserine becomes exposed on the outer leaflet of the plasma membrane, and the axon becomes fragmented in a manner requiring the calcium influx. Previous studies have shown that the axon degradation is mediated by the calcium-dependent proteases, calpains [122, 123]. Given that the axon is already essentially dead at the point of calcium-dependent fragmentation, Ko *et al.* suggest that catastrophic ATP loss is the point at which an injured axon commits to death by disrupting mitochondrial, calcium, and membrane homeostasis [115]. Yang *et al.* reported that the MAPK signalling pathway also plays an important role in triggering energy deficit downstream of SARM1 activation [124]. SARM1 activated the MAPK cascade within minutes of axon injury [124], and given that MAPK signalling is reported to increase turnover of NMNAT2 [125] this may function to propagate the axodegenerative response. JNK is activated as part of this pathway, and it has been speculated that this may contribute to the positive regulatory phosphorylation of SARM1

S548 [126]. The downstream events of SARM1 activation leading to axon degeneration are summarised in Figure 1.6.

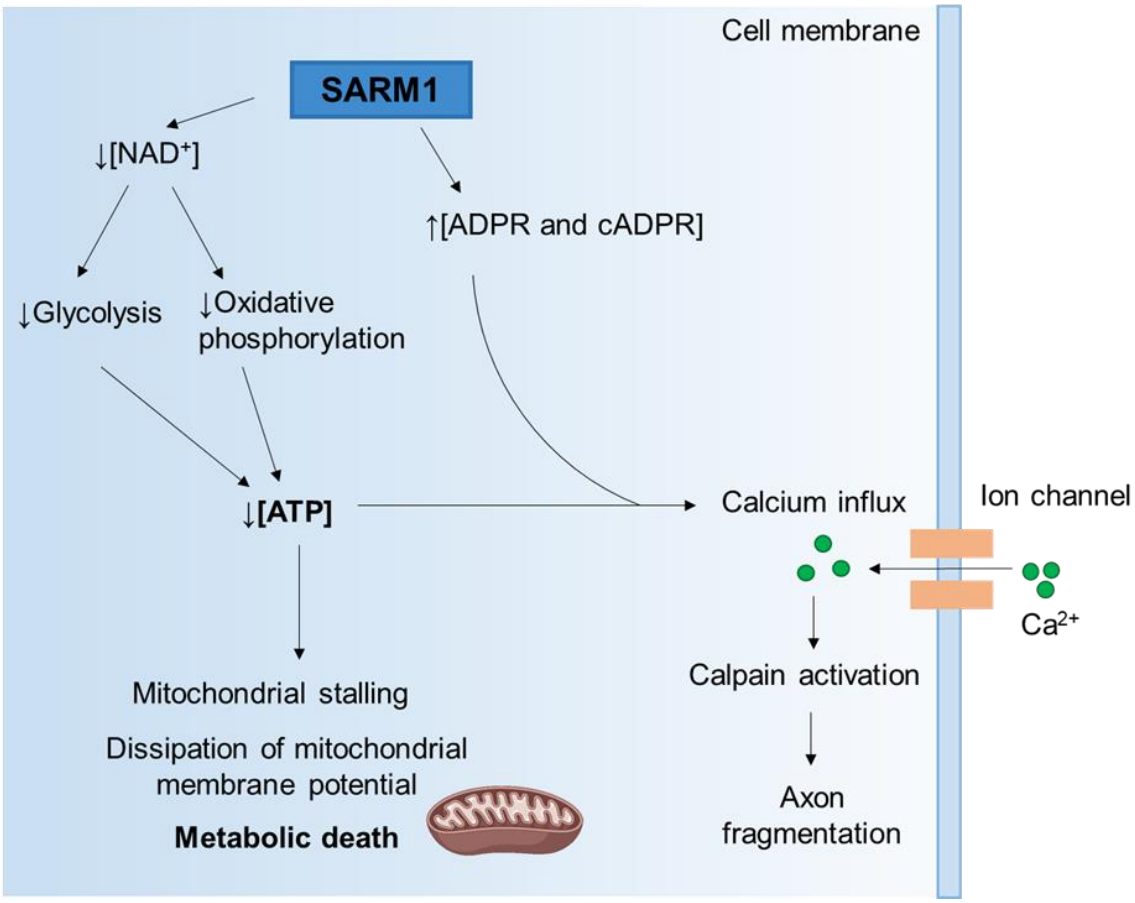

Figure 1.6 Events downstream of SARM1 activation which lead to axon degeneration

Upon SARM1 activation NAD^+ is cleaved. This leads to a reduction in NAD^+ levels and an increase in ADPR and cADPR levels. The reduction in NAD^+ causes a drop in the rate of glycolysis and oxidative phosphorylation, which causes catastrophic ATP depletion. This causes mitochondrial stalling and the dissipation of the mitochondrial membrane potential, and ultimately leads to metabolic cell death. This ATP depletion may contribute to disruption of ion channels, causing calcium influx. The increased concentration of ADPR and cADPR also contribute to the calcium influx by binding to ryanodine receptors and TRPM2. As a result of this calcium influx, calpains become activated and this ultimately leads to fragmentation of the axon. ADPR, adenosine diphosphate ribose; ATP, adenosine triphosphate; cADPR, cyclic ADPR; NAD^+, nicotine adenine dinucleotide; SARM1, sterile α- and armadillo motif-containing protein.

1.5 The discovery of SARM1 inhibitors and activators

Our understanding of SARM1 activation and function has progressed rapidly in the past few years and because of the enticing prospect of targeting SARM1 in neurodegenerative conditions, substantial effort has been devoted to the development of SARM1 modulators. A recent study demonstrated that SARM1-haploinsufficiency could delay axon degeneration in response to a variety of physical and toxic insults, and that SARM1-targeting by antisense oligonucleotides which reduce SARM1 expression to a similar level can similarly delay axon degeneration [127]. This illustrated that absolute abrogation of SARM1 expression is not essential to improve outcome in neurodegeneration. Gene therapy, wherein a dominant-negative SARM1 mutant is introduced into neurons by adeno-associated virus (AAV), has exhibited success in robustly protecting axons from destruction both *in vitro* and *in vivo* in mouse. In wild-type human induced pluripotent stem cells (iPSCs), expression of the same dominant negative mutant SARM1 could block injury-induced axon degeneration to a similar extent as is observed in *Sarm1* knockout human iPSCs [128]. A systematic review of clinical trials of AAV-based gene therapies has shown them to be safe and efficacious in humans [129]. Thus, this could be a promising therapeutic strategy in the treatment of neurodegenerative conditions, particularly in chemotherapy induced peripheral neuropathy where SARM1 targeting would only be temporarily required for the duration of chemotherapy treatment.

In addition to gene therapies, the first small molecule SARM1 inhibitors have been discovered. The first of these was reported by Hughes *et al.*, who identified a potent and selective inhibitor of SARM1 NADase activity based on isoquinoline [113]. This inhibitor was axoprotective in both mouse neurons and human iPSCs. SARM1 inhibition prevented axon destruction even when the inhibitor was applied to neurites up to 3 hours after axotomy. The authors of this study reported that transient mitochondrial injury with rotenone causes axons to enter an immediate state of axonal damage, which are fated to degenerate. Treatment with the SARM1 inhibitor not only prevented degeneration, but allowed recovery of axons in this state [113]. This could have profound implications in the treatment of human axodegenerative diseases, as there is evidence of a pool of recoverable axons in certain conditions [130, 131], and their restoration could result in improved function. Li *et al.* designed fluorescent probes which act as substrates of SARM1 and allow visualisation of SARM1 activation in live cells [132]. Using the probes, the authors could

screen candidate inhibitors, and discovered a nisoldipine derivative, called dHNN, which could block SARM1 activation and axon degeneration [132]. This inhibitor reacts with the cysteines in SARM1, and the cryo-EM structure showed that it locks SARM1 into the inactivate conformation [132].

In another exciting development, a recent report showed the discovery of potent, selective, but irreversible isothiazole inhibitors of SARM1 which are axoprotective in human and mouse axons *in vitro* [133]. The inhibitors were tested *in vivo* in a mouse model of chemotherapy induced peripheral neuropathy using paclitaxel, and remarkably could prevent loss of nerve fibres and conferred partial protection of axonal function [133]. The demonstration that small molecule inhibitors of SARM1 can successfully protect axons from degeneration both *in vitro* and *in vivo* is promising and bodes well for their use in neurodegenerative conditions. Potent activators of SARM1 have also been recently discovered. Vacor is a disused rodenticide and neurotoxin, which is metabolised to vacor mononucleotide (VMN) by nicotinamide phosphoribosyltransferase (NAMPT), and then to vacor adenine dinucleotide (VAD) by NMNAT2, similar to the production of NAD from nicotinamide [134]. Loreto *et al.* demonstrated that vacor-induced neuron and axon death is SARM1-dependent, and that it is the vacor metabolite VMN which strongly activates SARM1 through direct binding to the ARM domain [134]. Mutations in this binding pocket protected mouse neurons from vacor-induced neurite degeneration, and neither NMN nor VMN could activate SARM1 which harboured these mutations [134]. A similar study was published by Wu *et al.* identifying SARM1 as mediator of toxicity induced by the neurotoxin 3-acetylpyridine (3-AP) [135]. 3-AP is converted to 3-AP mononucleotide (3-APMN), which can activate SARM1 [135]. The authors could demonstrate that application of exposed peripheral nerves with 3-AP could trigger localised neurodegeneration, and suggest that targeted SARM1 activation may therefore be of use for therapeutic neurolysis in severe pain conditions [135].

Recently, acidic pH was found to irreversibly activate SARM1 even more efficiently than NMN by directly regulating the ARM-TIR interaction [136]. A protocol was devised by the authors of this study to differentiate the inhibitory mechanism of SARM1 inhibitors, in which cell lysates containing SARM1 lacking the mitochondrial targeting sequence were pre-treated with either acid or NMN, or left untreated, before incubation with a range of concentrations of each inhibitor [136]. The lysates which were not pre-treated screened for

inhibitors without distinction as to their mechanism. The NMN and acid pre-treated lysates, in which SARM1 was activated prior to exposure to inhibitors, were used to screen for inhibitors targeting the catalytic activity of SARM1. Using this protocol, the authors found that both disulfuram and the inhibitor they previously described, dHNN [132], mainly inhibited SARM1 activation as they failed to have an inhibitory effect on SARM1 which was pre-activated with NMN or acid. In contrast, nicotinamide and some detergents, including Tween-20 and Tween-80, inhibit SARM1 catalytic activity [136]. This screening method provides a robust tool for testing and understanding SARM1 inhibitors for drug discovery. The authors also speculate that acid-induced activation of SARM1 may occur physiologically in the lysosome [136].

Thus, great strides have been made in the development of SARM1-targeting strategies with therapeutic potential. Furthermore, many useful tools have been discovered and shared which will aid in expediting progress. It remains to be addressed if the targeted inhibition or activation of SARM1 will have implications for its roles in non-neuronal cell death (discussed in Section 1.6.4) or in the immune response (discussed in Section 1.3.3 and Section 3.1). Therefore it is essential that we understand the mechanisms through which SARM1 regulates each of these activities, and if inhibition of SARM1 catalytic activity will cause their dysregulation.

1.6 SARM1 and programmed cell death

Cells possess numerous molecular pathways to trigger their own death, termed programmed cell death. In the context of immunity, cell death can contribute to attenuating or propagating and directing further immune action, depending on the nature of the programme induced. Three of the most intensively investigated and well-characterised forms are apoptosis, pyroptosis, and necroptosis.

1.6.1 Programmed cell death

Apoptosis is a non-immunogenic contained form of cell death, wherein the plasma membrane stays intact and the cellular contents remain enclosed. Morphologically, apoptotic cells are characterised by extensive blebbing of the plasma membrane and condensation of the nucleus [137]. There are two forms of apoptosis, called the intrinsic and extrinsic pathway (reviewed in [138]). The intrinsic pathway is dependent on the release of factors from the mitochondria, which can be triggered by the absence of pro-survival signals or the presence of a toxic agent such as reactive oxygen species. The extrinsic pathway is initiated by the binding of death receptors on the cell to its cognate death ligand. The intrinsic and extrinsic pathways converge on the recruitment, cleavage, and activation of the zymogenic initiator caspases, caspase 9 [139] and caspase 8 [140] respectively. These initiator caspases then cleave and activate the executioner caspases, caspases 3 and 7 [141]. The executioner caspases initiate a cascade of events resulting in DNA fragmentation [142], disassembly of the cytoskeleton, extensive protein crosslinking [143], loss of mitochondrial membrane potential [144], and expression of ligands which act as an “eat me” signal for phagocytes [145, 146]. The apoptosed cells are quickly removed by efferocytosis, and the cells which engulf them do not produce inflammatory cytokines [147]. Apoptosis is particularly important in embryonic development [137] and in clearance of immune cells upon resolution of infection [148].

In contrast pyroptotic cell death is pro-inflammatory and lytic [149], and is mediated by formation of pores at the plasma membrane by the N-terminal fragment of gasdermin D (GSDMD). There is evidence that the GSDMD N-terminal fragment can also localise to the mitochondria, leading to decreased mitochondrial membrane potential and release of mitochondrial DNA [150]. This mitochondrial DNA can be released upon plasma

membrane rupture to act as a DAMP [151]. Pyroptosis proceeds following activation of canonical inflammasomes which comprise intracellular sensors, including nucleotide oligomerisation domain (NOD)-like receptors (NLRs) and absent in melanoma 2 (AIM2)-like receptors (ALRs), which oligomerise and recruit adaptor proteins, thus forming a scaffold to recruit the zymogenic pro-caspase-1 [152]. Through autocatalysis caspase-1 becomes active and, in addition to cleaving GSDMD and releasing the pore-forming N-terminus, cleaves the cytokines pro-IL-1β and pro-IL-18 to their active forms. Noncanonical inflammasome activation can also trigger pyroptosis. Caspases 4 and 5 in human (or 11 in mouse) act as cytosolic sensors of lipopolysaccharide (LPS) and upon activation, they can directly cleave GSDMD [153] and also trigger the formation of the NLRP3 inflammasome [154], leading to subsequent pyroptotic lysis and cytokine release. Recently it has been demonstrated that GSDME can also directly induce pyroptotic death in certain contexts [155, 156].

Necroptosis proceeds when death receptors bind their cognate ligands, but the apoptotic pathway is blocked. Necroptosis, unlike pyroptosis and apoptosis is caspase independent, and can only progress when caspase-8 activity is inhibited (reviewed in [138]). The core downstream components of the necroptotic pathway are receptor-interacting serine/threonine protein kinase 1 (RIPK1) [157], RIPK3 [158], and mixed-lineage kinase domain like (MLKL), which form a complex known as the necrosome. MLKL becomes phosphorylated [159], oligomerises, and translocates to intracellular and plasma membranes, disrupting their integrity [160]. This induces cell death and the pro-inflammatory release of cellular contents.

Additional less well-characterised forms of programmed cell death exist, including ferroptosis and parthanatos. Ferroptosis is inflammatory, and results from unconstrained iron-dependent peroxidation of polyunsaturated fatty acid chains in cell membranes, disrupting their integrity [161]. Parthanatos is induced by oxidative stress-induced DNA damage and mediated by hyperactive PARP1, which depletes cellular NAD^+ and ATP and dissipates the mitochondrial membrane potential [162]. Recent studies have indicated that programmed cell death pathways can display substantial flexibility and plasticity, and this blurs the previously clear distinctions between cell death pathways. For instance, the apoptotic caspase 8 can induce pyroptotis by cleavage of GSDMD in *Yersinia* infection [163]. Caspase 3, another apoptotic caspase, can also induce pyroptosis by cleavage of

GSDME [156]. The pyroptotic caspase-1 can initiate apoptosis in the absence of its substrate GSDMD [164]. Thus, some argue that many of different forms of programmed cell death could be considered a single coordinated system, in which the various pathways can compensate for one another as necessary (reviewed in [165]).

1.6.2 SARM1 and cell death in the nervous system

SARM1 is highly expressed in the neurons, and its role there in axon degeneration is well characterised (see Section 1.4). SARM1 has an additional role in neuronal cell death in some contexts, i.e. complete destruction of the entire cell, not only the axon. An early study by Kim *et al.* found that SARM1 associates with the mitochondria, where it recruits JNK3 [26]. Given that mitochondrial JNK3 signalling plays an important role in mediating apoptosis in neurons in the context of ischaemia [166], the group sought to investigate the effect of genetic SARM1 deletion in an *in vitro* model of oxygen and glucose deprivation. Hippocampal slices from WT mice and *Sarm1*$^{+/-}$ heterozygotes in this model exhibited massive cell death, which was substantially attenuated in hippocampal slices from *Sarm1*$^{-/-}$ mice [26]. The exact mechanism and form of cell death were unspecified, but presumed to be apoptosis due to the role of mitochondrial JNK3 in apoptosis in neurons. Similarly, in the context of Bunyavirus infection, SARM1 induces neuronal cell death which is at least partially reduced by the pan-caspase inhibitor zVAD [167]. In addition, the dying neurons were characterised by caspase-3 activity and positive terminal deoxynucleotidyl transferase dUTP nick end labelling (TUNEL) staining, both of which are characteristic of apoptotic cells [167]. Similarly, TLR7/TLR9 stimulation was shown to mediate neuronal cell in a SARM1-dependent, MyD88-independent manner [168]. These dying neurons showed significantly increased caspase-3 activity and positive TUNEL staining, and exhibited the classical apoptosis-associated nuclear condensation. Thus, in some contexts SARM1 mediates neuronal apoptosis.

This is not the universal role for SARM1 in neuronal cell death however. It has been reported that expression of the SARM1 truncation consisting only of the SAM and TIR domains could induce cell death in neurons [89]. This death could not be blocked by treatment with the pan-caspase inhibitor zVAD, by calpain inhibition, by chelation of extracellular calcium ions with ethylene glycol-bis(2-aminoethylether)-N,N,N',N'-tetraacetic acid (EGTA), or with overexpression of the anti-apoptotic protein Bcl-xL [89].

In this context SARM1 does not function upstream of the apoptotic pathway nor does it trigger pyroptosis, as caspase inhibition does not prevent cell death. Summers *et al*. showed that mitochondrial dysfunction induced by the protonophore CCCP, which depolarises the mitochondrial membrane, and rotenone, which strongly inhibits complex I of the electron transport chain, triggers a SARM1-dependent cell death pathway in neurons [62]. Remarkably, they found that this SARM1-dependent death was not sensitive to pharmacological inhibitors of critical steps of apoptosis, pyroptosis, necroptosis, ferroptosis, or parathantos [62]. Thus, this novel cell death pathway, which they dubbed SARMoptosis, is distinct from other previously characterised call death pathways, and does not share any of their key steps.

In contrast SARM1 was reported to have an anti-apoptotic role in the context of prion disease in the brain [169]. Zhu *et al.* showed that prion pathogenesis is accelerated in *Sarm1*$^{-/-}$ mice. This was associated with enhanced expression of the pro-apoptotic gene X-linked inhibitor of apoptosis (XIAP)-associated factor 1 (XAF1) in these mice, which antagonises the anti-apoptotic function of XIAP. This resulted in relief of the inhibitory IAP activity and enhanced apoptotic caspase activity [169]. The exact mechanism by which SARM1 regulated expression of *Xaf1* was not elucidated.

These studies indicate that the role of SARM1 in the central nervous system is not limited to axon degeneration, but also encompasses the regulation of multiple forms of cell death.

1.6.3 SARM1 and cell death in the eye

Retinal ganglion cells (RGCs) are neurons which conduct visual signals to the brain from the eyes, and RGC degeneration occurs in many retinal disease which lead to blindness, including glaucoma [170]. Excitotoxicity is induced by prolonged or excessive activation of excitatory amino acid receptors, and can induce RGC death accompanied by axon degeneration [171]. It has been reported that excitotoxicity upregulates the expression of SARM1 in the retina [172]. A study by Massoll *et al.* demonstrated that silencing of SARM1 in the eye by intravitreal injection of *Sarm1* siRNA was protective in a kainic acid model of excitotoxicity-induced RGC damage [172]. Compared to controls, *Sarm1* siRNA treated eyes showed attenuated kainic acid-induced RGC death and reduced axon fragmentation [172]. It was later discovered that, while excitotoxicity in neurons induces

apoptosis in the soma, excitotoxicity-mediated axon degeneration proceeds by a necroptotic mechanism and is blocked by inhibitors of necroptosis [173]. In an established neuroinflammatory model of glaucoma induced by intravitreal tumor necrosis factor (TNF) injection, WT mice exhibit substantial early axon degeneration, followed by later significant RGC loss, both of which are abrogated in *Sarm1*$^{-/-}$ mice [174]. The authors demonstrated that TNF-injection induced a noncanonical axonal necroptotic signalling mechanism in the RGC axons; rather than directly triggering degeneration, MLKL induced the loss of NMNAT2 [174] specifically in the axons and not soma, and thus activated SARM1 NADase activity and subsequent axon degeneration as described in Section 1.4. In fact, forced dimerization of MLKL was sufficient to induce axon degeneration of neurons *in vitro* [174]. Based on the temporal pattern of axon degeneration followed by RGC cell death, the authors suggests that RGC cell death may be downstream of axon degeneration [174]. Thus, SARM1 NADase activity mediates pathological axonal degeneration which results in cell death in RGCs, and may be an attractive target in retinal degenerative diseases which lead to blindness.

It has recently been reported that SARM1 is also expressed in photoreceptor cells in the neural retina [175]. Ozaki *et al.* found that overexpression of a truncation of SARM1 lacking the autoinhibitory N-terminus drives photoreceptor cell death [175]. The authors observed substantial NAD^+ depletion in the photoreceptor layer of retinal explants treated with CCCP, which was rescued by SARM1 deletion. SARM1 ablation could also promote survival of photoreceptor cells in a rhodopsin knockout mouse model of photoreceptor degeneration, and the visual function of these surviving cells was preserved [175]. Thus targeting SARM1 NADase activity may therefore be a useful therapeutic strategy for patients with photoreceptor dystrophies.

SARM1 has also recently been implicated as driver of photoreceptor cell death in Leber congenital amaurosis type 9 (LCA9), a childhood onset retinal degenerative disease caused by mutations in NMNAT1 [176, 177]. NMNAT1 deletion in mouse causes a similar phenotype to LCA9, and conditional knockout of NMNAT1 in the photoreceptor cells is necessary and sufficient for retinal degeneration [178]. Mechanistically, loss of NMNAT1 resulted in increased NMN levels within photoreceptors, which activated the NADase activity of SARM1. SARM1 ablation could block NMNAT1-deficiency induced

photoreceptor cell death and prevent loss of visual function [178]. This study reinforces that SARM1 is a potential therapeutic candidate in retinopathies.

Thus in addition to mediating axonal degradation in the specialised neurons of the eye, SARM1 plays a crucial role in regulating in the death of these cells. SARM1 therefore presents a potential therapeutic target in retinal degenerative disease which lead to blindness.

1.6.4 SARM1 and cell death in periphery

In addition to the CNS and the eye, SARM1 has a role in regulation of programmed cell death in the periphery, specifically in determining cell fate following inflammasome activation. GSDMD was initially proposed to be necessary and sufficient for pyroptotic lysis and concomitant release of IL-1β and IL-18 [179, 180]. These functional outcomes of inflammasome activation were considered to be coupled. However, there have been many studies published reporting IL-1β release from living cells following inflammasome activation [181-183]. Furthermore, NLRP3 activation with so-called hyperactivating ligands such as peptidoglycan (PGN), can induce GSDMD-dependent IL-1β release in macrophages without inducing pyroptotic death [184].

Until recently, the mechanisms defining cell fate following inflammasome activation in macrophages remained elusive. Our group showed for the first time that following inflammasome activation in murine macrophages, SARM1 is the key regulator of cell fate [25]. Macrophages from *Sarm1*$^{-/-}$ mice showed decreased pyroptotic lysis but increased IL-1β release in response to conventional NLRP3 inflammasome activators, a similar phenotype to WT macrophages stimulated with hyperactivating ligands. SARM1 was shown to play a dual role in conventional inflammasome outcomes; an inhibitory role in restraining the NLRP3 inflammasome through direct interaction, and positive role in mitochondrial events [25]. This is summarised in Figure 1.7. Following inflammasome activation with LPS and nigericin SARM1 was found to cluster at the mitochondria and induce depolarisation. This was followed by cell lysis, measured by the released of lactate dehydrogenase (LDH) from the cell. In SARM1-deficient macrophages, NLRP3 inflammasome activation did not result in loss of mitochondrial membrane potential and LDH release was abrogated [25]. However, despite reduced pyroptotic lysis, SARM1-

knockout macrophages showed enhanced secretion of IL-1β [25]. This adds to the body of literature reporting that pyroptotic lysis and IL-1β can be uncoupled. Indeed neutrophils, which lack SARM1 expression, exhibit sustained IL-1β secretion in response to conventional inflammasome activation without concomitant pyroptotic lysis [185]. Compulsory induction of mitochondrial depolarisation in neutrophils could significantly induce pyroptosis. Interestingly transfection of neutrophils with SARM1 resulted in a significant increase in inflammasome-induced mitochondrial depolarisation [185]. It is possible therefore that the absence of SARM1 expression in neutrophils is related to the uncoupling of inflammasome-induced IL-1β secretion and pyroptotic lysis in these cells.

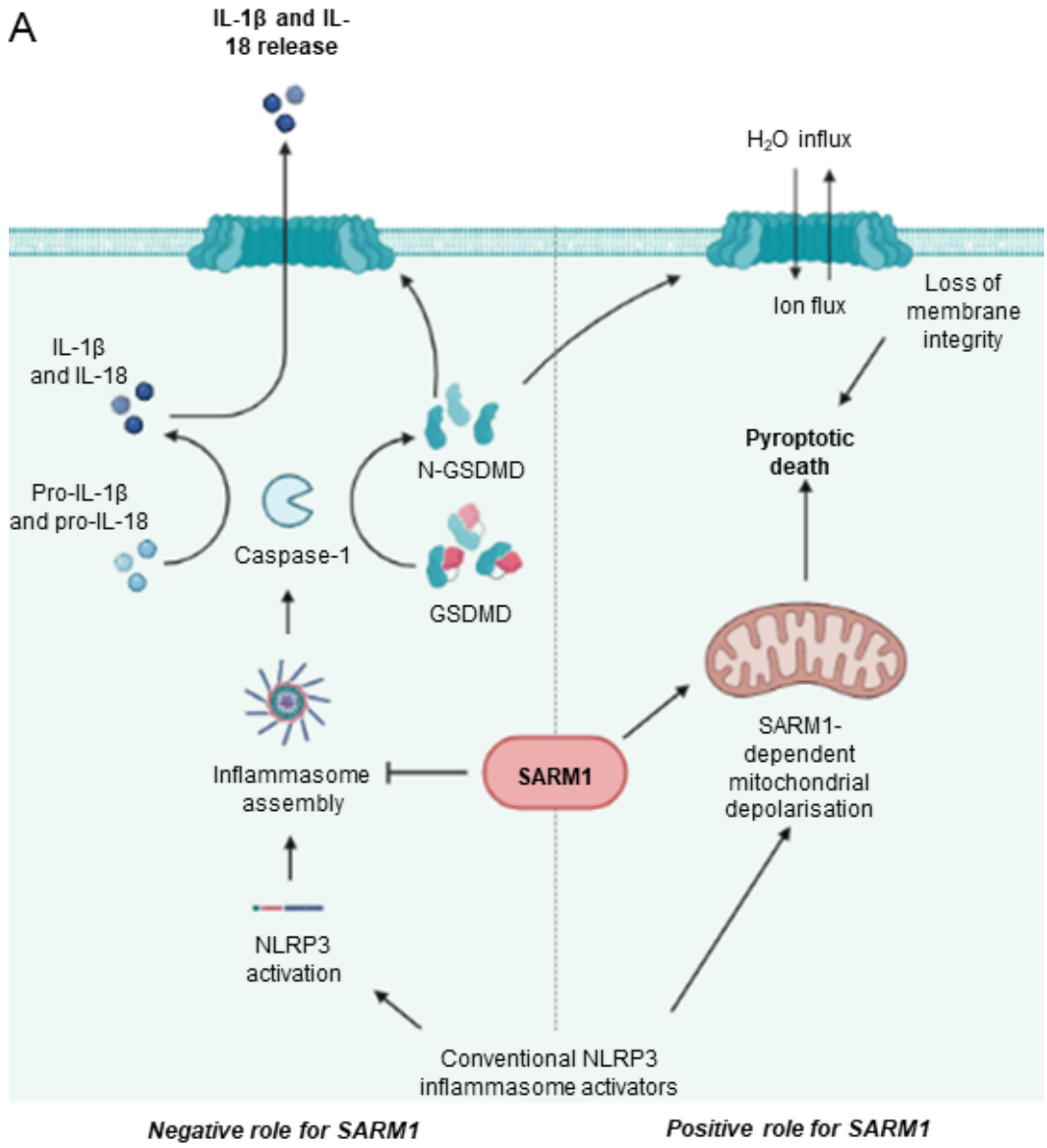

Figure 1.7 SARM1 regulates cell fate following inflammasome activation

(A) SARM1 physically interacts with NLRP3, restraining assembly of the NLRP3 inflammasome, and thereby attenuates IL-1β production and secretion. SARM1 also has a positive regulatory role in promoting pyroptotic cell death by mediating mitochondrial depolarisation. (B) Immune cells with lower SARM1 expression exhibit substantial IL-1 secretion without concomitant cell death. Cells which express more SARM1 exhibit pyroptotic cell death without substantial IL-1β release. Adapted from Carty *et al.*, 2019 [25].

SARM1 also has a crucial role in mediating apoptotic death of CD8 T cells to restore immune homeostasis following acute-phase infection [35]. Panneerselvam *et al*. reported that mitochondria-localised SARM1 perturbs mitochondrial integrity and causes generation of reactive oxygen species to induce apoptosis [35]. This was also associated with suppressed expression of the anti-apoptotic Bcl-xL and reduced phosphorylation of the pro-survival factor extracellular signal-regulated kinase (ERK). Knockdown of SARM1 could prevent CD8 T cell death in response to activation or neglect [35]. Thus, SARM1 has a physiologically beneficial role in this context, as failure to restore immune homeostasis following infection can lead to autoimmunity and lymphoproliferative diseases [186].

SARM1's pro-apoptotic function is also physiologically relevant in the context of active infection in macrophages. Upon recognition of PAMPs, a macrophage can propagate an immune response by secretion of cytokines or may undergo apoptosis. It has been reported that sensitive to apoptosis gene (SAG) governs macrophage survival in this context by modulating SARM1 levels [187]. Early in infection, SAG expression was observed to be upregulated in macrophages where it mediated the ubiquitination of SARM1, thus targeting it for proteasomal degradation [187]. This corresponded with minimal macrophage apoptosis in early infection. In later stages of infection, SAG expression dropped and SARM1 expression increased, and this was associated with induction of apoptosis in macrophages [187]. This SAG-dependent ubiquitin-proteasome system (SAG-UPS) is exploited to prevent apoptosis and promote tumorigenesis in early hepatocellular carcinoma [188]. SAG-mediated ubiquitination results in SARM1 and an additional pro-apoptotic protein, Noxa being targeted for degradation, and thus provides a survival advantage to the hepatocellular carcinoma cells [188]. The authors speculate that the SAG-UPS mediated degradation of SARM1 and Noxa could therefore be a potential therapeutic target. Thus SARM1 expression must be tightly controlled to ensure appropriate apoptosis during an immune response or homeostasis, and pathological dysregulation of its expression can result in cancer.

Further mechanistic insight into SARM1 regulation of non-neuronal apoptosis was gained by identification of a number of apoptosis-related binding partners. SARM1 is reported to interact with the mitochondrial NOD receptor NLRX1 [28], which has a role in promotion or inhibition of apoptosis in a stimulus dependent manner [189-191]. Killackey *et al.* demonstrated that SARM1 was required downstream of NLRX1 for induction of apoptosis

in murine fibroblasts cells [28]. In addition, the pro-apoptotic functions of SARM1 were reported to be subject to dual opposing regulatory effects by the two isoforms of ubiquitously expressed transcription (UXT), UXT V1 and UXT V2 [192]. SARM1 physically interacts with both isoforms of UXT. Co-expression of UXT V1 with SARM1 resulted in a reduction of caspase-8 activity, whereas UXT V2 caused enhanced caspase-8 activity, loss of mitochondrial membrane potential, and subsequent apoptosis when co-expressed with SARM1 [192].

An anti-apoptotic role for SARM1 has also been reported, wherein GFP-tagged SARM1 was observed to localise to the nucleus in response to apoptotic signalling, where it stabilised lamins and prevented DNA fragmentation from occurring [193]. However, this remains the sole study reporting nuclear localisation of SARM1; most studies report that SARM1 is localised to the mitochondria and cytosol. This may indicate that the GFP tag or overexpression of SARM1 impacted its localisation and activity. Thus, most studies agree that SARM1 is a pro-apoptotic factor whose expression and activity is strictly controlled to regulate cell death.

Overall, the role for SARM1 in cell death and degeneration is most intensively explored in the nervous system, where SARM1 is most highly expressed. However, the numerous studies defining a regulatory role for SARM1 in cell death in the periphery indicate that SARM1 expression and function are not limited to the central nervous system.

1.7 Aims

Mammalian SARM1 has numerous reported roles both within and outside of the nervous system. In the nervous system SARM1 is the central executioner of axon degeneration in a variety of contexts. As such, the ability to inhibit SARM1 would be of therapeutic benefit in pathological axodegenerative conditions, and the ability to locally augment SARM1 activity could be valuable in neurolysis for pain relief.

SARM1 also mediates multiple forms of cell death. The pro-apoptotic activity of SARM1 is regulated by direct binding with NLRX1 at the mitochondria [28], and is modulated by direct binding with UXT1 and UXT2 [192]. However, an anti-apoptotic role was also described for SARM1, which involved its translocation to the nuclear compartment to stabilise lamins [193]. SARM1 is also reported to inhibit pyroptosis through interaction with NLRP3 [25], and in neuronal cell death, SARM1 was reported to interact with JNK3 and recruit it to the mitochondria [26].

Additionally, mammalian SARM1 has a number of immune roles. Human SARM1 has a reported role in antagonising TLR signalling in immune cells by direct interaction with TRIF [36]. TLR antagonism has only been reported for murine SARM1 in the context of *B. pseudomallei* infection [194], and not with stimulation with TLR ligands in isolation [34]. However murine SARM1 exhibits TLR-independent regulation of specific chemokine gene induction in macrophages, which will be discussed in depth in Section 3.1.

This raises several questions. Given that structure of SARM1 is highly conserved between human and mouse, what underlies the disparate roles in TLR signalling and induction of immune genes between these species? While roles for SARM1 have been reported in immune cells, many of these studies rely on overexpression of SARM1, and a number of reports describe difficulty in detecting endogenous SARM1 expression in these cells. Could SARM1 expression and function actually be exclusively limited to neurons? Further, is it plausible that SARM1 is localised to the cytosol, the mitochondria, and the nucleus and has unrelated roles in each compartment? In addition, it is now accepted that SARM1 exists as an octamer even when inactive, with the TIR domains shielded from interacting with each other by associated with the ARM domains. Would this be amenable to the direct binding that SARM1 has reportedly exhibited with a range of proteins? Critically, would targeting

SARM1 activity therapeutically to modulate axon degeneration disrupt the other functions of SARM1?

This thesis aims to contribute to our understanding of SARM1 expression and function, and thereby begin to answer some of these questions. Specifically, it will examine the role ascribed to SARM1 in transcriptional regulation of *Ccl5* in murine macrophages. To do so, RNA sequencing was employed to identify any similarly regulated genes which may exist, and to shed light on the mechanism through which SARM1 regulates gene induction. Localisation of overexpressed epitope-tagged SARM1 was assessed to determine if SARM1 enters the nucleus to induce *Ccl5* transcription upon TLR stimulation. Importantly, several novel mice were generated using CRISPR/Cas9 genome editing, providing better models in which to assess the expression of endogenous epitope-tagged SARM1, and to examine the effects of *Sarm1* deletion and the loss of SARM1 NADase activity. Crucially, this thesis identifies issues with the widely used *Sarm1*$^{-/-}$ mouse model which warrant a critical re-evaluation of many of the phenotypes once ascribed to murine SARM1.

Chapter 2 Materials and Methods

2.1 Materials

2.1.1 Mouse lines

Table 2.1 Mouse lines

Mouse line	Background	Source
WT (as control for *Sarm1*$^{-/-}$)	C57BL/6J	Bred by TBSI animal facility
Sarm1$^{-/-}$ (*Sarm1*^{tm1Aidi})	C57BL/6J, <1% 129 (unspecified strain)	Generated by the Ding lab [26] JAX stock #018069
Sarm1$^{em1.1Tftc}$ *Sarm1*$^{em1.2Tftc}$ *Sarm1*$^{em1.3Tftc}$ Littermate WT	C57BL/6J	Commissioned by our lab, generated by TBSI transgenics facility [195] Heterozygous breeding pairs generated WT and knockout littermates
Sarm1^{Flag} Littermate WT	C57BL/6J	Commissioned by our lab, generated by TBSI transgenics facility [195] Heterozygous breeding pairs generated WT and epitope-tagged SARM1 littermates
Sarm1^{E682A} Littermate WT	C57BL/6J	Commissioned by our lab, generated by TBSI transgenics facility Heterozygous breeding pairs generated WT and NADase-inactive SARM1 littermates

2.1.2 Cells, cell culture reagents, and stimuli

Table 2.2 Cells

Cell Type	Genotypes	Description	Culture Medium
pBMDM	B6 congenic *Sarm1*$^{-/-}$ WT C57BL/6 *Sarm1*$^{em1.1Tftc}$ *Sarm1*$^{em1.2Tftc}$ *Sarm1*$^{em1.3Tftc}$ *Sarm1*^{Flag} *Sarm1*^{E682A}	Primary murine macrophages derived from bone marrow	• DMEM plus GlutaMax • 10% (v/v) FCS • Pen/strep [50 μg/mL] • 20% (v/v) L929 supernatant
iBMDM	WT C57BL/6 B6 congenic *Sarm1*$^{-/-}$	Immortalised BMDMs gifted by Professor K. Fitzgerald, University of Massachusetts Medical School, USA	• DMEM plus GlutaMax • 10% (v/v) FCS • Pen/strep [50 μg/mL]
iBMDM	B6 congenic *Sarm1*$^{-/-}$ stably expressing S724 or EV	Immortalised *Sarm1*$^{-/-}$ expressing Flag-tagged SARM1 (S724) and empty vector (EV) controls. Generation described in [25]	• DMEM plus GlutaMax • 10% (v/v) FCS • Pen/strep [50 μg/mL] • Puromycin [5 μg/mL]
iBMDM	*Sarm1*$^{em1.2Tftc}$ *Sarm1*$^{em1.3Tftc}$ *Sarm1*^{Flag} WT C57BL/6J	Immortalised BMDMs I generated in the course of this study	• DMEM plus GlutaMax • 10% (v/v) FCS • Pen/strep [50 μg/mL]
L929	N/A	Supernatant from these cells is used as a source of M-CSF to differentiate BMDMs	• RPMI • 10% (v/v) FCS • Pen/strep [50 μg/mL]
Cre-J2	N/A	Supernatant from these cells is used as a source of Cre-J2 retrovirus to immortalise BMDMs	• DMEM plus GlutaMax • 10% (v/v) FCS • Pen/strep [50 μg/mL]

Table 2.3 Cell culture reagents

Cell culture reagent	Manufacturer	Identifier
Dulbecco's modified eagle medium (DMEM) plus GlutaMAX™	Gibco	61965059
RPMI-1640 medium plus GlutaMAX	Gibco	61870044
Fetal calf serum (FCS)	Gibco	10500-064
Neurobasal™-A medium	Gibco	10888022
B-27™ supplement	Gibco	17504044
GlutaMAX supplement	Gibco	35050061
Penicillin/Streptomycin (pen/strep)	Sigma-Aldrich	P4333-100ML
Trypsin/EDTA solution (10X)	Sigma-Aldrich	T4174-100ml
Dulbecco's phosphate buffered saline (PBS)	Sigma-Aldrich	D8537-500ML
Dimethyl sulfoxide (DMSO)	Sigma-Aldrich	D8418-250ML
Gentamycin	Sigma Aldrich	G1397-100ml
Puromycin dihydrochloride	Sigma-Aldrich	P8833-100MG
Cytosine β-D-arabinofuranoside	Sigma-Aldrich	C1768-100MG
Poly-D-Lysine	Sigma-Aldrich	P4707-50ML
Trypan blue	Fisher Scientific	10593524
HyClone cell culture grade water (endotoxin free)	Fisher Scientific	10011342
Red Blood Cell Lysis Solution (10X)	Miltenyi Biotec	130-094-183

Adherent cells were cultured in vented, cell culture treated flasks (T25, T75, or T175 depending on the cell number) from Corning or in cell culture treated deep base 15 cm culture dishes from Greiner as indicated. Sterile cell scrapers were from Fisher Scientific.

Table 2.4 Stimuli

Stimulus	Description	Source	Identifier
LPS	Lipopolysaccharide from *E. coli*, serotype EH100(Ra)	Enzo	ALX-581-010
CL075	Thiazoloquinoline compound	InvivoGen	tlrl-c75-5
MPLA	Monophosphoryl lipid A	InvivoGen	tlrl-mpls
Vincristine sulfate	Chemotherapeutic agent which induces axon degeneration	Sigma Aldrich	V8879-1MG
Klebsiella pneumoniae	Hypervirulent strain CIP52.145	Gifted by Professor Jose Bengoechea, Queen's University Belfast	CIP52.145

2.1.3 Antibodies

Table 2.5 Antibodies

Antibody (anti-)	Raised in	Source	Identifier
β-actin	Mouse	Sigma-Aldrich	A5316
Flag	Mouse	Sigma-Aldrich	F1804
Vinculin	Rabbit	Cell Signaling Technology	4650
SARM1	Chicken	Established in our laboratory, described in [195]	N/A
H3	Mouse	Upstate	05-499
GAPDH	Rabbit	Cell Signaling Technology	2118
Mouse IRDye 680LT secondary antibody	Goat	LI-COR	926-68070
Rabbit IRDye 800CW secondary antibody	Goat	LI-COR	926-32211

2.1.4 Primers

Table 2.6 Quantitative real-time PCR primers

Target	Sequence (5'---3') Forward	Sequence (5'---3') Reverse
Acap1	GGC ATT GTC AGA TCC AAA TC	CAT CAG CCA TGG TAG GAA G
Atp5k	CAT CGG CAT GGC ATA CG	GCT GTC ATC TTG AGC TTC C
Ccl5	CTC ACC ATA TGG CTC GGA CA	ACA AAC ACG ACT GCA AGA TTG G
Ccl6	CTT TAT CCT TGT GGC TGT CC	TGA ATT ATT GGA GGG TTA TAG CG
Ccl9	TAA CTC ACG GAT TCA GTG TTC	CCA ATC TTT CAA TGC ATC TCT G
Ifnb	ATG GTG GTC CGA GCA GAG AT	CCA CCA CTC ATT CTG AGG CA
Il1b	GTG AAA TGC CAC CTT TTG ACA GTG ATG AG	CTG CTG CGA GAT TTG AAG CTG GAT G
Il6	AAG AGT TGT GCA ATG GCA ATT CTG	ATA GGC AAA TTT CCT GAT TAT ATC CAG T
Il10	AGG CGC TGT CAT CGA TTT CTC	GAC ACC TTG GTC TTG GAG CTT AT
Ifit1	CTG AGA TGT CAC TTC ACA TGG AA	GTG CAT CCC CAA TGG GTT CT
Isg15	CTA GAG CCT GCA GCA ATG	CAC CAA TCT TCT GGG CAA TC
Ndufb3	TGT CGT AAG AAA CTA GAG GAA AC	CAT GTC CAT GTC CAG CAG
Plscr3	CTG TGT CTG TCT AGC TGT TC	CCA CCG GCT CTG GAT AC
Rpl38	GGA GAT CAA GGA CTT TCT GC	GTG ATA ACC AGG GTG TAA AGG
Rps29	AGC TCT ACT GGA GTC ACC	TTC AGC CCG TAT TTG CG
Sarm1	GCT CAG TGC ATA GGA GCA TTC	AGT AAG AAA CCA GGC GTT TCA G
Tfrc	CTC GCT TAT ATT GGG CAG AC	CTC ACG AGG AGT GTA TGT ATT C
Tnf	TCC CCA AAG GGA TGA GAA GTT	GTT TGC TAC GAC GTG GGC TAC
Uqcrh	GTG TCT GAT GGA GTG AGT TC	CCT GAT TCC CAG TGA CAA G
β-actin	TCC AGC CTT CCT TCT TGG GT	GCA CTG TGT TGG CAT AGA GGT

Table 2.7 Genotyping primers

Mouse	Sequence (5'---3') Forward	Sequence (5'---3') Reverse
Sarm1$^{em1.1Tftc}$ *Sarm1*$^{em1.2Tftc}$ *Sarm1*$^{em1.3Tftc}$	CAT GGT CCT GAC GCT GCT C	CGC CTT GCA CCT CAG TGC
Sarm1^{Flag}	GTA CCA GGA GGC CAC CAT CGA G	CTC ATC TAA CCT GTG CCT GGC ATC
Sarm1^{E682A}	CTC ATC TAA CCT GTG CCT GGC ATC	CTC ATC TAA CCT GTG CCT GGC ATC

2.1.5 Buffers

Table 2.8 Buffers

Buffer	Composition
10x PBS	1.45 M NaCl 227 mM Na_2HPO_4 39 mM NaH_2PO_4
3x Western blot sample buffer	187.5 mM Tris pH 6.8 30% (v/v) Glycerol 6% (w/v) sodium dodecylsulfate (SDS) 0.3% (w/v) Bromophenol blue Added fresh: 150 mM Dithiothreitol (DTT)
10x Western blot running buffer	250 mM Tris 1.9 M Glycine 10% (w/v) SDS
10x Western blot transfer buffer	250 mM Tris 1.9 M Glycine
Radioimmunoprecipitation assay (RIPA) buffer	50 mM Tris-HCl, pH 8 150 mM NaCl 1% (v/v) TRITON X-100 0.1% (w/v) SDS 0.5% (w/v) Sodium deoxycholate

	5 mM EDTA
IP lysis buffer	50 mM Tris-HCl, pH 7.4 150 mM NaCl 1 mM EDTA 1% (v/v) TRITON X-100 Protease inhibitors added fresh
Cell fractionation cytoplasmic buffer	10 mM Tris/HCl, pH 7.4 10 mM NaCl 3 mM $MgCl_2$ 10 mM EDTA 1% (v/v) TRITON X-100 Protease inhibitors added fresh
Cell fractionation nuclear buffer	30 mM HEPES, pH 7.9 36% (v/v) Glycerol 600 mM NaCl 2 mM $MgCl_2$ 30 mM EDTA
50 x Tris-Acetate-EDTA (TAE) buffer	1 M Glacial acetic acid 2 M Tris 50 mM EDTA
Tissue lysis buffer	50 mM Tris-HCl, pH8.0 150 mM NaCl 1 % (v/v) TRITON-X 100 5 mM EDTA
6x DNA loading buffer	0.25% (w/v) Bromophenol blue 0.25% (w/v) Xylene cyanol ff 30% (v/v) Glycerol
10x TBS	200 mM Tris 1.5 M NaCl Adjust pH to pH 7.6

2.1.6 Method-specific materials

Table 2.9 Method-specific materials

ELISA materials	**Manufacturer**	**Identifier**
Murine CCL5(RANTES) DuoSet ELISA kit	R&D systems	DY-478
Murine TNF DuoSet ELISA kit	R&D systems	DY-410
Murine IL-6 DuoSet ELISA kit	R&D systems	DY-406
TMB Substrate Reagent Set	BD Biosciences	555214
Bovine serum albumin (BSA)	Sigma-Aldrich	A8022-500G
Genotyping PCR materials	**Manufacturer**	**Identifier**
5x Green GoTaq Flexi Buffer	Promega	M891A
25 mM $MgCl_2$	Promega	A351B
GoTaq G2 Hot Start Polymerase	Promega	M740A
dATP, dCTP, dGTP, dTTP, each [100 mM]	Brennan & Co	N0446S
Ultrapure DNase/RNase-free water	BioSciences Ltd	10977035
2-Log DNA ladder (0.1 – 10 kb)	Brennan & Co	N3200L
QIAquick PCR purification kit	Qiagen	28104
SYBR Safe DNA gel stain	Invitrogen	S33102
Agarose	Sigma-Aldrich	A9539-500G
Restriction enzymes and buffers	**Manufacturer**	**Identifier**
BsaWI	New England Biolabs	R0567S
CutSmart buffer	New England Biolabs	B7204
SmoI (SmII)	ThermoFisher Scientific	ER1981
Tango buffer	ThermoFisher Scientific	BY5

RNA isolation, reverse transcription, and quantitative real-time PCR	**Manufacturer**	**Identifier**
High Pure total RNA Isolation Kit	Roche	11828665001
RNA*later*	Sigma-Aldrich	R0901
TRIzol reagent	ThermoFisher Scientific	15596018
Ultrapure DNase/RNase-free water	Invitrogen	10977035
dATP, dCTP, dGTP, dTTP, each [100 mM]	Brennan & Co	N0446S
Random Hexamer	IDT	N/A
Moloney Murine Leukemia Virus Reverse Transcriptase (M-MLV RT)	Promega	M1701
M-MLV RT 5X Buffer	Promega	M531A
RNase OUT recombinant ribonuclease inhibitor	ThermoFisher Scientific	10777019
Tungsten Carbide Beads, 3 mm	Qiagen	69997
PowerUp SYBR Green Master Mix	ThermoFisher Scientific	A25778
Bioanalyzer RNA 6000 Nano kit	Agilent	5067-1511
Immunoprecipitation (IP)	**Manufacturer**	**Identifier**
Anti-Flag M2 magnetic beads	Sigma-Aldrich	M8823
MagRack 6	Cytiva	28-9489-64
SDS-PAGE and Western blot	**Manufacturer**	**Identifier**
Bicinchoninic acid (BCA) protein assay	Pierce	23227
Protogel (30% Acrylamide (w/v), 0.8% Bisacrylamide (w/v))	National Diagnostics	NAT1260
Tetramethylethylenediamine (TEMED)	Sigma-Aldrich	T7024-50ML
PageRuler plus protein ladder, 10 to 250 kDa	ThermoFisher Scientific	26620
Amersham Protran 0.45 μm Nitrocellulose membrane	Cytiva	GE10600007

BSA	Sigma-Aldrich	A8022-500G
Skimmed milk powder (SMP)	Lab M	MC027
Software	**Source**	**Identifier**
GraphPad Prism	GraphPad Software Inc.	v9.1.2
Bioanalyzer 2100 Expert Software	Agilent	G2946CA
Image Studio Lite	LI-COR Biosciences	v4.0
QuantStudio Design and Analysis software	Thermo Fisher Scientific	v1.4.2
Integrative Genomics Viewer	Broad Institute	N/A

2.2 Methods

2.2.1 Generation of mouse lines

2.2.1.1 C57BL/6 congenic Sarm1$^{-/-}$ mouse

Sarm1$^{-/-}$ mice were generated by the Ding lab by targeted gene disruption as described in [26]. Briefly, exon 3 through 6 of the *Sarm1* locus was disrupted by replacement with a neomycin-resistance replacement cassette in embryonic stem cells derived from an unspecified 129/SvJ mouse, known as the donor. These cells were implanted to a C57BL/6 blastocyst, the recipient, and following germline transmission and at least 15 generations of backcrossing, a SARM1-deficient mouse on the C57BL/6 background was achieved (Figure 2.1).

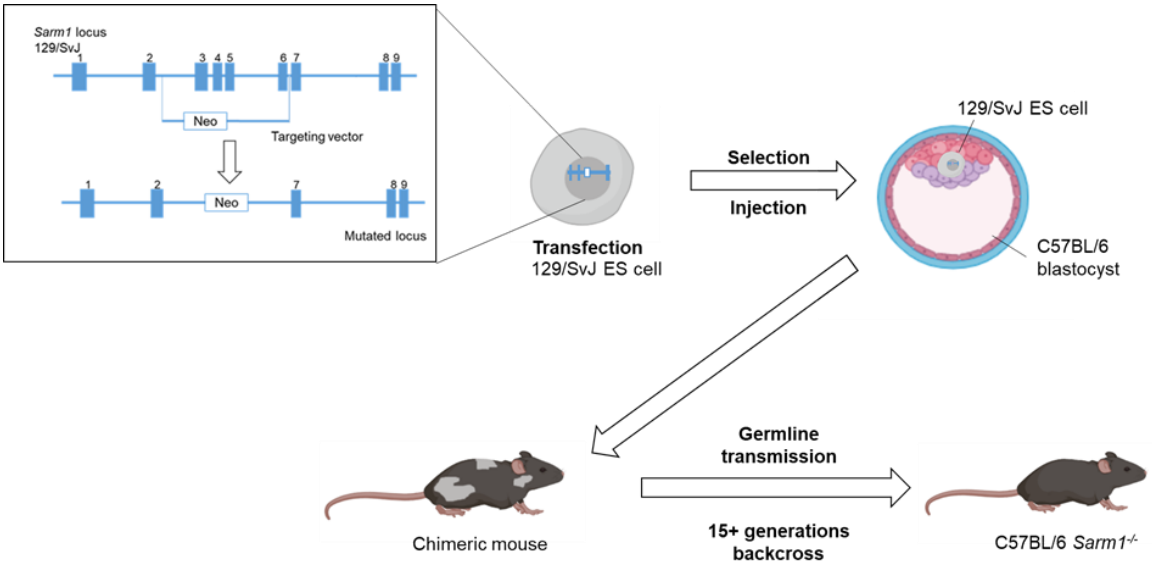

Figure 2.1 Generation of C57BL/6 congenic *Sarm1*$^{-/-}$ mouse by targeted gene disruption

Generated by the Ding lab [26]. Exon 3 through 6 of the *Sarm1* locus were replaced by a neomycin resistance cassette in embryonic stem cells from an unspecified 129/SvJ mouse. Cells which were successfully targeted were selected and injected into a C57BL/6 blastocyst, which was implanted into a pseudopregnant female mouse. The resulting offspring were chimeric. Following germline transmission and over 15 subsequent generations of backcrossing to C57BL/6 mice, the congenic *Sarm1*$^{-/-}$ mouse was almost entirely on the C57BL/6 background.

2.2.1.2 Sarm1$^{em1.1Tftc}$, Sarm1$^{em1.2Tftc}$, and Sarm1$^{em1.3Tftc}$ mice

Mice were generated by Dr Claire Fergus and Dr Vincent Kelly in the Trinity Biomedical Sciences Institute (TBSI) transgenics facility for the Bowie lab, and their generation is described in [195]. In brief, pre-assembled Cas9 ribonucleoparticles were microinjected into C57BL/6 zygotes. Exon 1 of the *Sarm1* locus was targeted 96 nucleotides downstream of the ATG start codon, using a guide RNA (gRNA) targeted against the sequence GCCACCACTCCGATCCGGTCCGG. The recovered offspring were screened by PCR and characterised by Sanger sequencing (MWG eurofins). Three knockout mutants were selected, carrying a 2 bp (*Sarm1$^{em1.1Tftc}$*), 34 bp (*Sarm1$^{em1.2Tftc}$*) and 5 bp (*Sarm1$^{em1.3Tftc}$*) deletion. The disrupted sequences in exon 1 of the *Sarm1* locus in these mice is shown in Figure 2.2.

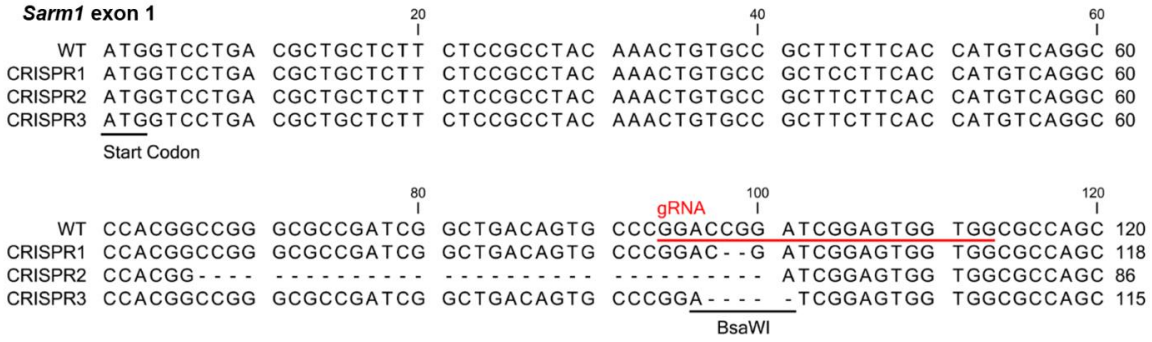

Figure 2.2 Multiple sequence alignment showing disrupted *Sarm1* locus in CRISPR/Cas9 SARM1 knockout mouse lines

The start codon is indicated by a black bar, the guide sequence is denoted by a red bar, and the BsaWI recognition site is indicated. Figure is from [195].

2.2.1.3 Sarm1$^{em2(FLAG\text{-}Strep)Tftc}$ (Sarm1^{Flag}) mouse

The mouse in which SARM1 is epitope tagged was generated by Dr Claire Fergus and Dr Vincent Kelly in the TBSI transgenics facility for the Bowie lab, and its generation is fully described in [195]. CRISPR/Cas9 was used to tag SARM1 in a C57BL/6 mouse by insertion of a C-terminal triple Flag, double Streptag II sequence in the *Sarm1* gene. The gRNA recognition sequence in exon 9 of *Sarm1*, CACAGTAGGGCACGGGAACTGG, was targeted and a repair construct introduced to remove the stop codon and introduce the Flag and Streptag II sequences. This targeting strategy is shown in Figure 2.3.

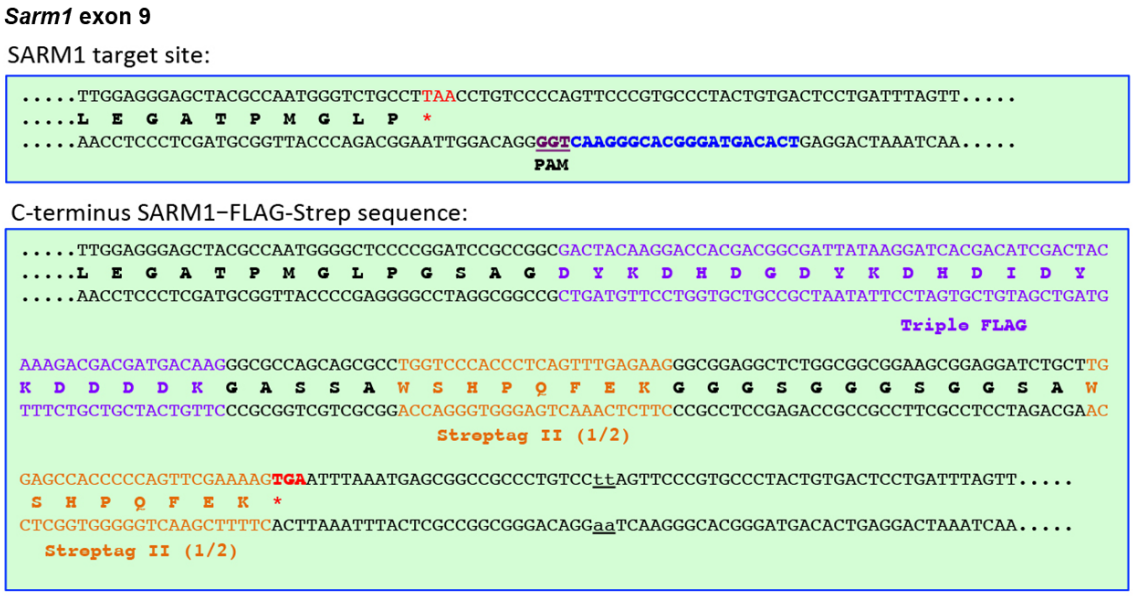

Figure 2.3 CRISPR/Cas9 targeting strategy used to generate a mouse in which SARM1 is epitope-tagged

The gRNA target sequence is shown in blue adjacent to a protospacer adjacent motif (PAM) sequence in exon 9 of the *Sarm1* locus. Upon Cas9 cutting at this site, a repair construct was used to remove the stop codon, shown in red, and introduce the triple Flag and Streptag II tags, shown in purple and orange respectively. Figure generated by Dr Claire Fergus.

2.2.1.4 Sarm1^{em1_E682A_Tftc} (Sarm1^{E682A}) mouse

Mice were generated by Dr Claire Fergus and Dr Vincent Kelly in the TBSI transgenics facility for the Bowie lab. The gRNA targeting sequence, TTAAAGCAGTCACAATCTCCTGG, was designed to target the first codon, for glutamic acid, in exon 8 of *Sarm1*. A repair vector was designed to alter this codon to a codon for alanine. A number of base changes resulting in synonymous codons were introduced beside this site to inhibit re-cutting by the Cas9 and to aid in genotyping. The crRNA was assembled into a Cas9 ribonucleoparticle (RNP) and mixed with the repair vector. This was microinjected into the pronuclei of C57BL/6 zygotes. Offspring were genotyped by PCR and a mutant was identified. Figure 2.4 shows the targeting strategy.

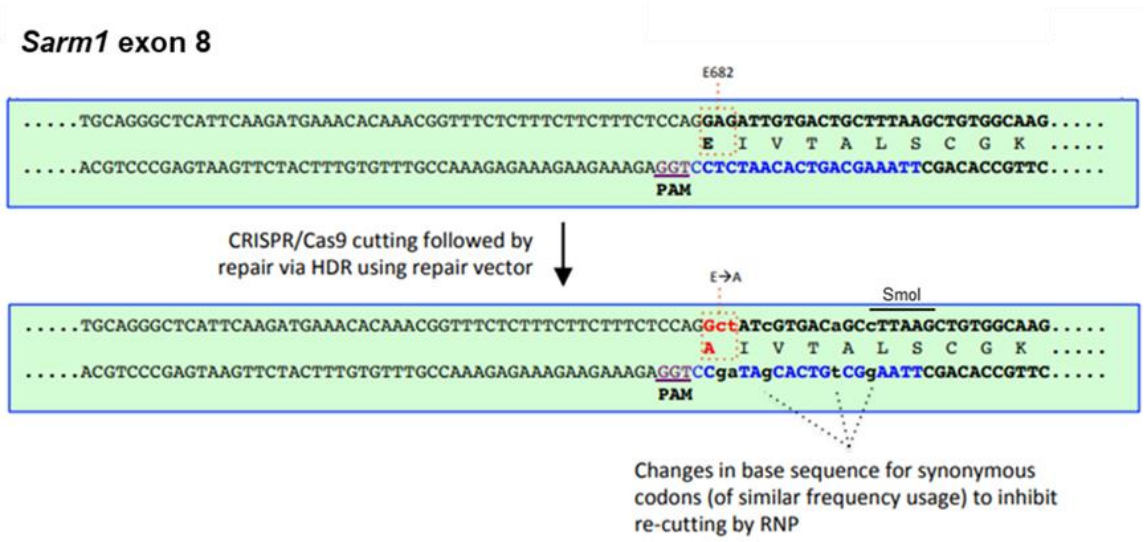

Figure 2.4 CRISPR/Cas9 targeting strategy used to generate a mouse in which SARM1 NADase activity is inactive

The gRNA target sequence is shown in blue adjacent to the PAM sequence, at the beginning of exon 8 of Sarm1 on the antisense strand. Upon Cas9 cutting at this site, the repair vector provides a template for homology directed repair. The repair vector contains base changes to modify the glutamic acid-682 residue (E682) to an alanine. It also contains the indicated base changes for synonymous codons to inhibit recutting by Cas9. Figure generated by Dr Claire Fergus.

2.2.2 Genotyping

2.2.2.1 DNA isolation from ear tissue

80 µL of 0.05 M sodium hydroxide solution was added to each ear punch sample. Samples were briefly centrifuged to ensure the tissue was submerged, and were then incubated at 95 °C on a heating block, shaking at 900 rpm for 40 minutes. 10 µL of 1 M Tris, pH 8 was added to each sample to neutralise the sodium hydroxide. The samples were vortexed for 5 minutes.

2.2.2.2 Genotyping protocol for Sarm1$^{em1.1Tftc}$, Sarm1$^{em1.2Tftc}$, and Sarm1$^{em1.3Tftc}$ mice

Heterozygous mice were bred to produce littermate WT and SARM1-knockout mice. Polymerase chain reaction (PCR) was used to amplify the WT or mutated allele. The PCR conditions are described in Table 2.10, and the programme displayed in Table 2.11 was used. The PCR product was purified and concentrated using the Qiagen QIAquick PCR purification kit. Half of the purified PCR product was digested using the restriction enzyme

BsaWI (New England Biolabs, R0567), half was left undigested. DNA was electrophoresed on a 2% (w/v) agarose TAE gel.

Table 2.10 PCR conditions for genotyping *Sarm1*$^{em1.1Tftc}$, *Sarm1*$^{em1.2Tftc}$, and *Sarm1*$^{em1.3Tftc}$ mice

GoTaq polymerase reaction	Final Volume	Final Concentration
5x Green GoTaq® buffer	12 µL	1x
25 mM $MgCl_2$	2 µL	1mM
dNTPs (2.5 mM each)	4 µL	200 µM
Forward primer (10 µM)	1.875 µL	0.5 µM
Reverse primer (10 µM)	1.875 µL	0.5 µM
GoTaq® DNA Polymerase (5u/µL)	0.5 µL	2.5 U
Template DNA	-	125 ng
PCR-grade water	to 50 µL	

Table 2.11 PCR programme for genotyping *Sarm1*$^{em1.1Tftc}$, *Sarm1*$^{em1.2Tftc}$, and *Sarm1*$^{em1.3Tftc}$ mice

Step	Temperature	Duration	Number of cycles
Initial denaturation	95 °C	2 minutes	1
Denaturation	94 °C	30 seconds	30
Annealing	61 °C	30 seconds	
Extension	72 °C	30 seconds	
Final extension	72 °C	5 minutes	1

2.2.2.3 Genotyping protocol for Sarm1^{Flag} mice

PCR was used to amplify the WT or tagged-allele. The PCR conditions are described in Table 2.12, and the programme displayed in Table 2.13 was used. The PCR product was electrophoresed on a 2% (w/v) agarose TAE gel.

Table 2.12 PCR conditions for genotyping *Sarm1^{Flag}* mice

GoTaq polymerase reaction	Final Volume	Final Concentration
5x Green GoTaq® buffer	4 µL	1 x
25 mM $MgCl_2$	0.8 µL	1 mM
dNTPs (2.5 mM each)	1.6 µL	200 µM
Forward primer (10 µM)	1 µL	0.5 µM
Reverse primer (10 µM)	1 µL	0.5 µM
GoTaq® DNA Polymerase (5u/µL)	0.2 µL	1 U
Template DNA	-	50 ng
PCR-grade water	to 20 µL	

Table 2.13 PCR programme for genotyping *Sarm1^{Flag}* mice

Step	Temperature	Duration	Number of cycles
Initial denaturation	95 °C	2 minutes	1
Denaturation	94 °C	30 seconds	30
Annealing	64 °C	30 seconds	
Extension	68 °C	30 seconds	
Final extension	72 °C	5 minutes	1

2.2.2.4 Genotyping protocol for Sarm1^{E682A} mice

Heterozygous mice were bred to produce littermate WT and knockout mice. PCR was used to amplify the WT or mutant allele. The PCR conditions are described in Table 2.14, and the programme displayed in Table 2.15 was used. The PCR product was purified and concentrated using the Qiagen QIAquick PCR purification kit. Half of the purified PCR product was digested using the restriction enzyme SmoI, and half was left undigested. The PCR product was then electrophoresed on a 2% (w/v) agarose TAE gel.

Table 2.14 PCR conditions for genotyping *Sarm1^{E682A}* mice

GoTaq polymerase reaction	Final Volume	Final Concentration
5x Green GoTaq® buffer	12 µL	1x
25 mM $MgCl_2$	2 µL	1mM
dNTPs (2.5 mM each)	4 µL	200 µM
Forward primer (10 µM)	2.5 µL	0.5 µM
Reverse primer (10 µM)	2.5 µL	0.5 µM
GoTaq® DNA Polymerase (5u/µL)	0.5 µL	2.5 U
Template DNA	-	125 ng
PCR-grade water	to 50 µL	

Table 2.15 PCR programme for genotyping *Sarm1^{E682A}* mice

Step	Temperature	Duration	Number of cycles
Initial denaturation	95 °C	2 minutes	1
Denaturation	94 °C	30 seconds	30
Annealing	57 °C	30 seconds	
Extension	72 °C	30 seconds	
Final extension	72 °C	8 minutes	1

2.2.3 Cell culture

2.2.3.1 BMDM passaging

Cells were cultured in sterile laminar flow hoods under asceptic conditions, and all materials and reagents used were sterile. Cells were cultured in a humidified incubator at 37 °C with 5% CO_2 in vented tissue culture (TC) treated flasks in the appropriate culture medium (see Table 2.2 in Section 2.1.2). Unless otherwise indicated, BMDMs were subcultured every two to three days once they reached 85% confluency. Immortalised BMDMs (iBMDMs) were scraped into their culture medium using a sterile cell scraper. They were transferred to a 50 mL conical tube and centrifuged at 180 g for 5 minutes. The supernatant was discarded, and the cell pellet resuspended in 10 mL of warm media. The appropriate volume of cell suspension was transferred to a new vented flask containing warmed culture medium in a ratio of 1:10 – 1:20. Excess iBMDMs were used for experiments. The generation and culture conditions for primary BMDMs (pBMDMs) is described later in Section 2.2.4.3. For experiments, cells were counted using the TC20 automated cell counter (Biorad). To exclude dead cells, the cell suspension was diluted 1/2 in Trypan blue solution and cells which include the dye were discounted. The appropriate volume of medium was added to reach the desired cell seeding density, which was 5 x 10^5 cells/mL unless otherwise indicated. Cells were added to the wells of the appropriate format plate, avoiding outer wells where possible to prevent evaporation loss. Plates were returned to the incubator to allow cells to adhere prior to stimulation or infection. The culture conditions for Cre-J2 cells and L929 cells are described in Section 2.2.4.1 and Section 2.2.5.1 respectively.

2.2.3.2 Culture of primary mouse neurons

Primary mouse neurons were dissected from P1 to P3 neonate brains and cultured as described by Beaudoin *et al.* in [196]. The cortex was dissected, trypsinized, and resuspended into the Neurobasal A medium containing B-27 supplement, 10 μM Cytosine β-D-arabinofuranoside, and 0.5 mM GlutaMax supplement. Cells were plated in wells coated overnight with 0.1 mg/ml Poly-D-lysine. At DIV2 (Days *in vitro*), the medium was replaced with Neurobasal A medium containing B27 and one-half of the media was replaced at DIV5. Cells were used for the assay at DIV7.

2.2.3.3 Freezing and resuscitation of cells

To freeze, cells were centrifuged and the supernatants discarded. The cell pellet was resuspended in FCS containing 10% DMSO (v/v). 1ml of cell suspension was swiftly transferred to a cryovial and placed in a Mr Frosty freezing container (Nalgene) containing isopropanol to facilitate a rate of cooling of approximately -1 °C/minute, the optimal rate for cell preservation. The container was kept in a -80 °C freezer overnight, and then cells were transferred to liquid nitrogen for long term storage. To resuscitate frozen cells, cryovials were removed from the liquid nitrogen and swiftly thawed in a 37 °C water bath until most of the cell suspension had thawed. The cell suspension was transferred directly into a 50 mL conical tube containing warmed media with the appropriate constituents (see Table 2.2), and centrifuged at 260 g for 5 minutes. The cell pellet was resuspended and then transferred to a 75 cm^2 flask and cultured as previously described.

2.2.4 Generation of pBMDMs

2.2.4.1 Generation of macrophage colony-stimulating factor (M-CSF) conditioned medium

Supernatants from L929 cells were used as a source of M-CSF for the differentiation of pBMDMs from bone marrow cells. To generate the M-CSF-conditioned medium, 2 x 10^7 L929 cells were seeded in 40 mL of complete medium (see Table 2.2) in a 175 cm^2 flask. In order to efficiently generate large volumes, 10+ flasks were seeded. The cells were cultured for 7 days without changing the medium. The L929 supernatants were transferred to 50 mL conical tubes, and centrifuged at 260 g for 10 minutes. Using a 45 μM filter, the L929 supernatants were filtered into a new 50 mL conical tube, and stored at -80 °C.

2.2.4.2 Isolation of bone marrow cells

Mice were euthanised in accordance with the institution's animal ethics guidelines. Hind legs were dissected from mice and feet were removed. The femurs and tibiae were transferred to cold medium, and moved to a laminar flow TC hood under sterile conditions. Using a sterile dissection kit the tissue surrounding the femurs and tibiae was removed, leaving the bones intact. Lint-free tissue was soaked in 70% ethanol, and used to desiccate any remaining muscle or connective tissue and to sterilise the bones. A small amount was cut off each end of the bones. The bone marrow was flushed from the bone cavity using 10 mL of medium in a syringe with a 25 G needle, until the bone appeared white. When all

bones had been flushed, the bone marrow cell suspensions were transferred to 50 mL conical tubes, and centrifuged for 5 minutes at ~500 g. The supernatant was discarded. At this point, bone marrow could be frozen for later use (see Section 2.2.3.2). Alternatively, for immediate use of cells the cell pellet was resuspended in 1 mL of red blood cell lysis buffer, and incubated at room temperature for 2 minutes. 20 mL of medium was added, and the suspension was centrifuged for 5 minutes at 500 x g. The supernatant was discarded, and the colour of the pellet inspected to ensure that all red blood cells had been lysed. If any red remained, the red blood cell lysis buffer step was repeated. As the freezing and thawing process causes red blood cell lysis, this step is not required for frozen bone marrow.

2.2.4.3 Differentiation of pBMDMs from bone marrow cells

Bone marrow cells were resuspended in cDMEM supplemented with 20% L929, then seeded in sterile vented 175 cm^2 flasks in 40 mL of cDMEM supplemented with 20% L929. Care was taken to ensure similar seeding densities between mice; generally bone marrow from a single mouse was split into 2-3 175 cm^2 flasks. The flasks were placed in the incubator. On day 3 (three days later) and again on day 5, 4 mL of warmed L929 supernatants was added per flask, and flasks were returned to the incubator. On day 7, cells were examined under the light microscope to ensure elongated morphology and complete confluency. The medium was removed and the now differentiated pBMDM were washed gently with warm PBS. Then 7 mL of warmed 1 x Trypsin solution was added, and the flasks were incubated for 3-5 minutes at 37 °C. When the cells detached, 20 mL of cDMEM was added to stop the reaction, and the cell suspension was transferred to a 50 mL conical tube. The cells were centrifuged at 260 g for 5 minutes, and seeded for experiments in the appropriate plate in complete medium (see Table 2.2).

2.2.5 Generation of iBMDMs

2.2.5.1 Production of Cre-J2 retrovirus-containing supernatant

iBMDMs were generated with J2 recombinant retrovirus carrying ν -myc and ν -raf/mil oncogenes [195, 197] with viral supernatants from Cre-J2 cells as the source. Cre-J2 cells were propagated in complete medium (see Table 2.2) in 175 cm^2 flasks in a humidified incubator at 37 °C with 5% CO_2 until the cells reached 100% confluence. The medium was removed, and the cells were washed with warm PBS, then harvested by trypsinisation as described previously in Section 2.2.4.3. The cell suspension was centrifuged, then the

supernatant was discarded, and the cells resuspended in complete medium. 75% of the cell suspension was added to a fresh 175 cm^2 flask, and the total volume was made up to 20 mL. The flasks were incubated in a humidified incubator at 37 °C with 5% CO_2 for 24 hours. The cell supernatants were then harvested into a sterile 50 mL conical tube, then filtered through a 0.45 μM filter. The viral supernatants were stored at -80 °C until use.

2.2.5.2 Immortalisation of BMDMs

Bone marrow from the tibiae and femurs from mice was flushed using a syringe, red blood cells were lysed, and the resulting cells were resuspended in cDMEM supplemented with 20% (v/v) L929 supernatant. Two T75 flasks were plated per mouse, one for immortalisation and one as a control flask. Approximately a quarter of the bone marrow from a mouse was plated per T75 flask, ensuring equal density between flasks. Remaining bone marrow was used to generate pBMDM (described in Section 2.2.4.3) to ensure normal phenotype in the cells being immortalised. Three days after plating (day 3), the media was aspirated from each flask of adherent macrophage progenitors being immortalised, and replaced with cDMEM media supplemented with 50% (v/v) Cre-J2 virus-containing supernatant and 20% (v/v) L929 conditioned media. The control flask media was aspirated and replaced with cDMEM supplemented with 20% (v/v) L929 conditioned media only, and both flasks were returned to the incubator. After 24 h, the media was aspirated from both flasks and replaced with cDMEM with 20% (v/v) L929, and flasks were returned to the incubator. On day 5, a second round of infection was performed identically to day 3. On day 6, media was aspirated, and replaced with cDMEM supplemented with 20% (v/v) L929 conditioned media. Cells were cultured in cDMEM containing 20% (v/v) L929 conditioned media, splitting gently (1/2) as necessary. 2 – 4 weeks after the second round of infection, over 50% of the flask surface area was covered by clusters of round cells. The cells were scraped with a sterile scraper, and then cultured in a fresh flask with cDMEM with 15% (v/v) L929. The concentration of L929 conditioned media in the culture media was gradually reduced over a number of weeks until BMDM could survive and proliferate as normal in the absence of L929 conditioned media (passaging 1/10 every other day), and the cells in the control flasks died. This process takes from 3-6 months. Maintenance of iBMDMs is described in Section 2.2.3.1.

2.2.6 Cell stimulation

2.2.6.1 Stimulation with TLR ligands

All TLR ligands for cell stimulation were diluted in serum-free media, then added to cells. LPS was used at 100 ng/mL, MPLA at 1 μg/mL, and CL075 at 5 μg/mL.

2.2.6.2 Infection with Klebsiella pneumoniae

BMDM were seeded in 24 well plates and allowed to adhere overnight. The following day, an hour prior to infection, the media was replaced with antibiotic-free cDMEM and cells were returned to the incubator. An hour later, cells were infected with the hypervirulent strain of *Klebsiella pneumoniae* CIP52.145 at a multiplicity of infection (MOI) of 100:1. The plates were gently shaken to spread the bacteria in the wells, and then centrifuged at 200 g for 5 minutes to synchronise the infection. After 1 hour, the plate was washed once with PBS to remove the extracellular bacteria. 500 μL of antibiotic-free cDMEM supplemented with 100 μg/mL gentamycin was added to each well to kill any remaining extracellular bacteria. After the indicated time cell supernatants were removed, centrifuged to remove debris, and analysed for cytokine secretion by ELISA as described in Section 2.2.10. Cells were washed twice with PBS, and RNA isolation was carried out as described in Section 2.2.7.2.

2.2.6.3 Axon degeneration assay

Neurons (DIV7) were treated with 1 nM vincristine sulfate salt (Sigma) or vehicle (DMSO), and then were set into Incucyte Live-Cell Analysis Systems (Sartorius). The first scan was made at 1 h after the treatment; the following scans were made every 6 h after the treatment. The neurite outgrowth was quantified using the semiautomatic tracing tool NeuronJ plugin [198] from the ImageJ package Fiji [199]. This was performed by Dr Ryoichi Sugisawa.

2.2.7 RNA isolation

2.2.7.1 RNA isolation from brainstems

Brainstems from *Sarm1*$^{em1.1/1.2/1.3Tftc}$ mice and WT littermate controls were harvested and stored in RNAlater prior to isolating RNA. RNA was isolated from brainstems using

TRIzol. Each brainstem was added to a sterile 2 mL microcentrifuge tube with 1ml TRIzol and 3 metal beads. The tissue was homogenised using the TissueLyserII from Qiagen, for 2 minutes at 20-30 Hz. The adaptor was rotated and the samples were homogenised again for 2 minutes at 20-30 Hz. Samples were centrifuged for 5 minutes at 12,000 g at 4 °C and transferred to a new sterile 2 mL tube, leaving the metal beads and any residual tissue. 200 µL of chloroform was added per sample, and they were mixed by inversion for approx. 15 seconds. The samples were then incubated at room temperature for 3 minutes, before centrifuging at 11,600 g at 4 °C for 15 minutes. The aqueous phase was carefully removed, and added to 500 µL isopropanol in a fresh 2 mL tube. RNA was precipitated by repeated pipetting, followed by incubation at room temperature for 10 minutes and then centrifugation at 11,600 g for 10 minutes. The RNA precipitate forms a translucent gel-like pellet. The supernatant was decanted, and the pellet was washed once with ice-cold 75% ethanol. The ethanol was removed and pellets allowed to air dry, before resuspension in nuclease-free water and incubation at 60 °C for 10 minutes. RNA was quantified using Nanodrop 2000, adjusted to 100 ng/µL, and stored at -80 °C until use, as RNA is highly labile.

2.2.7.2 RNA isolation from cells in culture

Total RNA was extracted using the High Pure RNA Isolation Kit. Cells were seeded at 5×10^5 cells/mL in 24-well plates, allowed to adhere overnight, and stimulated as indicated the next day. Medium was then removed from adherent cells, and 200 µL of lysis/binding buffer and 100 µL of PBS were added to each well. The plates were stored at -80 °C before further processing according to the manufacturer's instructions. In brief, the cell lysates were added to columns, and the RNA was bound to the membrane. An on-column DNase digestion was used to remove genomic DNA, followed by several washing steps. Finally the RNA was eluted using 50 µL elution buffer and stored at -80 °C until use.

2.2.8 RNA analysis by quantitative real time PCR (qRT-PCR)

2.2.8.1 Reverse transcription

Complementary DNA (cDNA) was synthesised from isolated RNA by the process of reverse transcription, catalysed by the enzyme reverse transcriptase from Moloney murine leukemia virus (M-MLV). The reaction mix, shown in Table 2.16, was prepared on ice and the RNA samples were thawed and kept on ice throughout the process. A negative control,

in which the reverse transcriptase enzyme was replaced with RNA and DNA free water, was prepared to control for residual genomic DNA amplified in the real-time PCR reaction. 5 µL RNA and 5 µL cDNA reaction mix were added to one tube of a PCR tube strip and mixed, then briefly centrifuged at 4 °C to remove air bubbles. Reaction was carried out in a thermocycler using thermal conditions in Table 2.17. cDNA was then diluted 1:2 with RNA and DNA free water, and stored at -20 °C until real-time PCR analysis.

Table 2.16 Conditions for reverse transcription

Component	Volume/reaction
Random Hexamers (1 µg/µL)	0.5 µL
5X RT buffer	2 µL
dNTPs (2.5 mM)	2 µL
RNase OUT recombinant ribonuclease inhibitor	0.25 µL
M-MLV Reverse transcriptase	0.25 µL
Total reaction volume per sample	5 µL

Table 2.17 Programme for reverse transcription

Duration	Temperature
10 minutes	20 °C
30 minutes	42 °C
3 minutes	95 °C

2.2.8.2 qRT-PCR

The resulting cDNA was analysed by qRT-PCR using the PowerUp SYBR Green Master Mix and the QuantStudio 3 Real-Time PCR system. 8 µL of PCR reaction mix containing gene-specific primer pairs (listed in Table 2.6), was added to each well of MicroAmp® Fast 96-well reaction plate, and 2 µL of cDNA sample was added. The plate was sealed

with adhesive film (Anachem), and briefly centrifuged to remove air bubbles. qRT-PCR was carried out in the QuantStudio 3 Real-Time PCR system, using the conditions in Table 2.18 and the programme shown in Table 2.19. A melting curve step (Table 2.20) was carried out following the first use of a set of primers to ensure that there is a single DNA product. Separately, each sample was analysed similarly for the housekeeping gene β-*actin*.

Table 2.18 Conditions for qRT-PCR

Component	Volume
Forward primer (5 pmol/μL)	0.5 μL
Reverse primer (5 pmol/μL)	0.5 μL
PowerUp SYBR Green Master Mix	5 μL
Molecular biology water	2 μL

Table 2.19 Programme for qRT-PCR

Temperature	Duration	Cycles
50 °C	2 minutes	1
95 °C	2 minutes	1
95 °C	1 second	40
60 °C	30 seconds	

Table 2.20 Melt-curve programme

Ramp rate	Temperature	Duration
1.6 °C/second	95 °C	15 seconds
1.6 °C/second	60 °C	1 minute
0.15 °C/second	95 °C	15 seconds

2.2.8.3 Calculation of relative quantification

Relative quantification (RQ) was calculated using the comparative C_t method, which compared the cycle numbers at which fluorescence crosses a certain threshold (C_t). To account for variation in input cDNA concentrations, each target sample was normalised to the respective *β-actin* value as in internal control using the following equation:

$$\Delta C_t = C_t\text{target} - C_t\beta\text{-}actin$$

The expression of the target gene was then determined relative to the mean of the unstimulated control sample, according to the following equation:

$$\Delta C_t\text{mean control} = (\Delta C_t\text{control 1} + \Delta C_t\text{control 2} + \Delta C_t\text{control 3})/3$$

$$\Delta\Delta C_t = \Delta C_t - \Delta C_t\text{mean control}$$

$$RQ = 2^{-\Delta\Delta Ct}$$

RQ values were calculated for each of three replicates per experimental condition. The mean RQ values were calculated and presented as fold induction relative to the WT unstimulated control, set to 1.

2.2.9 RNA sequencing

2.2.9.1 Sample preparation and sequencing

Primary BMDM were generated from femurs and tibiae of four 8-week old female WT and four *Sarm1*$^{-/-}$ mice as described in Section 2.2.4. Cells were stimulated for 3 hours with 5 μg/mL CL075, or 100 ng/mL LPS or left unstimulated. Total RNA was isolated prepared from samples as described in Section 2.2.7.2 and stored at -80°C. Bioanalysis was performed using Agilent RNA 6000 Nano Kit and Agilent 2100 bioanalyzer according to manufacturer's instructions. Only samples with a RNA integrity number (RIN) >8 and concentration greater than 20 ng/μL proceeded to the next stage. Library preparation and sequencing were performed by Macrogen Inc.. RNA libraries were prepared using TruSeq Stranded Total RNA with Ribo-zero (Illumina). Sequencing was carried out on the Illumina NovaSeq 6000 platform, in a 100 bp paired-ends read format, with a sequencing coverage of 40 million reads. Figure 2.5 summarises the process.

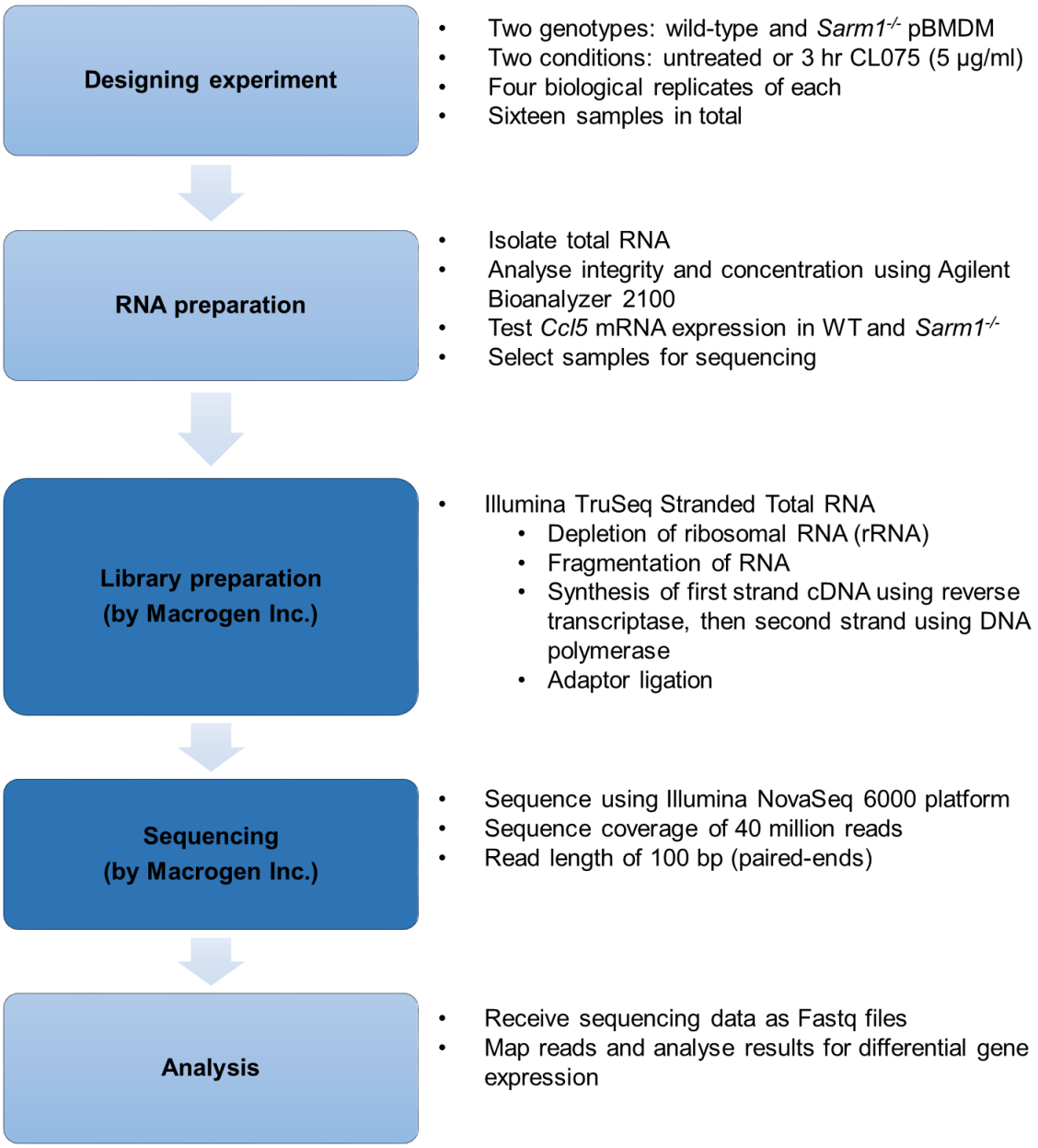

Figure 2.5 Summary of the process of sample preparation and RNA sequencing

2.2.9.2 Mapping reads

Sequencing data was received from Macrogen as Fastq files. Two different forms of alignment were carried out by Dr Karsten Hokamp from the School of Genetics and Microbiology, TCD. Hisat2 [200] was used to map reads directly to the GRCm38.p6 assembly of the C57BL/6 mouse genome, whereas kallisto [201] was used to map reads against the repeat-masked transcriptome, which were subsequently transposed onto the genome.

2.2.9.3 Differential gene expression analysis

Differential gene expression analysis was carried out by Dr Fiona Roche from the School of Genetics and Microbiology, TCD. Following mapping using kallisto, transcripts which were too short to have been captured at the library preparation step (<300bp in length) were filtered out of the analysis. Following this, transcripts which were very lowly expressed, having a transcript per million (TPM) count of less than one, were filtered out to remove background noise. DESeq2 [202] (version 1.22.2) was used for differential gene expression analysis of RNA sequencing data. As *Sarm1*$^{-/-}$ replicates exhibited a lot of variability, these samples were split into two pairs with similar expression profiles (SKO1/SKO2 and SKO3/SKO5) then compared to WT. Unstimulated *Sarm1*$^{-/-}$ and WT pBMDM were compared, and genes were deemed differentially expressed if the base mean was greater than 100 TPM, the fold change exceeded 1.6 fold, and the adjusted p-value was less than 0.05. The base mean refers to the mean of the normalised counts for a given gene across all samples (both untreated and CL075-treated BMDMs from both WT and *Sarm1*$^{-/-}$ mice). Here, setting a base mean threshold allowed us to exclude very low abundance transcripts from the analysis. Similarly, CL075-stimulated *Sarm1*$^{-/-}$ and WT pBMDM were compared, and genes were deemed differentially expressed if the base mean was greater than 100 TPM, and the fold change exceeded 1.6 fold. The p-value cut off for two replicates (SKO3 and SKO5) was relaxed to $p \leq 0.1$ to include *Ccl5*, which was the positive control. A heatmap was then generated using the ComplexHeatmap [203] package in R, showing genes which were differentially expressed either before or after stimulation in both SKO1/2 and SKO3/5 relative to WT, grouped according to chromosomal location. The expression of differentially expressed genes could then be compared in WT and *Sarm1*$^{-/-}$ BMDMs by qRT-PCR as described in Section 2.2.8.2.

2.2.9.4 Analysis of density of SNPs and indels relative to the reference genome

Analysis of density of SNPs and indels relative to the reference genome was carried out by Dr Fiona Roche from the School of Genetics and Microbiology, TCD. The samtools mpileup [204] tool was used to identify genetic variants between a representative unstimulated *Sarm1*$^{-/-}$ sample sequence (mapped using Hisat2) and the mm10 mouse reference genome. Genetic variants (both SNPs and INDELS) were filtered to only include: (1) Those with high quality score (QUAL > 100), and (2) Those with high sequencing depth (DP > 100). The mouse reference genome was divided into sliding windows of 10kb using

bedtools [205] makewindows. Genetic variants were counted within each of these windows using bedtools intersect. The count data was visualised in R with the IdeoViz package.

2.2.9.5 Visualising gene coverage, SNPs, and indels using Integrative Genomics Viewer

The integrative genomics viewer [206] (IGV) from the Broad Institute was used to visualise reads which were mapped to the genome using Hisat2. BAM files of these reads were loaded to IGV so that sequence variation from the reference sequence (denoted by a coloured bar) and gene coverage could be examined at a given locus. Figure 2.6 summarises the RNA sequencing analysis process from read alignment to validation.

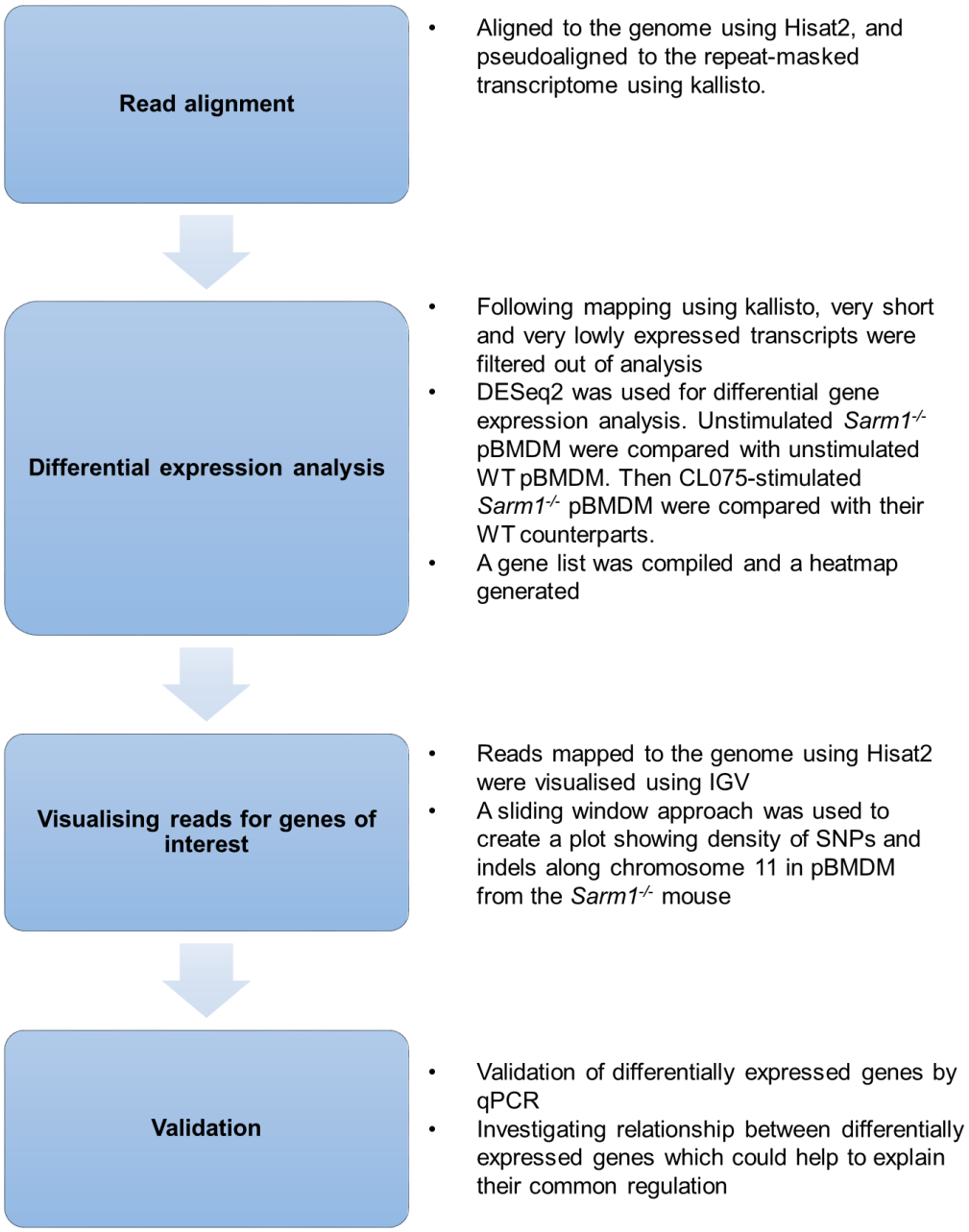

Figure 2.6 Summary of the analysis of RNA sequencing results

2.2.10 Enzyme-linked immunosorbent assay (ELISA)

After harvesting to a 96 well plate, supernatants were centrifuged at 260 g for 3 minutes to remove cellular debris, and transferred to a fresh 96 well plate. Supernatants were stored at -20 °C. Antibodies from the R&D DuoSet ELISA kits were reconstituted according to the manufacturer's instructions. The manufacturer's protocol was followed, but using half of the recommended volume of antibody for each step. Maxibinding 96 well ELISA plates (SPL Life Sciences) were coated with 50 µL of capture antibody diluted in PBS and incubated overnight at 4 °C. The following day, the plates were washed 4 times with PBS with 0.05% (v/v) Tween 20 to remove the unbound capture antibody. The plates were blocked by addition of 200 µL of 1% (w/v) BSA in PBS to each well, and incubated for 2 hours at room temperature. The blocking solution was discarded. The standards and samples were diluted appropriately in 1% (w/v) BSA in PBS, then 50 µL was added to the plate in triplicate. The plate was incubated overnight at 4 °C. The following day, the plates were washed 4 times with PBS with 0.05% (v/v) Tween 20 to remove the samples and standards. 50 µL of detection antibody diluted in 1% (w/v) BSA in PBS was added to each well. The plate was incubated for 2 hours at room temperature, then washed 4 times with PBS with 0.05% (v/v) Tween 20. 50 µL/well of diluted Streptavidin-horseradish peroxidase (HRP) solution was added to each well and the plate was incubated for 30 minutes. The plates were washed 4 more times, then 50 µL/well of 3, 3', 5, 5'-tetramethylbenzidine (TMB) substrate solution (1:1 mixture of Solution A and Solution B) was added. The reaction was stopped by addition of 25 µL 1N H_2SO_4 to each well. The optical density was assessed by measuring absorbance at 450 nm. The concentration of cytokines in the samples was interpolated from the standard curve.

2.2.11 Western blotting

2.2.11.1 Sample Preparation for Western blotting

Mice brains and brainstems were dissected and homogenized in ice-cold tissue lysis buffer supplemented with cOmplete^{TM} Mini Protease Inhibitor Cocktail (Roche) using BioMashers (Takara). Following incubation on ice for 30 minutes, samples were centrifuged for 20 minutes at 18,350 g at 4 °C. The supernatants (lysates) were transferred to a fresh tube, and were stored at -80 °C until further processing.

BMDMs were seeded at 5 x 10^5 cells/mL and allowed to adhere overnight, then stimulated as indicated. BMDMs were washed with PBS three times, then lysed with RIPA buffer supplemented with 1 mM sodium orthovanadate, 10 µL/mL aprotinin, and 1 mM phenylmethylsulfonyl fluoride (PMSF). Prior to preparing samples for Western Blot, protein concentrations were measured by BCA assay (Pierce) according to manufacturers' instructions, and adjusted as necessary.

2.2.11.2 SDS-poly acrylamide gel electrophoresis (SDS-PAGE)

A sample volume containing 30 µg of protein was mixed with 3X Western blot sample buffer and boiled at 99 °C for 5 minutes. The full sample volume was transferred to a well of an appropriate percentage SDS-polyacrylamide gel. The gel was prepared a day in advance according to Table 2.21, and stored at 4 °C in damp tissue. 3 – 5 µL of prestained protein marker was loaded so that the molecular weight of proteins of interest could be determined. Proteins were separated according to size by passing a 80 V current through the using the Mini-Protean Tetra system (Bio-Rad) and 1X running buffer, until the dye-front reached the end of the gel.

Table 2.21 SDS-polyacrylamide gel compositions

2 x SDS gels (1.5 mm)	**8% resolving gel**	**10% resolving gel**	**12% resolving gel**	**Stacking gel**
Protogel	5.3 mL	6.6 mL	8 mL	1.3 mL
Tris-HCl	5 mL (1.5 M, pH 8.8)	5 mL (1.5 M, pH 8.8)	5 mL (1.5 M, pH 8.8)	1 mL (1 M, pH 6.8)
10% SDS (w/v)	200 µL	200 µL	200 µL	80 µL
10% Ammonium persulfate (APS) (w/v)	200 µL	200 µL	200 µL	80 µL
H_2O	9.3 mL	8.2 mL	6.6 mL	5.5 mL
TEMED	12 µL	10 µL	8 µL	8 µL

2.2.11.3 Transfer

Proteins were transferred from the gel to a 0.45 µm nitrocellulose membrane (Whatman Protran) using the semi-dry transfer method. Three sheets of blotting paper were soaked in 1X transfer buffer and place on the semi-dry transfer apparatus (Biometra). The nitrocellulose membrane was then soaked in transfer buffer and placed on top of the blotting paper. The stacking gel was removed and discarded, and the resolving gel was placed face down on the membrane, then covered by three more soaked sheets of blotting paper. Air bubbles were removed by rolling a 50 mL conical tube over the transfer sandwich. A current of 75 mA per gel was applied for 90 minutes. The membrane was then washed in PBS/ Tween 0.1% (v/v).

2.2.11.4 Immunoblotting

To prevent the antibody from non-specifically binding to unoccupied sites, the nitrocellulose membrane was blocked by incubation in 5% (w/v) skimmed milk powder (SMP) in PBS/ Tween 0.1% (v/v) for 1 hour at room temperature. The membrane was then incubated overnight at 4 °C with the antibody diluted in 5% SMP in PBS/ Tween 0.1% (v/v). The following day, the membrane was washed 3 times for 5 minutes in PBS/ Tween 0.1% (v/v), then incubated for 1 hour with the fluorescent-labelled secondary antibody. The proteins were detected using the Odyssey Imaging System (LI-COR Biosciences).

2.2.12 Cell fractionation

Cells were seeded at 5 x 10^5 cells/mL in 10 cm culture dishes and allowed to adhere overnight. The next day, cells were stimulated as indicated. Following stimulation, supernatants were removed and discarded, and cells were washed twice with ice-cold phosphate buffered saline (PBS) on ice. Cells were scraped in 5 mL ice-cold PBS then pelleted by centrifugation at 1,000 g for 5 minutes at 4 °C. Cells were resuspended in 200 µL cytosolic lysis buffer supplemented with 1 mM sodium orthovanadate, 10 µL/mL aprotinin (Sigma), and 1 mM PMSF (protease inhibitors). The cell suspension was incubated for 30 minutes on ice to lyse the plasma membrane, then centrifuged for 30 minutes at 325 g at 4 °C. The supernatant, containing an impure cytoplasmic fraction, was removed and stored at -80 °C. The pellet, containing a pure nuclear fraction was washed twice with 1 mL of unsupplemented cytoplasmic lysis buffer, then resuspended in 200 µL nuclear lysis buffer supplemented with 1 mM sodium orthovanadate, 10 µL/mL aprotinin,

and 1 mM PMSF. During a 30 minute incubation on ice, samples were vigorously vortexed three times. The samples were then centrifuged at 14,220 g. Supernatants containing nuclear proteins was removed and stored at -80 °C, then were subject to SDS-PAGE as described in Section 2.2.11.

2.2.13 Immunoprecipitation

WT and *Sarm1*^{Flag} iBMDM were seeded at a density of 5 x 10^5 cells/mL in 15 cm dishes and allowed to adhere overnight. The following day, supernatants were removed and cells were washed three times with ice-cold PBS. Cells were then lysed using IP lysis buffer supplemented with 1 mM sodium orthovanadate, 10 µL/mL aprotinin, and 1 mM PMSF. Immunoprecipitation was carried out using anti-Flag M2 Magnetic Beads (Sigma, M8823) according to the manufacturer's instructions. Immunoprecipitated proteins were eluted from the beads by incubation with glycine-HCl (0.1 M, pH 3), then neutralised with 1 M Tris-HCl. IP and input lysates were subjected to SDS-PAGE as described in Section 2.2.11.

2.2.14 Griess assay

To assess nitric oxide (NO) production, cells were 5 × 10^5 cells/mL in 96-well plates, allowed to adhere overnight, and stimulated with the indicated agonist for 24 hours. Griess assay was then performed on freshly removed supernatants, to determine nitrite levels in supernatants as a surrogate measure of NO. 50 µL of sample was pipetted into a well of a flat-bottomed 96 well plate in triplicate. Sodium nitrite was used to prepare a standard curve, using a top standard of 100 µM. 50 µL of sulphanilamide (1% in 5% phosphoric acid) was pipetted into each well. This was incubated for 5 minutes at room temperature protected from light. 50 µL of N-(1-Naphthyl)ethylenediamine (0.1% in H_2O) was added to each well, followed by a further five minute incubation in the dark. A magenta colour appears immediately in the presence of nitrites. Absorbance was measured using a wavelength of 550 nm on a spectrophotometer. Concentration of nitrite in the samples was interpolated from the standard curve.

2.2.15 Statistical analysis

All data were analysed with GraphPad Prism 9. Data are presented as mean ± SEM; *p < 0.05 indicates significance compared to the respective control group. Specific statistical tests and significance levels are described in figure legends.

Chapter 3 Passenger Genes Flank the *Sarm1* Locus and Confound Interpretation of Results in *Sarm1*$^{-/-}$ Mice

3.1 Introduction

The role of SARM1 and, more specifically, of its enzymatic activity in axon degeneration is well-characterised. With the recent discovery of potent inhibitors and activators of the SARM1 NADase, the prospect of therapeutic modulation of SARM1 activity to treat axodegeneration and for relief from intractable pain is close to being realised. With this in mind, it is vital that the less well-explored functions of SARM1 are investigated, and that the impact that SARM1 modulation may have on these activities is understood. The role of murine SARM1 as a transcriptional regulator of the immune response is one such function requiring further investigation. While numerous studies report aberrant transcriptional phenotypes in SARM1-deficient mice, definitive mechanistic insights into the process by which SARM1 regulates transcription have remained largely elusive.

3.1.1 Murine SARM1 regulates resistance or susceptibility to neurotropic viral infections

An early study in SARM1-deficient mice by Kim *et al.* found that, surprisingly for a TLR-adaptor protein, murine SARM1 expression was particularly abundant in neurons in the brain [26]. This is consistent with the now well-characterised role for SARM1 in mediating axon degeneration (discussed in detail in Section 1.4). The SARM1-deficient mice generated for that study and used in this project were congenic. Congenic mice differ from wild type mice of the desired strain only at the gene of interest and a segment of chromosome that is linked to this gene, which is derived from another strain. The SARM1-deficient mice in question are C57BL/6 congenic 129 embryonic stem cell-derived *Sarm1*$^{-/-}$ mice: they are on the C57BL/6 background, and the *Sarm1* locus and linked segment of chromosome is derived from the 129 strain embryonic stem cells in which the *Sarm1* locus was disrupted. These mice and similarly generated SARM1-deficient mice will herein be referred to as B6 congenic *Sarm1*$^{-/-}$ mice. Using these mice, several studies have demonstrated that SARM1's function in the nervous system extends beyond neurodegeneration alone; numerous groups have published an apparent role for SARM1 in

susceptibility to neurotropic viruses. B6 congenic *Sarm1*$^{-/-}$ mice showed enhanced susceptibility to West Nile virus (WNV) in a study by the Diamond lab [44]. WNV replication was augmented in the brainstem of B6 congenic *Sarm1*$^{-/-}$ mice relative to WT controls, and this was associated with reduced TNF levels in the brainstem and increased neuronal cell death. In contrast, B6 congenic *Sarm1*$^{-/-}$ mice were protected from lethality following infection with La Crosse virus (LACV), a zoonotic neurotropic Bunyavirus. LACV replication was equivalent between WT and *Sarm1*$^{-/-}$ neurons, however *Sarm1*$^{-/-}$ neurons were protected from cell death [167]. While the mitochondria in WT neurons were damaged following LACV infection, the mitochondria in *Sarm1*$^{-/-}$ neurons remained fully intact. This corresponded with abrogated superoxide production in the LACV-infected *Sarm1*$^{-/-}$ neurons, and stunted expression of genes which are induced in response to oxidative stress in *Sarm1*$^{-/-}$ neurons compared to WT. Similar to LACV, B6 congenic *Sarm1*$^{-/-}$ mice were protected from lethal infection with vesicular stomatitis virus (VSV) [207]. Expression of a range of cytokines and chemokines was reduced in non-haematopoietic cells of the brain in VSV-infected B6 congenic *Sarm1*$^{-/-}$ mice relative to WT. The protection also correlated with reduced injury to the CNS. The susceptibility of B6 congenic *Sarm1*$^{-/-}$ mice to *Mycobacterium tuberculosis*, *Listeria monocytogenes*, and *Influenza A* virus was also assessed in this study and found to be similar to WT [207], indicating that SARM1 does not indiscriminately influence susceptibility to all infections. Overall, using B6 congenic *Sarm1*$^{-/-}$ mice as a model, numerous studies report a role for SARM1 in determining resistance or sensitivity to neurotropic viruses, in association with altered cytokine production.

3.1.2 Murine SARM1 has a role in regulating transcription in the nervous system

It is difficult to define if the role for SARM1 in determining susceptibility to neurotropic viruses is separable from its roles in axon degeneration and cell death, and if it is partially attributable to a role in regulating cytokine production. There is however a clearly defined role for SARM1 in regulation of expression of specific chemokines in neurons following axotomy, which is spatially and temporally separated from the injury-induced axon degeneration. Both *in vitro* and *in vivo* following traumatic axon injury by transection, *Ccl2, Ccl7, Ccl12,* and *Csf1* expression are specifically upregulated in neurons [208], and it was determined that SARM1 was required for this upregulation. Indeed, expression of these chemokines was abolished in transected neurons from B6 congenic *Sarm1*$^{-/-}$ mice

compared to WT. Remarkably, the authors found that activation of SARM1 by forced dimerization of the TIR domain alone was sufficient to drive rapid expression of these chemokines, even in the absence of traumatic axon injury [208]. SARM1-stimulated chemokines preceded the induction of axon degeneration, which remained undetectable 12 hours post SARM1 activation.

Another study using B6 congenic *Sarm1*$^{-/-}$ mice examined the effects of SARM1-deficiency on transcription in the brain in the context of prion disease. Whole transcriptome analysis showed dramatically increased expression of *Xaf1* in both uninfected and prion-infected brains of B6 congenic *Sarm1*$^{-/-}$ mice compared to WT [169]. Unexpectedly, given that *Sarm1*$^{-/-}$ mice are generally protected from neurodegeneration, SARM1-deficiency was deleterious in prion disease and led to accelerated pathogenesis. X-linked inhibitor of apoptosis (XIAP)-associated factor 1 (XAF1) is a pro-apoptotic protein. It binds to XIAP and triggers its relocalisation to the nucleus, thus antagonising XIAP's suppression of caspase activation and cell death [209]. XAF1 can also coordinate with TNF to induce cytochrome *c* release and apoptosis, in a mechanism distinct from antagonising XIAP [210]. It has been shown that the ratio of XAF1 to XIAP in a motor neuron governs how resistant or susceptible it is to apoptotic cell death [211]. Thus, the exacerbated progression of prion pathogenesis seen in B6 congenic *Sarm1*$^{-/-}$ mice brains relative to WT could be attributed to this enhanced *Xaf1* expression in *Sarm1*$^{-/-}$ brains, as cytokine profiles in the brain and neuroinflammation were equivalent to WT. Interestingly, a similar increase in expression of *Xaf1* was also seen in VSV-infected brainstem from B6 congenic *Sarm1*$^{-/-}$ mice compared to WT [207]. Thus, aside from roles in cell death and axon degeneration in the nervous system, SARM1 also has a reported role in regulation of transcription both basally, for example regulating *Xaf1* expression in uninfected brains, and following traumatic axon injury.

3.1.3 SARM1 regulates Ccl5 expression in murine BMDMs

The roles for murine SARM1 in regulating cell death and transcription are well-characterised in neurons and the brain, where it is highly expressed. However the roles for murine SARM1 in peripheral immune cells, where expression is lower, remain underexplored. Human SARM1 was originally characterised as a TRIF-antagonist in human PBMCs [36], and was subsequently found to antagonise MyD88 signalling in

addition [43]. There is no evidence that murine SARM1 has a similar role. In fact, in a study published by our laboratory, expression of *Ccl2, Cxcl10, Il1b,* and *Tnf* was normal in bone marrow derived macrophages (BMDMs) from B6 congenic *Sarm1*$^{-/-}$ mice following various TLR stimulations [34]. This indicates that SARM1 is not negatively regulating TRIF or MyD88 signalling in this context. However *Ccl5* expression was specifically and consistently diminished in BMDMs from B6 congenic *Sarm1*$^{-/-}$ mice compared to WT controls stimulated with a range of TLR and non-TLR ligands. Ectopic expression of SARM1 protein in these *Sarm1*$^{-/-}$ BMDMs could rescue *Ccl5* expression, and in WT BMDMs could augment *Ccl5* expression [34]. Concerningly however, when I followed a similar protocol using the same cell lines, the finding of restored *Ccl5* expression by ectopic SARM1 expression in *Sarm1*$^{-/-}$ iBMDMs could not be subsequently repeated.

It has been previously demonstrated that delayed gene expression following stimulation can result from extended splicing time rather than hindered initiation of transcription [212]. *Ccl5* pre-messenger RNA (pre-mRNA) would be expected to accumulate in *Sarm1*$^{-/-}$ BMDMs relative to WT if the absence of SARM1 resulted in inefficient or defective splicing, which was not the case when pre-mRNA and mature messenger RNA (mRNA) were measured by qRT-PCR. Instead, both pre-mRNA and mature RNA were reduced in the *Sarm1*$^{-/-}$ BMDMs relative to WT over a series of time-points [34], indicating that SARM1 regulation of *Ccl5* expression occurs at the point of or prior to transcription. Western blots showed that activation of the transcription factors NF-κB and IRF3 was normal in *Sarm1*$^{-/-}$ BMDMs following stimulation with LPS, as was their nuclear translocation as determined by confocal microscopy. The first indication of a mechanism came from chromatin immunoprecipitation (ChIP) analysis of BMDMs stimulated with TLR4 or TLR7 agonists, which showed impaired recruitment of IRF3 and NF-κB, as well as RNA polymerase II (PolII), to the *Ccl5* promoter in *Sarm1*$^{-/-}$ BMDMs compared to WT. How SARM1 regulates the recruitment of transcription factors to *Ccl5* promoter to regulate transcription remains unclear. Intriguingly, SARM1 was also required for optimal *Ccl5* expression following cytosolic PRR stimulation with VACV-70mer and polyinosinic:polycytidylic acid (poly(I:C)), indicating that this regulation is TLR-independent (summarised in Figure 3.1). This is contrary to the function of human SARM1 as an inhibitor of TLR signalling [36].

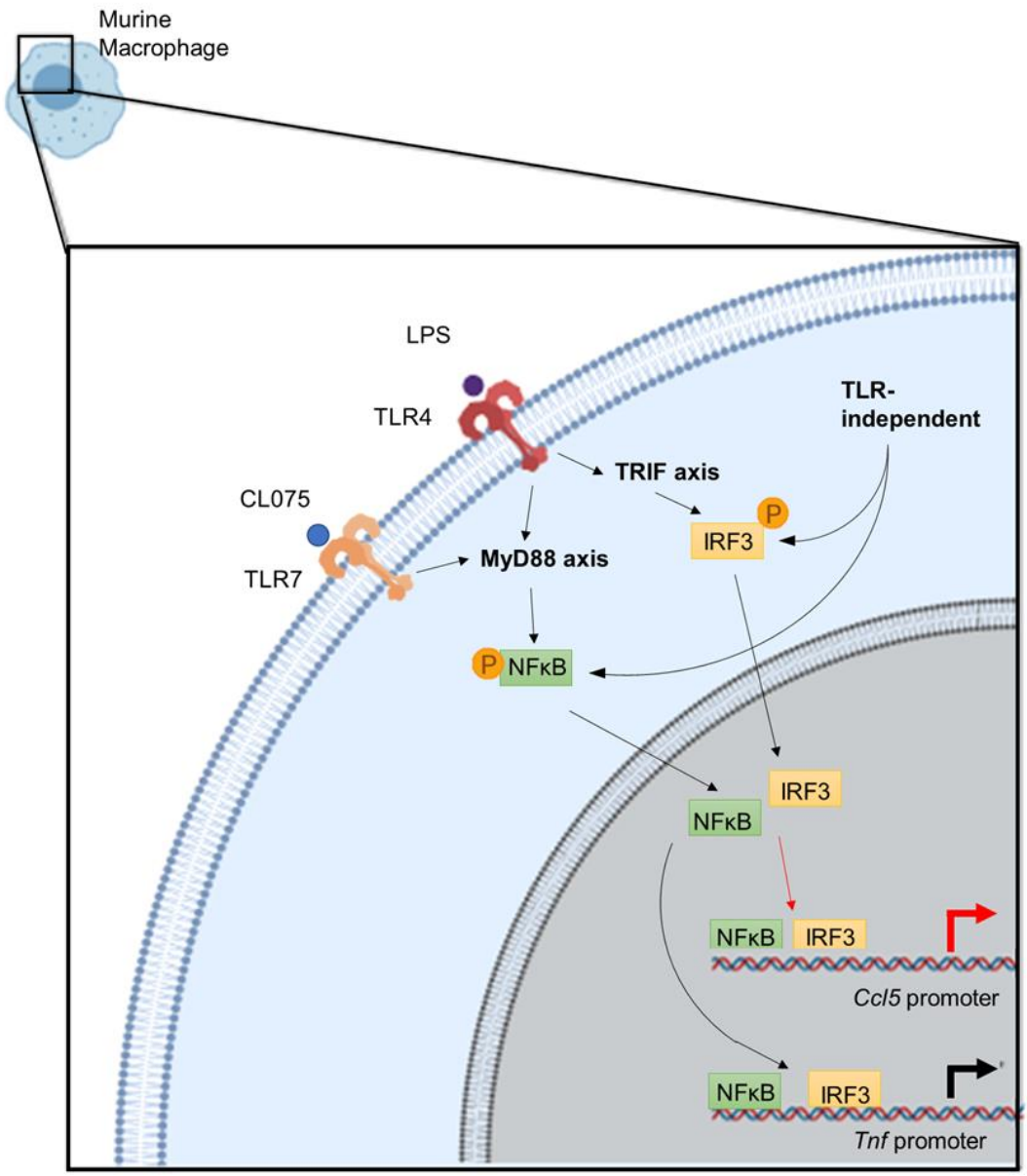

Figure 3.1 Schematic showing steps leading to *Ccl5* expression in BMDMs following stimulation

Steps which proceed as normal in BMDMs from B6 congenic *Sarm1*$^{-/-}$ mice are indicated by a solid black line. Those which are impaired in *Sarm1*$^{-/-}$ BMDMs relative to WT are denoted by a solid red line. LPS, lipopolysaccharide; TLR4, toll-like receptor 4; MyD88, Myeloid differentiation factor 88; TRIF, TIR-domain-containing adaptor protein inducing IFNβ; IRF3, Interferon regulatory factor 3; NF-κB, Nuclear factor kappa B; *Ccl5*, C-C motif chemokine ligand 5 gene; *Tnf*, tumor necrosis factor gene

To contribute to our understanding of SARM1 as a transcriptional regulator, I aimed to build upon the report published by Gürtler *et al.* defining a role of SARM1 in regulating *Ccl5* expression in macrophages. Specifically, I sought to further scrutinise the mechanism by which SARM1 regulates *Ccl5* expression and to identify any potential additional SARM1-regulated genes. Since the publication of this study in 2014, the number of studies investigating a role for SARM1 has grown rapidly, and much more is now known about the structure and function of SARM1 on a molecular level. In 2017 it was discovered that SARM1 possesses intrinsic NADase enzymatic activity which is essential for axon degeneration [30] (discussed in detail in Section 1.4.7). Whether this NAD^+ cleavage activity is required for SARM1 regulation of *Ccl5* expression is as yet unknown. However it is known that cellular NAD levels can play an important role in transcriptional reprogramming [213]. Sirtuins are a family of NAD^+-dependent enzymes, which post-translationally modify their substrates by adenosine diphosphate (ADP)-ribosylation or by deacetylation. A number of these sirtuins are nuclear, and through post-translational modifications, can alter chromatin accessibility and thus transcription [214]. Poly (ADP-ribose) polymerase-1 (PARP-1) is another NAD^+-dependent enzyme which modifies chromatin structure through its intrinsic enzyme activity, thus modulating chromatin accessibility [215]. SARM1 NADase activity could potentially disrupt the availability of NAD^+, and thus impair the function of sirtuins and PARP-1 and by extension result in altered chromatin accessibility. However, NAD^+ levels are maintained in a compartment specific manner, with NMNAT1, NMNAT2, and NMNAT3 mediating NAD^+ biosynthesis in the nucleus, in the cytoplasm and in the mitochondria respectively in mammals [216]. Therefore, in order to cause altered chromatin accessibility by modulating NAD^+ availability to sirtuins or PARP-1, SARM1 would have to localise to the nucleus. Sethman *et al*. reported C-terminal GFP-tagged SARM1 translocating to the nucleus to stabilise lamins and prevent DNA fragmentation following stimulation of human embryonic kidney (HEK 293) cells with pro-apoptotic stimuli [193]. However, this remains the sole study reporting nuclear SARM. Furthermore, *in silico* analysis of the SARM1 sequence does not reveal any putative nuclear localisation sequence (NLS) [193]. Most studies report that SARM1 localises predominantly at the mitochondria across a number of species, including amphioxus [38], shrimp [217], grass carp [218], and mice [26], and it has been suggested that both a cytosolic and mitochondrial pool of SARM1 may exist [28]. Therefore, in order to more fully understand the role of SARM1 in transcription, the subcellular localisation of SARM1 in BMDMs following TLR stimulation requires further investigation.

The overall aim of this thesis is to understand the role for murine SARM1 in transcriptional regulation in macrophages. To achieve this, the initial stage of my project focused on confirming that *Ccl5* expression is reduced in BMDMs from B6 congenic *Sarm1*$^{-/-}$ mice relative to WT, and that TLR-signalling was not enhanced in the absence of SARM1. The subcellular localisation of SARM1 in BMDMs was assessed using subcellular fractionation, in an effort to gain further insight into the mechanism by which SARM1 regulates *Ccl5* expression. Finally, RNA sequencing was employed as an unbiased and global assessment of the role of SARM1 in transcription following stimulation with TLR agonists, using *Ccl5* as a positive control. This was intended to identify any additional genes which are similarly SARM1-regulated, and to shed light on the mechanism of regulation.

3.2 Results

3.2.1 Ccl5 induction is impaired in immortalised and primary BMDMs from B6 congenic Sarm1$^{-/-}$ mice

A previous study in our laboratory demonstrated that macrophages derived from B6 congenic *Sarm1*$^{-/-}$ mice show reduced *Ccl5* induction compared to their WT counterparts following a range of stimuli [34]. Prior to further investigation, I initially sought to validate this phenotype in both pBMDMs and iBMDMs. There are numerous experimental advantages associated with iBMDMs; large numbers of cells can be generated quickly and easily, the cells can be manipulated to stably express proteins, and their use is ethically advantageous as it reduces the use of animals in research. Crucially however, the results are only representative of the individual mouse from which the BMDMs are derived. That is to say that biological variation is unaccounted for in results gathered using iBMDMs, regardless of how many times the experiment is carried out. Alternatively, results gathered from multiple biological replicates of pBMDMs can show real biological variation, and are therefore a better representative of the whole population. They are however somewhat time-consuming to produce, and there are limitations on the number of cells that can be generated per mouse. Thus, both iBMDMs and pBMDMs were employed in this study, taking into account their respective advantages and limitations when selecting the appropriate cell type for each experiment.

To confirm that *Ccl5* induction was reduced in *Sarm1*$^{-/-}$ BMDMs relative to WT BMDMs, the cells were stimulated either with LPS, a potent agonist of TLR4 which employs both TRIF-mediated and MyD88-mediated signalling, or CL075, a synthetic agonist of TLR7 in mice, which signals exclusively through MyD88. The stimulations were carried out over a 24 hour timecourse to determine a kinetic profile of CCL5 expression in these cells, and to establish whether it is impaired or delayed. In accordance with previously published results from our laboratory, *Ccl5* gene induction was decreased in *Sarm1*$^{-/-}$ iBMDMs (Figure 3.2) relative to their WT counterparts following stimulation with either CL075 (Figure 3.2A) or LPS (Figure 3.2B). This trend was observed over a 24 hour period for both stimuli. In contrast, *Tnf* gene induction was not significantly reduced in *Sarm1*$^{-/-}$ iBMDMs compared to WT controls following stimulation with CL075 (Figure 3.2C) or LPS (Figure 3.2D), indicating that the absence of SARM1 does not globally impair the transcription of

inducible immune genes in mouse BMDMs. To determine if there were functional consequences to reduced *Ccl5* gene induction, I then measured the secreted CCL5 protein in the supernatants of these BMDMs. In agreement with their reduced *Ccl5* mRNA levels, *Sarm1*$^{-/-}$ iBMDMs had significantly reduced CCL5 secretion over the course 24 hours following stimulation with CL075 (Figure 3.2E) or LPS (Figure 3.2F), without a concomitant decrease in TNF secretion (Figure 3.2G, H).

Similarly, *Sarm1*$^{-/-}$ pBMDMs showed impaired *Ccl5* expression compared to WT controls following stimulation with CL075 (Figure 3.3A) and LPS (Figure 3.3B). While the difference in *Ccl5* expression between LPS-stimulated WT and *Sarm1*$^{-/-}$ pBMDMs fell short of significance, there was a consistent trend among all replicates. *Tnf* expression in these cells was not significantly or consistently decreased in *Sarm1*$^{-/-}$ pBMDMs compared to WT (Figure 3.3C, D). The *Sarm1*$^{-/-}$ pBMDMs also secreted less significantly less CCL5 than their WT counterparts after either stimulation (Figure 3.3E, F). There were no significant differences in TNF secretion following CL075 (Figure 3.3G) or LPS (Figure 3.3H) in pBMDMs.

3.2.2 ***Phenotypic differences exist between Sarm1$^{-/-}$ iBMDMs and pBMDMs***

Having established that both iBMDMs and pBMDMs from B6 congenic *Sarm1*$^{-/-}$ mice share the common phenotype of reduced *Ccl5* expression relative to WT controls, I sought to determine if there were differences in inflammatory mediators commonly associated with pro-inflammatory macrophages in *Sarm1*$^{-/-}$ iBMDMs or pBMDMs compared to WT. A key marker of pro-inflammatory macrophages is the upregulation of inducible nitric oxide synthase (iNOS), which results in the production of nitric oxide (NO) from L-arginine [219]. Following stimulation with LPS, nitric oxide production by WT and *Sarm1*$^{-/-}$ BMDMs was measured indirectly by detection of nitrites in supernatants by Griess assay. Following LPS stimulation for 24 hours, the *Sarm1*$^{-/-}$ iBMDMs produced significantly less nitric oxide than their WT counterparts (Figure 3.4A). In contrast, *Sarm1*$^{-/-}$ pBMDMs produced equivalent nitric oxide levels to WT (Figure 3.4B). Overall, WT pBMDMs and iBMDMs produced similar levels of nitric oxide. This phenotypic difference between *Sarm1*$^{-/-}$ iBMDMs and pBMDMs affects their suitability in further experiments.

In contrast to their diminished nitric oxide production, *Sarm1*$^{-/-}$ iBMDMs produced significantly more of the pro-inflammatory cytokine IL-6 than WT iBMDMs following both CL075 (Figure 3.4C) and LPS (Figure 3.4D) stimulation. However, there were no differences in IL-6 production between WT and *Sarm1*$^{-/-}$ pBMDMs with either stimulus (Figure 3.4E, F). Thus, *Sarm1*$^{-/-}$ iBMDMs maintain the phenotype of impaired *Ccl5* expression and remain suitable to explore the mechanism by which SARM1 exerts regulation on this specific gene. However, the deviations in iBMDMs from pBMDMs with respect to induction of other inflammatory immune genes disqualifies them from use in investigating a broader, transcriptional role for SARM1.

3.2.3 Ccl5 induction is impaired in Sarm1$^{-/-}$ *pBMDMs following stimulation with MPLA*

Mammalian SARM1 was originally described as a negative regulator of TRIF signalling in human peripheral immune cells [36]. Murine SARM1 therefore may have two conflicting regulatory roles in BMDMs stimulated with LPS – a potential negative role through TRIF inhibition and the experimentally validated positive role in promoting *Ccl5* expression following TLR stimulation. Thus, before proceeding with further experiments interrogating the mechanism through which SARM1 positive regulates *Ccl5* expression following stimulation with LPS, I sought to determine if the results were confounded by a concurrent inhibitory role on TRIF signalling.

Monophosphoryl lipid A (MPLA) is produced by hydrolysis of diphosphoryl lipid A, the component of LPS which is recognised by TLR4. This results in the removal of all but one phosphate groups, and varying levels of deacylation. The result is a reduced toxicity TLR4 ligand, which is used as a vaccine adjuvant in humans. Numerous studies have demonstrated that it is primarily TRIF signalling, and not MyD88 signalling, which proceeds following TLR4 stimulation with MPLA [220, 221]. To determine if SARM1-deficiency augmented TRIF-dependent *Ccl5* expression by relieving the SARM1-mediated inhibition of TRIF signalling, or diminished *Ccl5* expression by removing SARM1's positive regulatory action, a time-course of MPLA stimulations was performed on WT and *Sarm1*$^{-/-}$ pBMDMs and the expression of *Ccl5*, *Tnf*, and *Il6* was measured. If SARM1 were inhibiting TRIF under these conditions, the SARM1-deficient BMDMs should show

increased expression of *Tnf* and *Il6*, genes which were previously shown not to be positively SARM1 regulated.

Following MPLA stimulation, there were no significant differences in *Tnf* (Figure 3.5C) or *Il6* (Figure 3.5E) gene expression between the WT and the *Sarm1*$^{-/-}$ pBMDMs, indicating that SARM1 does not antagonise TRIF signalling in murine BMDMs. In agreement with a positive regulatory role for SARM1, *Ccl5* expression was significantly decreased in the *Sarm1*$^{-/-}$ pBMDMs relative to the WT (Figure 3.5A). CCL5, TNF and IL-6 protein secretion was also measured in the supernatants of WT and *Sarm1*$^{-/-}$ pBMDMs following MPLA stimulation. CCL5 secretion was significantly reduced in the *Sarm1*$^{-/-}$ pBMDMs relative to WT (Figure 3.5B). While TNF secretion was also lower in *Sarm1*$^{-/-}$ pBMDMs than in WT (Figure 3.5D), IL-6 levels were equivalent between the two genotypes (Figure 3.5F), indicating that cytokine production is not globally impaired in SARM1-deficient cells following MPLA stimulation, nor is it augmented due to the absence of SARM1 antagonism of TRIF. Therefore, LPS remains a suitable ligand to study the mechanism by which SARM1 regulates *Ccl5* expression, and the results are not confounded by an opposing inhibitory function of SARM1.

3.2.4 SARM1 does not enter the nucleus to regulate Ccl5 expression

Unfortunately, endogenous SARM1 is difficult to detect in macrophages, and this has resulted in uncertainty surrounding the subcellular localisation of SARM1. While most agree that SARM1 resides exclusively at the mitochondria [24] or that there is both a mitochondrial and cytoplasmic pool of SARM1 [28], overexpressed SARM1 was reported by one group to localise to the nucleus to stabilise lamins following treatment with apoptotic stimuli [193]. Previous work from our laboratory found that the activation and nuclear translocation of the transcription factors NF-κB and IRF3 in *Sarm1*$^{-/-}$ pBMDMs proceeds as normal. However NF-κB and IRF3 recruitment to the *Ccl5* promoter, and not the *Tnf* promoter, were found to be impaired in *Sarm1*$^{-/-}$ BMDMs relative to WT [34]. This suggested that SARM1 may be exerting its regulatory effects from the nucleus. Given that SARM1 possesses intrinsic NADase activity, its presence in the nucleus could potentially locally deplete the available pool of NAD^+, thus altering the activity of sirtuins and poly (ADP-ribose) polymerases, leading to altered chromatin accessibility and by extension, transcription. Alternatively, if present in the nucleus SARM1 could physically interact with

a known transcriptional regulator and modulate its function. Understanding if SARM1 is ever present in the nucleus could therefore shed light on the mechanism by which it could regulate transcription. Thus, I examined the localisation of SARM1 using subcellular fractionation.

To overcome the issue of SARM1 being difficult to detect in macrophages *Sarm1*$^{-/-}$ iBMDMs which had been transduced to stably express the 724 aa isoform of SARM1 with a C-terminal Flag tag, henceforth called S724, were used for localisation studies. Previous work from our laboratory has shown that SARM1 can be readily detected in these cells using commercially available antibodies specific to the Flag tag. *Sarm1*$^{-/-}$ iBMDMs stably expressing an empty vector (EV) were used as a control. To determine if SARM1 was constitutively present at the nucleus, or translocated there after stimulation, S724 and EV *Sarm1*$^{-/-}$ iBMDMs were briefly treated with LPS or left untreated. A nuclear fraction and a mixed cytoplasmic fraction were isolated from these cells, and the presence of Flag-tagged SARM1 and subcellular location markers was assessed by Western blot (Figure 3.6). The cytoplasmic fraction contained both the cytoplasmic marker glyceraldehyde 3-phosphate dehydrogenase (GAPDH) and the nuclear marker, histone 3 (H3), indicating it is an impure cytoplasmic rather than cytosolic fraction. The isolated nuclear fraction contained H3 and not GAPDH, indicating that it was devoid of detectable cytoplasmic contamination. Flag-tagged SARM1 was not detectable in either the cytoplasm or the nucleus of EV *Sarm1*$^{-/-}$ iBMDMs. In unstimulated S724 *Sarm1*$^{-/-}$ iBMDMs, Flag-tagged SARM1 was detectable only in the cytoplasmic fraction and not the nucleus. Stimulation with LPS did not induce nuclear translocation of SARM1 (Figure 3.6). Thus, SARM1 does not reside at the nucleus under resting conditions, nor does it translocate there following TLR stimulation.

3.2.5 RNA sequencing reveals a disproportionate number of differentially expressed genes on chromosome 11 surrounding the Sarm1 locus

Data heretofore indicate that SARM1 specifically regulates *Ccl5* expression in a stimulus-independent manner without entering the nucleus, though little light has been shed on the mechanism through which this could occur and whether this regulation is exclusive to *Ccl5*. Therefore in order to obtain a broad and unbiased view of the role SARM1 in the regulation of inducible immune gene expression, RNA sequencing was performed on untreated and

CL075-treated WT and *Sarm1*$^{-/-}$ BMDMs. For this purpose, pBMDMs were used rather than iBMDMs for two reasons. Firstly, all iBMDMs were derived from a single mouse so their use would preclude the inclusion of numerous real biological replicates. Secondly, as discussed in Section 3.2.2, some phenotypes observed in SARM1-deficient iBMDMs are not seen in pBMDMs, indicating that the results would not be broadly representative.

CL075 was used to stimulate the BMDMs through TLR7 for three hours, as *Ccl5* expression was previously shown to be substantially reduced in *Sarm1*$^{-/-}$ pBMDMs relative to WT at this time-point. Furthermore, following the relatively short stimulation time gene induction is likely to be a direct response to CL075 treatment, rather than a secondary response to genes expressed at an earlier time-point. RNA from unstimulated BMDMs was also examined by RNA sequencing to determine if any differences exist basally in the transcriptional landscape of BMDMs from WT and B6 congenic *Sarm1*$^{-/-}$ mice. BMDMs from five mice per genotype were stimulated as described or left untreated, and total RNA was isolated. The mice were all female and age-matched to remove any confounding factors associated with sex or age differences in immune response. It is important to note that as the data generated in this RNA sequencing experiment is exclusively from female mice, it may not reflect the transcriptional landscape in male *Sarm1*$^{-/-}$ mice. The quality and concentration of the resulting RNA was assessed as described in Section 2.2.9.1 and four biological replicates of WT and of *Sarm1*$^{-/-}$ pBMDMs were selected for sequencing on that basis. RNA is exceptionally labile and prone to degradation, and the integrity of RNA samples is of paramount importance to obtain sequencing data which faithfully reflects the transcriptome. The RIN, which measures RNA intactness on a scale from 1 -10, was found to be between 9.5 and 10 for all selected samples, indicating minimal degradation. All selected samples were also of adequate concentration. Samples were sent to Macrogen, Inc. where library preparation and sequencing were performed as described in Section 2.2.9.1

Sequencing data was received from Macrogen, Inc. and mapped to the genome and repeat mapped transcriptome by Dr Karsten Hokamp. Differential gene expression analysis was then performed by Dr Fiona Roche, as described in Section 2.2.9.3. The *Sarm1*$^{-/-}$ replicates exhibited substantial variability, which was clearly visible from the principal component analysis (PCA) plot (data not shown). When the *Sarm1*$^{-/-}$ replicates were collectively subjected to differential gene expression analysis compared to wild type, no genes were found to be significantly differentially expressed, including the positive control *Ccl5*. An

alternative strategy was therefore employed to identify the genes which were differentially expressed in *Sarm1*$^{-/-}$ BMDMs relative to WT BMDMs to a similar degree as *Ccl5*. The four *Sarm1*$^{-/-}$ samples were split into two pairs with similar expression profiles (SKO1/SKO2 and SKO3/SKO5) then compared to WT. Unstimulated *Sarm1*$^{-/-}$ and WT pBMDMs were compared, and genes were deemed differentially expressed if the DESeq2 base mean was greater than 100, the fold change exceeded 1.6 fold, and the adjusted p-value was less than 0.05. Similarly, CL075-stimulated *Sarm1*$^{-/-}$ and WT pBMDMs were compared, and genes were deemed differentially expressed if the DESeq2 base mean was greater than 100, and the fold change exceeded 1.6 fold. The p-value cut off for two replicates (SKO3 and SKO5) was relaxed to $p \leq 0.1$ to include *Ccl5*, which was the positive control). This strategy is shown in Figure 3.7A. It is important to note that dividing the *Sarm1*$^{-/-}$ BMDM samples for analysis and redefining the significance threshold for differential gene expression to include *Ccl5* may bias the results. It is therefore important that an additional measure is used to verify differential gene expression, hence differences in the abundance of mRNA of selected genes of interest were later measured by qPCR.

The differentially expressed genes (DEGs) from both comparisons were compiled into a single gene list, which was then interrogated for patterns which may shed light on the mechanism by which SARM1 influenced their expression. Transcription factor binding site analysis was employed to identify transcription factor binding sites which are overrepresented among the DEGs compared to genes whose expression was similar in WT and *Sarm1*$^{-/-}$ pBMDMs using oPOSSUM-3 [222]. However, no significant results emerged. Pathway analysis was also carried out to investigate if any relationship existed between the DEGs, or if they may be commonly associated with a process that may be SARM1-regulated, but no clear patterns were observed (data not shown). Together, this suggested that the identified DEGs were not differentially expressed due to regulation of a known regulatory protein or transcription factor by SARM1.

When a heatmap was generated by Dr Fiona Roche with DEGs clustered by chromosomal location it became clear that chromosome 11, on which the *Sarm1* and *Ccl5* loci reside, was disproportionately represented. Eight out of the total 22 DEGs reside on chromosome 11 (Figure 3.7B). Three of these differentially expressed genes (*Ccl6, Ccl9,* and *Acap1*) were experimentally validated by qRT-PCR. In agreement with the sequencing data, the expression of *Ccl6* (Figure 3.8A) and *Ccl9* (Figure 3.8B) mRNA were reduced in *Sarm1*$^{-/-}$

relative to WT BMDMs both basally and following stimulation with CL075 for 3 hours. *Acap1* expression also mirrored the RNA sequencing results, with *Sarm1*$^{-/-}$ BMDMs having elevated basal *Acap1* levels relative to WT (Figure 3.8C). Stimulation with CL075 for 3 hours caused a small reduction in *Acap1* expression in both WT and *Sarm1*$^{-/-}$ BMDMs, but it remained significantly higher in the *Sarm1*$^{-/-}$ cells.

3.2.6 Passenger genes flank the Sarm1 locus in Sarm1$^{-/-}$ *BMDMs*

A large proportion of the genes which are differentially expressed in pBMDMs from B6 congenic *Sarm1*$^{-/-}$ mice compared to WT controls were on chromosome 11, the chromosome on which the *Sarm1* locus resides, and three of these were experimentally validated. This prompted a re-examination of the B6 congenic *Sarm1*$^{-/-}$ mouse used in this study, which is commonly used in mouse SARM1 studies. This mouse was generated by targeted gene disruption, as described in Section 2.2.1.1. Briefly, the *Sarm1* locus was disrupted by replacement with a targeting vector in embryonic stem cells derived from an unspecified 129/SvJ mouse, known as the donor. These cells were implanted to a C57BL/6 blastocyst, the recipient, and following germline transmission and at least 15 generations of backcrossing, a SARM1-deficient mouse on the C57BL/6 background was achieved. It is now appreciated however that mice generated in this manner harbour residual donor-derived genetic material in the region flanking the targeted locus, termed passenger genes or passenger mutations. The probability of a given gene being of donor origin is dependent on proximity to the targeted locus and the number of generations of backcrossing to C57BL/6 mice.

Thus, a map of chromosome 11 was drawn (Figure 3.9), showing the position of DEGs relative to the *Sarm1* locus and indicating the distance between the DEGs and the *Sarm1* locus. This distance is measured in centimorgans (cM), a unit for measuring genetic linkage, specifically the interval at which there is a 1% chance of recombination during meiosis. Indeed all eight DEGs on chromosome 11 reside in close proximity to the *Sarm1* locus. The most distal upstream and downstream DEGs, *Tnfsf13* and *Ccl6* respectively, are separated from *Sarm1* by an interval of less than 5 cM (Figure 3.9). Assuming 16 - 20 generations of backcrossing to C57BL/6, the probability of a passenger gene being retained within 5 cM from the targeted gene is 46.3 – 37.7%. It is therefore feasible that the DEGs found on chromosome 11 in B6 congenic *Sarm1*$^{-/-}$ mice are differentially expressed because

of strain differences between C57BL/6 and 129SvJ mice, rather than due to the absence of SARM1 protein. To investigate this further, the density of single nucleotide polymorphisms (SNPs) and insertions and deletions (indels) in RNA isolated from *Sarm1*$^{-/-}$ BMDMs relative to the C57BL/6 reference sequence was investigated across chromosome 11 (Figure 3.10), using a sliding window approach as described in Section 2.2.9.4, performed by Dr Fiona Roche. There was a high density of SNPs and indels flanking the *Sarm1* locus on chromosome 11. There were some sporadic instances of SNPs and indels on other chromosomes, these were not closely packed and are likely due to genetic drift (Figure 3.10).

To interrogate the possibility that DEGs in *Sarm1*$^{-/-}$ BMDMs are donor-derived passenger genes, the RNA sequence of genes of interest from *Sarm1*$^{-/-}$ BMDMs was examined using IGV from the Broad Institute. The deviations from the reference sequence in *Sarm1*$^{-/-}$ RNA were manually recorded, and compared to the SNPs listed by the Sanger Mouse Genomes Project (SMGP) to be associated with 129 strains. As the exact 129 strain used in the generation of B6 congenic *Sarm1*$^{-/-}$ mice was not specified, all three 129 strains annotated in the SMGP were used in the comparison. Sequence variations were first examined in DEGs which were experimentally validated to be differentially expressed in *Sarm1*$^{-/-}$ BMDMs, namely *Ccl6*, *Ccl9*, and *Acap1*. Unsurprisingly, no SNPs or indels were visible in the *Ccl6* locus in *Sarm1*$^{-/-}$ BMDMs (Figure 3.11), as there are no exonic 129-associated variations listed by the SMGP. However, deviations from the reference sequence were found in both the *Ccl9* (Figure 3.12) and *Acap1* (Figure 3.13) loci in RNA from *Sarm1*$^{-/-}$ BMDMs. Where these sequence deviations existed, they were present in all reads. By manual comparison, these were found to be 129-associated variants (Tables 3.1 and 3.2 respectively). There were no instances of a 129-associated variant not being detected in RNA from *Sarm1*$^{-/-}$ BMDMs when there were reads mapped to the position of the variant. The sequence at the *Ccl5* locus in RNA from *Sarm1*$^{-/-}$ BMDMs was next examined. Here, RNA from CL075-stimulated WT and *Sarm1*$^{-/-}$ were compared to the reference sequence rather than unstimulated, as *Ccl5* is not basally expressed in these cells. A small number of sequence deviations from the reference sequence were seen in RNA from *Sarm1*$^{-/-}$ and not WT BMDMs (Figure 3.14). They were once again found to be 129-associated SNPs (Table 3.3).

Xaf1 was among the genes found to be differentially expressed in BMDMs from B6 congenic *Sarm1*$^{-/-}$ mice, and is of interest due to its role in promoting cell death. In agreement with the published literature in B6 congenic *Sarm1*$^{-/-}$ mice [169, 207] *Xaf1* expression appeared higher in *Sarm1*$^{-/-}$ BMDMs than in WT. However, there was a multitude of sequence deviations visible in the RNA from *Sarm1*$^{-/-}$ BMDMs relative to the reference sequence at the *Xaf1* locus, and this was not seen in the corresponding WT RNA (Figure 3.15). These numerous SNPs all corresponded to known 129-associated variants (Table 3.4). Additionally, the *Sarm1*$^{-/-}$ *Xaf1* sequence contains a premature stop codon, which results in truncation of the final 3 amino acids of the protein (Table 3.4, highlighted in red). This could have implications for all studies using these mice to study the role of SARM1 in regulating cell death.

While analysis was proceeding on the initial RNA sequence experiment, a second set of BMDMs RNA samples, from WT (four biological replicates) and B6 congenic *Sarm1*$^{-/-}$ mice (five biological replicates), was generated and sent for sequencing. The BMDMs were either treated for 3h with LPS to stimulate TLR4 or left untreated. The samples were processed and analysed identically to the previous experiment, as described in Section 2.2.9.1, and once again mapping was performed by Dr Karsten Hokamp. Data to this point have demonstrated that passenger genes on chromosome 11 confound the differential gene expression analysis, therefore the focus of this experiment was on the basally differentially expressed genes on chromosome 11. In agreement with previous results, a disproportionate fraction of basal DEGs reside on chromosome 11. A heatmap was compiled by Dr Fiona Roche of genes on chromosome 11 which are basally upregulated (Figure 3.16A) and downregulated (Figure 3.16B) in *Sarm1*$^{-/-}$ BMDMs relative to WT ordered by their position on chromosome 11, with the position of the *Sarm1* locus indicated. Strikingly, all of these genes were within 5 cM of the *Sarm1* locus and are therefore likely to be donor-derived passenger genes (Figure 3.16). The eight chromosome 11 DEGs described in the previous experiment (Figure 3.7) (*Tnfsf13, Plscr3, Acap1, Nlrp1c-ps, Xaf1, Ccl5, Ccl9,* and *Ccl6*) were confirmed here to be differentially expressed. Consistent with Figure 3.7, *Ccl6* (Figure 3.17A) and *Ccl9* (Figure 3.17B) expression was reduced in *Sarm1*$^{-/-}$ BMDMs relative to WT, both basally and following LPS stimulation. *Acap1* expression also mirrored the previous results, being higher in both untreated and LPS-treated *Sarm1*$^{-/-}$ BMDMs than in their WT counterparts (Figure 3.17C).

In addition, the *Nlrp1a*, *Nlrp1b*, and *Nlrp1c-ps* transcripts expressed in *Sarm1*$^{-/-}$ BMDMs varied greatly from those found in WT BMDMs. In contrast to WT, there was almost no *Nlrp1a* expression in *Sarm1*$^{-/-}$ BMDMs, with reads only mapping to a single exon (Figure 3.18). This corresponds with the differential expression seen in the DEG analysis (Figure 3.16). While *Nlrp1b* was expressed in both WT and *Sarm1*$^{-/-}$ BMDMs, the transcript expressed in *Sarm1*$^{-/-}$ lacked a number of early exons (Figure 3.19). *Nlrp1c-ps*, the pseudogene, was expressed in WT BMDMs but not in *Sarm1*$^{-/-}$ (Figure 3.20). Using the Mouse Genomics Informatics (MGI) multiple genome viewer (MGV) tool [223], the transcripts of *Nlrp1a*, *Nlrp1b*, and *Nlrp1c-ps* which are expressed by C57BL/6J and 129S1/SvImJ strains were compared, to see if passenger genes could account for the aberrant transcripts observed in the *Sarm1*$^{-/-}$ BMDMs. Indeed, *Nlrp1b* transcripts expressed in the 129 strain mouse lack expression of a number of early exons that are present in the transcripts expressed by the C57BL/6 strain mouse (Figure 3.21). This corresponds with an absence of reads mapping to those exons of *Nlrp1b* in *Sarm1*$^{-/-}$ BMDMs (Figure 3.19). In addition, the *Nlrp1c-ps* pseudogene is absent from the genome of the 129 strain mouse (Figure 3.21), and no reads were mapped to this locus in BMDMs from the *Sarm1*$^{-/-}$ mouse (Figure 3.20). The lack of expression of *Nlrp1a* in BMDMs from *Sarm1*$^{-/-}$ mice (Figure 3.18) is not reflective of the pattern of *Nlrp1a* transcription in 129 strain mouse (Figure 3.21). The absence of reads mapping to the *Nlrp1a* locus in BMDMs from *Sarm1*$^{-/-}$ mice could indicate that *Nlrp1a* is simply not expressed in this mouse, or that substantial sequence deviations in the *Sarm1*$^{-/-}$ *Nlrp1a* locus prevented the reads from being mapped to this locus in the C57BL/6 reference sequence. *Nlrp1a* and *Nlrp1b* encode the NLRs NLRP1a and NLRP1b, which act as the sensor components for the NLRP1a and NLRP1b inflammasomes. This is an additional confounding factor in the B6 congenic *Sarm1*$^{-/-}$ mice which may misguide interpretation of results in studies using these mice to investigate the role of SARM1 in cell death.

3.2.7 Stable expression of SARM1 does not rescue Ccl5 expression in B6 congenic Sarm1$^{-/-}$ *mice*

The data thus far confirms that *Ccl5* expression is reduced in *Sarm1*$^{-/-}$ BMDMs relative to WT, and that the region flanking the *Sarm1* locus on chromosome 11 retains donor-derived passenger genes. It has yet to be elucidated however if it is the absence of SARM1, or the presence of these passenger genes which results in impaired *Ccl5* expression in BMDMs.

Thus, the ability of stably expressed SARM1 to enhance *Ccl5* induction in iBMDMs derived from B6 congenic *Sarm1*$^{-/-}$ mice was assessed. It was previously confirmed that CCL5 protein secretion is reduced in *Sarm1*$^{-/-}$ iBMDMs relative to WT following LPS stimulation (Figure 3.2). SARM1 expression was evaluated by Western blot in *Sarm1*$^{-/-}$ iBMDMs stably expressing Flag-tagged SARM1 to ensure that SARM1 was expressed at sufficiently high levels (Figure 3.22A). Within days of this, CCL5 secretion was measured in EV and S724 *Sarm1*$^{-/-}$ iBMDMs which were stimulated for 3 or 24 hours with LPS or left unstimulated. Stable expression of SARM1 did not result in enhanced CCL5 secretion in *Sarm1*$^{-/-}$ iBMDMs following short or long LPS stimulation (Figure 3.22B). Concerningly, this is in disagreement with previously published results from our lab, where exogenous expression of SARM1 in *Sarm1*$^{-/-}$ iBMDM restored *Ccl5* expression. TNF secretion was therefore measured as a control to ensure that overall protein secretion by EV or S724 expressing *Sarm1* BMDMs was not disrupted due to an underlying contamination or discrepancies in cell number. There were no substantial differences between the EV and S724 expressing *Sarm1*$^{-/-}$ iBMDMs (Figure 3.22C). This additional control was not included in our lab's previously published experiments. It is therefore possible that the previously observed enhancement of CCL5 secretion by ectopic SARM1 expression in *Sarm1*$^{-/-}$ iBMDMs was not a specific effect resulting from the action of SARM1, but rather a result of discrepancies in cell number or presence of an underlying infection. Therefore, the phenotype of impaired *Ccl5* induction in *Sarm1*$^{-/-}$ iBMDMs was misattributed to a regulatory role for SARM1, and is likely due to the presence of passenger genes in the genome of the B6 congenic *Sarm1*$^{-/-}$ mice.

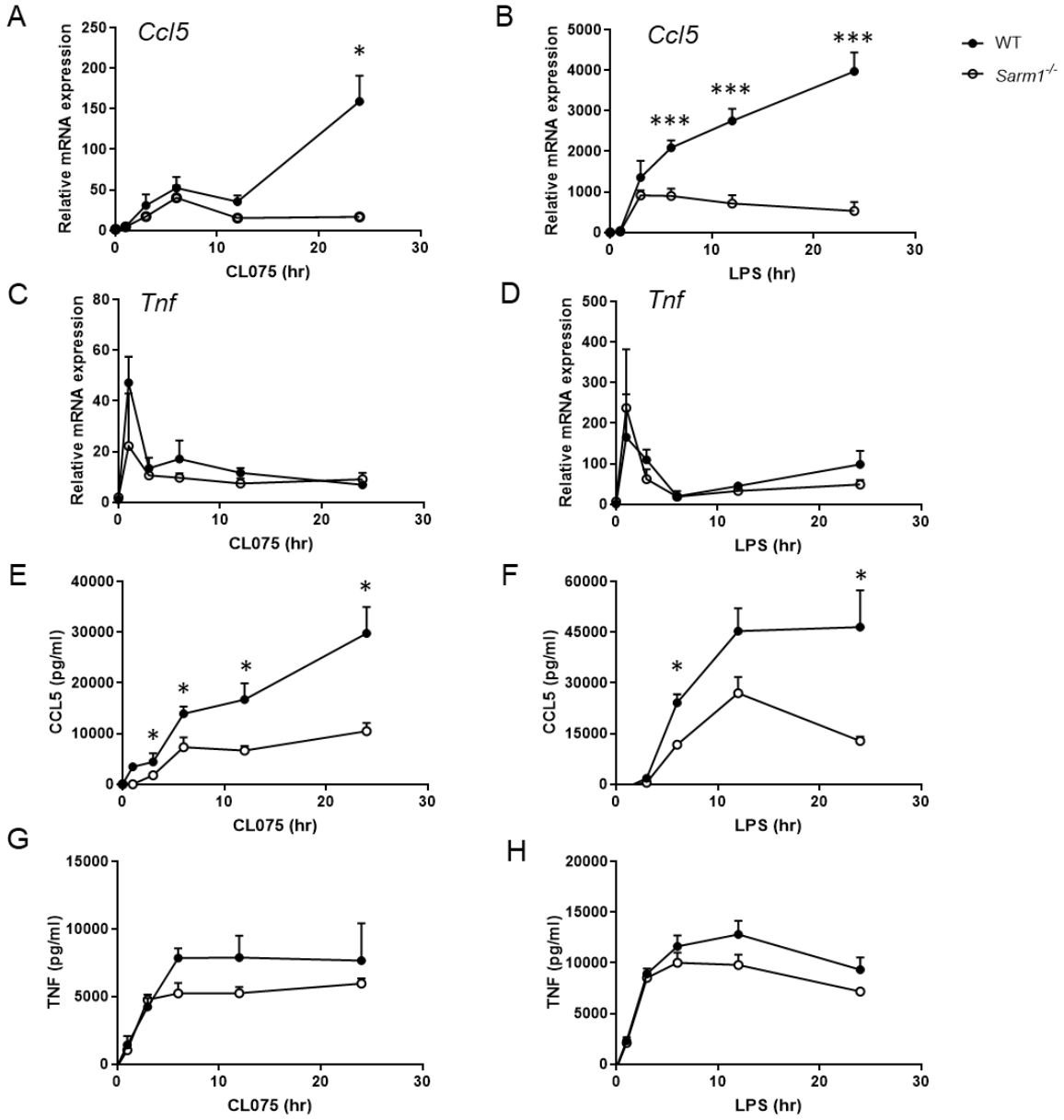

Figure 3.2 *Ccl5* expression is reduced in immortalised BMDMs from B6 congenic *Sarm1*$^{-/-}$ mice compared to WT mice

WT and *Sarm1*$^{-/-}$ iBMDMs were stimulated with 5 μg/ml CL075 (A, C, E, G) or 100 ng/ml LPS (B, D, F, H) for the indicated times. *Ccl5* (A, B) and *Tnf* (C, D) mRNA were assayed by qRT-PCR, normalized to the housekeeping gene β-actin, and are presented relative to the untreated WT control. Supernatants were assayed for CCL5 (E, F) and TNF (G, H) protein by ELISA. Graphs show mean ±SD of triplicate samples and are representative of at least three independent experiments. * $p< 0.05$, ** $p< 0.01$, *** $p< 0.001$ compared with WT, multiple unpaired *t*-test with Holm-Šídák multiple comparisons test).

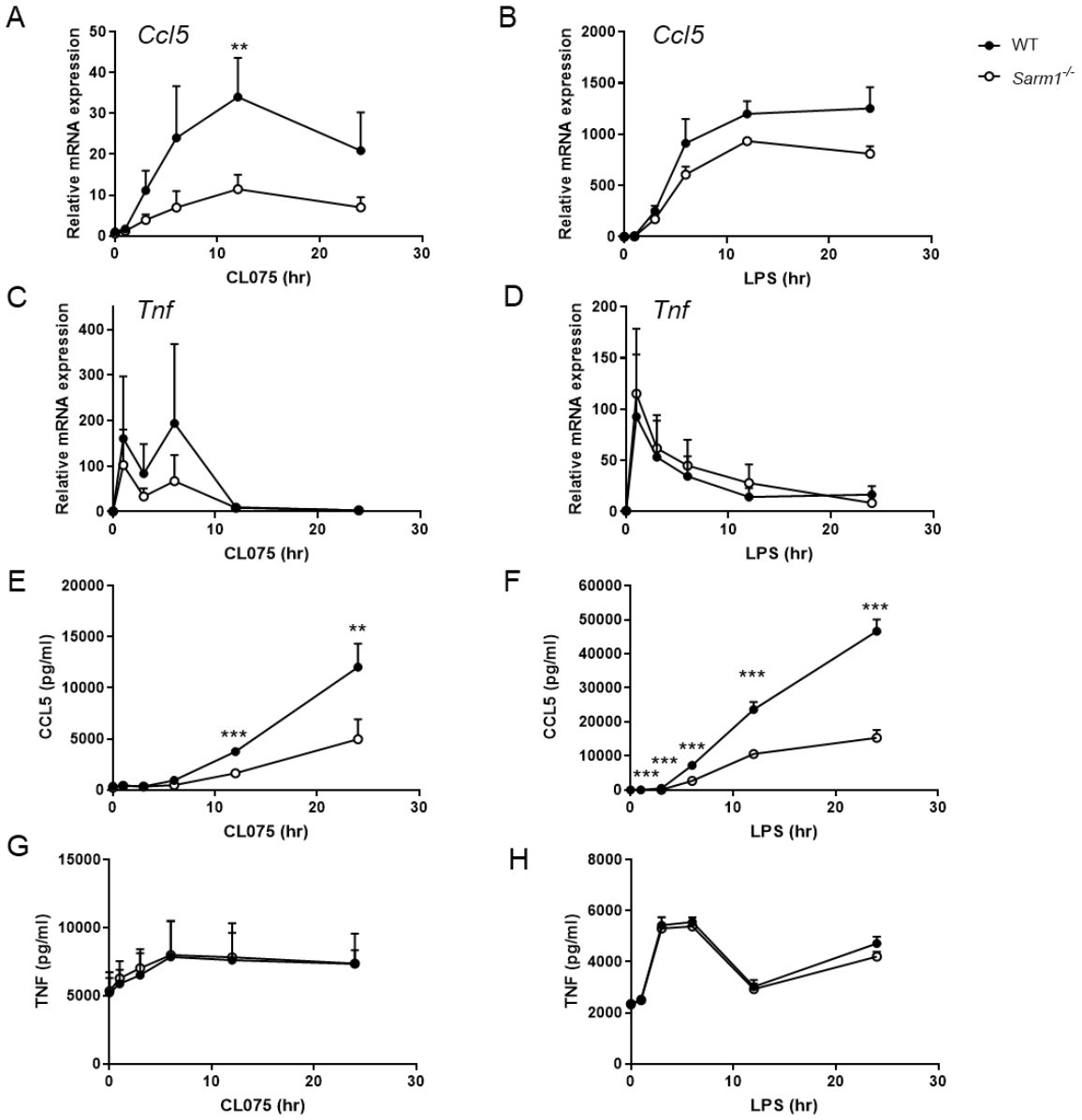

Figure 3.3 *Ccl5* expression is reduced in primary BMDMs from B6 congenic *Sarm1*$^{-/-}$ mice compared to WT mice

WT and *Sarm1*$^{-/-}$ pBMDMs were stimulated with 5 μg/ml CL075 (A, C, E, G) or 100 ng/ml LPS (B, D, F, H) for the indicated times. *Ccl5* (A, B) and *Tnf* (C, D) mRNA were assayed by qRT-PCR, normalized to the housekeeping gene β-actin, and are presented relative to the untreated WT control. Supernatants were assayed for CCL5 (E, F) and TNF (G H) protein by ELISA. Graphs show mean ±SEM from 3-5 mice per genotype, performed in triplicate. *p<0.05, **p<0.01, ***p<0.001 multiple Mann-Whitney tests with Holm-Šídák multiple comparisons test.

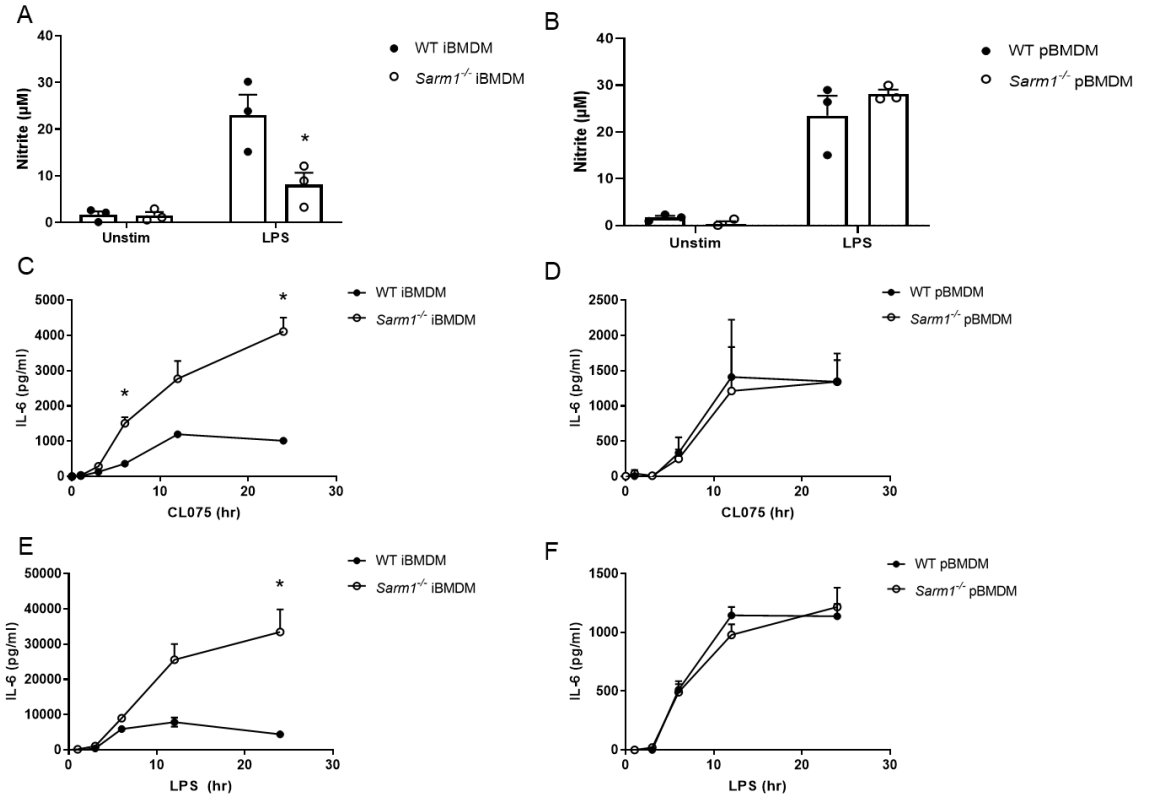

Figure 3.4 Nitric oxide production and IL-6 secretion are dysregulated in *Sarm1*$^{-/-}$ iBMDMs, but not in *Sarm1*$^{-/-}$ pBMDMs, relative to WT

WT and *Sarm1*$^{-/-}$ iBMDMs (A, C, E) and pBMDMs (B, D, F) were stimulated with 5 μg/ml CL075 (C, D) or 100 ng/ml LPS (A, B, E, F) for the indicated times. Supernatants were assayed for nitrite as a surrogate measurement of NO production by Griess assay after 24 h LPS stimulation (A, B). IL-6 (C, D, E, F) protein was assayed by ELISA after the indicated times. Graphs show mean ±SEM from 3-5 experiments with for iBMDMs (A, C, E) and 3-5 mice per genotype for pBMDMs (B, D, F) performed in triplicate. *p<0.05, **p<0.01, ***p<0.001 multiple Mann-Whitney tests with Holm-Šídák multiple comparisons test.

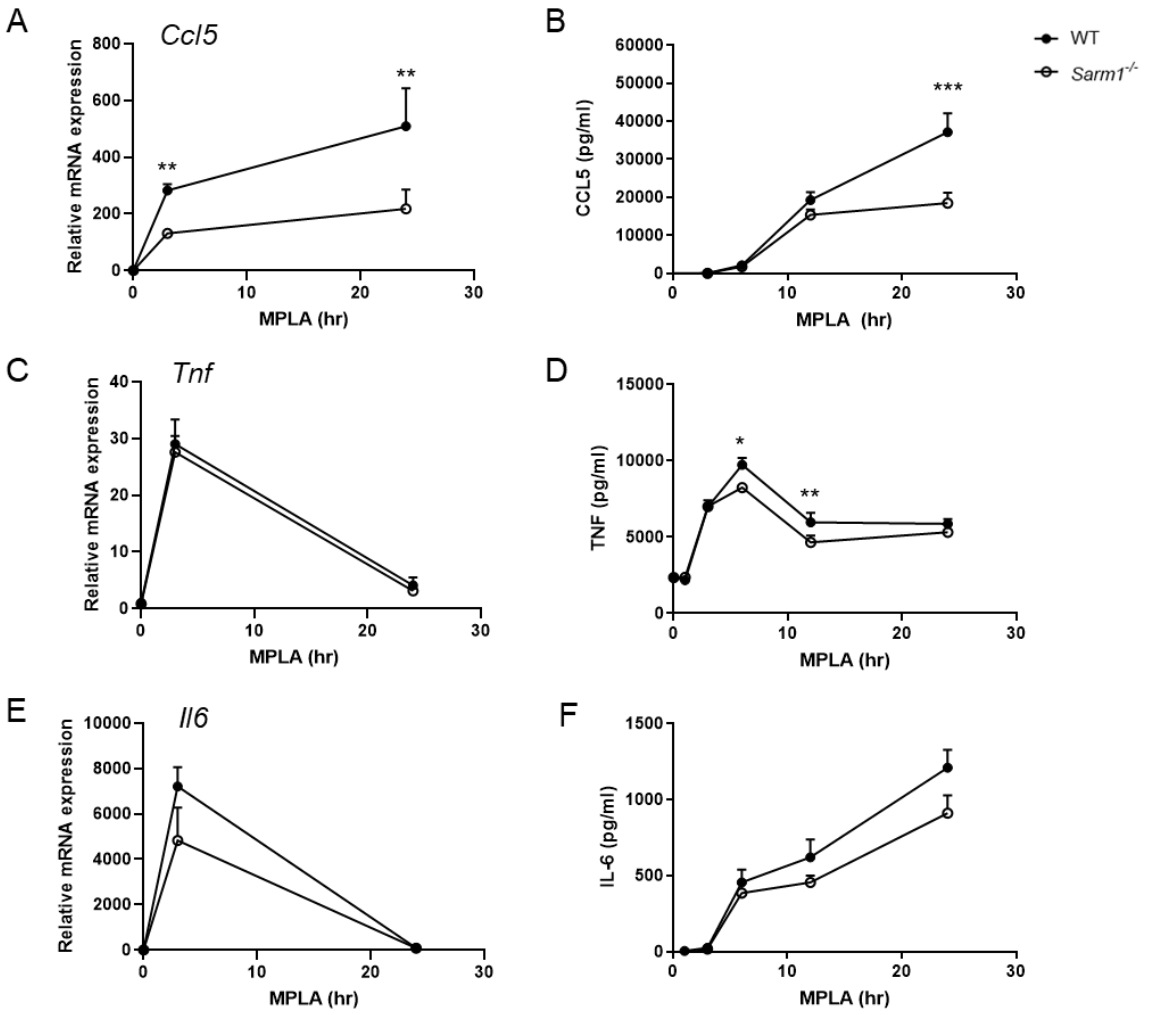

Figure 3.5 *Ccl5* induction is reduced in pBMDMs from B6 congenic *Sarm1*$^{-/-}$ mice compared to WT mice following stimulation with MPLA

WT and *Sarm1*$^{-/-}$ pBMDMs were stimulated with 1 μg/ml MPLA for the indicated times. *Ccl5* (A), *Tnf* (C), and *Il6* (E) mRNA were assayed by qRT-PCR, normalized to the housekeeping gene β-actin, and are presented relative to the untreated WT control. Supernatants were assayed for CCL5 (B), TNF (D), and IL-6 (F) protein by ELISA. Graphs show mean ±SEM from 3-5 mice per genotype, performed in triplicate. *p<0.05, **p<0.01, ***p<0.001 multiple Mann-Whitney tests with Holm-Šídák multiple comparisons test.

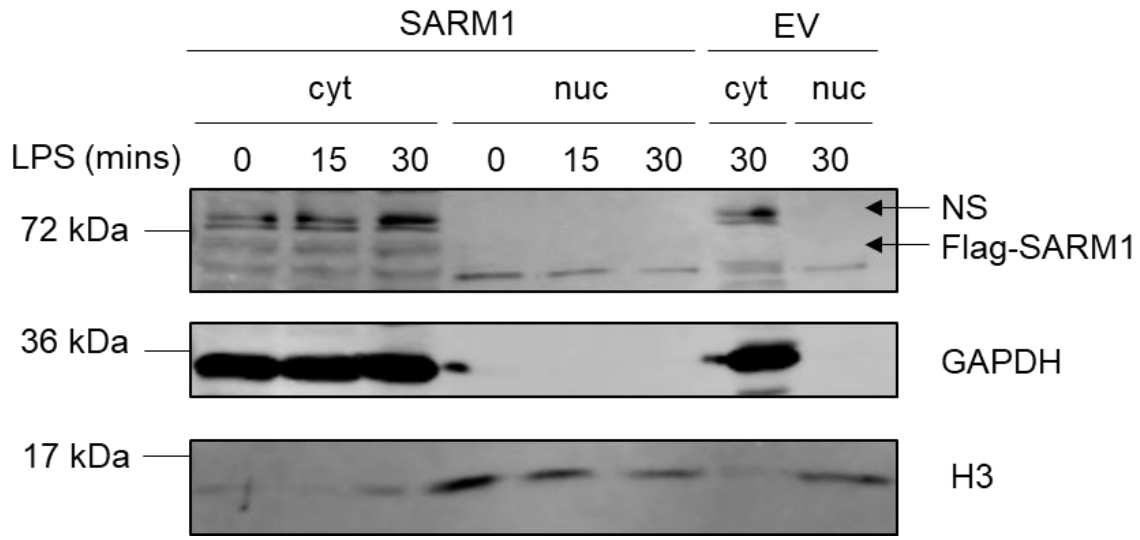

Figure 3.6 SARM1 is expressed in the cytoplasm and not the nucleus

Sarm1$^{-/-}$ iBMDMs stably expressing EV or Flag-tagged SARM1 were stimulated with 100 ng/ml LPS as indicated, then a nuclear fraction (nuc) and cytoplasmic (cyt) fraction were isolated by fractionation and subjected to SDS-PAGE. Immunoblotting was performed for SARM1 using a specific antibody to Flag, with H3 as a nuclear marker, and GAPDH as a cytoplasmic marker. NS indicates a non-specific band. Blot is representative of three independent experiments.

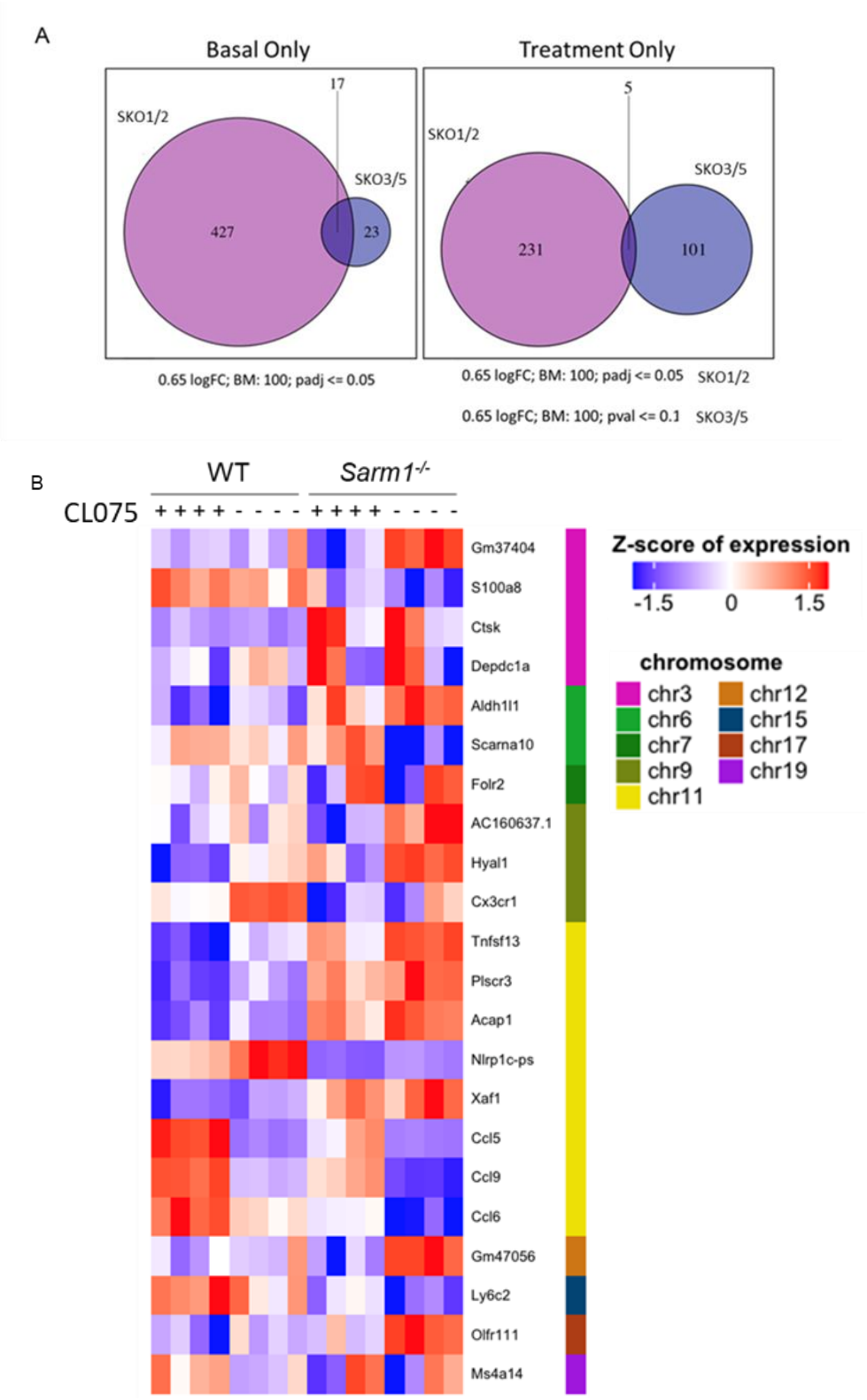

Figure 3.7 Transcriptome analysis of pBMDMs from B6 congenic *Sarm1*$^{-/-}$ mice compared to WT pBMDMs reveals numerous differentially expressed genes on chromosome 11

(A) Strategy employed to generate a list of genes which are differentially regulated in all *Sarm1*$^{-/-}$ replicates relative to WT, basally and following CL075 treatment. FC = fold change, BM = base mean.

(B) Heatmap displaying genes which are differentially expressed between WT and *Sarm1*$^{-/-}$ pBMDMs, either basally or following CL075 stimulation for three hours, grouped according to chromosome.

Figure generated by Dr Fiona Roche.

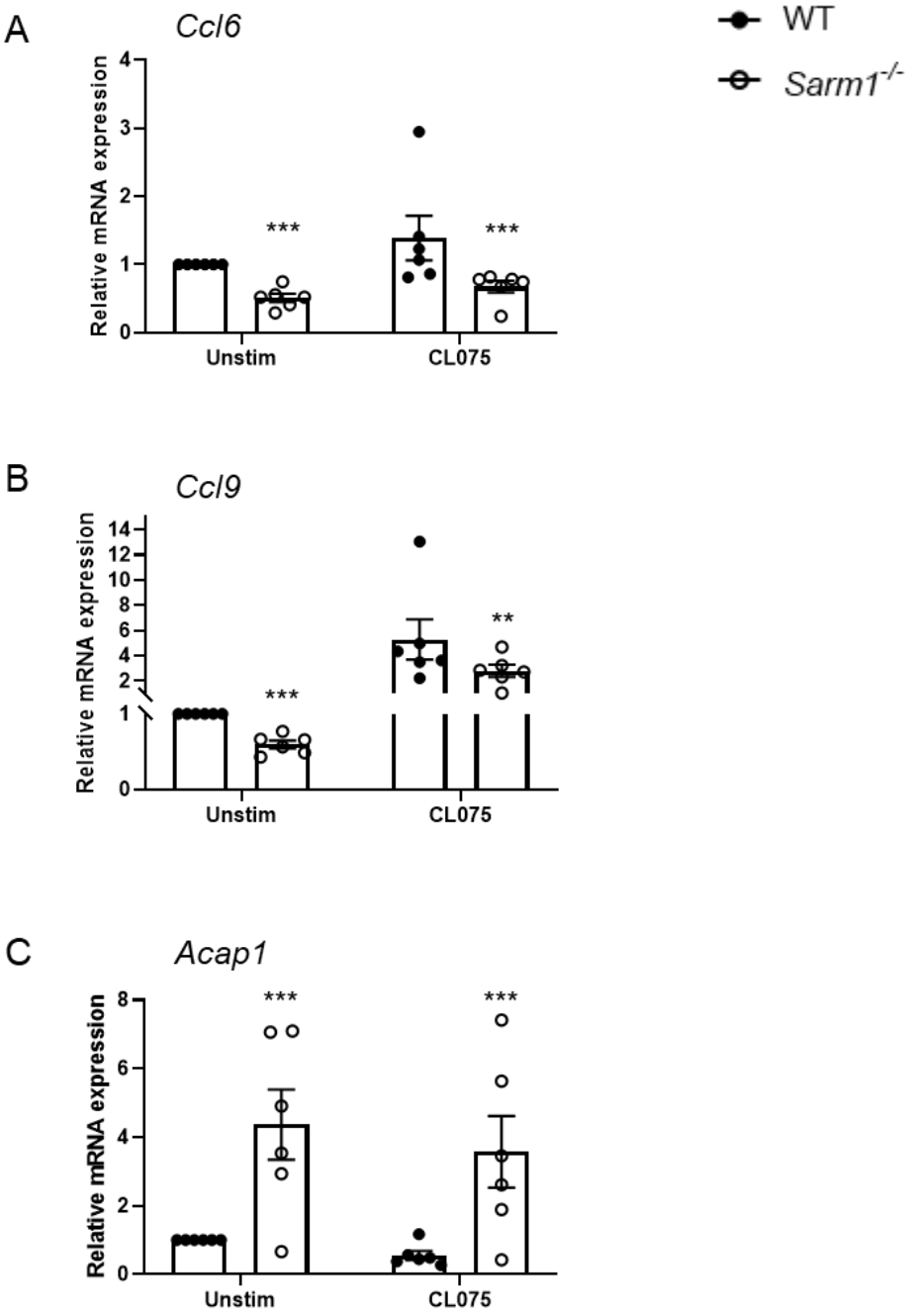

Figure 3.8 *Ccl6, Ccl9,* and *Acap1* are confirmed to be differentially expressed in *Sarm1*$^{-/-}$ pBMDMs relative to WT pBMDMs

WT and *Sarm1*$^{-/-}$ pBMDMs were stimulated with 5 μg/ml CL075 for three hours, or medium as a control. *Ccl6* (A), *Ccl9* (B), and *Acap1* (C) mRNA were measured by qRT-PCR, normalized to the housekeeping gene β-actin, and are presented relative to the untreated WT control. Graphs show mean ± SEM from 6 mice per genotype, performed in triplicate. **p<0.01, ***p<0.001, multiple Mann-Whitney tests with Holm-Šídák multiple comparisons test.

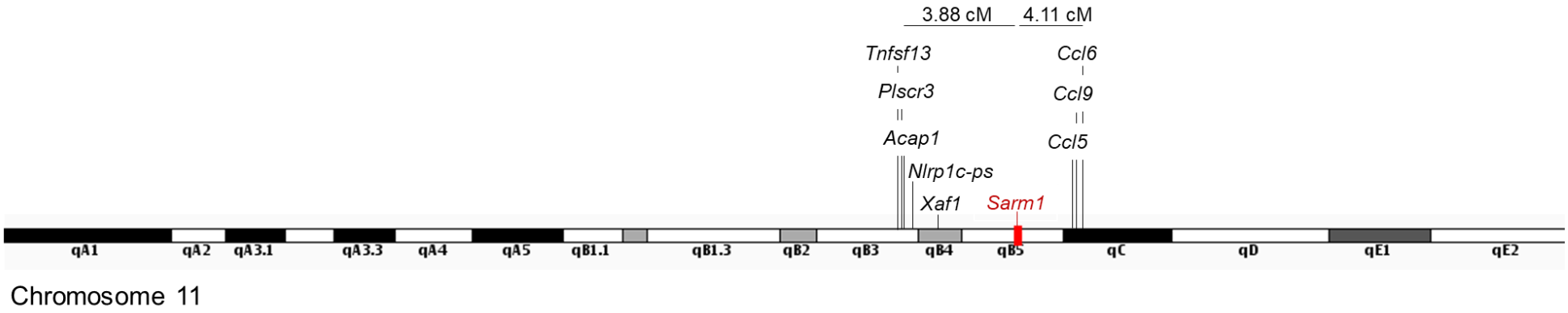

Figure 3.9 Graph of chromosome 11 indicating the position of genes which are differentially expressed in pBMDMs from B6 congenic *Sarm1*$^{-/-}$ mice compared to WT, shown relative to the *Sarm1* locus

cM = centimorgan.

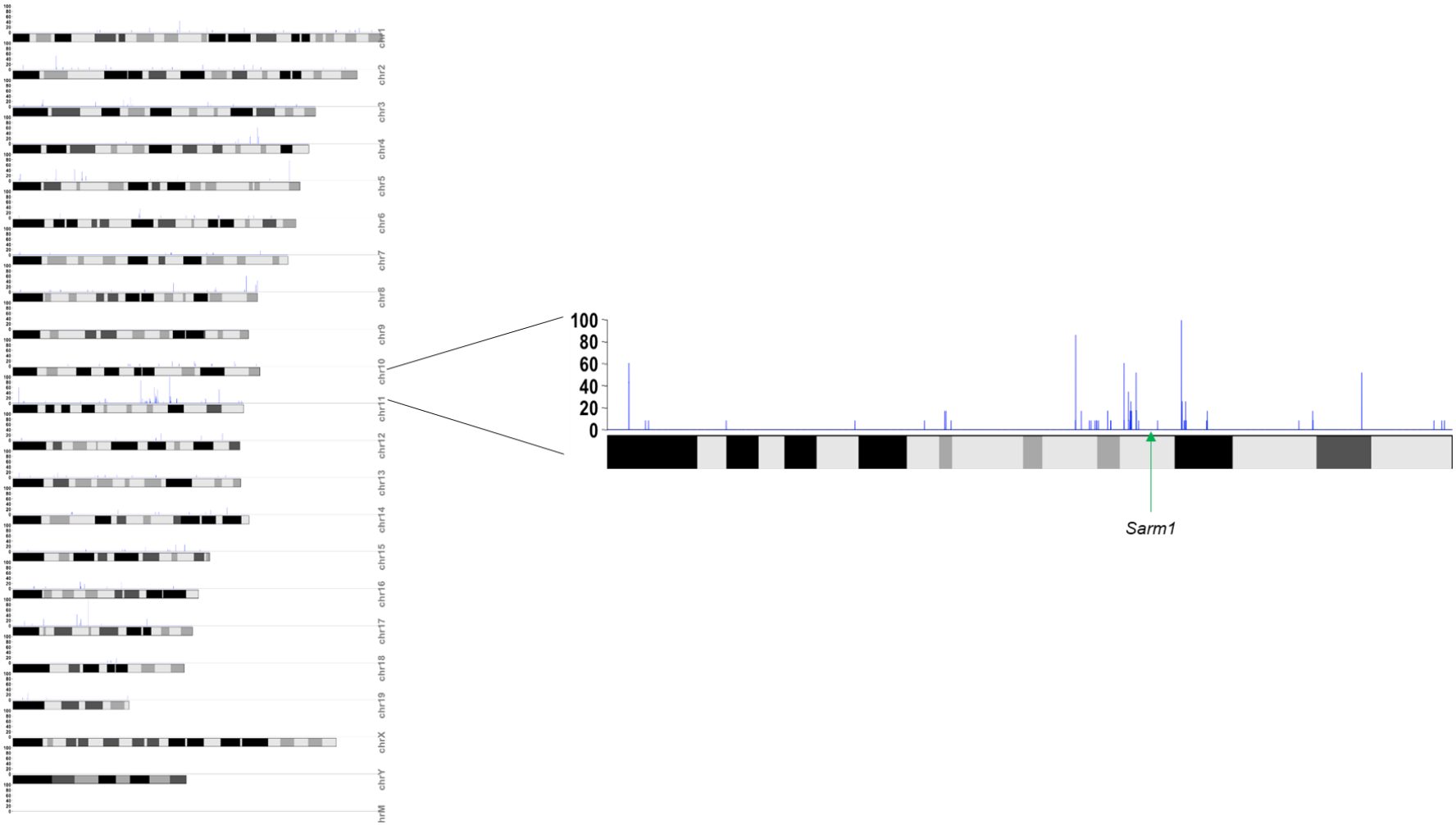

Figure 3.10 Graph showing density of SNPs and indels per 10 kb section of each chromosome in *Sarm1*$^{-/-}$ BMDMs relative to the C57BL/6 reference sequence

Density of SNPs and indels is indicated by blue bars. A larger view of chromosome 11 is shown, with the *Sarm1* locus indicated by a green arrow. Figure was generated by Dr Fiona Roche.

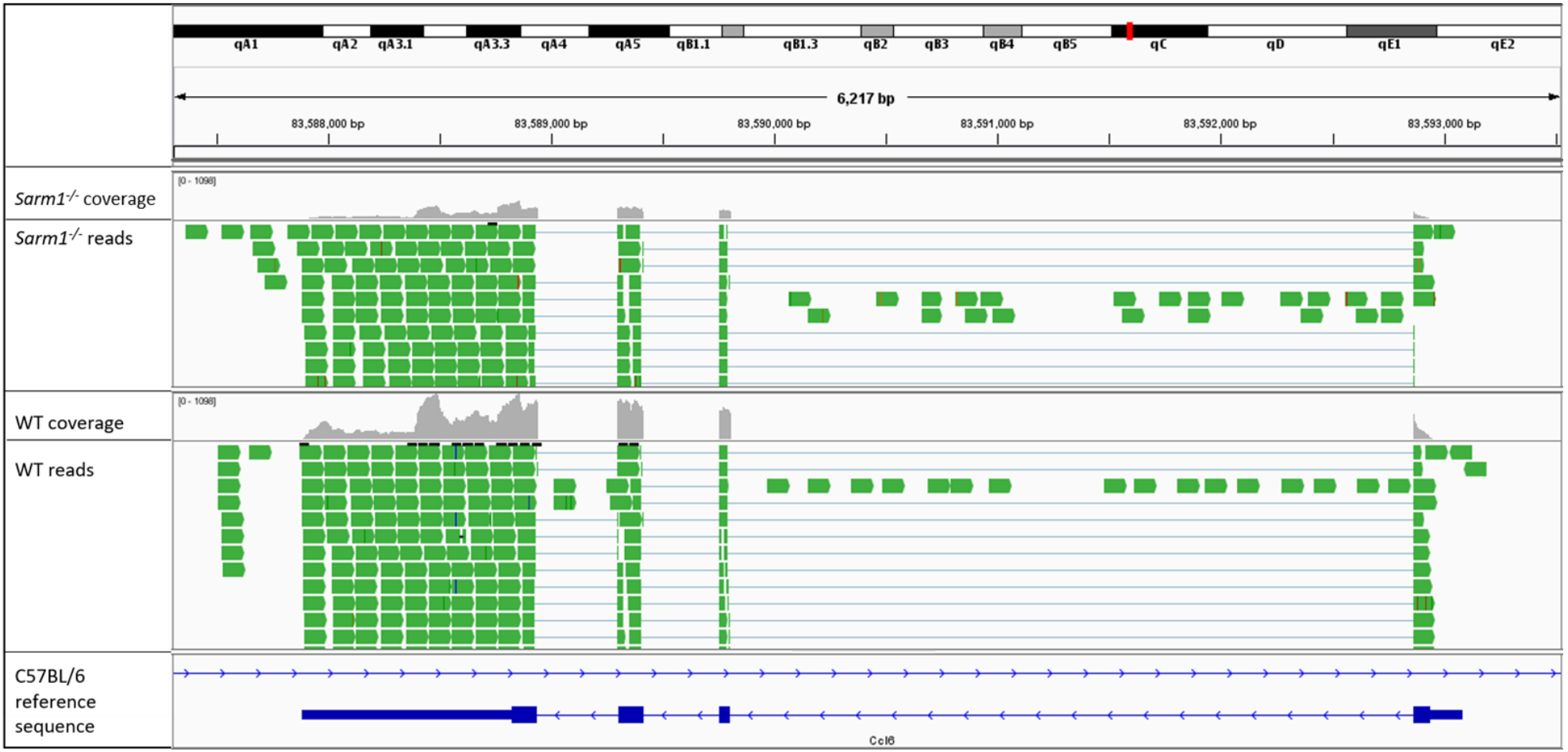

Figure 3.11 Aligned reads at the *Ccl6* locus in unstimulated *Sarm1*$^{-/-}$ and WT BMDMs visualized using IGV

Image shows coverage of the genes in grey, with variations from the C57BL/6 reference sequence denoted by coloured vertical bars.

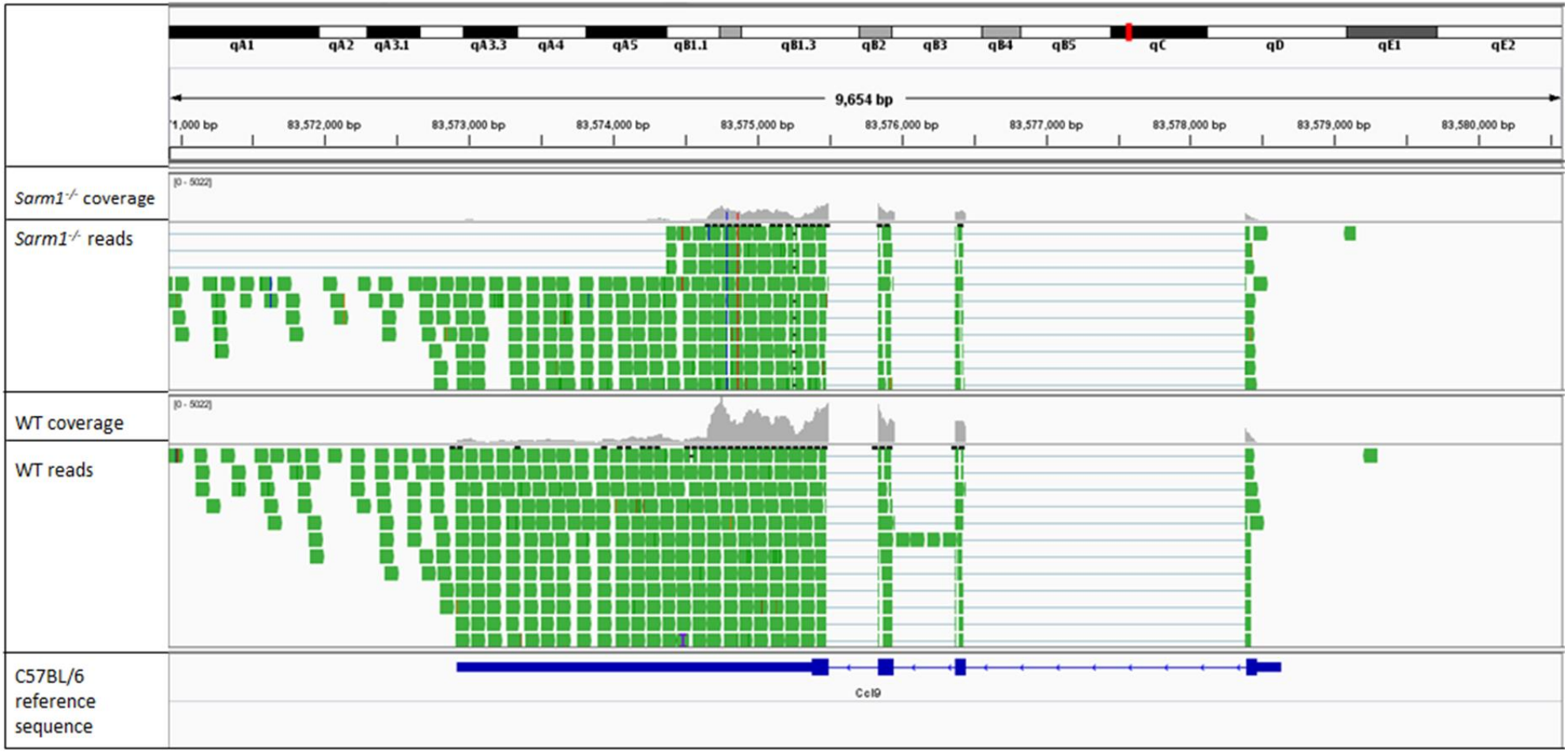

Figure 3.12 Aligned reads at the *Ccl9* locus in unstimulated *Sarm1*$^{-/-}$ and WT BMDMs visualized using IGV

Image shows coverage of the gene in grey, with variations from the C57BL/6 reference sequence denoted by coloured vertical bars.

Table 3.1 129-associated SNPs in the *Ccl9* locus in *Sarm1*$^{-/-}$ mice

Position	Reference sequence	129P2_OlaHsd	129S1_SvImJ	129S5SvEvBrd	*Sarm1*$^{-/-}$	WT
83573506	T	A	A	A	A	T
83574358	G	A	A	A	A	G
83574483	A	T	T	T	T	A
83574789	T	C	C	C	C	T
83574865	A	T	T	T	T	A
83577352	A	G	G	G	G	A
83577717	G	A	A	A	A	G
83577950	G	T	T	T	T	G
83578064	A	G	G	G	G	A
83578065	G	A	A	A	A	G
83578135	C	T	T	T	T	C

The sequence of RNA in the *Ccl9* locus in pBMDMs from WT and B6 congenic *Sarm1*$^{-/-}$ mice was compared to that of the C57BL/6 reference sequence at positions where SNPs are found in 129 strain mice. A dash (-) indicates that no reads are present at that position.

Figure 3.13 Aligned reads at the *Acap1* locus in CL075-stimulated *Sarm1*$^{-/-}$ and WT BMDMs visualized using IGV

Image shows coverage of the gene in grey, with variations from the C57BL/6 reference sequence denoted by coloured vertical bars.

Table 3.2 129-associated SNPs in the *Acap1* locus in B6 congenic *Sarm1*$^{-/-}$ mice

Position	Reference sequence	129P2_OlaHsd	129S1_SvImJ	129S5SvEvBrd	*Sarm1*$^{-/-}$	WT
69883722	A	G	G	G	G	A
69884416	T	C	C	C	C	T
69886650	A	G	G	G	-	A
69886669	A	G	G	G	-	-
69887144	A	G	G	G	-	-
69887572	A	T	T	T	T	-
69887826	C	T	T	T	T	-
69888122	C	T	T	T	-	-
69888207	G	A	A	A	A	-
69888255	C	A	A	A	-	-
69889594	G	C	C	C	-	-
69889775	A	G	G	G	G	-
69890754	C	T	T	T	-	-
69890799	A	C	C	C	-	-
69892453	C	C/G	~	C/G	G	-
69892463	C	C/G	G	~	G	-
69893032	A	G	G	G	G	-
69893127	A	G	G	G	-	-
69893537	A	T	T	T	T	-
69893845	T	C	C	C	C	T
69894408	G	A	A	A	-	G
69894987	C	T	T	T	-	-
69895070	T	C	C	C	-	-
69895170	T	A	A	A	-	-
69895222	T	~	T/G	-	-	-
69895499	A	G	G	G	G	A

The sequence of RNA in the *Acap1* locus in pBMDMs from WT and B6 congenic *Sarm1*$^{-/-}$ mice was compared to that of the C57BL/6 reference sequence at positions where SNPs are found in 129 strain mice. A dash (-) indicates that no reads are present at that position.

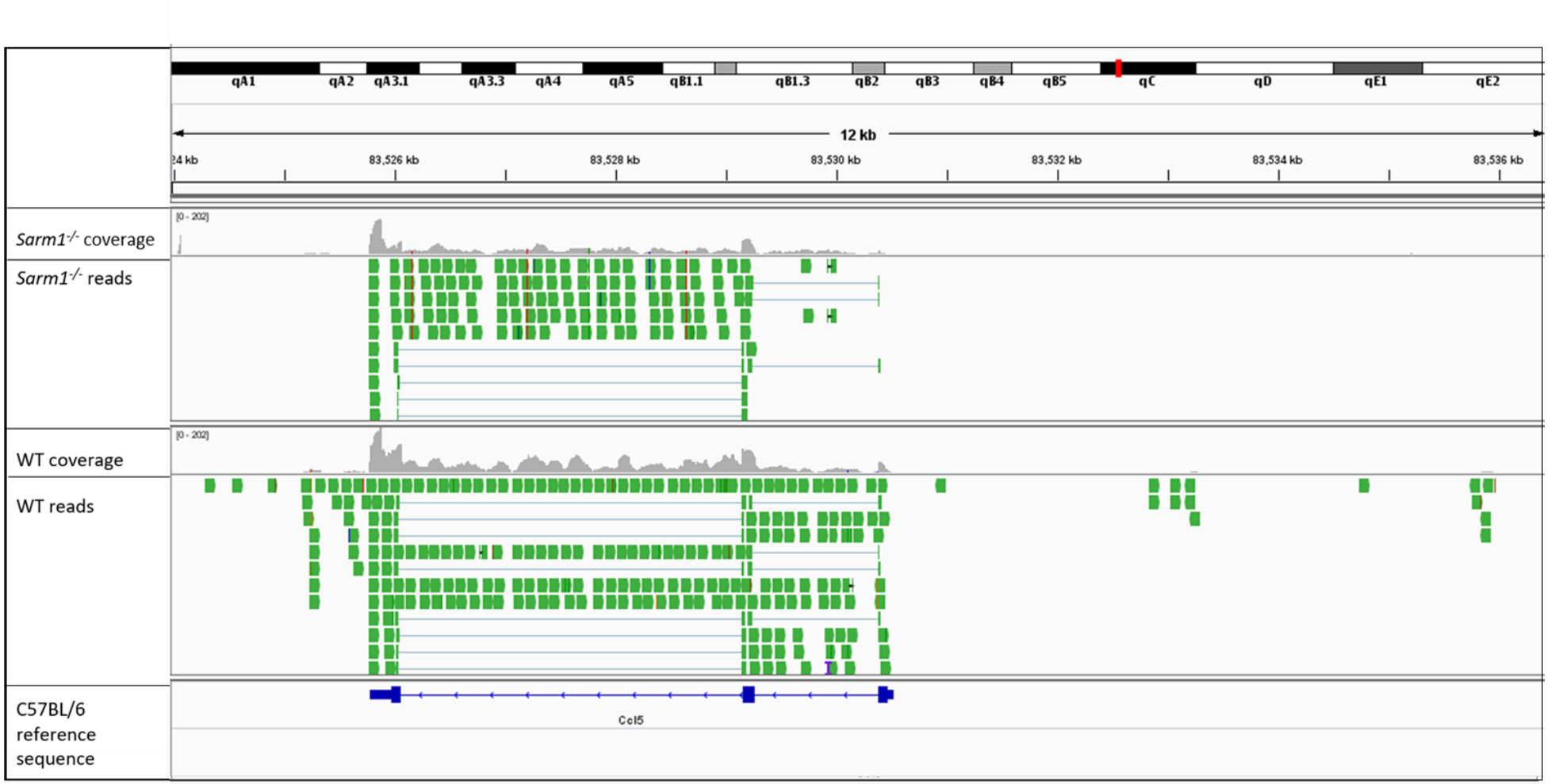

Figure 3.14 Aligned reads at the *Ccl5* locus in CL075-stimulated *Sarm1*$^{-/-}$ and WT BMDMs visualized using IGV

Image shows coverage of the gene in grey, with variations from the C57BL/6 reference sequence denoted by coloured vertical bars.

Table 3.3 129-associated SNPs in the *Ccl5* locus in B6 congenic *Sarm1*$^{-/-}$ mice

Position	Reference sequence	129P2_OlaHsd	129S1_SvImJ	129S5SvEvBrd	*Sarm1*$^{-/-}$	WT
83527207	C	T	T	T	T	C
83527768	G	A	A	A	A	G
83528313	T	C	C	C	C	T
83528651	G	T	T	T	T	G

The sequence of RNA in the *Ccl5* locus in pBMDMs from WT and B6 congenic *Sarm1*$^{-/-}$ mice was compared to that of the C57BL/6 reference sequence at positions where SNPs are found in 129 strain mice.

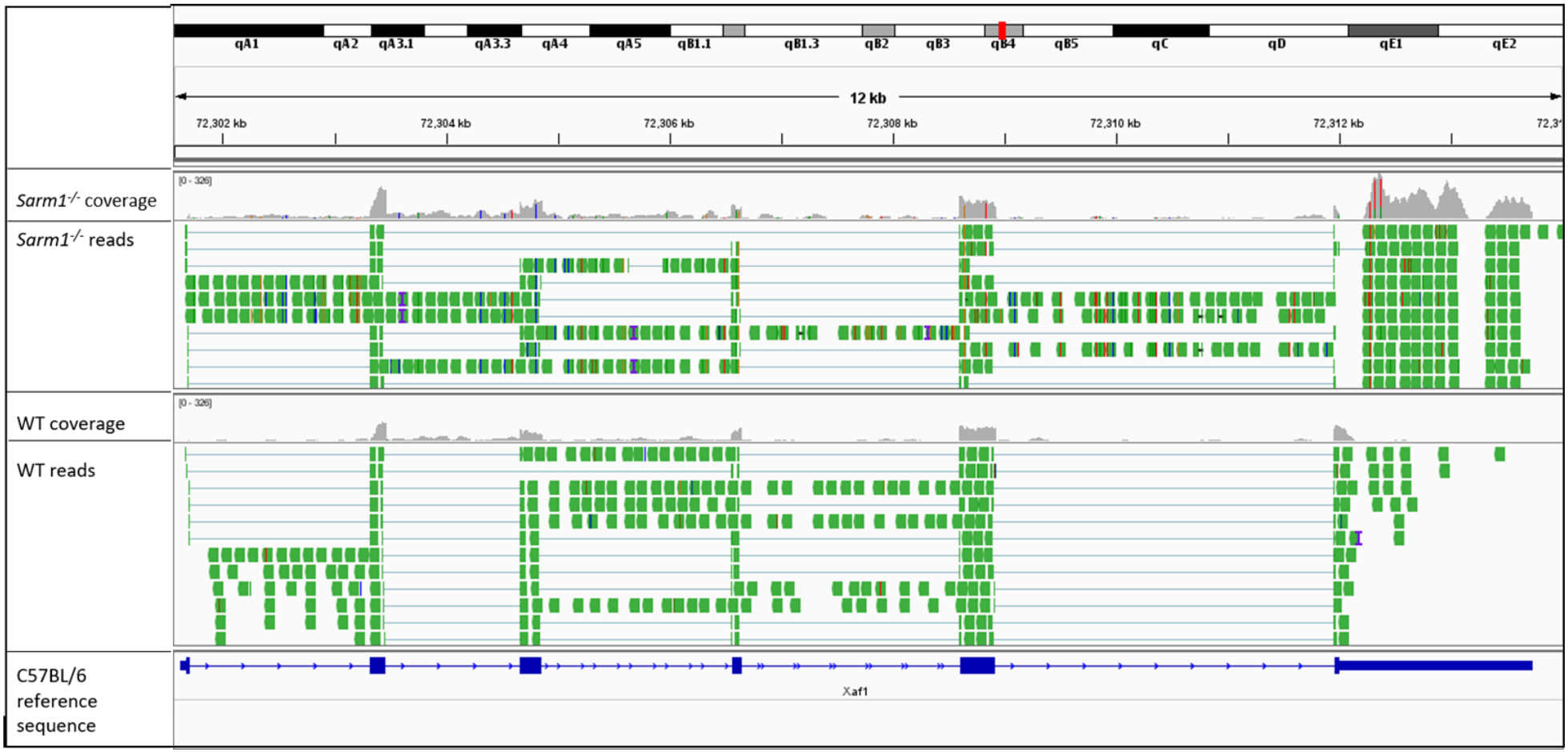

Figure 3.15 Aligned reads at the *Xaf1* locus in CL075-stimulated *Sarm1*$^{-/-}$ and WT BMDMs visualized using IGV

Image shows coverage of the gene in grey, with variations from the C57BL/6 reference sequence denoted by coloured vertical bars.

Table 3.4 129-associated SNPs in the *Xaf1* locus in B6 congenic *Sarm1*$^{-/-}$ mice

Position	Reference sequence	129P2_OlaHsd	129S1_SvImJ	129S5SvEvBrd	*Sarm1*$^{-/-}$	WT
72301750	C	A	A	A	A	C
72302259	A	G	G	G	G	A
72302345	A	G	G	G	G	-
72302580	G	C	C	C	C	G
72302826	G	A	A	A	A	G
72302834	T	C	C	C	C	T
72302846	T	C	C	C	C	T
72302908	A	G	G	G	G	A
72302959	C	A	A	A	A	C
72303085	G	A	A	A	A	G
72303149	G	A	A	A	A	G
72303151	C	G	G	G	G	C
72303205	A	T	T	T	T	A
72303231	C	G	G	G	G	C
72303583	T	C	C	C	C	T
72303758	G	A	A	A	A	G
72304311	T	C	C	C	C	T
72304402	A	G	G	G	G	A
72304534	T	C	C	C	C	T
72304593	C	T	T	T	T	C
72304815	T	C	C	C	C	T
72304984	T	C	C	C	C	T
72305104	T	C	C	C	C	T
72305144	G	A	A	A	A	G
72305218	C	T	T	T	T	C
72305344	G	A	A	A	A	G
72305417	G	A	A	A	A	G
72305594	C	G	G	G	G	C
72305980	G	A	A	A	A	G
72306243	A	G	G	G	-	A
72306300	G	A	A	A	A	G
72306341	A	G	G	G	G	A
72306449	G	A	A	A	A	G
72306452	T	C	C	C	C	T
72306493	A	T	T	T	T	A
72306600	G	A	A	A	A	G
72306603	G	C	C	C	C	G
72306608	C	A	A	A	A	C
72306628	A	G	G	G	G	A

Position	Reference sequence	129P2_OlaHsd	129S1_SvImJ	129S5SvEvBrd	*Sarm1*$^{-/-}$	WT
72306708	G	A	A	A	A	G
72306971	C	A	A	A	A	C
72306984	C	A	A	A	A	C
72307017	G	A	A	A	A	G
72307018	C	T	T	T	T	C
72307034	G	T	T	T	T	G
72307128	T	C	C	C	C	T
72307250	C	A	A	A	A	-
72307259	G	A	A	A	A	-
72307644	G	C	C	C	C	G
72307666	C	T	T	T	T	C
72307778	A	G	G	G	G	A
72307801	A	G	G	G	G	A
72307820	T	A	A	A	A	T
72307905	C	T	T	T	T	C
72308017	T	t/c	-	t/c	T	T
72308062	A	G	G	G	G	A
72308198	C	T	T	T	T	C
72308241	T	A	A	A	A	T
72308342	T	G	G	G	G	T
72308444	A	C	C	C	C	A
72308490	T	C	C	C	C	T
72308491	G	A	A	A	A	G
72308542	C	T	T	T	T	C
72308557	A	C	C	C	C	A
72308563	T	G	G	G	G	T
72308650	A	G	G	G	G	A
72308837	C	T	T	T	T	C
72308966	T	G	G	G	G	T
72309030	G	C	C	C	-	G
72309055	T	C	C	C	C	T
72309097	A	C	C	C	C	-
72309152	G	A	A	A	A	-
72309388	T	G		~	-	T
72309427	G	A	A	A	-	G
72311997	G	A	A	A	A	G
72312000	C	A	A	A	-	C
72312278	C	T	T	T	T	C
72312302	A	-	A/T	-	A	A
72312320	T	-	T/A	T/A	T/A	T

The sequence of RNA in the *Xaf1* locus in pBMDMs from WT and B6 congenic *Sarm1*$^{-/-}$ mice was compared to that of the C57BL/6 reference sequence at positions where SNPs are found in 129 strain mice. Indicated in red is the position at which the SNP described in 129 mice results in a premature stop codon. A dash (-) indicates that no reads are present at that position.

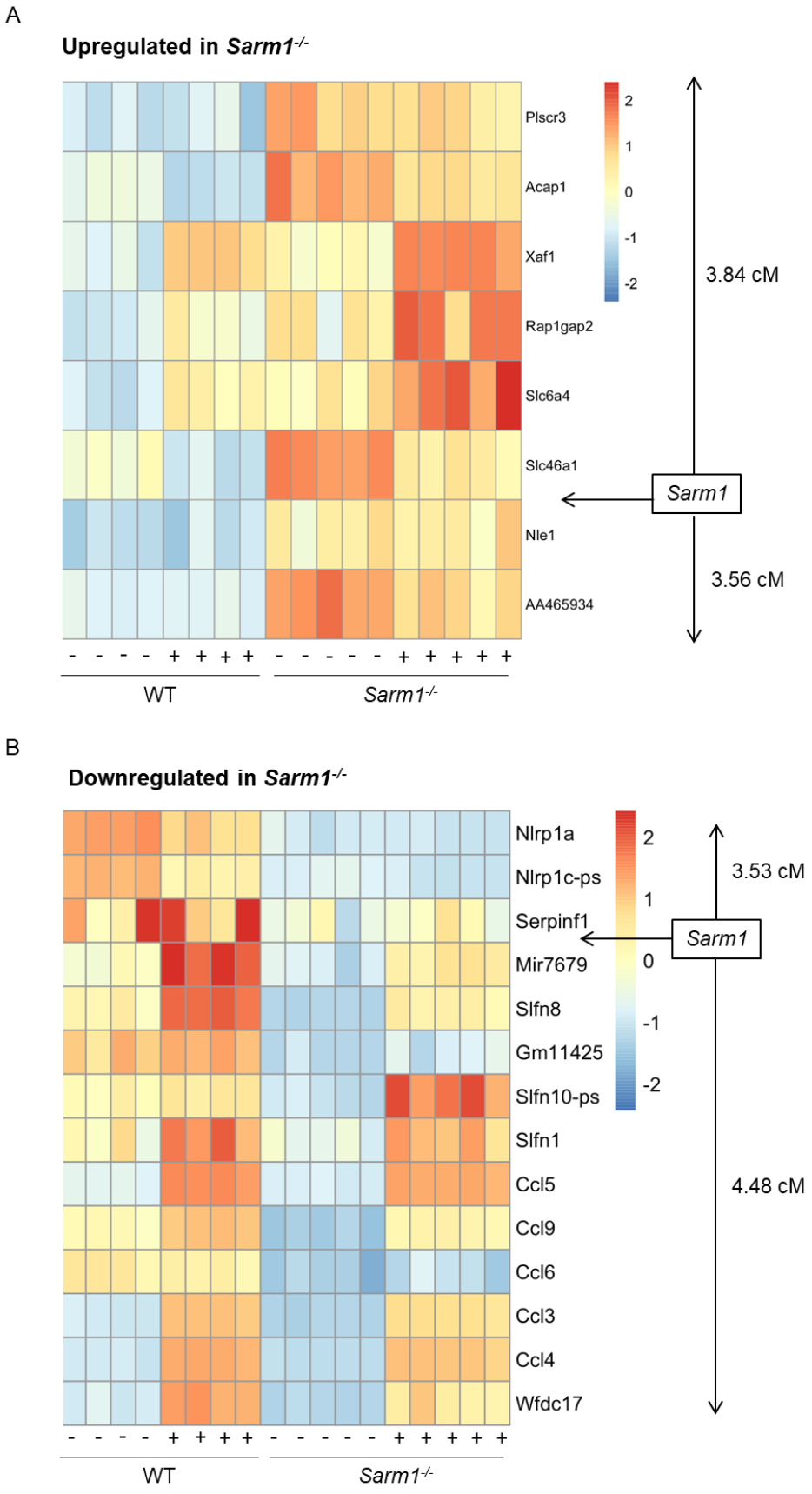

Figure 3.16 Heatmaps showing genes which are basally differentially expressed in *Sarm1*$^{-/-}$ pBMDMs relative to WT

Heatmaps were generated showing the genes on chromosome 11 which are basally upregulated (A) or downregulated (B) in *Sarm1*$^{-/-}$ pBMDMs relative to WT, ordered according to their position relative to the *Sarm1* locus. Figure generated by Dr Fiona Roche.

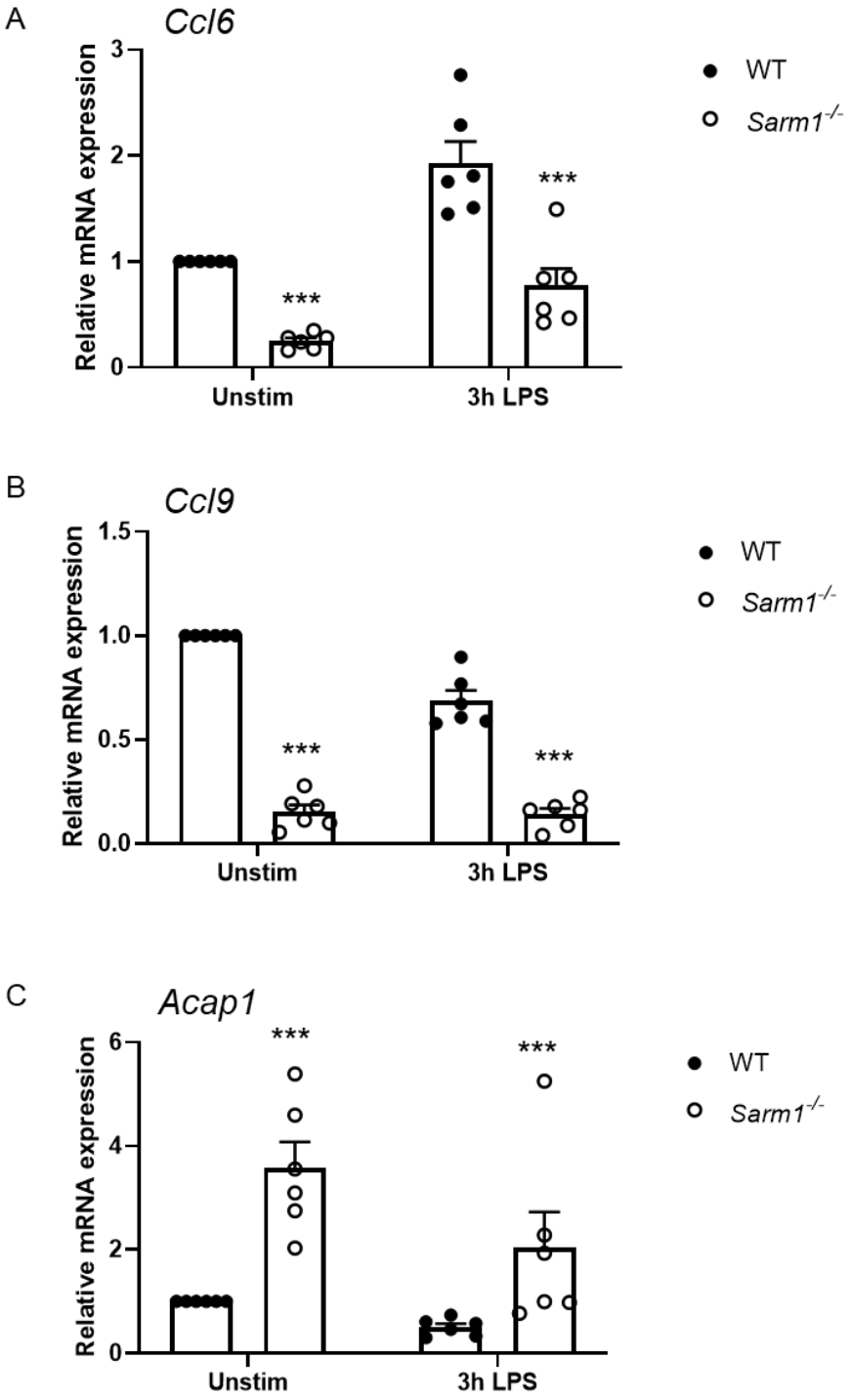

Figure 3.17 *Ccl6*, *Ccl9*, and *Acap1* are confirmed to be differentially expressed in *Sarm1*$^{-/-}$ pBMDMs relative to WT pBMDMs

WT and *Sarm1*$^{-/-}$ pBMDMs were stimulated with 100 ng/ml LPS for three hours, or medium as a control. *Ccl6* (A), *Ccl9* (B), and *Acap1* (C) mRNA were measured by qRT-PCR, normalized to the housekeeping gene β-actin, and are presented relative to the untreated WT control. Graphs show mean ± SEM from 6 mice per genotype, performed in triplicate. **p<0.01, ***p<0.001, multiple Mann-Whitney tests with Holm-Šídák multiple comparisons test.

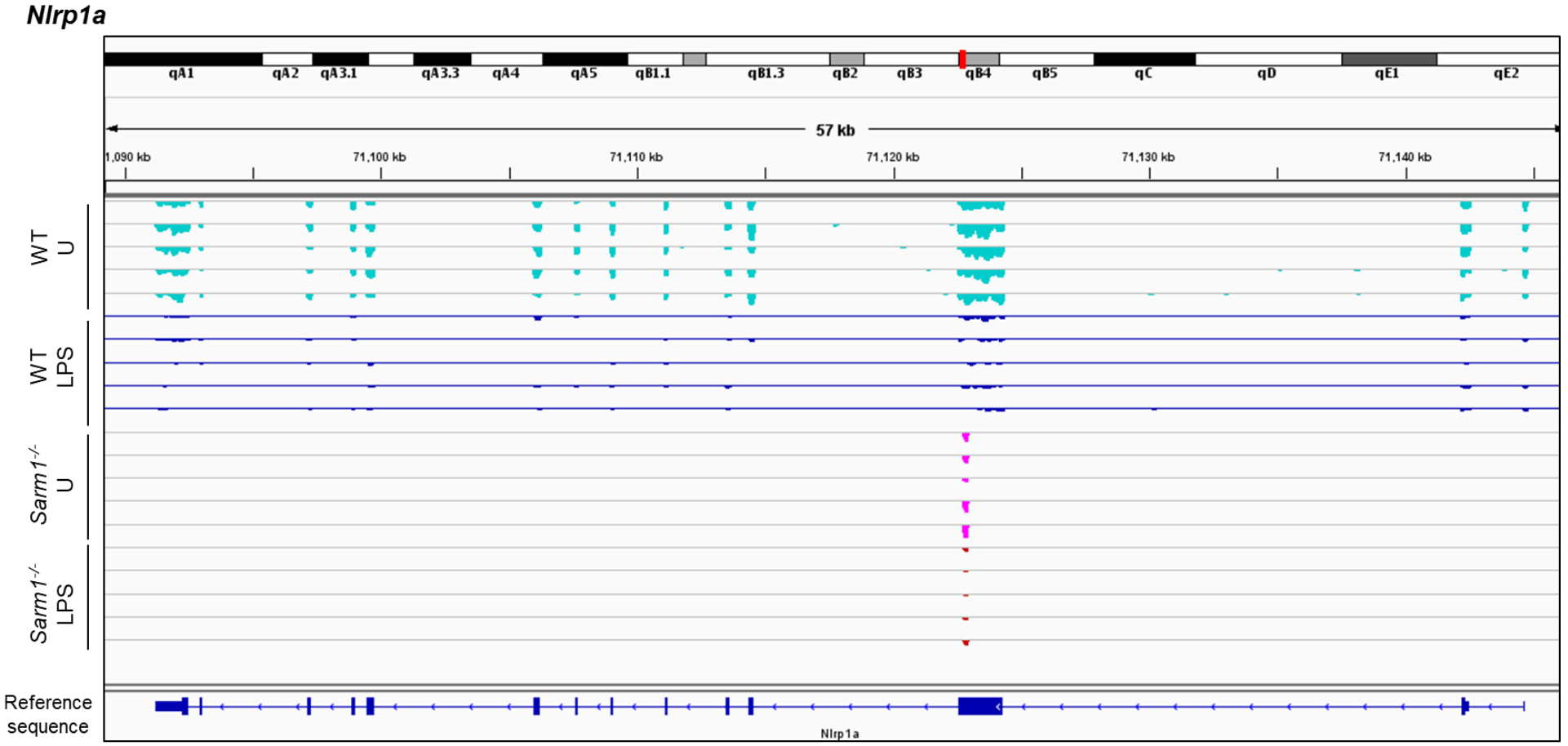

Figure 3.18 Different *Nlrp1a* transcripts are expressed in WT and *Sarm1*$^{-/-}$ BMDMs

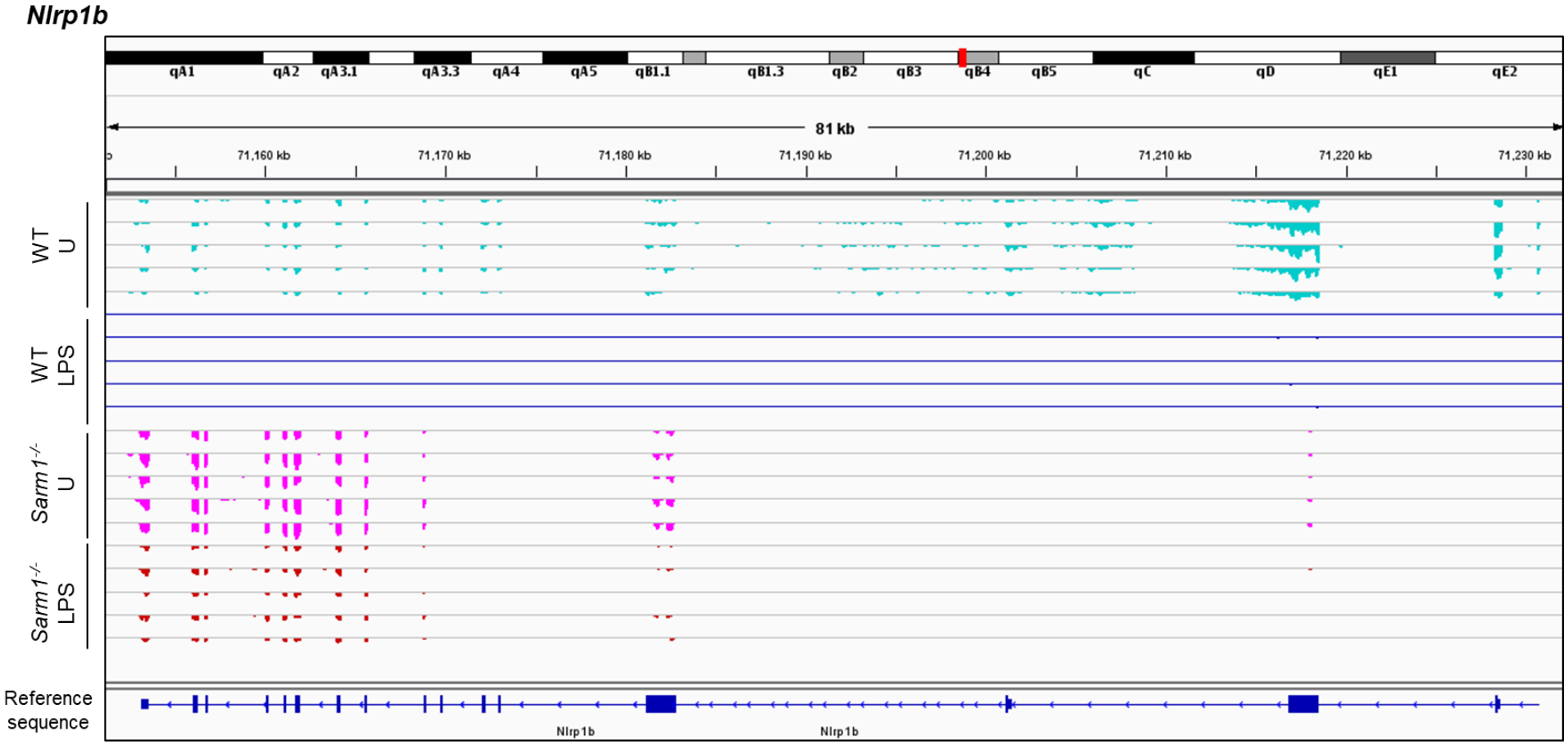

Figure 3.19 Different *Nlrp1b* transcripts are expressed in WT and *Sarm1*$^{-/-}$ BMDMs

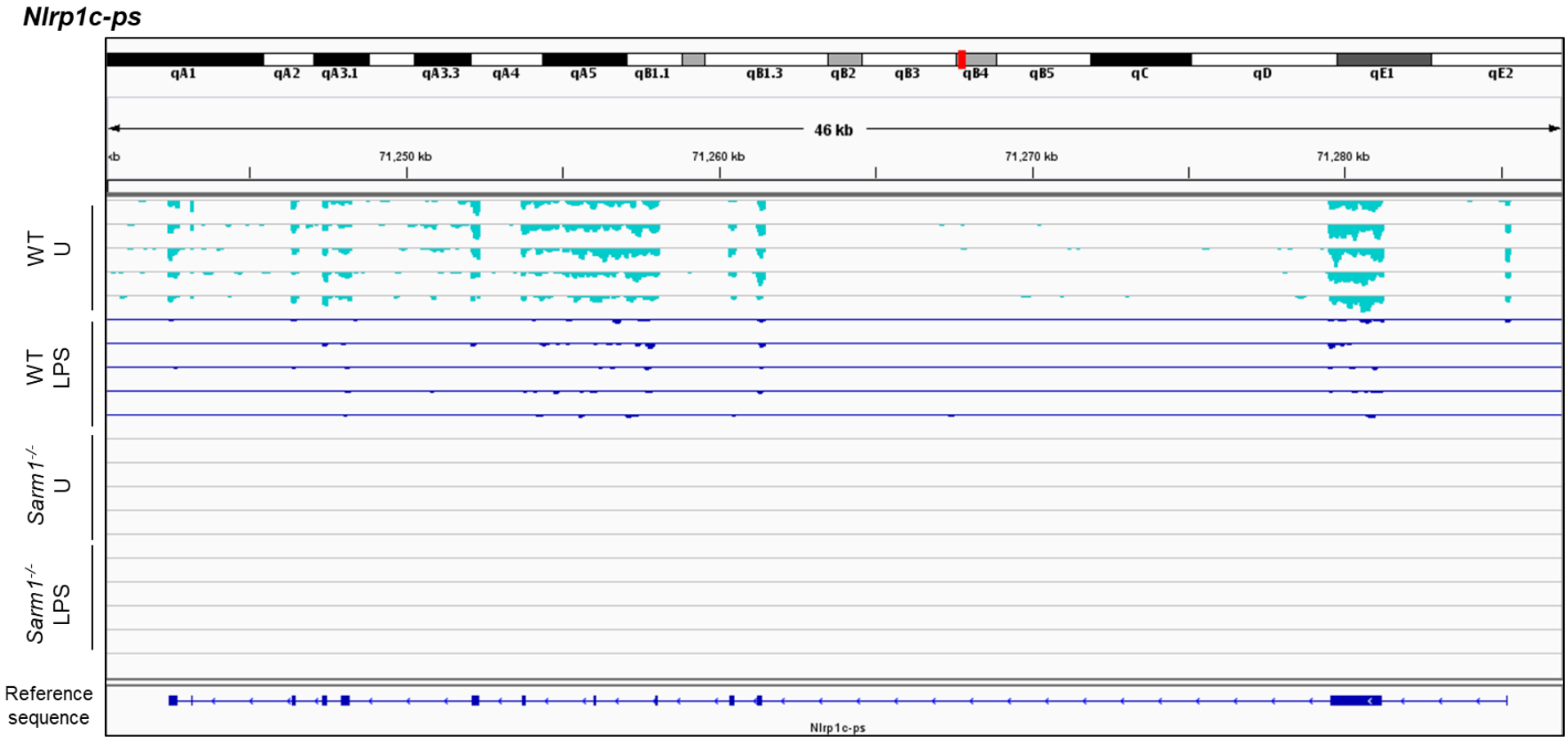

Figure 3.20 *Nlrp1c-ps* is expressed in WT but not *Sarm1*$^{-/-}$ BMDMs

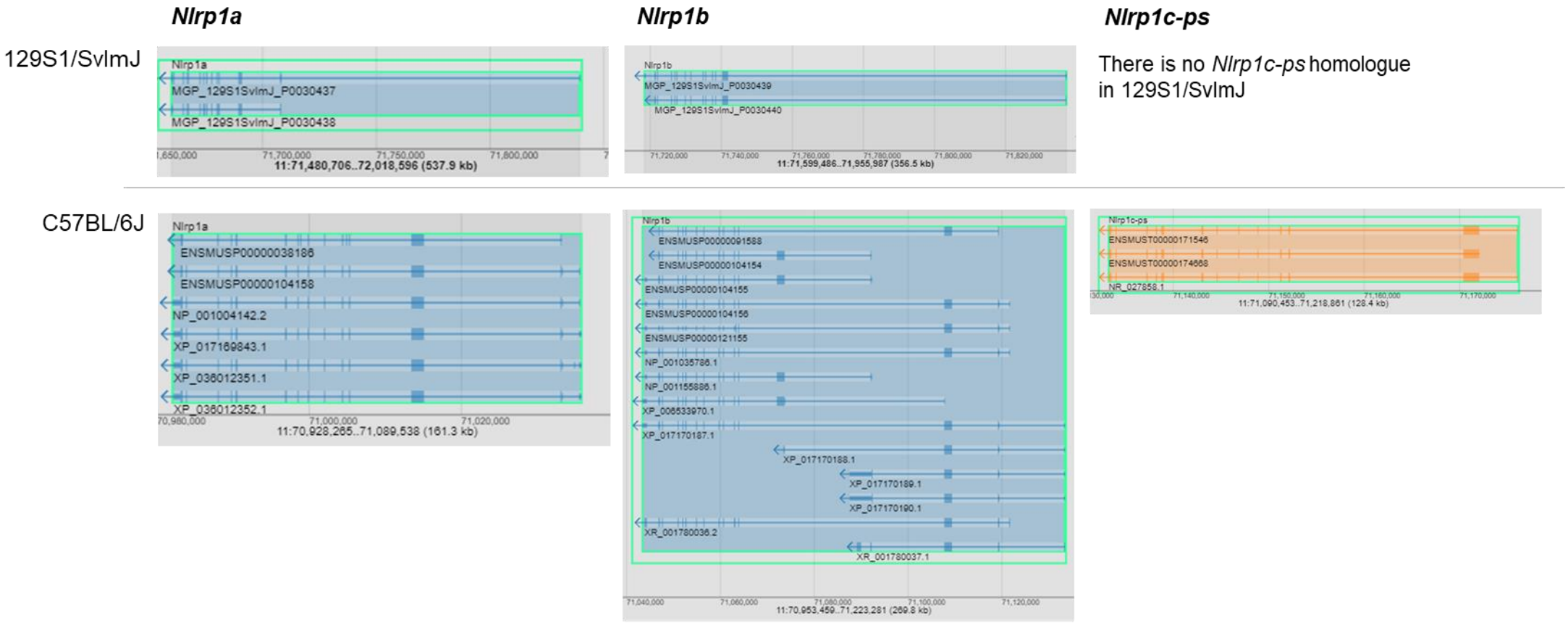

Figure 3.21 Different transcripts of the *Nlrp1* paralogues are expressed in C57BL/6 and 129 strains of mice

Images from the MGI MGV showing the different transcripts of *Nlrp1a*, *Nlrp1b*, and *Nlrp1c-ps* expressed in 129S1/SvImJ mice and C57BL/6J mice.

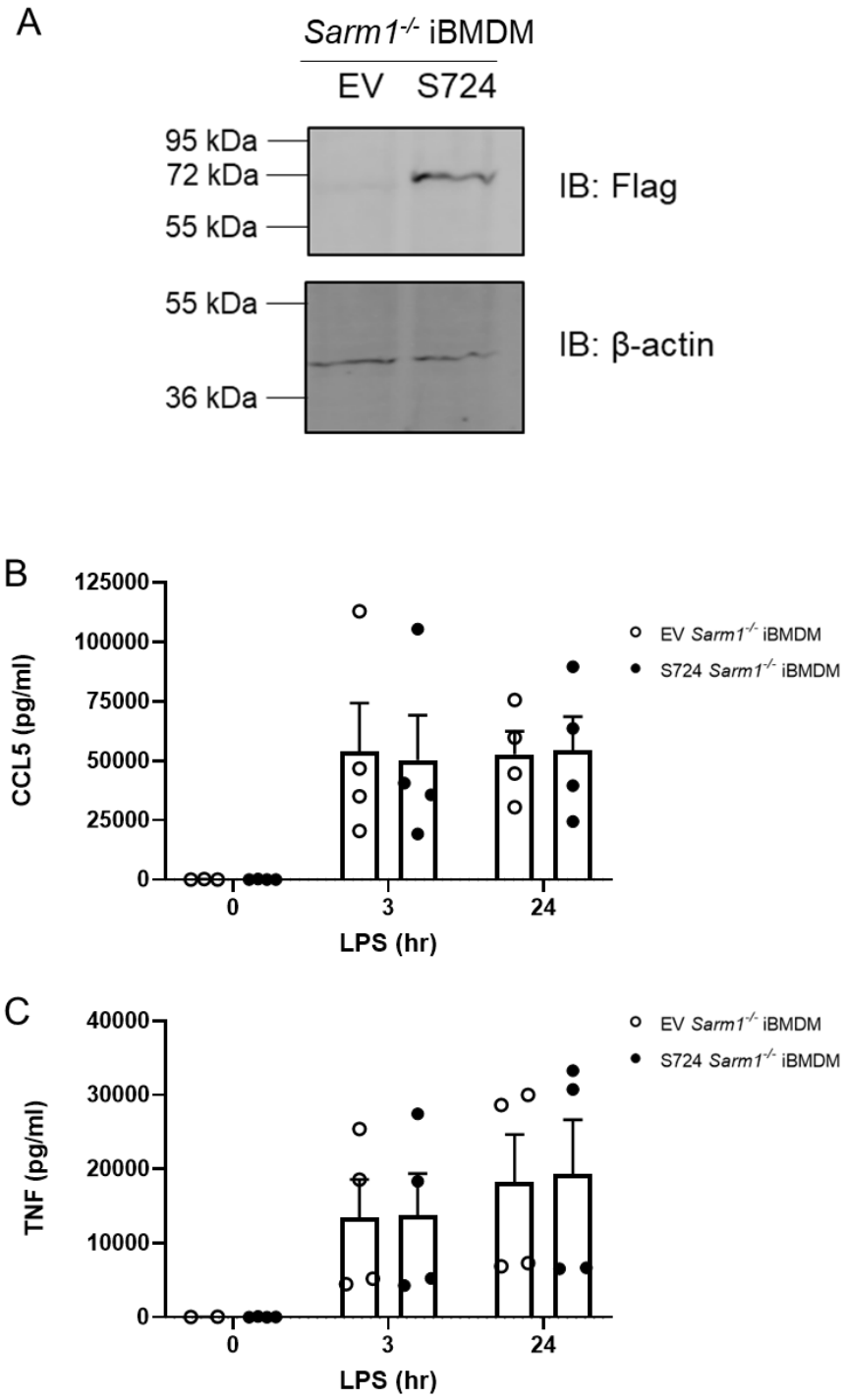

Figure 3.22 Stable expression of SARM1 does not augment CCL5 secretion in *Sarm1*$^{-/-}$ iBMDMs

(A) Immunoblot confirming expression of Flag-tagged SARM1 in S724 expressing *Sarm1*$^{-/-}$ iBMDMs and not in EV.
(B, C) S724 and EV expressing *Sarm1*$^{-/-}$ iBMDMs were stimulated for 3 h or 24 h with 100 ng/ml LPS, or with medium as a control. Supernatants were assayed for CCL5 (B) and TNF (C) protein by ELISA. Data are mean ±SEM from 4 mice per genotype, performed in triplicate. There were no significant differences determined by multiple Mann-Whitney tests with Holm-Šídák multiple comparisons test.

3.3 Discussion

While the role of SARM1 is well-characterised in the murine nervous system, much less is known currently about the function of SARM1 in murine immune cells. Thus the initial aim of this study was to determine the mechanism by which SARM1 regulates *Ccl5* expression in murine BMDMs, and to investigate which other genes, if any, are similarly regulated. Having confirmed that *Ccl5* expression was impaired in both primary and immortalised BMDMs, I sought to ascertain if there were any differences in transcriptional phenotype between *Sarm1*$^{-/-}$ iBMDMs and pBMDMs which may influence their suitability for various experiments. In her PhD thesis, Dr Claudia Gürtler characterised the expression of IRF3 in these iBMDMs. She found that basal IRF3 expression was reduced in the *Sarm1*$^{-/-}$ iBMDM, but not pBMDM, relative to their WT counterparts on the mRNA and protein level. Given that IRF3 contributes to NO induction in murine macrophages after TLR stimulation [224], I measured the NO levels in supernatants of *Sarm1*$^{-/-}$ iBMDM and pBMDM compared to WT after LPS stimulation. Interestingly, in keeping with their reduced IRF3 levels, NO production was dramatically reduced in *Sarm1*$^{-/-}$ iBMDM. This reduction was not observed in *Sarm1*$^{-/-}$ pBMDM under similar conditions. *Il6* expression is also regulated by IRF3 in mouse macrophages [225] and IL-6 has been implicated as a driver of NO production in mouse macrophages [224]. Thus I measured IL-6 production in *Sarm1*$^{-/-}$ iBMDM and pBMDM compared to their WT counterparts. Surprisingly, following both TLR4 and TLR7 stimulation, IL-6 production was consistently augmented in *Sarm1*$^{-/-}$ iBMDM compared to WT. In contrast, *Sarm1*$^{-/-}$ pBMDM had similar IL-6 production to WT. Reduced NO production in *Sarm1*$^{-/-}$ iBMDM is congruent with their reduced IRF3 levels. However, it is unclear why IL-6 production is elevated in the *Sarm1*$^{-/-}$ iBMDM, as the anticipated effect of reduced IRF3 would be reduced IL-6.

Given that *Sarm1*$^{-/-}$ pBMDM did not display diminished NO production and enhanced IL-6 production as seen in *Sarm1*$^{-/-}$ iBMDM, these phenotypes are not attributable to the absence of SARM1. Rather, it is possible that the process of differentiating and immortalising BMDMs, described in detail in Section 2.2.5, created or amplified differences in phenotype between the WT and B6 congenic *Sarm1*$^{-/-}$ mice from which these iBMDM were derived. A study published in 2013 found that bone marrow cells plated at a low density during differentiation secreted higher levels of pro-inflammatory cytokines including IL-6 and TNF, but lower NO levels, than those plated at higher densities [226].

It is possible therefore that bone marrow cells from which the *Sarm1*$^{-/-}$ iBMDM were derived were seeded at a lower density than their WT counterparts. However, this explanation cannot account for the observation that TNF production was not significantly different between WT and *Sarm1*$^{-/-}$ iBMDM. Another factor which must be considered is that each of the immortalised cell lines is only representative of a single mouse. Thus, differences in gene expression may be a result of biological variation. Further, it is unclear if these iBMDM were derived from sex- and age-matched mice. If the WT and B6 congenic *Sarm1*$^{-/-}$ mice used to generate these iBMDM were not sex-matched, they may exhibit different immune responses due sexual dimorphism [227]. Similarly, age is a factor which governs expression of pro-inflammatory genes in murine BMDMs [228], so aberrant gene expression could be due to the mice from which these cells were derived not being age-matched. Regardless of the source of disparity in phenotype between immortalised and primary *Sarm1*$^{-/-}$ iBMDM, it is clear that the iBMDM are unsuitable as a tool for broad study of transcription of inflammatory genes in the absence of SARM1. This emphasises the importance of exercising caution when interpreting results from cell lines such as these, particularly where details of the provenance are unclear.

Despite these limitations, *Sarm1*$^{-/-}$ iBMDM which stably expressed S724 were useful in determining the subcellular localisation of SARM1 under resting and stimulated conditions. SARM1 is difficult to detect in murine macrophages using commercially available antibodies, and as a result this and other similar studies rely on exogenous stably expressed epitope-tagged SARM1. We have no evidence that this tag influences SARM1 activity, however. In agreement with published data from our lab [25] and from others, SARM1 was not detected in the nucleus of murine BMDMs. It remains possible that the C-terminal Flag-tag appended to SARM1 may interfere with the localisation and function of SARM1, as reconstitution of *Sarm1*$^{-/-}$ iBMDMs with this epitope-tagged protein did not restore the purported function of SARM1 of increasing CCL5 expression. However, the SARM1 sequence contains an N-terminal mitochondrial localisation sequence (MLS) [24], and does not contain any predicted NLS according to the Rost lab NLSdb [229]. Additionally, there are no reported instances in the literature of endogenous SARM1 localising to the nucleus. Thus, as it is likely restricted to the cytoplasm and mitochondria, SARM1 is likely to be excluded from interacting with known regulatory protein in the nucleus. Additionally, any NAD^+ depletion caused by SARM1 NADase activity would be

locally in the cytoplasmic or mitochondrial, and not nuclear, compartments, and would therefore be unlikely to alter the activity of chromatin accessibility modulating enzymes.

Having disqualified SARM1 presence in the nucleus as a contributor to transcriptional regulation of *Ccl5* expression, and confirmed the absence of the confounding impact of SARM1 antagonism of TLR signalling, I sought to examine the broader role for SARM1 in transcription. Thus, RNA sequencing was employed with the intention of finding out which genes other than *Ccl5*, if any, are differentially expressed in *Sarm1*$^{-/-}$ BMDMs relative to WT, and to shed some light on the mechanism by which they are regulated by SARM1. However, it emerged that the common factor among a disproportionate fraction of the DEGs was their location on chromosome 11, the chromosome on which both the *Sarm1* and *Ccl5* loci reside. As the B6 congenic *Sarm1*$^{-/-}$ mice from which these BMDMs are derived were generated by targeted gene disruption using unspecified 129X1/SvJ mouse embryonic stem cells, proximity to the targeted *Sarm1* locus was examined. All eight of the differentially expressed genes on chromosome 11 were located within 5 cM of the *Sarm1* locus. During their development, these B6 congenic *Sarm1*$^{-/-}$ mice were reportedly backcrossed to C56BL/6 mice for 15 generations to exclude as much 129X1/SvJ donor genetic material as possible and create a *Sarm1*$^{-/-}$ mouse on the C57BL/6 background. However it is now appreciated that the region flanking the target gene in congenic mice made this way remains of donor origin, unless separated by recombination [230]. The probability that a region of 5 cM flanking either side of the SARM1 locus remains of donor 129/SvJ origin after 16 generations of backcrossing to C57BL/6 is 46.3%. Given the very high density of SNPs and indels that was visible in the region flanking the *Sarm1* locus in the *Sarm1*$^{-/-}$ BMDMs relative to the C57BL/6 reference sequence, it seems likely that the portion of chromosome 11 on which these DEGs reside is of donor origin and that the DEGs are passenger genes. It is important to acknowledge that the density of SNPs and indels was calculated from the transcriptome, and therefore represents only the parts of the genome which was transcribed at the time of the experiment. This is a limitation of this experiment, as it likely masks the extent to which the region flanking the *Sarm1* locus in the genome of *Sarm1*$^{-/-}$ BMDMs deviates from the C57BL/6 reference sequence.

The mRNA expression of three of the DEGs in this region on chromosome 11, *Ccl6, Ccl9,* and *Acap1,* was experimentally confirmed to differ between WT and *Sarm1*$^{-/-}$ BMDMs both with and without stimulation. As these are likely passenger genes, the sequence of reads

mapping to these loci in *Sarm1*$^{-/-}$ BMDMs was examined at the base pair level, and compared to that of WT BMDMs, the C57BL/6 reference sequence, and SNPs which are associated with a number of 129 strains. Indeed, reads mapped to *Ccl9* and *Acap1* in *Sarm1*$^{-/-}$ BMDMs both harboured all of the listed 129-associated SNPs, and each of these SNPs were present in 100% of reads at the given location. None of these SNPs were detected in the WT BMDMs, which matched the C57BL/6 reference sequence. No SNPs were present in the reads mapping to the *Ccl6* locus in *Sarm1*$^{-/-}$ BMDMs, however the only listed 129-associated SNPs were in intronic sequences in the gene and so no reads were mapped to those parts. How the sequence of promoters and enhancers associated with the DEGs may differ between WT and *Sarm1*$^{-/-}$ remains unknown, as the sequence of only the transcribed mRNA is available through this RNA sequencing experiment. Whether the presence of passenger mutations in the DEGs observed in *Sarm1*$^{-/-}$ BMDMs is responsible for their altered transcription is also unclear at this point. Thus, we can't currently delineate if differential gene expression in *Sarm1*$^{-/-}$ BMDMs is due to the presence of passenger genes or the absence of SARM1, and this will be the focus of Chapter 4.

In addition to discovering genes on chromosome 11 with a different level of expression in *Sarm1*$^{-/-}$ BMDMs compared to WT, some genes expressed different transcripts in *Sarm1*$^{-/-}$ and WT BMDMs. This includes *Xaf1*, the transcript of which possessed an extended 3' untranslated region (UTR) in *Sarm1*$^{-/-}$ BMDMs relative to WT. The 3' UTR plays a major role in determining the posttranscriptional fate of an mRNA transcript, particularly its stability. The 3' UTR contains many regulatory elements and sites, and can be targets of micro RNAs (miRNAs) and RNA binding proteins (RBPs) [231]. Whether these specific interactions are negative or positive determines if an extended 3' UTR enhances or diminishes the mRNA stability. Perhaps the augmented expression of *Xaf1* mRNA in *Sarm1*$^{-/-}$ is a consequence of enhanced mRNA stability as a result of the extended 3'UTR relative to the WT transcript, rather than increased transcription of the gene. Closer inspection of the *Xaf1* sequence revealed many 129-associated SNPs, indicating that it is a passenger gene of 129/SvJ origin. One such SNP results in a premature stop codon, truncating the final 3 amino acids of the XAF1 protein in *Sarm1*$^{-/-}$ BMDMs. The impact that this may have on the resulting protein's stability could not be measured, as commercially available antibodies lacked the required specificity to measure XAF1 protein levels by Western blot. However, similar findings were published by the García-Sastre lab during the course in this study, wherein they generated *Xaf1*$^{-/-}$cells and used them to discern

which of the many bands detected by an XAF1 antibody was the correct band. They could then measure XAF1 expression in splenocytes from poly(I:C) treated WT and B6 congenic *Sarm1*$^{-/-}$ mice, and found that a novel band of lower molecular weight exclusively in the *Sarm1*$^{-/-}$ splenocytes. This could be representative of a truncated XAF1, the translated product of the *Sarm1*$^{-/-}$ transcript with a premature stop codon. This truncated C-terminus could affect the protein's function; it is the C-terminal region of XAF1 which mediates binding to XIAP [232]. This warrants re-examination of studies pertaining to cell death which were performed in B6 congenic *Sarm1*$^{-/-}$ mice, including that defining a role of SARM1 in slowing the progression of prion disease [169].

Each of the three *Nlrp1* paralogues also show a different pattern of expression in *Sarm1*$^{-/-}$ BMDMs relative to WT, and this may be further reason to disqualify B6 congenic *Sarm1*$^{-/-}$ mice for use in studies pertaining pyroptosis in certain contexts. The *Nlrp1b* transcript expressed in *Sarm1*$^{-/-}$ BMDMs shows similarities to those expressed by 129 strain mice, and the lack of *Nlrp1c-ps* expression observed in the *Sarm1*$^{-/-}$ BMDMs corresponds with the absence of an *Nlrp1c-ps* homologue in 129 strain mice. The absence of *Nlrp1a* expression in BMDMs from the *Sarm1*$^{-/-}$ mouse is not reflective of an absence of *Nlrp1a* in 129 strain mice, however it still deviates from the transcriptional profile observe in the WT BMDMs. NLRP1b is the best characterised of the murine NLRP1 paralogues, and it is activated by proteolytic cleavage mediated by *Bacillus anthracis* lethal toxin [233]. This results N-end rule-mediated degradation of the NLRP1b N-terminus, freeing the C-terminus to activate caspase-1 and thus induce pyroptosis. The transcription of the *Nlrp1a, Nlrp1b* and *Nlrp1c-ps* genes was analysed in a range of mouse strains which were either sensitive or resistant to *B. anthracis* lethal toxin (LT) in a study by Sastalla *et al.* They showed that in macrophages from mice which are LT-resistant, including C57BL/6J, *Nlrp1a* and *Nlrp1c-ps* are expressed. In contrast, macrophages from mice which are sensitive to LT, which includes the strain 129S1/SvlmJ, do not express *Nlrp1a* or *Nlrp1c-ps.* There are multiple splice variants of *Nlrp1b,* only two of which (denoted SV1 and SV2) contain exon 1 and 2 of the gene. In this study, they examined expression of *Nlrp1b* SV1 and SV2 compared to other variants, and found that macrophages from C57BL/6 mice expressed SV1 and SV2 in addition to other variants, but that 129S1/SvlmJ macrophages did not express *Nlrp1b* SV1 and SV2 [234]. This is similar to my findings in *Sarm1*$^{-/-}$ mice, where *Nlrp1c-ps* was not expressed, very few reads mapping to *Nlrp1a* were detected, and exon 1 and 2 of *Nlrp1b* were not expressed. This striking similarity in

expression of the three *Nlrp1* paralogues between macrophages from *Sarm1*$^{-/-}$ and 129 strain mice is an additional indicator that passenger genes may account for phenotypes which are observed in B6 congenic *Sarm1*$^{-/-}$ mice, specifically relating to cell death.

It appears likely that passenger genes on chromosome 11 contribute to differential gene expression in the *Sarm1*$^{-/-}$ mouse. However, the 129-derived genetic material cannot necessarily account for the differential expression of genes on chromosomes other than chromosome 11 in the initial RNA sequencing experiment, shown in the heatmap in Figure 3.7. Differential expression of a number of these genes could potentially affect the immune response in *Sarm1*$^{-/-}$ mice. S100A8 can act as a DAMP when released from a cell, and is recognised by TLR4 to induce inflammatory cytokine production [235]. *Hyal1* encodes a hyaluronidase, which breaks down the endogenous molecule hyaluronan to saccharides of smaller molecular weights which can activate the NLRP3 inflammasome to induce IL-1β secretion and pyroptosis [236]. The differential expression of these genes could therefore potentially have an impact on cytokine expression and cell death in the *Sarm1*$^{-/-}$ mouse. Additionally, *Ctsk* encodes the cysteine protease cathepsin k, deficiency of which in the CNS is associated with memory and learning deficits [237]. Thus, differential expression of these genes would be an additional factor which renders these mice unsuitable for studies into inflammatory cytokine responses and inflammasome-mediated cell death as well as studies testing cognition. I initially considered that these genes may be legitimately differentially expressed in macrophages in the absence of SARM1, or that they may be downstream of the passenger gene-driven DEGs on chromosome 11. However, it is visibly noticeable that the expression levels of a number of these genes are inconsistent in the SKO replicates. I therefore sought to investigate the possibility that these are spurious results, possibly caused by the splitting up the SKO replicates for analysis and relaxing the threshold for significance. All of the non-chromosome 11 DEGs shown in the heatmap in Figure 3.7 appeared to differentially expressed in unstimulated cells. I could therefore examine if these genes were differentially expressed in the unstimulated WT and *Sarm1*$^{-/-}$ samples from the second RNA sequencing experiment, in which LPS was the stimulus used. Interestingly, none of these genes emerged as DEGs in unstimulated BMDMs in the second RNA sequencing experiment, suggesting that they are spurious results. This emphasises the importance of validating the RNA sequencing results by qPCR to ensure that results did not arise from bias within the analysis.

One limitation of this study stems from the use of transcriptomics rather than genomics. RNA sequencing can only provide information on the sequence of the genes that are transcribed in the specific conditions under which the samples were generated. Thus, no information is available on the sequence of genes which are not expressed basally or with TLR stimulation for a short period, and it therefore cannot be confirmed if these genes are of C57BL/6 or 129 origin. Additionally, transcriptomics only offers information about the transcribed portion of the gene, and thus it is not known what differences may exist in the promoters or enhancers of any given gene between BMDMs from WT and *Sarm1*$^{-/-}$ mice. However, one advantage of employing transcriptomics over genomics is that transcript variants between BMDMs from WT and *Sarm1*$^{-/-}$ mice, such as *Xaf1* and the *Nlrp1* paralogues could be identified.

Chapter 4 CRISPR/Cas9 SARM1-Knockout Mice Clarify the Role of Murine SARM1 in Transcription

4.1 Introduction

4.1.1 The need for a CRISPR/Cas9 SARM1-knockout mouse

B6 congenic *Sarm1*$^{-/-}$ mice have been widely used in studies into the function of murine SARM1 as discussed in Chapter 3 and I have shown that passenger genes, derived from the 129 strain, flank the *Sarm1* locus in these mice. This is a common feature in congenic mice made by targeted gene disruption; even after 20 generations of backcrossing, there is an ~83% likelihood that the region flanking the target locus at an interval of 1 cM remains of donor origin [230]. This limits the usefulness of the B6 congenic *Sarm1*$^{-/-}$ mouse, and obscures the actual phenotype resulting from the absence of SARM1. Thus, there is a pressing need for an alternative knockout mouse model which can clarify the roles for murine SARM1 in the absence of confounding passenger genes, particularly in respect to transcriptional phenotypes.

Genome editing was revolutionised with the advent of CRISPR/Cas9 (clustered regularly interspaced short palindromic repeats/CRISPR-associated 9) technology [238], for which Doudna and Charpentier received the Nobel Prize in Chemistry in 2020. The CRISPR-Cas system on which this technology is based originates in prokaryotes [239], where it acts as a form of adaptive immunity against viruses and plasmids [240] by using RNA-guided nucleases to cleave non-self genetic material. This system was harnessed as a means of genome editing. In brief, a single guide RNA (sgRNA) is designed complementary to the genomic target sequence of interest and provides specificity [241]. In addition to the sgRNA, Cas9 endonuclease must also be introduced. This may be in the form of mRNA, a plasmid, or protein in combination with the sgRNA as a preassembled ribonucleoparticle (RNP) [242]. Cas9, bound to the sgRNA is targeted to the sequence of interest, which must be in proximity to a Cas9-specific protospacer adjacent motif (PAM) sequence [243]. Here, the endonuclease activity of Cas9 induces a double strand break (DSB) 3-4 nucleotides upstream of the PAM sequence, which may be repaired by non-homologous end joining

(NHEJ) or if a homologous DNA sequence is present, by homology directed repair (HDR). Repair *via* NHEJ is error-prone, introducing indels, which leads to frame-shifts or the introduction of a premature stop codon and can result in knockout of the gene product. HDR is less error prone and through this pathway new sequences, such as an epitope tag, can be introduced to the genome by homologous recombination of the desired repair construct. The technology is reviewed in [244]. Thus CRISPR/Cas9 is a valuable genomic editing tool which can create both knockout and mutant animals. Crucially, while off-target mutagenesis may occur it is based on target sequence similarity [229, 245], unlike the proximity-based off-target effects observed in congenic mice made by targeted gene disruption.

Data from this study thus far has revealed that there are passenger genes flanking the *Sarm1* locus in B6 congenic *Sarm1*$^{-/-}$ mice, and this led us to question the fundamental cause of phenotypes previously observed by us and others in these mice. Specifically, I speculated that the transcriptional regulation of *Ccl5* in murine macrophages previously attributed to SARM1 [34] may actually be an artefact of the manner in which the congenic mice were made. Clearly, there was an urgent need for an improved mouse in which to examine the effects of solely the absence of SARM1. Thus, the TBSI transgenics facility was commissioned to generate a number of SARM1-deficient mice using CRISPR/Cas9 so that the roles for SARM1 in transcription and beyond could be interrogated in an alternative knockout model.

4.1.2 The susceptibility of SARM1-deficient mice generated by CRISPR/Cas9 to neurotropic viruses

Meanwhile, similar scrutiny was directed at the role of SARM1 in determining susceptibility to neurotropic viruses in the absence of passenger genes by the García-Sastre lab, whose previous work showed that B6 congenic *Sarm1*$^{-/-}$ mice are protected from VSV [207]. To address the contribution of passenger genes to this phenotype, a number of SARM1-deficient mice were generated by CRISPR/Cas9 genome-editing and their susceptibility to neurotropic viruses were assessed [246]. This was compared with the responses seen in two different strains of B6 congenic *Sarm1*$^{-/-}$ mice which were independently generated in separate labs using similar techniques. The first strain was generated by the Ding lab [26], and is the B6 congenic *Sarm1*$^{-/-}$ mouse which has been used

in this thesis. This strain includes a neomycin-resistance cassette in the disrupted *Sarm1* locus, which facilitated selection of the embryonic stem cells which had been successfully genome-edited. The second strain was generated by the Diamond lab [44], and lack a neomycin cassette. For the purpose of comparison, for the remainder of Section 4.1 these mice will be referred to as $Sarm1^{AD}$ and $Sarm1^{MSD}$ respectively.

The role for SARM1 in determining susceptibility to VSV was originally determined in $Sarm1^{AD}$ mice, which exhibited reduced cytokine and chemokine levels in the brain compared to WT, and were therefore protected from lethal infection [207]. In contrast, the two CRISPR/Cas9 SARM1-deficient mice generated by the García-Sastre lab, termed $Sarm1^{AGS3}$ and $Sarm^{AGS12}$, displayed similar cytokine and chemokine expression to WT controls and succumbed to VSV infection [246]. This was not due to technical differences in how the experiment was performed between the studies, as the authors confirmed that $Sarm1^{AD}$ mice exhibited enhanced survival and diminished cytokine production in the same experiment. Thus, the protection against VSV originally observed in $Sarm1^{AD}$ was conferred by passenger genes and not by the absence of SARM1. Importantly, this demonstrates that there are functional consequences to the retention of 129-derived genetic material in B6 congenic $Sarm1^{-/-}$ mice.

The contribution of SARM1 in the immune response to WNV was previously assessed in $Sarm1^{MSD}$ mice, which were more susceptible to WNV than WT controls and produced less TNF [44]. This phenotype was recapitulated in $Sarm1^{AGS3}$ mice, which succumbed to lethal WNV infection while WT mice survived [246]. As the $Sarm1^{MSD}$ colony was retired by the Diamond lab, the previously observed phenotype could not be simultaneously confirmed in these mice. In lieu of this, $Sarm1^{AD}$ mice were infected with WNV. Surprisingly, unlike $Sarm1^{MSD}$ and $Sarm1^{AGS3}$ mice, $Sarm1^{AD}$ mice did not exhibit enhanced susceptibility to WNV, and were similar to WT. The exact reason for the discrepancy between the phenotypes observed in the two B6 congenic $Sarm1^{-/-}$ mouse strain is not obvious. However, this is a clear demonstration that phenotypes which result from the absence of SARM1 may also be masked in B6 congenic $Sarm1^{-/-}$ mice, though whether or not it is related to passenger genes is unclear.

Additionally, a previous study demonstrated that $Sarm1^{MSD}$ mice were protected from lethal LACV infection [167]. Uccellini *et al.* examined the susceptibility of $Sarm1^{AD}$, $Sarm1^{AGS3}$,

Sarm1^{AGS12} mice to LACV compared to WT. In contrast to the *Sarm1*^{MSD} mice, *Sarm1*^{AD} mice were not protected from lethal LACV infection, nor were *Sarm1*^{AGS3} or *Sarm1*^{AGS12} mice [246]. Thus as a consequence of the confounding factor of passenger genes in B6 congenic *Sarm1*$^{-/-}$ mice, phenotypes have been misattributed to the absence of SARM1. These passenger genes may also mask phenotypes which would be observed in the absence of SARM1 without additional confounding factors, as seen in the case of WNV. Similar examination is required of the published roles for SARM1 in determining susceptibility or resistance to diseases outside of the CNS in the absence of passenger genes.

4.1.3 Passenger genes cause differential gene expression in macrophages from B6 congenic Sarm1$^{-/-}$ *mice*

In addition to investigating the role for SARM1 in neurotropic disease in CRISPR/Cas9 SARM1-knockout mice, Uccellini *et al.* assessed differential gene expression in macrophages from B6 congenic *Sarm1*$^{-/-}$ mice compared to WT following LPS stimulation. The authors then evaluated the expression of these genes in macrophages from *Sarm1*^{AGS3} mice. In agreement with my findings in Chapter 3, while no differences were observed between WT and *Sarm1*^{AD} macrophages in LPS-induced TNF or IL6 production, *Ccl5* expression was diminished in *Sarm1*^{AD} BMDMs. In addition, the expression of chemokines *Ccl3* and *Ccl4* were found to be reduced in *Sarm1*^{AD} BMDMs stimulated with LPS relative to WT [246]. Similar to the genes I found to be differentially expressed through RNA sequencing analysis, these chemokine genes are on chromosome 11. Strikingly, all of these genes were expressed to an equal level in *Sarm1*^{AGS3} and WT BMDMs [246], demonstrating that passenger genes accounted for the differential gene expression which was observed in B6 congenic *Sarm1*$^{-/-}$ macrophages. In further support of the absence of a role for murine SARM1 in regulating the transcription of *Ccl5*, exogenous expression of SARM1 in RAW264.7 cells failed to augment LPS-induced *Ccl5* expression in this study [246]. This mirrors the results I observed in *Sarm1*$^{-/-}$ BMDMs stably expressing SARM1 in Section 3.2.7, but is contrary to the enhanced *Ccl5* previously observed in a similar experiment in our lab [34]. It therefore seems likely that no deficit in *Ccl5* induction will be observed in the SARM1-deficient mice which we independently generated. The study by Uccellini *et al.* also reported a similar *Xaf1* transcript in both brains and splenocytes from B6 congenic *Sarm1*$^{-/-}$ mouse as was observed in *Sarm1*$^{-/-}$ BMDM in Section 3.2.6 and confirmed that this unique isoform is present in 129 mice and absent in *Sarm1*^{AGS3} and *Sarm1*^{AGS12} mice

[246]. However the expression of further DEGs which I uncovered in B6 congenic *Sarm1*$^{-/-}$ by RNA sequencing in Section 3.2.5, has not yet been assessed in any SARM1-deficient mouse in the absence of passenger genes. Using BMDMs from our independently generated SARM1-deficient mice, in this chapter I will delineate whether it is the absence of SARM1 or the presence of passenger gene which accounts for the differential gene expression previously observed in BMDMs from B6 congenic *Sarm1*$^{-/-}$ mice.

4.2 Results

4.2.1 The characterisation of SARM1-deficient mice generated using CRISPR/Cas9

To investigate the role for SARM1 in transcriptional regulation in murine BMDM without the confounding factor of passenger genes, SARM1-deficient mice were generated by CRISPR/Cas9-mediated genome engineering by the TBSI transgenics facility. The targeting strategy is described in detail in Section 2.2.1.2. The three novel SARM1-deficient mice each contained a deletion within the first exon of the *Sarm1* locus; *Sarm1*$^{em1.1Tftc}$ (2 bp deletion), *Sarm1*$^{em1.2Tftc}$ (34 bp deletion), and *Sarm1*$^{em1.3Tftc}$ (5 bp deletion) (Figure 2.2). Each of these deletions resulted in a premature stop codon, and interrupted the recognition sequence of the restriction enzyme BsaWI. This facilitated the use of this restriction enzyme in genotyping. Following PCR of genomic DNA, the amplicon containing WT sequence contains the BsaWI recognition sequence and thus is cleaved by the enzyme resulting in a higher cleaved band. Meanwhile, the amplicons containing the *Sarm1*$^{em1.1Tftc}$, *Sarm1*$^{em1.2Tftc}$, and *Sarm1*$^{em1.3Tftc}$ sequences are not cleaved by BsaWI, and appear as an intact, lower band (Figure 4.1A and B). Variation in the intestinal microbiota between mice can influence mouse phenotypes. The use of littermates is the optimal mode of establishing a near-homogeneous microbiome [247] to limit the confounding influence of the microbiota in mouse studies. Thus, heterozygous breeding pairs were established to produce WT and SARM1-deficient littermate mice for all further experiments. Crucially, the offspring of these heterozygous breeding pairs are also genetically homologous, aside from the targeted gene of interest. That is to say that genomes of the SARM1-deficient and WT progeny vary only at the *Sarm1* locus. Additionally, the SARM1-knockout and WT littermate control mice are perfectly age-matched by the nature of their generation.

SARM1 expression is high in the brain [26], thus SARM1 protein expression was confirmed to be abrogated in the brains of *Sarm1*$^{em1.1Tftc}$, *Sarm1*$^{em1.2Tftc}$, and *Sarm1*$^{em1.3Tftc}$ mice compared to WT littermate controls by Dr Ryoichi Sugisawa (Figure 4.1C) [195]. As SARM1 is difficult to detect using commercially available antibodies, an antibody generated by our lab specific to the TIR domain of SARM1 was used [195]. SARM1 is required for axon degeneration in neurons following a range of cellular and mitochondrial insults (discussed in detail in Section 1.4), including the chemotherapeutic agent

vincristine. This phenotype was exploited by Dr Ryoichi Sugisawa to confirm the functional loss of SARM1 activity in neurons from the three novel CRISPR SARM1-deficient mice. Remarkably, similar to axons from B6 congenic *Sarm1*$^{-/-}$ mice, axons remained intact for 72 hours after vincristine treatment in neurons from *Sarm1*$^{em1.1Tftc}$, *Sarm1*$^{em1.2Tftc}$, and *Sarm1*$^{em1.3Tftc}$ mice. In contrast, WT axons exhibited dramatic and significant loss of length after 24 hours (Figure 4.2) [195].

4.2.2 In the absence of passenger genes, SARM1-deficient BMDMs display normal TLR4-dependent transcription

After our laboratory had verified that SARM1 protein is not expressed in *Sarm1*$^{em1.1Tftc}$, *Sarm1*$^{em1.2Tftc}$, and *Sarm1*$^{em1.3Tftc}$ and shown that the CRISPR/Cas9 knockouts faithfully recapitulate the axoprotective phenotype seen in B6 congenic *Sarm1*$^{-/-}$ neurons, I could then interrogate the transcriptional phenotype in BMDMs without the confounding factor of passenger genes. In particular since *Ccl5* resides on chromosome 11, less than 5 cM from the *Sarm1* locus, passenger genes could be responsible for the differential *Ccl5* expression previously observed in B6 congenic *Sarm1*$^{-/-}$ BMDMs (Figures 3.2 and 3.3). Indeed, contrary to what was seen in B6 congenic *Sarm1*$^{-/-}$ BMDMs, *Ccl5* transcription (Figure 4.3A) and subsequent CCL5 secretion (Figure 4.3C) was not significantly different *Sarm1*$^{em1.3Tftc}$ BMDMs and their WT littermate controls following stimulation with LPS over a 24 hour period. In addition, *Tnf* mRNA (Figure 4.3B) and protein levels (Figure 4.3D) were equivalent between *Sarm1*$^{em1.3Tftc}$ and WT BMDMs. Thus, the reduced *Ccl5* expression previously observed in B6 congenic *Sarm1*$^{-/-}$ BMDMs was not as a result of SARM1-deficiency, but likely due to the presence of passenger genes. A similar phenotype was observed in BMDMs derived from both *Sarm1*$^{em1.1Tftc}$ and *Sarm1*$^{em1.2Tftc}$ mice compared to WT littermate controls (Figure 4.4). Hence, all three novel SARM1-deficient mice generated by CRISPR/Cas9, which are verified knockouts, show similar transcriptional responses to TLR-4 stimulation. Thus, when necessary, experiments performed on different CRISPR knockout lines were combined, and are referred to as *Sarm1*^{em1Tftc} in these instances. In addition, in response to TLR4 stimulation with MPLA, CCL5 and TNF secretion were found to be similar in SARM1-deficient BMDMs from CRISPR knockout mice and WT controls (Figure 4.5), contrary to B6 congenic *Sarm1*$^{-/-}$ BMDMs.

Ccl6, Ccl9 and *Acap1* were previously identified as differentially expressed genes in B6 congenic *Sarm1*$^{-/-}$ BMDMs compared to WT by RNA sequencing (Section 3.2.6). The mRNA expression of each of these genes was confirmed to be differentially expressed both basally and following stimulation with CL075 or LPS for 3 hours. However, I observed that the sequence of each of these genes in B6 congenic *Sarm1*$^{-/-}$ BMDMs showed significant deviation from the C57BL/6 reference, which suggested that passenger mutations may contribute to the altered expression compared to WT. Thus, I examined the expression of *Ccl6, Ccl9,* and *Acap1* in *Sarm1*$^{em1.3Tftc}$ pBMDMs. Compellingly, all three genes were expressed equally in BMDMs from *Sarm1*$^{em1.3Tftc}$ mice and their WT littermates, both basally and following LPS stimulation over a 24 hour time course (Figure 4.6). Therefore, the previously observed differential expression resulted from the presence of passenger genes and not the absence of SARM1.

4.2.3 Generation and characterisation of iBMDMs from Sarm1$^{em1.1Tftc}$ *and Sarm1*$^{em1.2Tftc}$ *mice*

Having assessed the transcriptional phenotype in pBMDMs from SARM1-deficient mice generated by CRISPR, I then sought to derive iBMDMs from these mice. These are a useful tool for further studies into SARM1-deficient macrophages which may require more material than is easily attainable from pBMDMs. The use of iBMDMs in studies is now commonplace, as they can be easily and rapidly expanded, and they reduce the number of research animals required. Thus it is important to characterise these cells, and ensure they recapitulate the phenotype observed in primary cells. The iBMDMs were generated using Cre-J2 viral supernatants as described in Section 2.2.5, employing the same method used to create the B6 congenic *Sarm1*$^{-/-}$ iBMDMs which were used in Chapter 3. The potential pitfalls in the immortalisation process which can result in non-gene driven variations between gene-edited iBMDMs and their WT controls were outlined previously. Here, measures were taken to avoid the introduction of variability at each step. To ensure sex- or age-related differences, iBMDMs were derived from littermate WT and *Sarm1*^{em1Tftc} mice. Bone marrow cells were counted and seeded at an equal density, as discrepancies in seeding density during BMDM differentiation can cause phenotypic differences [226]. As each line of iBMDMs represents only the single mouse from which it is derived, iBMDMs were generated from both a *Sarm1*$^{em1.2Tftc}$ mouse and a *Sarm1*$^{em1.3Tftc}$ mouse, as well as their WT littermates. Bone marrow from these same mice was used to generate pBMDMs which

were used in Figure 4.3 and Figure 4.4, and their transcription was similar to other biological replicates. Thus, these mice are suitable representatives from which to derive iBMDMs.

As there were no differences in LPS-induced gene induction between WT and *Sarm1*$^{em1.2Tftc}$ or *Sarm1*$^{em1.3Tftc}$ pBMDMs, it is reasonable to anticipate that the *Sarm1*$^{em1.2Tftc}$ and *Sarm1*$^{em1.3Tftc}$ iBMDMs would also be similar to their WT controls. However, I previously observed differences in phenotype between B6 congenic *Sarm1*$^{-/-}$ pBMDMs and iBMDMs (Section 3.2.2) and the cause for this could not be conclusively defined. It remains possible that in the absence of SARM1, immortalisation of BMDMs results in differential expression of certain genes. To test this, CCL5 and TNF levels were measured in the supernatants of *Sarm1*$^{em1.2Tftc}$ and *Sarm1*$^{em1.3Tftc}$ iBMDMs and their respective WT controls, basally and after 3 hour or 24 hour treatment with LPS. As anticipated, there were no differences in CCL5 or TNF secretion between *Sarm1*$^{em1.2Tftc}$ and WT iBMDMs basally or after TLR4 stimulation with LPS (Figure 4.7A and 4.7C). This is consistent with the data in pBMDMs, which suggests that there is no role for SARM1 in specific regulation of *Ccl5* or in TRIF antagonism in murine BMDMs. Contrary to this however, CCL5 production was reduced in *Sarm1*$^{em1.3Tftc}$ iBMDMs relative to WT after treatment with LPS for 24 hours (Figure 4.7B). This is not indicative of SARM1 regulation specifically of CCL5 production, as TNF secretion was also diminished in *Sarm1*$^{em1.3Tftc}$ iBMDMs compared to WT 24 hours post LPS stimulation (Figure 4.7D). Both CCL5 and TNF production were equivalent between WT and *Sarm1*$^{em1.3Tftc}$ iBMDMs basally and 3 hours after TLR4 stimulation.

As cytokine induction was impaired in *Sarm1*$^{em1.3Tftc}$ iBMDMs but not *Sarm1*$^{em1.2Tftc}$ iBMDMs compared to WT, I wondered if other TLR4-dependent innate responses may differ between iBMDMs from these two CRISPR/Cas9 SARM1-knockout mice. NO is one such TLR4-induced immune effector molecule. Previously I observed that iBMDMs, and not pBMDMs, from B6 congenic *Sarm1*$^{-/-}$ mice produced substantially less NO than their WT counterparts following LPS stimulation for 24 hours (Figure 3.4A and B), The density at which bone marrow cells are seeded prior to differentiation can influence the phenotype of the resulting BMDMs, with cells seeded at a lower density having increased pro-inflammatory cytokine production but decreased NO production relative to cells seeded at a higher density [226]. Thus, I sought to measure production of nitric oxide of *Sarm1*$^{em1.2Tftc}$ and *Sarm1*$^{em1.3Tftc}$ iBMDMs compared to WT, as differences between either of the SARM1-

deficient cell lines and their WT control could indicate differences in seeding density at the time at which they were derived. NO production was equivalent between *Sarm1*$^{em1.2Tftc}$ iBMDMs and their WT controls following TLR4 stimulation with either LPS or MPLA (Figure 4.8A). Similarly, there was no difference in NO production between *Sarm1*$^{em1.3Tftc}$ and WT iBMDMs (Figure 4.8B), indicating that differences in bone marrow cell density during the time of differentiation are not responsible for the reduced cytokine secretion observed in *Sarm1*$^{em1.3Tftc}$ iBMDMs relative to WT. Overall, no differences in NO production were observed between *Sarm1*^{em1Tftc} and WT pBMDMs (Figure 4.8D) or between *Sarm1*^{em1Tftc} and WT iBMDMs (Figure 4.8C, data is from Figures 4.8A and 4.8B combined). Thus, SARM1 does not regulate NO production in pBMDMs or iBMDMs in the absence of passenger genes.

4.2.4 The characterisation of BMDMs expressing enzymatically inactive SARM1 from mice generated using CRISPR/Cas9

SARM1 possesses intrinsic NADase enzymatic activity, which it essential for mediating axon degeneration [30] (discussed in detail in Section 1.4). It has been shown in human SARM1 that substitution of the glutamic acid E642 with alanine (E642A) results in an enzymatically disabled SARM1 which is unable to cleave NAD^+ [30]. The TBSI transgenics facility generated mice with an NADase-inactive SARM1 using CRISPR/Cas9, by substituting SARM1 glutamic acid E682, the murine equivalent of the human SARM1 E642, with alanine (E682A) as described in Section 2.2.1.4. The resulting mouse, *Sarm1*$^{em1\_E682A\_Tftc}$, will be henceforth called *Sarm1*^{E682A}. To prevent re-cutting by Cas9, a number of bases surrounding E682 were also substituted while maintaining synonymous codons, and this facilitated the use of the restriction enzyme SmoI when genotyping these mice. The SmoI recognition site is present in the WT SARM1 sequence, but is absent in the *Sarm1*^{E682A} sequence as result of the base substitutions. Heterozygous breeding pairs were established to generate *Sarm1*^{E682A} and WT littermate pairs for use in experiments (Figure 4.9A).

Using this mouse, we could discern whether it was the NADase activity of SARM1 or an unrelated structural activity, such as TIR domain binding, which mediates a given phenotype. The outcome of SARM1 NADase activity is not only the local depletion of NAD^+, but also the production of cADPR [30]. It is unlikely that a phenotype which is

absent in SARM1-deficient BMDMs would be present in the SARM1 NADase-inactive BMDMs, unless SARM1 NADase has an opposing function to the rest of SARM1 in cytokine regulation. However, both the *Sarm1*^{E682A} and *Sarm1*^{em1Tftc} mice became available for studies at the same time, and experiments using these mice were therefore carried out simultaneously. Thus, the requirement for SARM1 NADase activity for optimal *Ccl5* production was examined using these BMDMs from *Sarm1*^{E682A} mice. Unsurprisingly, there was no difference in the expression of *Ccl5* mRNA between WT and *Sarm1*^{E682A} pBMDMs stimulated over a 24 hour timecourse with LPS (Figure 4.9B). *Tnf* expression also remained equivalent between the genotypes (Figure 4.9C). However, while *Sarm1* mRNA was detectable in these cells, SARM1 protein could not be detected by Western blot (R. Sugisawa, personal communication). Thus, it remains possible that this mouse acts as an additional SARM1-knockout mouse rather than an NADase-inactive SARM1 expressing mouse. Regardless of whether or not SARM1 protein is expressed in this mouse, it further confirms that SARM1 does not regulate *Ccl5* induction in macrophages.

4.2.5 Examining the role for SARM1 in Klebsiella pneumoniae infection of primary macrophages

The role for SARM1 in determining resistance or susceptibility to a number of neurotropic infections has been re-evaluated by the García-Sastre lab, using SARM1-deficient mice they generated independently using CRISPR/Cas9. As previously discussed in Section 4.1, in contrast to B6 congenic *Sarm1*$^{-/-}$ mice, SARM1-deficient mice generated by CRISPR were similar to WT in their susceptibility to VSV and LACV [246]. Thus, passenger genes accounted for the previously observed phenotypes. In contrast to this, a similar phenotype was observed in B6 congenic *Sarm1*$^{-/-}$ mice and our *Sarm1*$^{em1.1Tftc}$ mice following *Klebsiella pneumoniae* infection in a study by our collaborator, Professor Jose Bengoechea. In that study (currently under review for publication, accessible on bioRxiv), SARM1-deficiency was found to be beneficial, and resulted in reduced intracellular survival of *K. pneumoniae* in macrophages *in vitro* and improved bacterial clearance *in vivo* [248]. This corresponded with enhanced expression of TNF, IL-1β, and type I interferons in B6 congenic *Sarm1*$^{-/-}$ iBMDM compared to WT following *K. pneumoniae* infection, and by extension, augmented expression of the interferon stimulated genes *Ifit1* and *Isg15* [248]. In addition, *K. pneumoniae*-induced *Il10* expression was diminished in *Sarm1*$^{-/-}$ iBMDM relative to WT. Overall, this resulted in enhanced inflammation in the B6 congenic *Sarm1*$^{-/-}$ iBMDMs

relative to WT [248]. As discussed in Section 3.2.2, iBMDMs do not always faithfully recapitulate the phenotype of pBMDMs, and caution must therefore be exercised in the interpretation of observations in iBMDMs. However, here the authors also observed enhanced inflammatory cytokine expression in the lungs of B6 congenic *Sarm1*$^{-/-}$ mice. These phenotypes were confirmed in *Sarm1*$^{em1.1Tftc}$ mice, both in the lung and in iBMDMs derived from *Sarm1*$^{em1.1Tftc}$ bone marrow [248].

I sought to investigate if the same phenotype of enhanced inflammation would be observed in primary BMDMs from *Sarm1*^{em1Tftc} mice. TLR4 is one of the major PRRs for detection of *K. pneumoniae* in the mouse [249-251]. While the induction of all genes which were measured was normal in pBMDMs from *Sarm1*^{em1Tftc} mice in response to TLR4 stimulation with an isolated ligand (Figures 4.3 – 4.6), this may not be the case upon stimulation with a complex pathogen containing multiple various PAMPs. *Sarm1*^{em1Tftc} pBMDMs and their WT littermates were infected with *K. pneumoniae* for 3, 6, or 16 h, or mock infected with media as a control as described in Section 2.2.6.2. *Ccl5* mRNA (Figure 4.10C) and CCL5 protein expression (Figure 4.10A) were measured, and found to be equivalent between *Sarm1*^{em1Tftc} pBMDMs and WT controls. This is in agreement with data to date, which shows that there is no role for SARM1 in the regulation of *Ccl5* expression in the absence of passenger mutations. Surprisingly, in contrast to the results observed in B6 congenic *Sarm1*$^{-/-}$ iBMDMs by the Bengoechea lab, the expression of inflammatory genes did not differ between *Sarm1*^{em1Tftc} pBMDMs and their WT littermate controls here. *Tnf* mRNA expression was similar in WT and *Sarm1*^{em1Tftc} (Figure 4.10D). TNF protein secretion was also equivalent between the two genotypes (Figure 4.10B). *Il1b* expression did not vary between *Sarm1*^{em1Tftc} and WT pBMDMs at any time point (Figure 4.11A), nor did *Ifnb* (Figure 4.11B). The Bengoechea lab observed diminished *Klebsiella*-induced *Il10* expression in *Sarm1*$^{-/-}$ iBMDMs compared to WT [248]. Here *Il10* expression was only induced at a very low level by infection with *K. pneumoniae*, and it was unaffected by the absence of SARM1 (Figure 4.11C). Similar expression levels of the interferon stimulated genes *Ifit1* (Figure 4.11D) and *Isg15* (Figure 4.11E) was observed in WT and *Sarm1*^{em1Tftc} pBMDMs. What underlies the difference in transcriptional response between *Sarm1*^{em1Tftc} pBMDMs and *Sarm1*$^{em1.1Tftc}$ iBMDMs is unclear.

A similar preliminary experiment was performed in *Sarm1*^{E682A} pBMDMs and their WT littermate controls. There were no significant differences in expression of *Ccl5* (Figure

4.12A), *Tnf* (Figure 4.12B), or *Il1* (Figure 4.12C) between *Sarm1*^{em1Tftc} and WT pBMDMs. *Ifnb* was barely induced by *Klebsiella* infection in either genotype, and was unaffected by the absence of SARM1 (Figure 4.12D). Unsurprisingly therefore the expression of *Ifit1* (Figure 4.12F) and *Isg15* (Figure 4.12G) was also very low and equal among genotypes. Again, *Il10* expression was low and equal between WT and *Sarm1*^{em1Tftc} pBMDMs (Figure 4.12E). As discussed earlier, SARM1 expression cannot be verified in this mouse, and it may be acting as an additional knockout.

Given that the Bengoechea group saw a similar phenotype in SARM1-deficient mice generated by targeted gene disruption and by CRISPR/Cas9 genome engineering [248], it is unlikely that passenger genes could account for the enhanced inflammation observed in *Sarm1*$^{-/-}$ iBMDMs infected with *Klebsiella*. Nonetheless to address this possibility, a preliminary experiment was performed in which pBMDMs from age-matched WT and B6 congenic *Sarm1*$^{-/-}$ mice were infected with *K. pneumoniae*. While the difference was not significant, *Ccl5* expression was lower in *Sarm1*$^{-/-}$ pBMDMs than WT controls 6 and 16 hours post-infection (Figure 4.13A). There were no significant differences in expression of *Tnf* (Figure 4.13B), *Ifnb* (Figure 4.13C), or *Il1b* (Figure 4.13D) between WT and *Sarm1*$^{-/-}$ pBMDMs. The expression of *Ifit1* (Figure 4.13E), *Il10* (Figure 4.13F), and *Isg15* (Figure 4.13G) were reduced in *Sarm1*$^{-/-}$ pBMDMs compared to WT, however the expression levels were extremely low. Further, with the exception of *Il10*, this is in disagreement with the findings of the Bengoechea lab, who observed enhanced *Ifit1* and *Isg15* in B6 congenic *Sarm1*$^{-/-}$ iBMDMs [248]. Thus, it is unclear if there is a general role for SARM1 in the transcriptional response to *Klebsiella pneumoniae* in BMDMs, or if it is unique to immortalised cells.

Overall, data from the novel CRISPR/Cas9 SARM1-knockout mice do not support a role for SARM1 in the transcriptional regulation of any gene which was investigated in pBMDMs, either in response to isolated TLR4 ligands or to infection with a complex pathogen. Passenger genes can account for the differential gene expression previously observed both basally and following TLR4 stimulation in BMDMs from B6 congenic *Sarm1*$^{-/-}$ mice. However, it is less clear why differential gene expression was observed in both B6 congenic and CRISPR/Cas9 SARM1-knockout iBMDMs compared to WT in response to *K. pneumoniae* infection by the Bengoechea lab, but no such differences were observed in pBMDMs from the same mice in my hands.

A

Mouse name	Deletion size
Sarm1$^{em1.1Tftc}$	2 bp
Sarm1$^{em1.2Tftc}$	34 bp
Sarm1$^{em1.3Tftc}$	5 bp

B

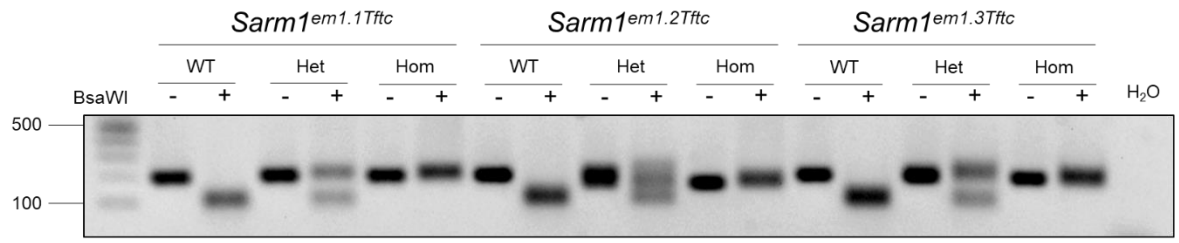

C

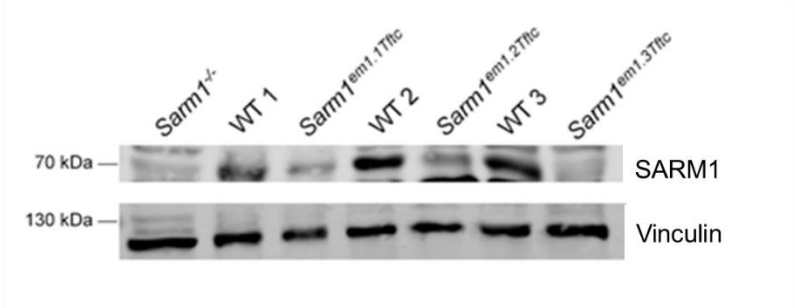

Figure 4.1 Genotyping of three novel SARM1-deficient mice generated using CRISPR by the TBSI transgenics facility

(A) Table shows the deletion size and official name for each CRISPR/Cas9 SARM1-deficient mouse line. Each of these deletions resulted in a premature stop codon.
(B) Genotyping results for CRISPR littermates. PCR amplicon from mouse genomic DNA was incubated with (+) or without (-) BsaWI enzyme. The amplicon containing WT sequence is recognised by the enzyme and shows a cleaved band whereas the disrupted sequence does not.
WT, wild type; het, heterozygote; hom, homozyote.
(C) Immunoblot analysis of brain lysate for SARM1, with vinculin as a loading control. WT1, WT2, and WT3 are littermates of *Sarm1*$^{em1.1Tftc}$, *Sarm1*$^{em1.2Tftc}$, and *Sarm1*$^{em1.3Tftc}$ respectively. *Sarm1*$^{-/-}$ is the B6 congenic *Sarm1*$^{-/-}$ and serves as a negative control for SARM1 expression. Figure 4.1C was generated by Dr Ryoichi Sugisawa, taken from Doran, Sugisawa *et al,* 2021 [195]

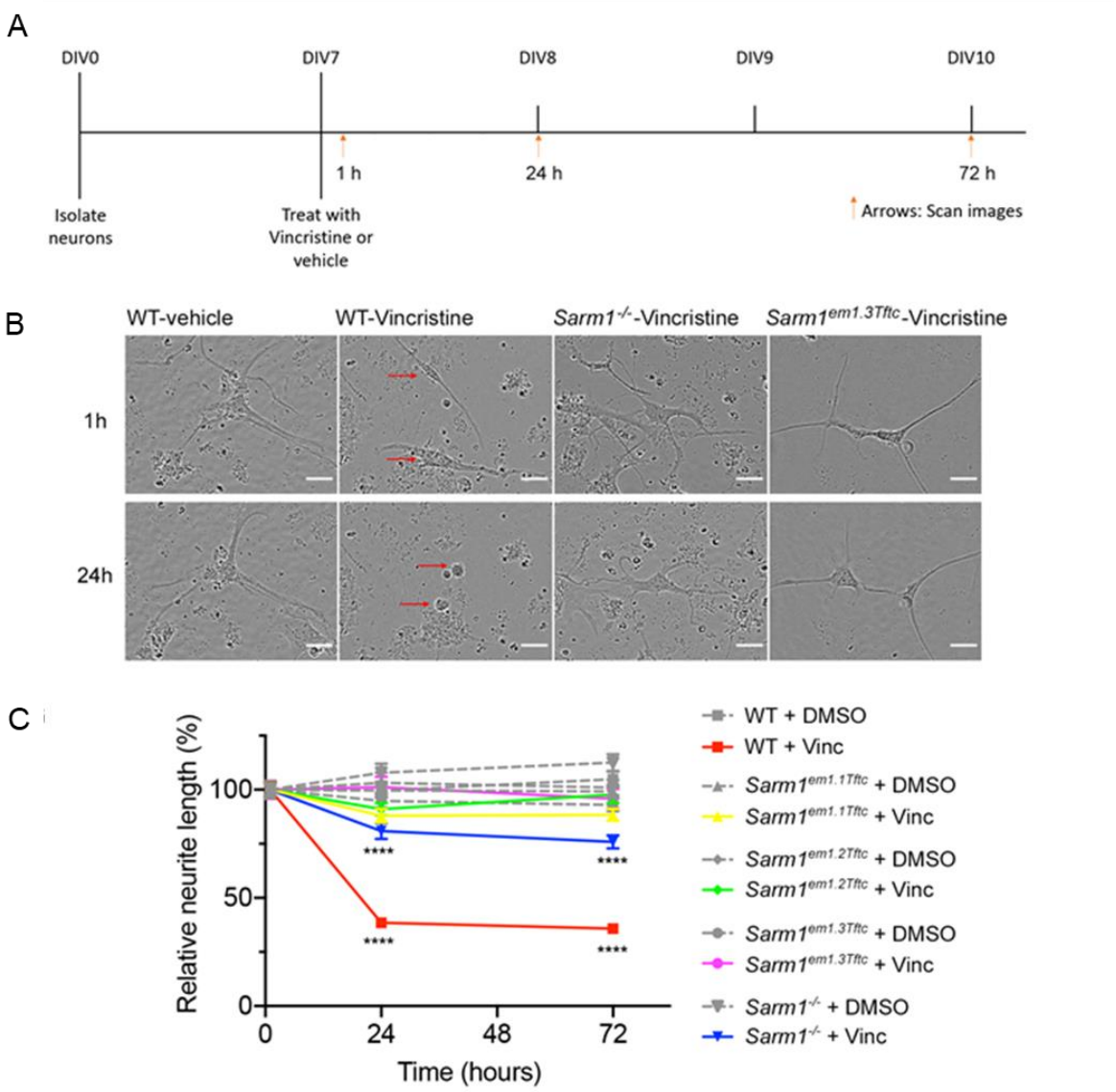

Figure 4.2 Neurons from *Sarm1*$^{em1.1Tftc}$, *Sarm1*$^{em1.2Tftc}$, and *Sarm1*$^{em1.3Tftc}$ mice are protected from vincristine-induced axon degeneration

(A) Schematic of axon degeneration protocol. DMSO is used as a vehicle. Primary neurons DIV (days in vitro) 7 were treated with vincristine or vehicle and images are scanned after 1 h, 24 h, and 72 h for analysis used in (B and C).
(B) Representative images of neurons after 1 h or 24 h treatment of vincristine or DMSO. "*Sarm1*$^{-/-}$" refers to B6 congenic *Sarm1*$^{-/-}$ mice. Red arrows indicate cell bodies of WT neurons which lose their neurites after 24 h vincristine treatment. White scale bar, 25 μm.
(C) Graph of relative neurite length over time for different mice and treatments. Neurite lengths are normalized to the mean of its own length at 1 h as 100 (%). All data are mean ± SEM of four or five mice used per genotype. Data were tested with a two-way ANOVA showing significant main effects of group $F(9, 4973) = 59.02$, $p < 0.0001$; time $F(2, 4973) = 25.08$, $p < 0.0001$; and interaction $F(18, 4973) = 14.90$, $p < 0.0001$; Tukey's multiple comparisons test, ****$p < 0.0001$ vincristine versus vehicle (DMSO) in WT and *Sarm1*$^{-/-}$ at 24 h and 72 h.
Figure 4.Z (A-C) and the data therein were generated by Dr Ryoichi Sugisawa, and taken from Doran, Sugisawa *et al.*, 2021 [195].

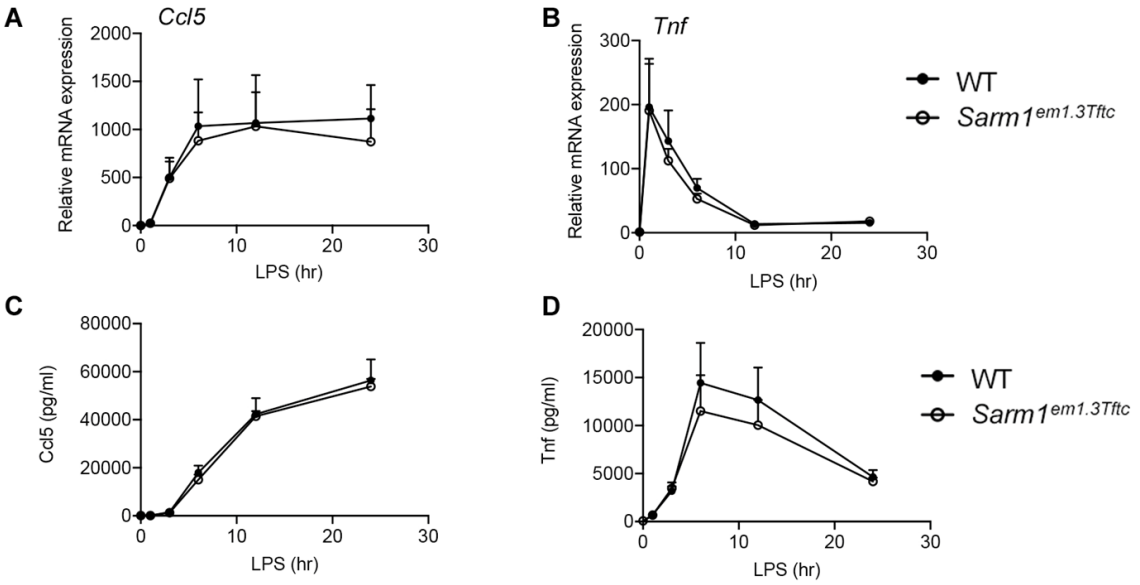

Figure 4.3 Macrophages from *Sarm1*$^{em1.3Tftc}$ mice show no defect in induction of *Ccl5* compared to WT littermates

WT and *Sarm1*$^{em1.3Tftc}$ pBMDMs were stimulated with 100 ng/ml LPS for the indicated times, or with medium as a control. Expression of *Ccl5* (A) and *Tnf* (B) mRNA were assayed by qRT-PCR, normalized to the housekeeping gene β-actin, and are presented relative to the untreated WT control. Supernatants were assayed for CCL5 (C) and TNF (D) protein by ELISA. Graphs show mean ±SEM from 3 mice per genotype, performed in triplicate. There were no significant differences determined by multiple Mann-Whitney tests with Holm-Šídák multiple comparisons test.

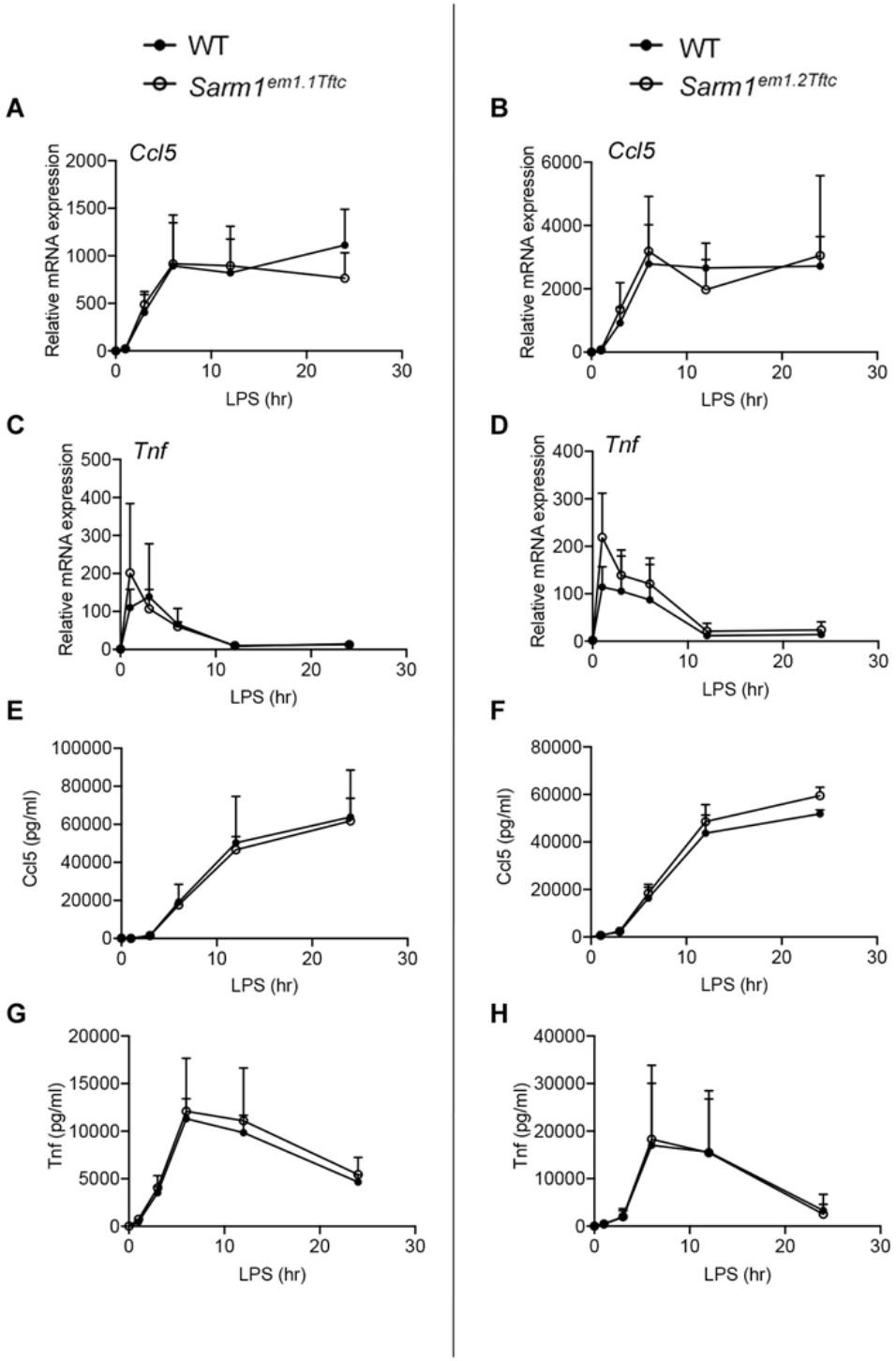

Figure 4.4 Normal induction of *Ccl5* and *Tnf* in macrophages from *Sarm1*$^{em1.1Tftc}$ and *Sarm1*$^{em1.2Tftc}$ mice compared to WT littermates

Sarm1$^{em1.1Tftc}$ (A, C, E, G) or *Sarm1*$^{em1.2Tftc}$ (B, D, F, H) pBMDM and their WT littermate controls were stimulated with 100 ng/ml LPS for the indicated times, or medium as a control. Expression of *Ccl5* (A, B) and *Tnf* (C, D) mRNA were assayed by qRT-PCR, normalized to the housekeeping gene β-actin, and are presented relative to the untreated WT control. Supernatants were assayed for CCL5 (E, F) and TNF (G, H) protein by ELISA. Data are mean ± SEM from 2 mice per genotype, performed in triplicate. No significant differences determined by multiple Mann-Whitney tests with Holm-Šídák multiple comparisons test.

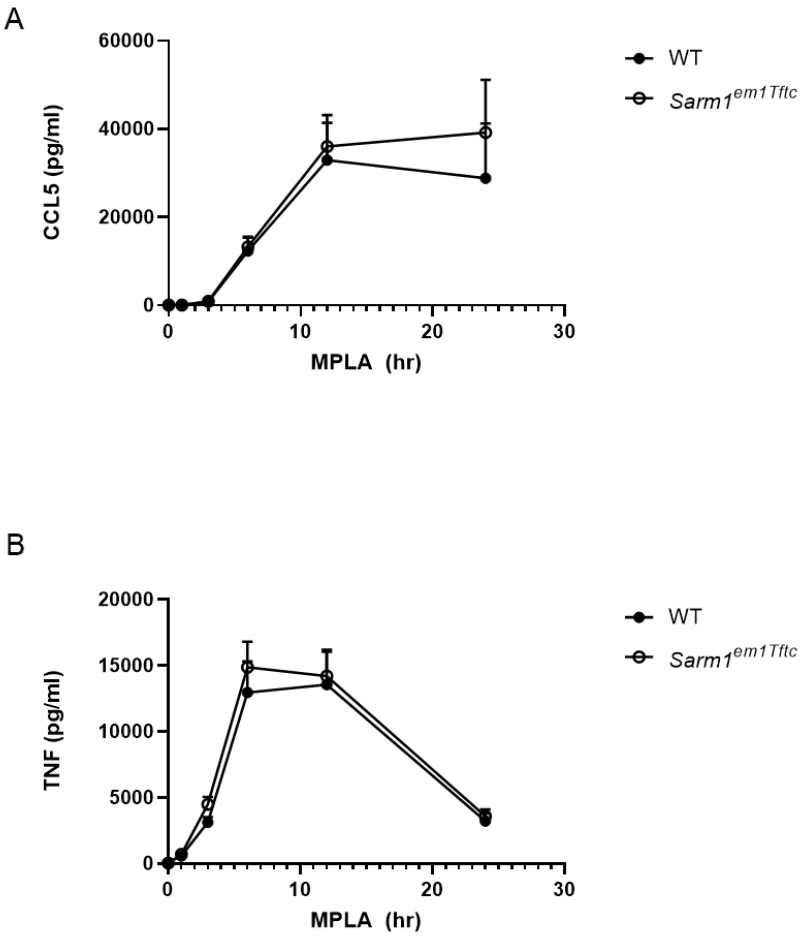

Figure 4.5 MPLA-induced CCL5 secretion is normal in pBMDMs from *Sarm*^{em1Tftc} mice compared to WT littermates

WT and *Sarm*^{em1Tftc} pBMDMs were stimulated with 1 μg/ml MPLA for the indicated times. Supernatants were assayed for CCL5 (A) and TNF (B) protein by ELISA. Graphs show mean ±SEM from 5 mice per genotype, performed in triplicate. No significant differences were determined by multiple Mann-Whitney tests with Holm-Šídák multiple comparisons test.

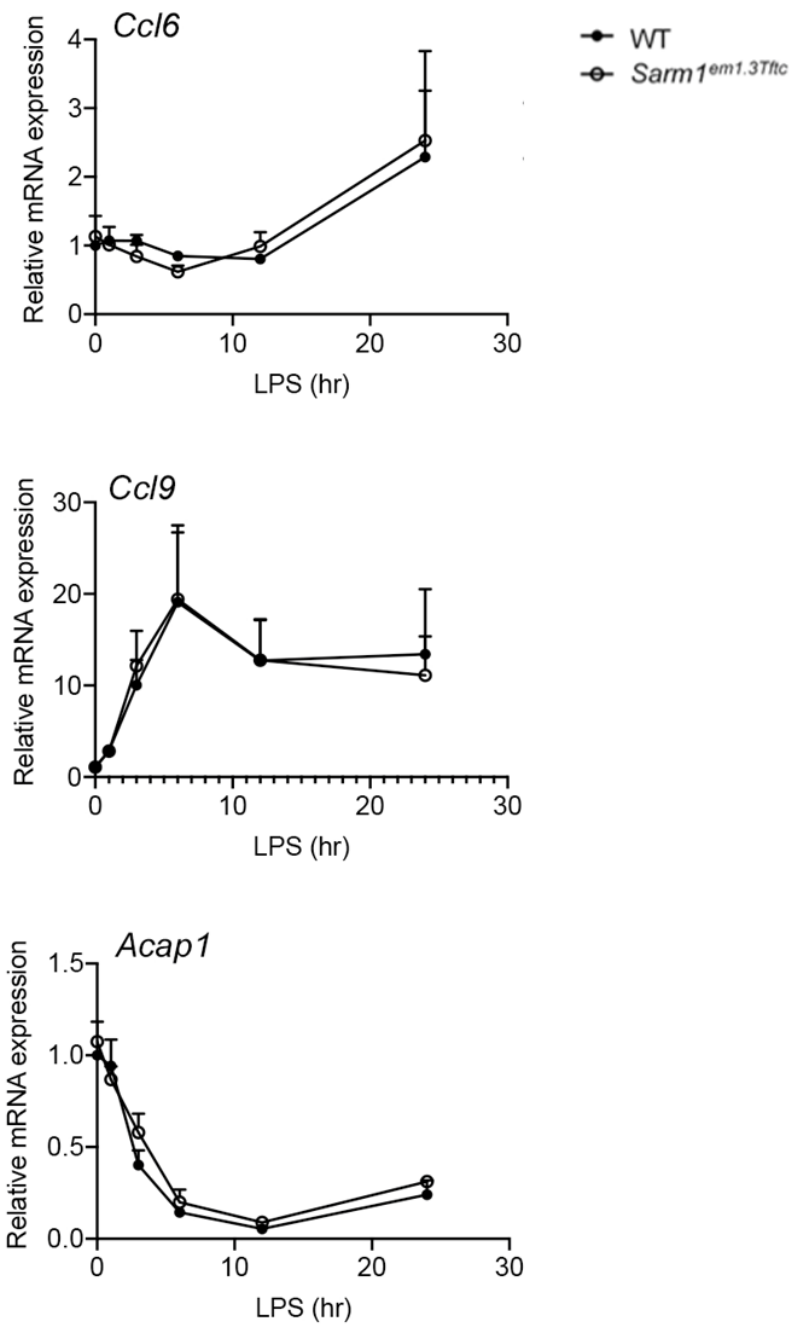

Figure 4.6 Macrophages from *Sarm1*$^{em1.3Tftc}$ mice show no defect in induction of select genes on chromosome 11 compared to WT littermates

WT and *Sarm1*$^{em1.3Tftc}$ pBMDMs were stimulated with 100 ng/ml LPS for the indicated times, or medium as a control. Expression of *Ccl6* (A), *Ccl9* (B), and *Tnf* (C) mRNA in were assayed by qRT-PCR, normalized to the housekeeping gene β-actin, and are presented relative to the untreated WT control. Graphs show mean ±SEM from 3 mice per genotype, performed in triplicate. There were no significant differences determined by multiple Mann-Whitney tests with Holm-Šídák multiple comparisons test.

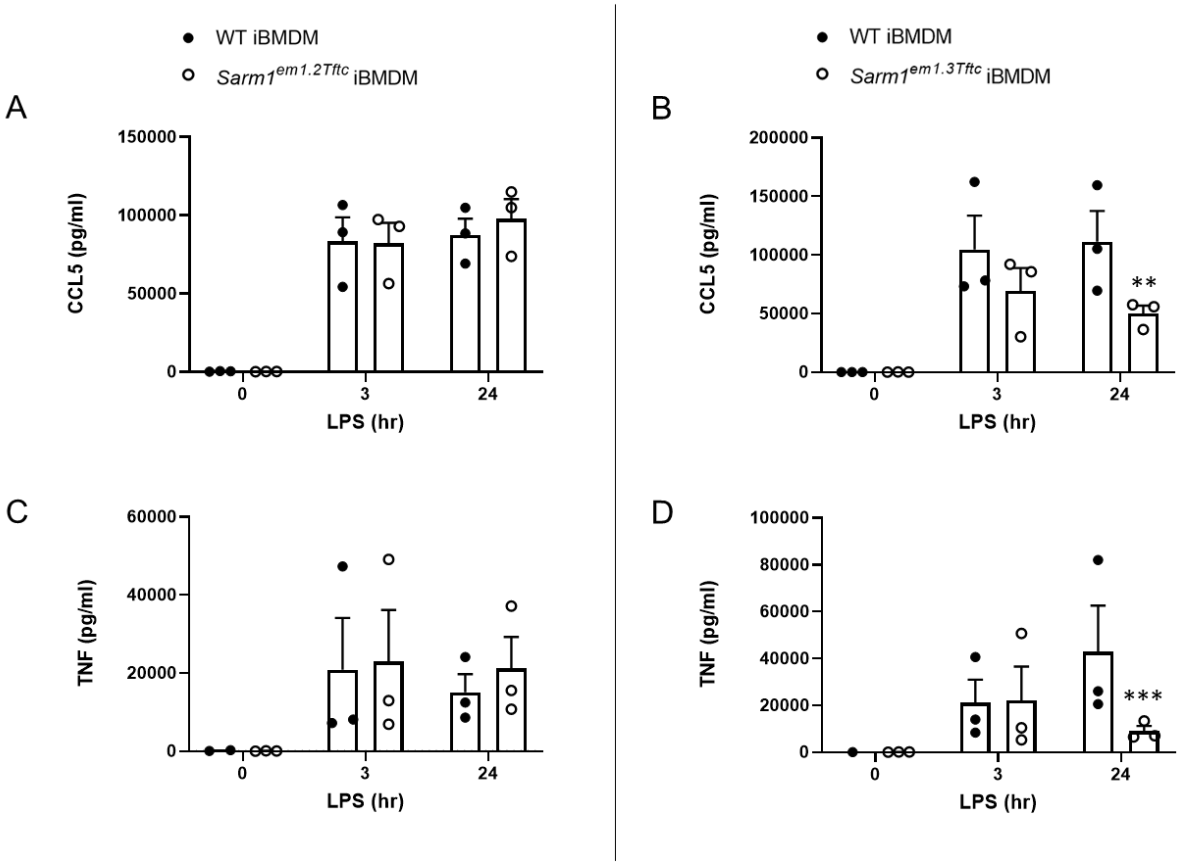

Figure 4.7 CCL5 and TNF secretion is normal in *Sarm1*$^{em1.2Tftc}$ iBMDMs, but impaired in *Sarm1*$^{em1.3Tftc}$ iBMDMs relative to WT

Sarm1$^{em1.2Tftc}$ (A, C) and *Sarm1*$^{em1.3Tftc}$ iBMDMs (B, D) and WT controls were stimulated with 100 ng/ml LPS for the indicated times. Supernatants were assayed for CCL5 (A, B) and TNF (C, D) protein by ELISA. Graphs show mean ±SEM from 3 experiments, performed in triplicate. **p<0.01, ***p<0.001 multiple Mann-Whitney tests with Holm-Šídák multiple comparisons test.

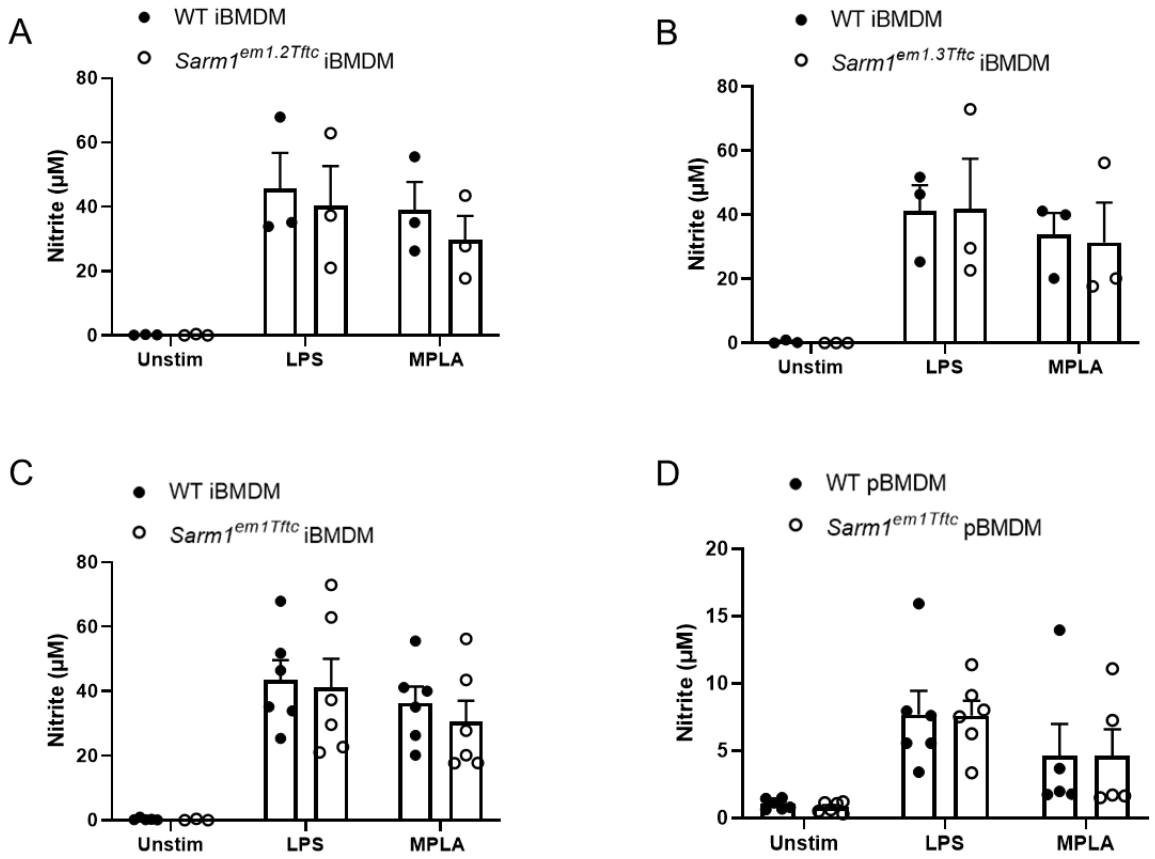

Figure 4.8 Nitric oxide production is normal in both primary and immortalised *Sarm1*^{em1Tftc} BMDMs

Sarm1$^{em1.2Tftc}$ iBMDMs (A), *Sarm1*$^{em1.3Tftc}$ iBMDMs (B), *Sarm1*^{em1Tftc} pBMDMs (D) and their respective WT controls were stimulated for 24 h with 1 μg/ml MPLA or 100ng/ml LPS or left unstimulated as indicated. Supernatants were assayed for nitric oxide production by Griess assay. Data from (A) and (B) are combined in (C). Graphs show mean ±SEM from 3 experiments (A and B), 6 experiments (C), and 5-6 mice per genotype (D), all performed in triplicate. There were no significant differences determined by multiple Mann-Whitney tests with Holm-Šídák multiple comparisons test.

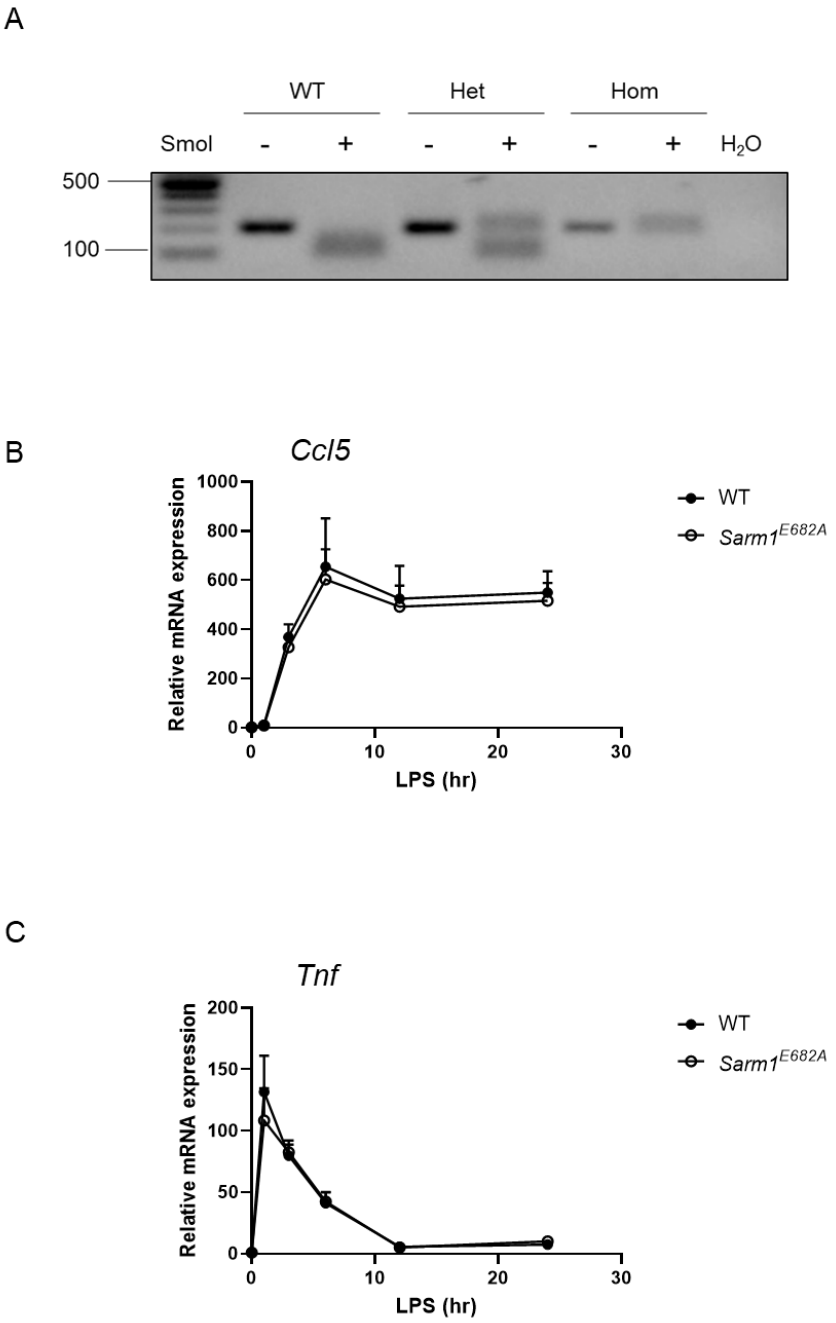

Figure 4.9 Genotyping and cytokine responses of a novel SARM1 NADase-deficient mouse generated using CRISPR

(A) Genotyping results for *Sarm1*^{E682A} littermates. PCR amplicon from mouse genomic DNA was incubated with (+) or without (-) SmoI enzyme. The amplicon containing WT sequence is not recognised by the enzyme, whereas the mutant sequence contains the SmoI restriction site and is cleaved. WT, wild type; het, heterozygote; hom, homozyote.
(B, C) WT and *Sarm1*^{E682A} pBMDMs were stimulated with 100 ng/ml LPS for the indicated times, or medium as a control. Expression of *Ccl5* (B) and *Tnf* (C) mRNA in were assayed by qRT-PCR, normalized to the housekeeping gene β-actin, and are presented relative to the untreated WT control. Graphs show mean ±SEM from 4-5 mice per genotype. There were no significant differences determined by multiple Mann-Whitney tests with Holm-Šídák multiple comparisons test.

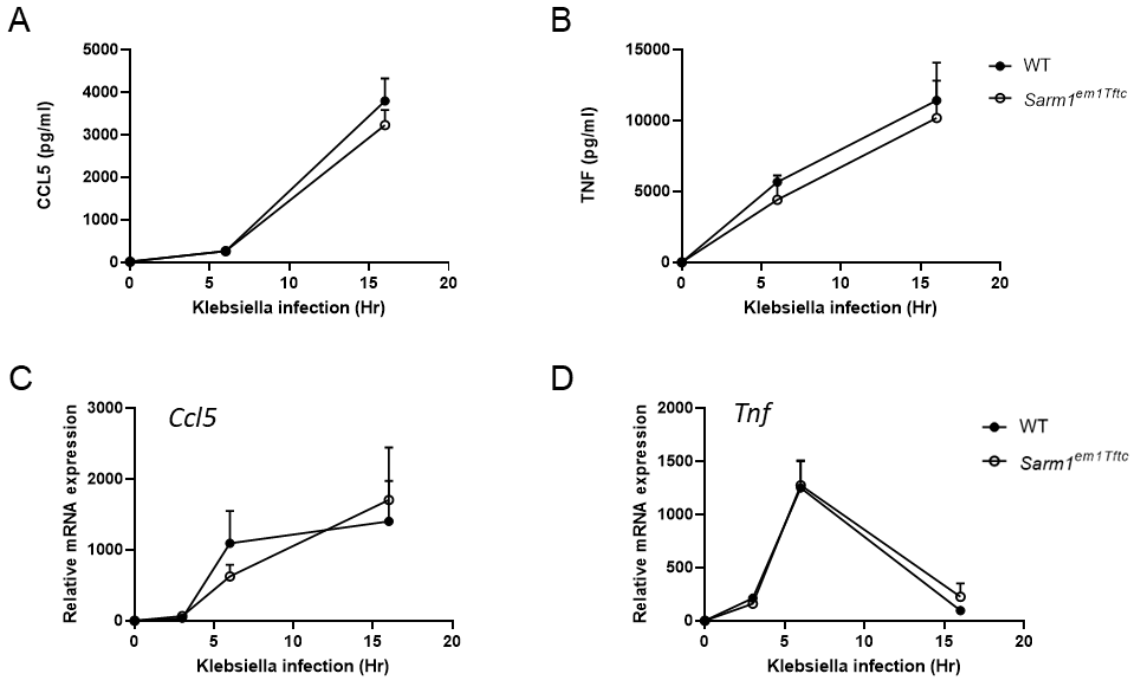

Figure 4.10 *Ccl5* and *Tnf* induction is similar in WT and *Sarm1*^{em1Tftc} pBMDMs following *Klebsiella pneumoniae* infection

(A - D) WT and *Sarm1*^{em1Tftc} pBMDMs were infected for the indicated times with *Klebsiella pneumoniae* or mock infected with media as a control. Expression of *Ccl5* (A) and *Tnf* (B) mRNA were assayed by qRT-PCR, normalized to the housekeeping gene β-actin, and are presented relative to the untreated WT control. Supernatants were assayed for CCL5 (C) and TNF (D) protein by ELISA. Data are mean ±SEM from 3 mice per genotype, performed in triplicate. There were no significant differences determined by multiple Mann-Whitney tests with Holm-Šídák multiple comparisons test.

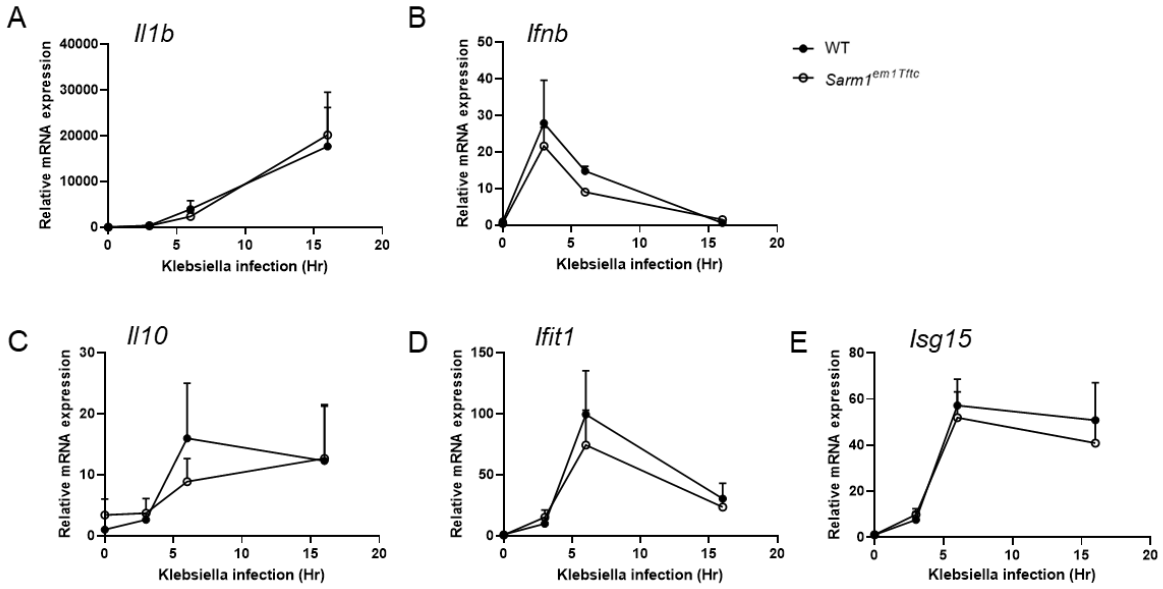

Figure 4.11 Gene induction is similar in WT and *Sarm1*^{em1Tftc} pBMDMs following *Klebsiella pneumoniae* infection

(A - E) WT and *Sarm1*^{em1Tftc} pBMDMs were infected for the indicated times with *Klebsiella pneumoniae* or mock infected with media as a control. Expression of *Il1* (A), *Ifnb* (B), *Il10* (C), *Ifit1* (D) and *Isg15* (E) mRNA were assayed by qRT-PCR, normalized to the housekeeping gene β-actin, and are presented relative to the untreated WT control. Data are mean ±SEM from 3 mice per genotype, performed in triplicate. There were no significant differences determined by multiple Mann-Whitney tests with Holm-Šídák multiple comparisons test.

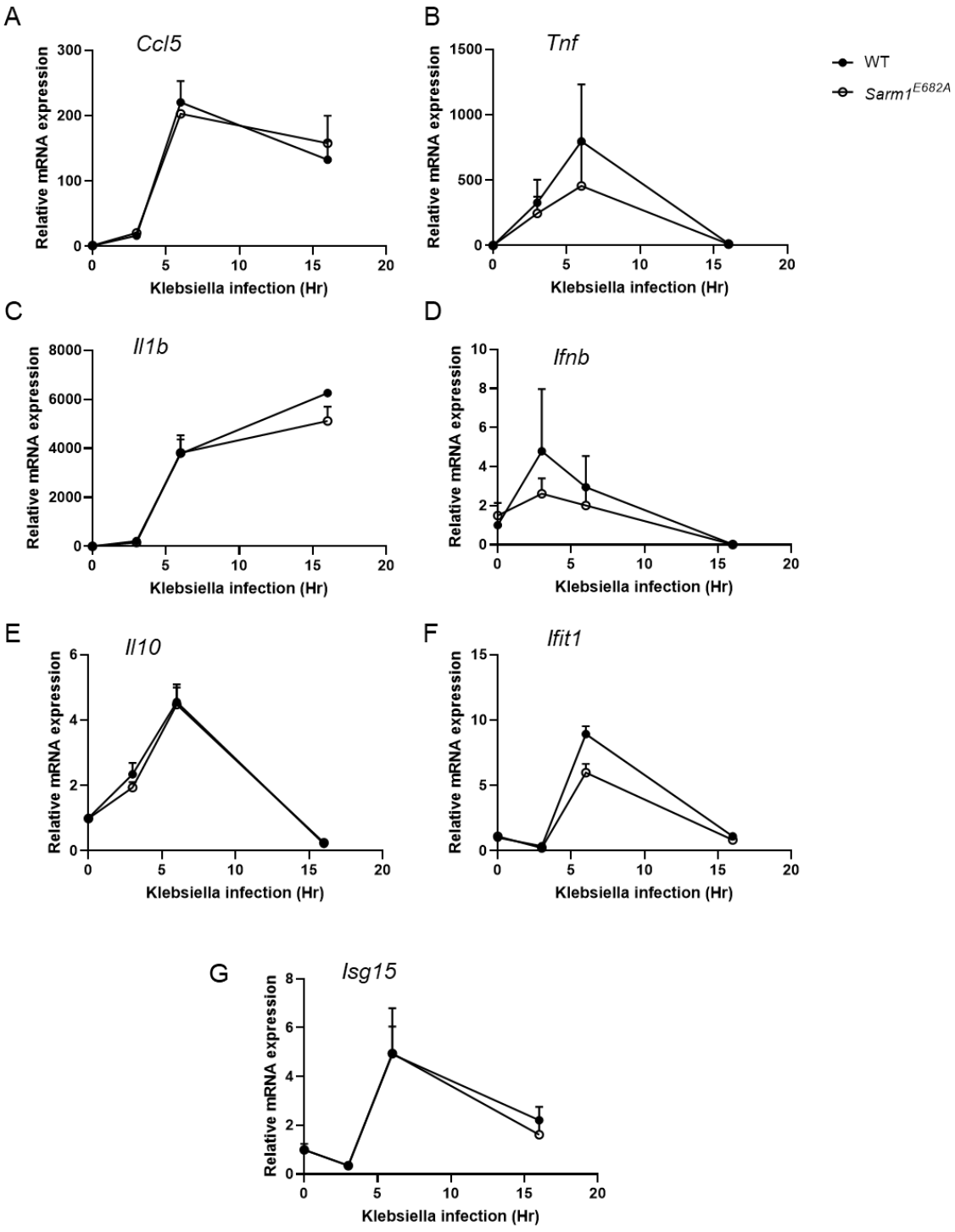

Figure 4.12 Gene induction is similar in WT and *Sarm1*^{E682A} pBMDMs following *Klebsiella pneumoniae* infection

(A - E) WT and *Sarm1*^{E682A} pBMDMs were infected for the indicated times with *Klebsiella pneumoniae* or mock infected with media as a control. Expression of *Ccl5* (A), *Tnf* (B), *Il1* (C), *Ifnb* (D), *Il10* (E), *Ifit1* (F) and *Isg15* (G) mRNA were assayed by qRT-PCR, normalized to the housekeeping gene β-actin, and are presented relative to the untreated WT control. Data are mean ±SEM from 2 mice per genotype, performed in triplicate. There were no significant differences determined by multiple Mann-Whitney tests with Holm-Šídák multiple comparisons test.

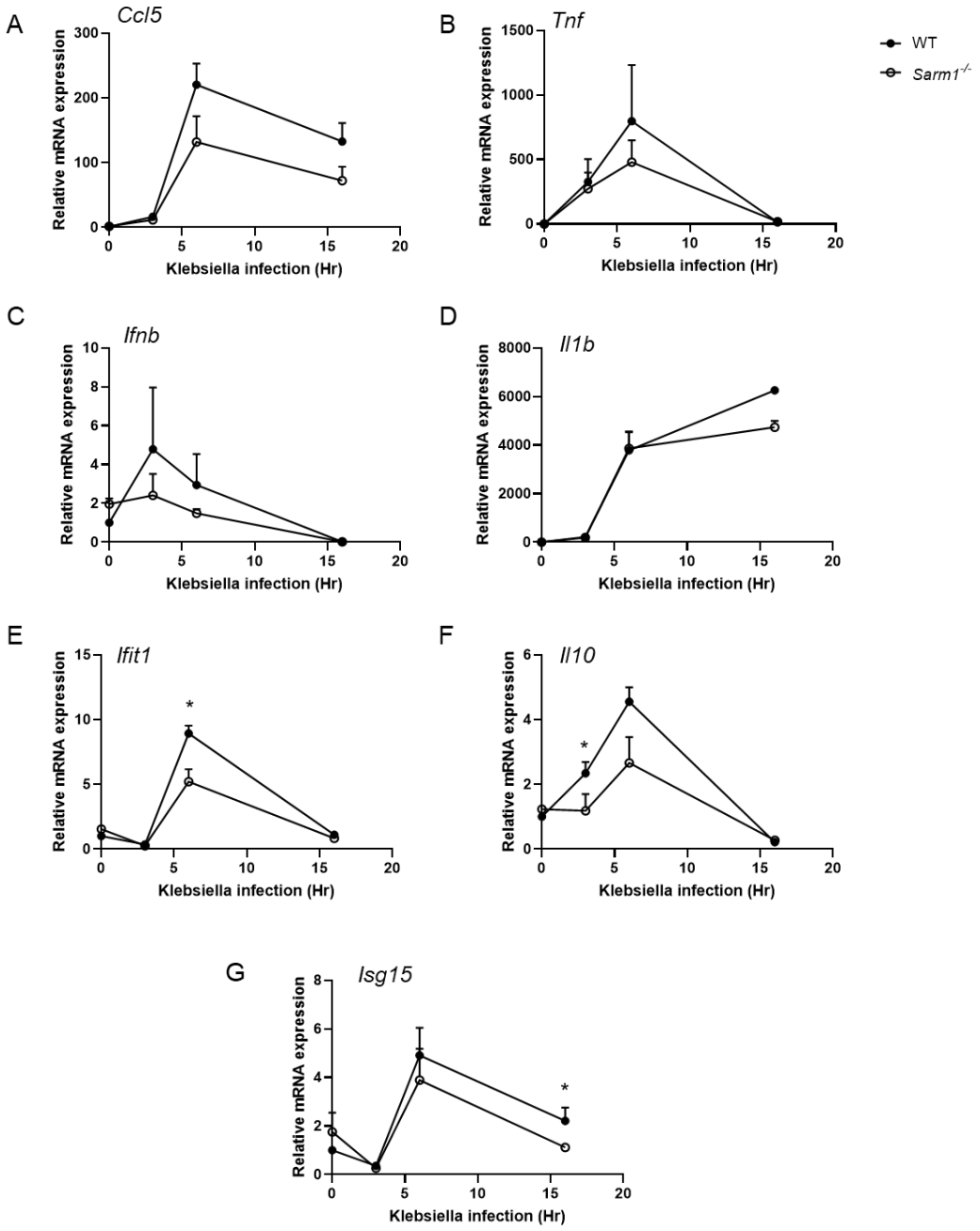

Figure 4.13 Gene induction is similar in WT and B6 congenic *Sarm1*$^{-/-}$ pBMDMs following *Klebsiella pneumoniae* infection

(A - E) WT and B6 congenic *Sarm1*$^{-/-}$ pBMDMs were infected for the indicated times with *Klebsiella pneumoniae* or mock infected with media as a control. Expression of *Ccl5* (A), *Tnf* (B), *Il1* (C), *Ifnb* (D), *Il10* (E), *Ifit1* (F) and *Isg15* (G) mRNA were assayed by qRT-PCR, normalized to the housekeeping gene β-actin, and are presented relative to the untreated WT control. Data are mean ±SEM from 2 mice per genotype, performed in triplicate. * $p < 0.05$ multiple Mann-Whitney tests with Holm-Šídák multiple comparisons test.

4.3 Discussion

The aim of this chapter was to ascertain if macrophages from SARM1-deficient mice exhibited differential gene expression after TLR4 stimulation in the absence of additional confounding variables. The presence of residual 129-derived genetic material surrounding the *Sarm1* locus precluded such comprehensive investigation in B6 congenic *Sarm1*$^{-/-}$ mice. Thus, we commissioned the TBSI transgenics facility to generate independent SARM1-deficient mice using CRISPR/Cas9 genome engineering, named *Sarm1*$^{em1.1Tftc}$, *Sarm1*$^{em1.2Tftc}$, and *Sarm1*$^{em1.3Tftc}$, or collectively *Sarm1*^{em1Tftc}. Crucially, these mice are on a fully C57BL/6 background. Unlike the B6 congenic *Sarm1*$^{-/-}$ mice, the novel CRISPR/Cas9 SARM1-knockout mice do not possess confounding passenger genes, and thus present an improved model in which to study the effects of SARM1 deletion. We could therefore use these CRISPR knockout mice to delineate which phenotypes previously observed in B6 congenic *Sarm1*$^{-/-}$ BMDMs are attributable to the absence of SARM1, and which were caused by the presence of passenger genes. Heterozygous breeding pairs were established for each CRISPR/Cas9 SARM1-deficient mouse line to generate littermate pairs of SARM1-deficient mice and WT controls. This is a labour-intensive process, as it requires that all mice are genotyped as shown in Figure 4.1, however it is essential to minimise the introduction of variability between the *Sarm1*^{em1Tftc} mice and their respective WT controls.

Another member of our laboratory verified that SARM1 protein expression was lost in *Sarm1*^{em1Tftc} by Western blot, and that the mice retained the axoprotective phenotype which has been reported in neurons from B6 congenic *Sarm1*$^{-/-}$ neurons [195]. This confirmed the functional loss of SARM1 in these mice, and ensured that they were an appropriate tool in which to test the role for SARM1 in transcriptional regulation. Thus I measured the LPS-induced expression of *Ccl5* in BMDMs from *Sarm1*^{em1Tftc} mice compared to littermate WT controls to test the role for SARM1 in transcriptional regulation of this gene, which was previously reported by our lab [34]. A timecourse of stimulations ranging from an hour to 24 hours was carried out, which would allow us to observe differential gene expression or altered expression kinetics between the WT and SARM1-knockout mice. BMDMs from all three SARM1-deficient mice generated by CRISPR/Cas9 showed a similar phenotype; there were no significant differences in LPS-induced *Ccl5* expression compared to their WT controls at any stimulation time point. The LPS-induced expression of *Tnf* was also unaffected by the absence of SARM1. This strengthens the case that, contrary to its role in

human myeloid cells [36], SARM1 does not antagonise TLR4-signalling in murine macrophages. Given that SARM1 protein expression and functional activity were confirmed to be abrogated in all three SARM1-deficient mice, and that they displayed a similar transcriptional phenotype, results from experiments carried out on the three CRISPR/Cas9-derived mice could be combined as appropriate. Similar to LPS, MPLA-induced CCL5 was equivalent between WT and *Sarm1*^{em1Tftc} BMDMs and their littermate WT counterparts. Hence, we conclude that SARM1 does not regulate transcription of *Ccl5* in murine macrophages, and that the phenotype observed in BMDMs from B6 congenic *Sarm1*$^{-/-}$ mice resulted from 129-derived passenger genes introduced when the mice were generated. This is reinforced by the fact that stable expression of SARM1 in B6 congenic *Sarm1*$^{-/-}$ BMDMs did not enhance CCL5 production, as seen in Section 3.2.7. In further support of this conclusion, during the course of this study, the García-Sastre lab reported similar findings in SARM1-deficient mice which they independently generated by CRISPR/Cas9 [246]. Thus, while the observations in the study previously published by our lab describing a role for SARM1 in transcriptional regulation of *Ccl5* by murine SARM1 in macrophages were correct, the interpretation was confounded by the presence of passenger genes, which had not yet been identified in the B6 congenic *Sarm1*$^{-/-}$ mouse.

In addition to *Ccl5*, the LPS-induced expression of *Ccl6*, *Ccl9*, and *Acap1* was measured in *Sarm1*^{emTftc} mice compared to WT littermate controls. Differential expression of these genes in BMDMs from B6 congenic *Sarm1*$^{-/-}$ mice was previously revealed by RNA sequencing and confirmed experimentally by qRT-PCR both basally and following stimulation with LPS for 3 hours (Chapter 3). However, suspicions were raised that this differential gene expression may be an artefact resulting from passenger genes based on the fact that these genes are located in close proximity to each other and to the *Sarm1* locus, and that their expression is disrupted basally. While I could previously confirm that 129-associated sequence variations were present at these loci in the B6 congenic *Sarm1*$^{-/-}$ BMDMs, it remained essential to demonstrate that these passenger genes were accountable for the altered gene expression. Thus, a timecourse of stimulations was carried out over a period of 24 hours, to facilitate identification of differential gene expression or disrupted expression kinetics in the SARM1-deficient macrophages. The expression of *Ccl6* and *Ccl9* were previously observed to be diminished in B6 congenic *Sarm1*$^{-/-}$ BMDMs relative to WT both basally and following LPS stimulation for 3 hours (Section 3.2.6). However, in

the absence of passenger genes, *Ccl6* and *Ccl9* expression was equivalent between *Sarm1*$^{em1.3Tftc}$ BMDMs and their WT control at every stimulation time point. Similarly, in the absence of passenger genes, basal and LPS-induced *Acap1* expression was equivalent between *Sarm1*$^{em1.3Tftc}$. This is in contrast to the enhanced *Acap1* expression observed in B6 congenic *Sarm1*$^{-/-}$ BMDMs compared to WT, both basally and following LPS treatment. Thus the previously observed differential gene expression is attributable to passenger genes, and not the absence of SARM1 in B6 congenic *Sarm1*$^{-/-}$ macrophages. The extent to which this passenger gene induced differential gene expression may contribute to other phenotypes attributed to SARM1-deficiency based on studies performed on B6 congenic *Sarm1*$^{-/-}$ is not known. However, it is increasingly clear that they are an unsuitable model in which to study the roles for murine SARM1. We propose that the SARM1-deficient mice which we generated through CRISPR/Cas9, characterised in this thesis and in our recent publication [195], present a superior alternative. These mice could be used to re-evaluate phenotypes previously ascribed to SARM1 based on results from B6 congenic *Sarm1*$^{-/-}$ mice, particularly where the products of genes which flank *Sarm1* on chromosome 11 are implicated in the mechanism of action. One such study reported accelerated progression of prion disease in B6 congenic *Sarm1*$^{-/-}$ mice, which was attributed to their enhanced *Xaf1* expression relative to WT [169]. Given that *Xaf1* is a passenger gene in B6 congenic *Sarm1*$^{-/-}$ mice, one may speculate that the same phenotype would not be observed in *Sarm1*^{em1Tftc} mice.

CRISPR/Cas9 was also used to generate a mouse in which SARM1 lacked NADase activity, called *Sarm*^{E682A}. The objective was to use this mouse to define which SARM1-mediated activities specifically required the NADase function of SARM1, which depletes NAD^+ and produces cADPR, and not the structural activity. I observed similar expression of all genes of interest in pBMDMs from *Sarm1*^{E682A} and WT littermate controls. This was the anticipated result, as it is implausible that the NADase activity of SARM1 would be required for the induction of genes whose expression is normal in pBMDMs completely lacking SARM1. However, difficulties have been encountered in detecting SARM1 protein in *Sarm1*^{E682A} neurons, where murine SARM1 is highly expressed [26, 195]. Thus, it is unclear if these mice are actually an NADase-inactive mutant or if they act as an additional SARM1 knockout mouse. Further investigation is required to determine why SARM1 is protein is not detectable in these mice. This could be due to disruption of the epitope which is recognised by SARM1 antibodies or due to lack of expression of SARM1 in these mice

as a result of the genetic manipulations done to generate the mice, although resolving this is beyond the scope of this project.

The B6 congenic *Sarm1*$^{-/-}$ and WT iBMDMs which were kindly gifted to our lab by Prof. Kate Fitzgerald were a useful resource as large number of cells could be generated quickly and with ease. In addition, by stably expressing flag-tagged SARM1 in the B6 congenic *Sarm1*$^{-/-}$ iBMDMs, we could examine the effect of reconstitution on transcription of *Ccl5* and determine that SARM1 did not localise to the nucleus. However, these cells retain passenger genes flanking the *Sarm1* locus, which limits their usefulness. Additionally, it is not known if the mice from which they were derived were age-matched, sex-matched, or co-housed, or if the bone marrow cells were seeded at similar densities at the point of differentiation. Differences in phenotype were observed between the primary and immortalised B6 congenic *Sarm1*$^{-/-}$ BMDMs (Section 3.2.2), which may relate to one of the factors listed above or may be for an unrelated reason. Further, these cells represented only the one mouse from which they were derived. I therefore sought to generate iBMDMs from SARM1-deficient cells which did not harbour passenger genes, and with optimally matched WT controls, which could be used in the place of B6 congenic *Sarm*$^{-/-}$ iBMDMs. Bone marrow cells from *Sarm1*$^{em1.2Tftc}$ and *Sarm1*$^{em1.3Tftc}$ and their respective WT littermates were seeded at similar densities, to prevent the introduction of variability, and immortalised. *Sarm1*$^{em1.2Tftc}$ iBMDMs and their WT controls showed similar secretion of CCL5 and TNF basally and following treatment with LPS for 3 or 24 hours, which mirrored the phenotype seen in *Sarm1*$^{em1.2Tftc}$ pBMDMs. In contrast, in *Sarm1*$^{em1.3Tftc}$ iBMDMs the secretion of CCL5 and TNF was similar to WT basally and following 3 hour treatment with LPS, but significantly reduced after 24 hours. It is unlikely that this is due to the absence of SARM1, given that it was not observed in *Sarm1*$^{em1.2Tftc}$ iBMDMs or *Sarm1*$^{em1.3Tftc}$ pBMDMs. Perhaps it may be attributable to subtle differences in the process of immortalisation with the J2 recombinant retrovirus when SARM1 is absent, or clonality arising from the long cultures required in this process. In contrast to the diminished NO production observed in B6 congenic *Sarm1*$^{-/-}$ iBMDMs, NO production was equivalent to WT in both *Sarm1*$^{em1.2Tftc}$ and *Sarm1*$^{em1.3Tftc}$ iBMDMs. Thus, while iBMDMs remain a valuable tool, the factors that influence their phenotype independent of gene-targeting are complicated. Even when all possible variables are controlled during the stages of mouse breeding and differentiation and immortalisation, the resulting iBMDMs will still be reflective only of the mice from which they derive, and will exhibit biological variation.

Therefore, care should be taken when generating iBMDM, and caution should be exercised when interpreting results from them.

Ideally, all publications reporting a role for murine SARM1 based on experiments performed with B6 congenic *Sarm1*$^{-/-}$ mice would be replicated in CRISPR/Cas9 SARM1-knockouts. Uccellini *et al.* re-examined the role for SARM1 in the response to a number of neurotropic diseases. The authors demonstrated that the role they previously reported for SARM1 in determining susceptibility to VSV in B6 congenic *Sarm1*$^{-/-}$ was not recapitulated in SARM1-deficient mice generated by CRISPR/Cas9, and stemmed from passenger genes [246]. Our collaborators in the Bengoechea lab examined the effect of SARM1-deficiency in *K. pneumoniae* infection in both B6 congenic *Sarm1*$^{-/-}$ and *Sarm1*$^{em1.1Tftc}$ mice and found a similar phenotype of enhanced cytokine secretion in the lung compared to WT [248]. *In vitro,* both B6 congenic *Sarm1*$^{-/-}$ and *Sarm1*$^{em1.1Tftc}$ iBMDMs also displayed augmented inflammatory cytokine secretion compared to their respective WT controls [248].

Given the limitations and uncertainties associated with iBMDMs I discussed previously, I investigated if a similar phenotype would be observed in *Sarm1*^{em1Tftc} pBMDMs. Surprisingly, I saw no significant differences in expression of the genes which the Bengoechea lab previously observed to be elevated in iBMDMs from *Sarm1*^{em1Tftc} compared to their littermate WT controls, namely *Il1b, Ifnb, Il10, Ifit1,* and *Isg15* [248]. In addition I measured the expression and secretion of CCL5 and TNF to see if SARM1 may have a role in their transcription in the context of a complex pathogenic infection. Again, there were no significant differences between WT and *Sarm1*^{em1Tftc}. Similarly, *K. pneumoniae*-induced gene induction was equivalent between pBMDMs from *Sarm1*^{E682A} mice and WT controls.

It seemed unlikely that passenger genes could account for the enhanced *K. pneumoniae*-induced cytokine expression observed by our collaborators in macrophages lacking SARM1, as both B6 congenic *Sarm1*$^{-/-}$ iBMDMs and *Sarm1*$^{em1.1Tftc}$ iBMDMs exhibited this same phenotype [248]. Nonetheless, I decided to examine the response to *K. pneumoniae* in pBMDMs from B6 congenic *Sarm1*$^{-/-}$, to ensure that we observe a similar phenotype. Surprisingly, enhanced expression of *Tnf, Ifnb, Il1b, Il10, Ifit1,* or *Isg15* was not observed in B6 congenic *Sarm1*$^{-/-}$ pBMDMs compared to WT. In fact, at some time-points, *Sarm1*$^{-/-}$ pBMDMs showed lower expression of some of these genes than their WT counterparts. As

anticipated, *K. pneumoniae*-induced *Ccl5* was reduced in pBMDMs from B6 congenic *Sarm1*$^{-/-}$ mice compared to WT due to the presence of passenger genes, though this did not meet the threshold of significance.

I noticed that the level of induction of some genes, particularly *Il10*, *Ifnb*, and the interferon-stimulated genes, was much lower in pBMDMs here than in iBMDMs by our collaborators. However it is unlikely that iBMDM/pBMDM differences explain why I did not observe the expected phenotype in pBMDMs from B6 congenic *Sarm1*$^{-/-}$ mice, as the Bengoechea lab observed enhanced IL-1, TNF and TRIF-dependent cytokines in pBMDMs from B6 congenic *Sarm1*$^{-/-}$ compared to WT as well as iBMDMs [248]. While the same protocol, time points, and strain of *Klebsiella* were used here and in the Bengoechea lab study, it remains possible that inter-institutional differences, or even technical differences in how each individual researcher performs the experiments, may have contributed the inconsistency in phenotype observed. For instance, here 24 well plates were used rather than 12 well plates to allow for more infection time-points, and cell number per well was adjusted to maintain a similar cell density and MOI. Perhaps differences in the preparation of the bacteria prior to infection could have resulted in the actual MOI being different to the calculated MOI, which may explain differences in gene induction.

The *in vivo* experiments were carried out by the Bengoechea lab in *Sarm1*$^{em1.1Tftc}$ mice sent by us from the TSBI animal facility, however it ought to be noted that littermate wild type controls were not used in these studies. The animals of different genotype have therefore experienced different environments and will vary in their microbiota. The WT C57BL/6 control mice used were purchased from Charles River Laboratories. It is not clear whether the controls are of the C57BL/6N or C57BL/6J strain, however if they are of the C57BL/6N strain this may result in phenotypic differences to the *Sarm1*$^{em1.1Tftc}$ mice which we generated on a C57BL/6J background. Additionally, due to genetic drift the wild type C57BL/6J mice would differ in genome sequence to the CRISPR SARM1-knockout mouse in additional locations to the *Sarm1* locus. These factors may all effect the response to infection. Further, a recent study compared the phenotype observed in two genetically identical mice in Harvard and the Broad Institute, and showed that differences in abundance of immune-stimulating bacteria between the two facilities resulted in two different phenotypes [252]. Inter-institutional environmental differences may influence the phenotypes observed by us and by the Bengoechea lab. A final possibility is that the

phenotype of enhanced inflammatory cytokine secretion observed in SARM1-deficient iBMDMs by the Bengoechea group does not occur in SARM1-deficient pBMDMs in absence of passenger genes, and is unrelated to the *in vivo* phenotype of improved bacterial clearance in SARM1-knockout mice. Therefore, while some results from the Bengoechea lab suggest that murine SARM1 has a role in the transcriptional response to *K. pneumoniae*, the extent to which confounding variables unrelated to the absence of SARM1 contribute to these results remains unclear

Thus, using the SARM1-deficient mice which we independently generated by CRISPR/Cas9, I have demonstrated that murine SARM1 does not have a role in regulating the transcription of *Ccl5* or a number of additional genes which were identified as DEGs in B6 congenic *Sarm1*$^{-/-}$ mice. Rather, the confounding influence of 129-derived passenger genes in B6 congenic *Sarm1*$^{-/-}$ mice resulted in differential gene expression. Copious studies have relied on B6 congenic *Sarm1*$^{-/-}$ mice to investigate the effect of SARM1 deletion, and it is not yet clear how far-reaching the impact of these confounding passenger genes may be on this field as a whole. Thus, the novel *Sarm1*^{em1Tftc} mice presented in this thesis and our recent publication [195] are a more appropriate model in which to examine the roles for murine SARM1, and could also be used to validate the results from previous studies. The *Sarm1*^{em1Tftc} mice also provided further confirmation that SARM1 does not have a role in antagonising MyD88 or TRIF signalling following TLR4 stimulation, as the LPS- and MPLA-induced expression of pro-inflammatory cytokines is normal in these mice. BMDMs from two of the three CRISPR/Cas9 SARM1-knockout mice were immortalised, and the resulting iBMDMs were characterised to ensure they were an appropriate tool in which to study the effects of SARM1-deficiency. However, impaired cytokines secretion was observed in iBMDMs from the *Sarm1*$^{em1.3Tftc}$ mouse, which is inconsistent with the normal cytokine induction observed in iBMDMs from *Sarm1*$^{em1.2Tftc}$ mouse and in pBMDMs from all three CRISPR/Cas9 SARM1-knockout mice. This once again emphasises the importance of careful generation of iBMDMs and judicious interpretation of results from these cells. Finally, the role for SARM1 in the cytokine response to *K. pneumoniae* was assessed in pBMDMs from B6 congenic mice, *Sarm1*^{em1Tftc} mice, and *Sarm1*^{E682A} mice. In contrast to results observed by the Bengoechea lab in iBMDMs from *Sarm1*^{em1Tftc} mice and *Sarm1*^{E682A} mice, SARM1-deletion had no impact on the *K. pneumoniae*-induced expression of pro-inflammatory cytokines in pBMDMs.

Chapter 5 SARM1 Expression in the Brain and Macrophages

5.1 Introduction

Data from this thesis thus far do not support a role for SARM1 in transcription in macrophages, as the differential gene expression previously observed in B6 congenic *Sarm1*$^{-/-}$ mice can be attributed to passenger genes. In contrast to macrophages where SARM1 expression is low, neurons express SARM1 abundantly [26]. Thus I wondered if differential gene expression may be observed in the CNS of our novel CRISPR/Cas9 SARM1-knockout mice.

5.1.1 Transcriptional regulation in the brainstem by SARM1

SARM1 is highly expressed in the nervous system, and its roles there are numerous and varied (as described in Sections 1.4, 1.6.2, and 3.1). In addition to the extensively studied function for SARM1 in mediating axon degeneration, and the recently verified role for SARM1 in determining resistance to WNV [246], there are also reports of SARM1 regulating transcription within the nervous system. The García-Sastre lab reported that a number of genes are basally differentially expressed in the brainstem of their independently generated CRISPR/Cas9 SARM1 knockout mice compared to WT, as determined by RNA sequencing [246]. Interestingly, among the differentially expressed transcripts were components of the mitochondrial electron transport chain, including the complex I subunits *Ndufa3* and *Ndufb3*, the complex III subunit *Uqcrh*, and the complex V subunit *Atp5k*. These genes were reportedly more highly expressed in the brainstem of SARM1-deficient mice than in WT controls. This may add support to the reported role for SARM1 in inhibition of mitochondrial respiration, which was observed by Murata *et al.* in HEK293T cells overexpressing SARM1, and in SH-SY5Y neuronal cells in which SARM1 was knocked-down [31]. Additional genes which the García-Sastre lab reported to be differentially expressed in the CRISPR/Cas9 SARM1-knockout mouse brainstem included *Rps29* and *Rpl38*, which encode ribosomal proteins, as well as the transferrin receptor gene *Tfrc* [246].

The RNA sequencing data was not accompanied by qRT-PCR measurement of mRNA levels of these genes in the brainstem of WT and SARM1-deficient mice. Nonetheless, I was interested in determining whether this differential gene expression would also be observed in the brainstem of each our three CRISPR/Cas9 SARM1-knockout mice compared to WT littermate controls when measured by qRT-PCR. In addition, recent data from our lab suggests that macrophages from *Sarm1*^{em1Tftc} show altered mitochondrial respiration compared to WT (K. Shanahan, personal communication). I wondered whether this may also be related to enhanced expression of components of the electron transport chain. While differential expression of these genes was not detected by RNA sequencing of BMDMs from B6 congenic *Sarm1*$^{-/-}$ compared to WT (Section 3.2.5), it remains possible that the presence of 129-derived passenger genes resulted in other legitimate DEGs being masked. Thus, one aim of this chapter was to examine the expression of the DEGs reported by the García-Sastre lab in both macrophages and brainstems from our *Sarm1*^{em1Tftc} mice.

5.1.2 SARM1 is difficult to detect outside of the nervous system

The focus of this thesis has so far been on investigating the role for murine SARM1 in transcriptional regulation exclusively in macrophages. Data from the CRISPR/Cas9 knockout mice did not reveal any such role. It showed instead that the reduced expression of *Ccl5* previously observed in SARM1-deficient macrophages [34] was a consequence of the 129-derived passenger genes present in the genome of B6 congenic *Sarm1*$^{-/-}$ mice. It is currently unclear how many other roles ascribed to SARM1 in macrophages may have been similarly derived from the incorrect interpretation of observations in B6 congenic *Sarm1*$^{-/-}$ mice. In fact, there is some contention surrounding the expression of SARM1 in macrophages. While we and others can detect SARM1 mRNA in WT BMDMs [34, 195], some groups have reported difficulty in detecting SARM1 expression in this cell type [44, 246].

In contrast, SARM1 is highly expressed in the nervous system [26]. This abundant expression correlates with numerous aforementioned reported roles for SARM1 in this setting; SARM1 mediates axonal degeneration following a variety of cellular insults [29, 89], regulates transcription of a discrete set of cytokines and chemokines following traumatic axon injury [208], regulates transcription in the brainstem [246], and determines resistance to WNV [246]. SARM1 protein expression is readily detectable in the brain.

However like many members of the TLR-adaptor family, SARM1 protein expression is challenging to specifically and reliably detect in many cell types, including macrophages, with the currently commercially available antibodies. Thus it is difficult to conclusively define the tissues and cell types where SARM1 is expressed, and this has impeded studies into the functions for SARM1 outside of the nervous system. Many studies therefore rely on exogenous expression of SARM1 to examine its functions in cell types where it is difficult to detect. This introduces a number of confounding factors, including potential effects the tag may have on the function or localisation of SARM1, and exogenous expression levels which may differ dramatically from endogenous levels. Hence it is difficult to conclude if the phenotypes observed in cells overexpressing SARM1 occur physiologically. Additionally, phenotypes considered to result from the absence of SARM1 outside of the nervous system may actually be attributable to passenger genes in cases where the experiments were carried out in B6 congenic *Sarm1*$^{-/-}$ mice, as was described earlier in this thesis. Thus, the possibility remains that SARM1 expression and function may be confined to the nervous system.

To address this we commissioned the TBSI transgenics facility to generate, to our knowledge, the first mouse expressing an epitope-tagged SARM1 endogenously [195]. In this mouse, named *Sarm1*$^{em2(FLAG\text{-}Strep)Tftc}$ and herein referred to as *Sarm1*^{Flag}, CRISPR/Cas9 mediated genome engineering was used to insert a triple Flag tag and double strep tag to the C-terminus of SARM1. These tags are readily detected by commercially available antibodies, and this facilitates detection of SARM1 in cells and tissues derived from this mouse. An important aim of this chapter was to determine if SARM1 expression, and by extension function, is limited to the nervous system or detectable in macrophages using the *Sarm1*^{Flag} mouse.

5.2 Results

5.2.1 SARM1 does not regulate the expression of Tfrc, Rps29, Rpl38, Ndufb3, or Atp5k in BMDMs

Data from our three novel CRISPR/Cas9 SARM1-knockout mice did not reveal any role for murine SARM1 in transcription of the specific genes of interest in BMDMs. However, in a study by the García-Sastre laboratory, RNA sequencing revealed that a number of genes were basally differentially expressed in the brainstem of CRISPR/Cas9 SARM1-deficient mice compared to WT controls [246]. A number of these genes encode components of the mitochondrial electron transport chain. I wondered if they may also be differential expressed in BMDMs from *Sarm1*^{em1Tftc} mice, as altered mitochondrial respiration has been observed in these cells by another member of the lab.

To address this, I designed qRT-PCR primers for a panel of genes selected from the list of DEGs reported by the García-Sastre lab, which included *Tfrc*, *Rps29*, *Rpl38*, *Ndufa3*, *Ndufb3*, *Uqcrh*, and *Atp5k* [246]. Expression of *Ndufa3* and *Uqcrh* was not consistently detected, or was detected at very low levels. Therefore they were excluded from further analysis. The expression of *Tfrc*, *Rps29*, *Rpl38*, *Ndufb3*, and *Atp5k* was measured in BMDMs from *Sarm1*^{em1Tftc} mice compared to WT littermate control. Both basal expression and TLR4-induced expression was examined over a 24 hour timecourse. No significant differences emerged in the expression of these genes before or after LPS treatment (Figure 5.1). In addition, with the exception of *Tfrc*, the expression of these genes was similar in BMDMs from *Sarm1*^{E682A} mice and WT littermate controls, both basally and following treatment with LPS (Figure 5.2). Basal *Tfrc* was reduced in *Sarm1*^{E682A} pBMDMs relative to WT, though this difference did not persist following LPS stimulation (Figure 5.2). It is unlikely that there is a legitimate role for SARM1 NADase in the homeostatic expression of *Tfrc* in pBMDMs, given that the absence of SARM1 has no impact on *Tfrc* expression. It is more plausible that this is an artefact. Thus, SARM1 does not regulate the expression of *Tfrc*, *Rps29*, *Rpl38*, *Ndufb3*, or *Atp5k* in BMDMs.

5.2.2 SARM1 does not regulate the expression of Tfrc, Rps29, Rpl38, Ndufb3, or Atp5k in the brainstem

I also sought to examine the expression of these genes in the brainstems of our novel CRISPR/Cas9 SARM1-knockout mice compared to WT. RNA was isolated from the brainstems of *Sarm1*$^{em1.1Tftc}$ mice and WT littermate controls, and using qRT-PCR the expression of *Tfrc*, *Rps29*, *Rpl38*, *Ndufb3*, and *Atp5k* was measured. The expression of *Ccl5* was also examined, though it was previously demonstrated to be normally expressed in SARM1-deficient macrophages in the absence of passenger genes (Section 3.2.5). In contrast to the differential expression of these genes observed by the García-Sastre lab through RNA sequencing [246], no significant differences in gene expression were observed between brainstems of WT and *Sarm1*$^{em1.1Tftc}$ mice by qRT-PCR (Figure 5.3). To ensure that this result was not exclusive to the *Sarm1*$^{em1.1Tftc}$ line of mice, the same experiment was performed in *Sarm1*$^{em1.2Tftc}$ and *Sarm1*$^{em1.3Tftc}$ mice and their respective WT littermate controls. Again, no significant differences were observed in the expression of these genes in the brainstems of *Sarm1*$^{em1.2Tftc}$ mice compared to WT (Figure 5.4 A, C, E, G, I, K), and *Sarm1*$^{em1.3Tftc}$ mice followed the same trend (Figure 5.4 B, D, F, H, J, L). Thus in three different CRISPR/Cas9 SARM1-knockout mice, it appears that the absence of SARM1 has no effect on transcription in the brainstem. This is in contradiction with the results observed by the García-Sastre lab by RNA sequencing, although their RNA sequencing results were not confirmed by qRT-PCR. Both we and the García-Sastre lab observed abrogated axon degeneration in neurons from our respective CRISPR/Cas9 SARM1-knockout mice [195], confirming functional loss of SARM1 Thus it is unclear why differences in transcriptional phenotype are observed between our groups. It may relate to the difference in sensitivity between the methods used by each group to measure gene expression.

5.2.3 SARM1 expression is not limited to the central nervous system

Although I did not observe a role for SARM1 in regulating transcription in the brainstem, the reported roles for SARM1 in the central nervous system are numerous and diverse. This is consistent with high SARM1 expression in neurons relative to other tissues and cell types [26], including BMDMs. We and others have previously reported roles for SARM1 in

murine macrophages [25, 45]. However, SARM1 is difficult to reliably and specifically detect in tissues outside of the brain using commercially available antibodies, and this has impeded the study of functions of SARM1 outside of the nervous system. To address this, we commissioned the TBSI transgenics facility to generate a mouse in which SARM1 possesses a C-terminal epitope tag using CRISPR/Cas9 (see Figure 2.3 for targeting strategy and generation of mouse).

In the resulting *Sarm1*^{Flag} mouse, the C-terminus of SARM1 is tagged by insertion of a triple Flag tag and double strep tag to facilitate detection. Heterozygous breeding pairs were established to generate *Sarm1*^{Flag} mice with littermate WT controls, and each litter was genotyped (Figure 5.5 A). Another lab member confirmed that this epitope-tagged SARM1 retained functionality by demonstrating that neurons from *Sarm1*^{Flag} mouse show similar axon degeneration to WT controls following treatment with vincristine [195]. Furthermore, expression of SARM1 mRNA in *Sarm1*^{Flag} mice was similar to that in WT counterparts across a range of tissues [195]. I then assessed the LPS-induced transcription (Figure 5.5 B and C) and subsequent secretion (Figure 5.5 D and E) of CCL5 and TNF in BMDMs from the *Sarm1*^{Flag} mouse compared to WT littermate controls, and found that they were unaffected by the presence of the epitope tag on SARM1. Thus, SARM1 is expressed to normal levels in this mouse, and the C-terminal tags do not interfere with the normal activation or catalytic activity of the protein which are required for vincristine-induced axon degeneration. Therefore this mouse is a useful model in which SARM1 expression can be examined while retaining the characteristic axodegenerative activity of wild type SARM1.

I used the *Sarm1*^{Flag} mouse to determine if SARM1 is expressed equally in the brain and brainstem, and to ascertain if SARM1 is expressed to a detectable level in BMDMs. Firstly, I showed by anti-Flag immunoblotting that SARM1 is as highly expressed in the brainstem as it is in the cerebrum (Figure 5.6 A). This makes sense given SARM1's roles within the CNS. In contrast, SARM1 was undetectable in primary BMDMs from *Sarm1*^{Flag} mice by Western blotting (Figure 5.6 A). It was however detectable at the mRNA level by qRT-PCR in these cells (Figure 5.6 B). The possibility therefore remained that SARM1 protein was expressed in these cells, but below the limit of detection by Western blotting. Thus, I then attempted to detect SARM1 expression in *Sarm1*^{Flag} pBMDMs by Flag immunoprecipitation followed by anti-Flag immunoblot. Once again, SARM1 was not

detectable in pBMDMs (Figure 5.7 A). This was not due to problems with the anti-Flag antibody as SARM1 was easily detected in the positive control, which was *Sarm1*^{Flag} brain lysate. (Figure 5.7 A). To overcome the experimental constraints associated with limited primary BMDM numbers, I then established iBMDMs from *Sarm1*^{Flag} bone marrow. In these cells, Flag-tagged SARM1 was readily detectable by Flag immunoprecipitation followed by Flag immunoblotting (Figure 5.7B). Flag-tagged SARM1 was also detectable by Western blot in these iBMDMs, albeit at lower levels than in the brain of *Sarm1*^{Flag} mice (Figure 5.7 B). This may suggest that immortalisation may increase SARM1 expression. Alternatively, continued proliferation of iBMDMs and not pBMDMs after the cells were seeded may have resulted in more iBMDMs being used in this experiment, thus resulting in SARM1 being easier to detect in these cells. Overall, data from the *Sarm1*^{Flag} mouse has demonstrated that SARM1 expression is not limited to the nervous system. This mouse will be a useful tool for us and others to examine SARM1 expression and function.

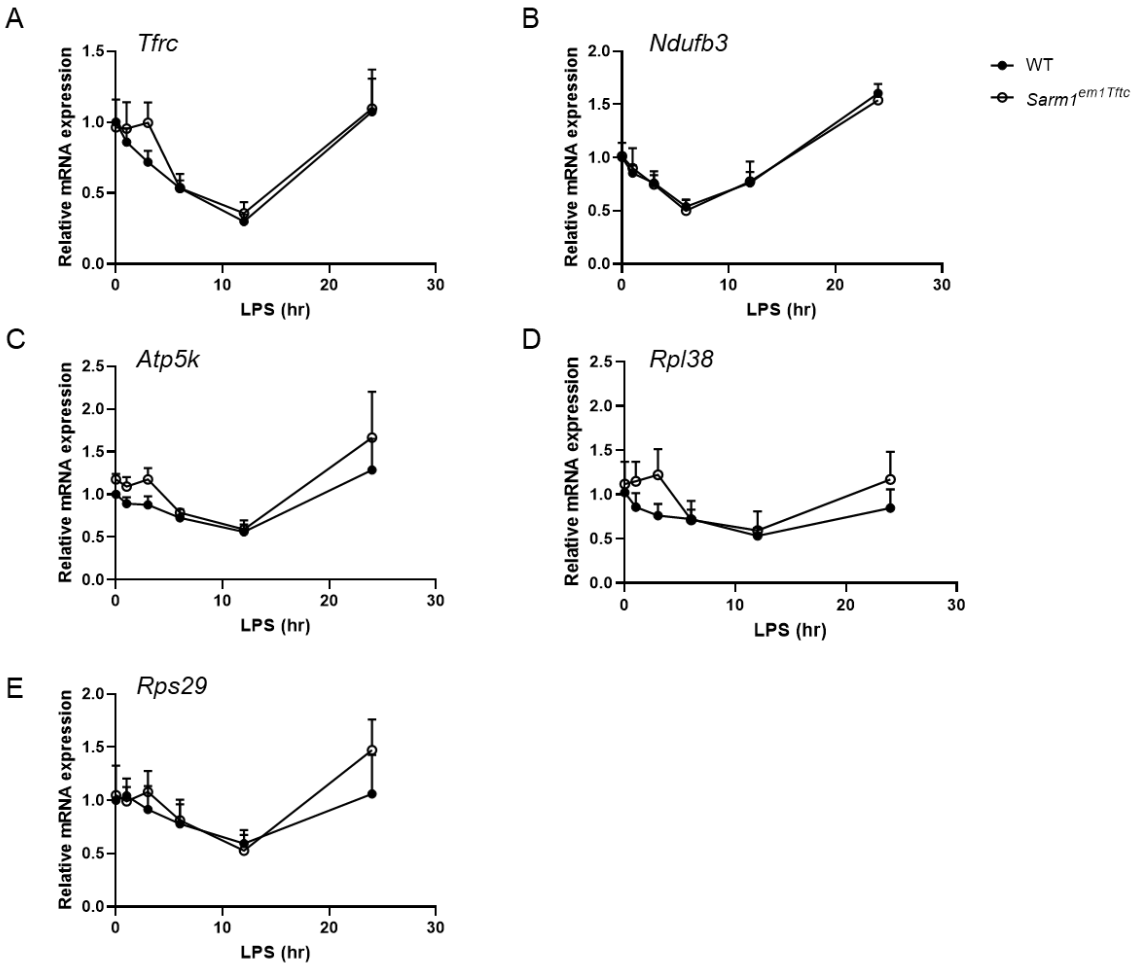

Figure 5.1 Transcription of selected genes is normal in pBMDM from *Sarm1*^{em1Tftc} mice relative to WT

(A-E) WT and *Sarm1*^{em1Tftc} pBMDM were stimulated with 100 ng/ml LPS for the indicated times, or medium as a control. Expression of *Tftc* (A), *Ndufb3* (B), *Atp5k* (C), *Rpl38* (D), and *Rps29* (E) mRNA in were assayed by qRT-PCR, normalized to the housekeeping gene β-actin, and are presented relative to the untreated WT control. Graphs show mean ±SEM from 4 mice per genotype, performed in triplicate. There were no significant differences determined by multiple Mann-Whitney tests with Holm-Šídák multiple comparisons test.

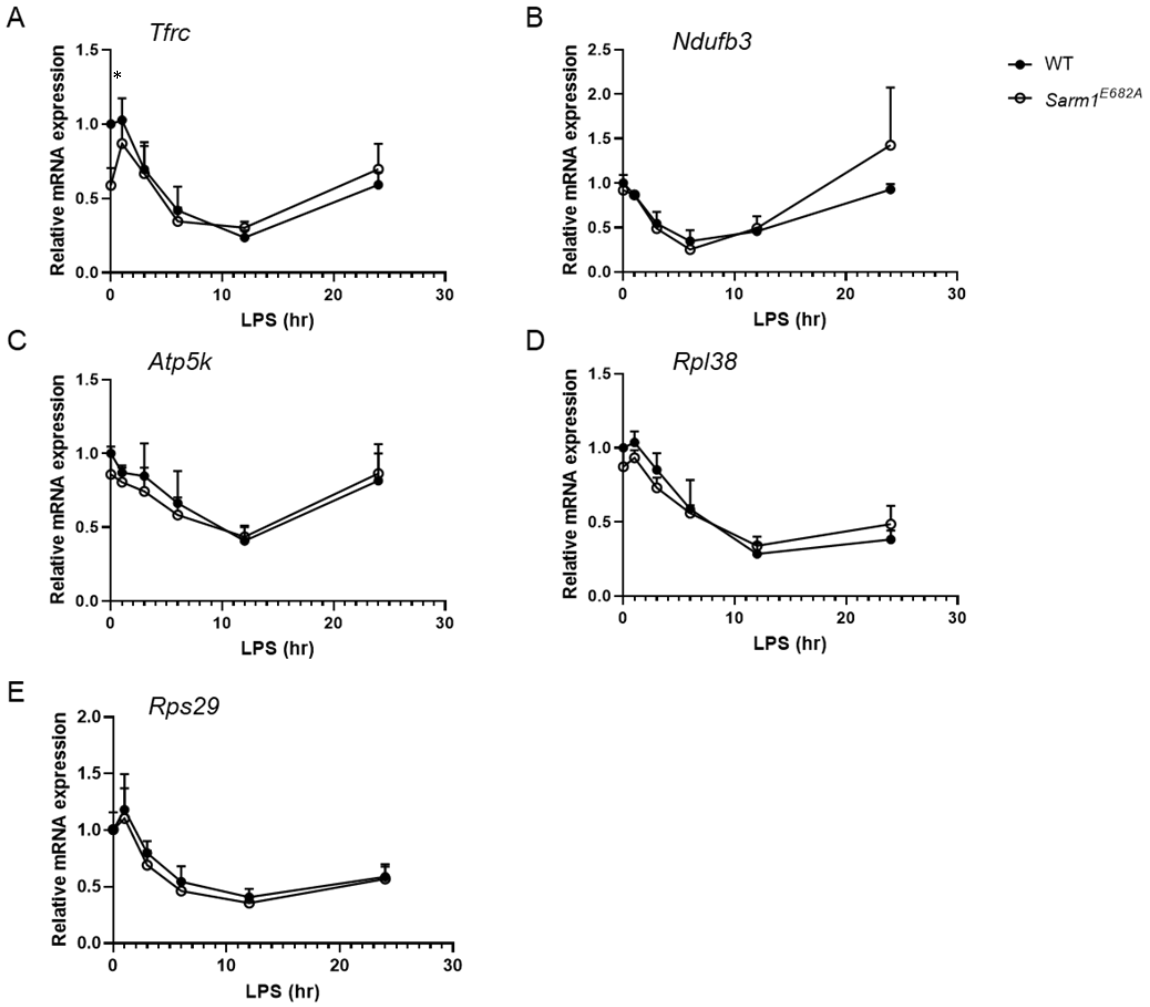

Figure 5.2 Transcription of selected genes is normal in pBMDM from *Sarm*^{E682A} mice relative to WT

(A-E) WT and *Sarm1*^{E682A} pBMDM were stimulated with 100 ng/ml LPS for the indicated times, or medium as a control. Expression of *Tftc* (A), *Ndufb3* (B), *Atp5k* (C), *Rpl38* (D), and *Rps29* (E) mRNA in were assayed by qRT-PCR, normalized to the housekeeping gene β-actin, and are presented relative to the untreated WT control. Graphs show mean ±SEM from 4-5 mice per genotype, performed in triplicate. * $p < 0.05$ compared to WT control as determined by multiple Mann-Whitney tests with Holm-Šídák multiple comparisons test.

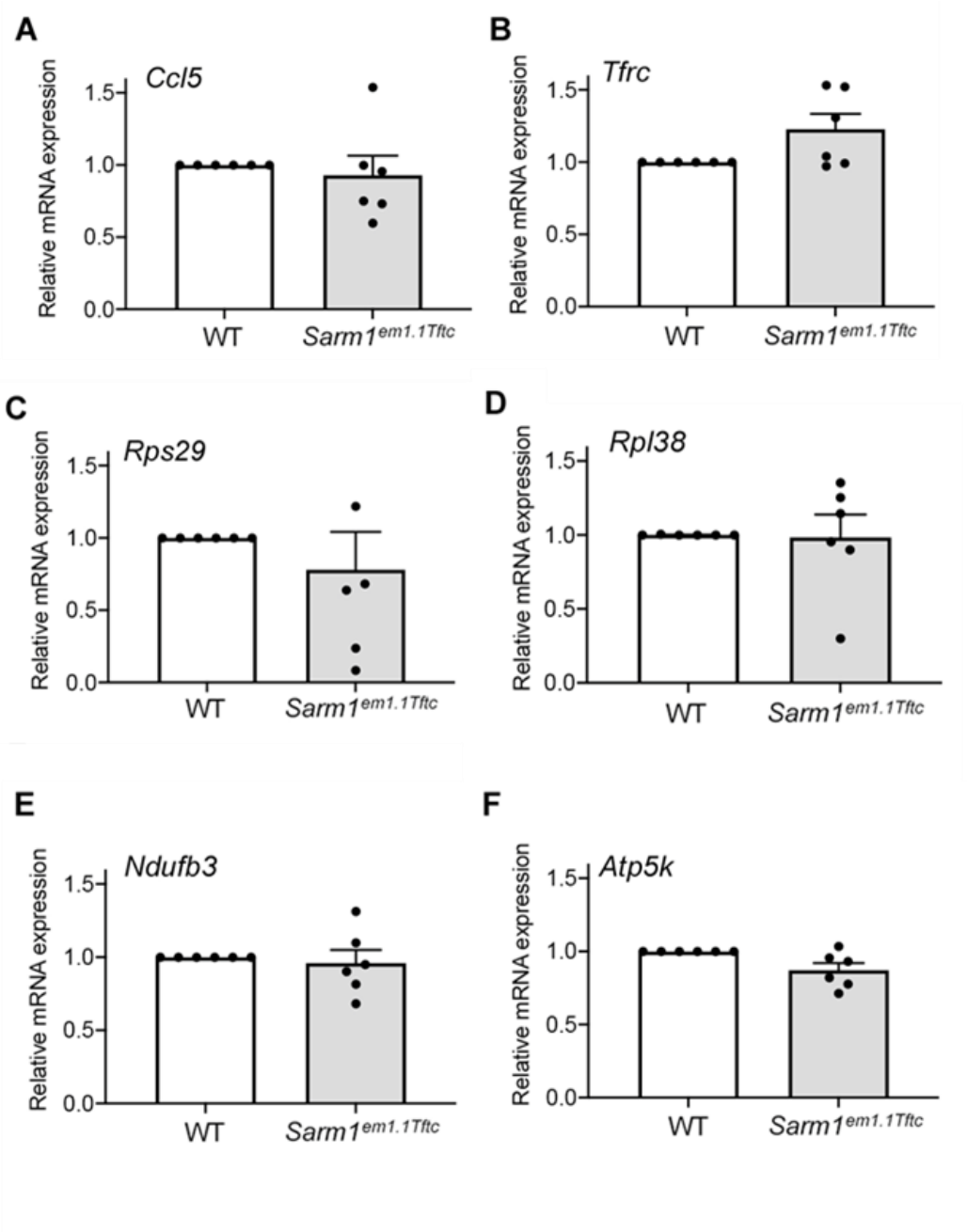

Figure 5.3 Transcription of selected genes is normal in the brainstem of *Sarm1*$^{em1.1Tftc}$ mice relative to WT

(A-F) Expression of *Ccl5* (A), *Tfrc* (B), *Rps29* (C), *Rpl38* (D), *Ndufb3* (E), and *Atp5k* (F) in the brainstem of WT and *Sarm1*$^{em1.1Tftc}$ littermate mice were measured by qRT-PCR, normalized to β-actin, and are presented relative to the littermate WT. Data are mean ±SEM from 6 mice per genotype, performed in triplicate, with no significant differences determined by two-tailed Wilcoxon matched-pairs signed rank test.

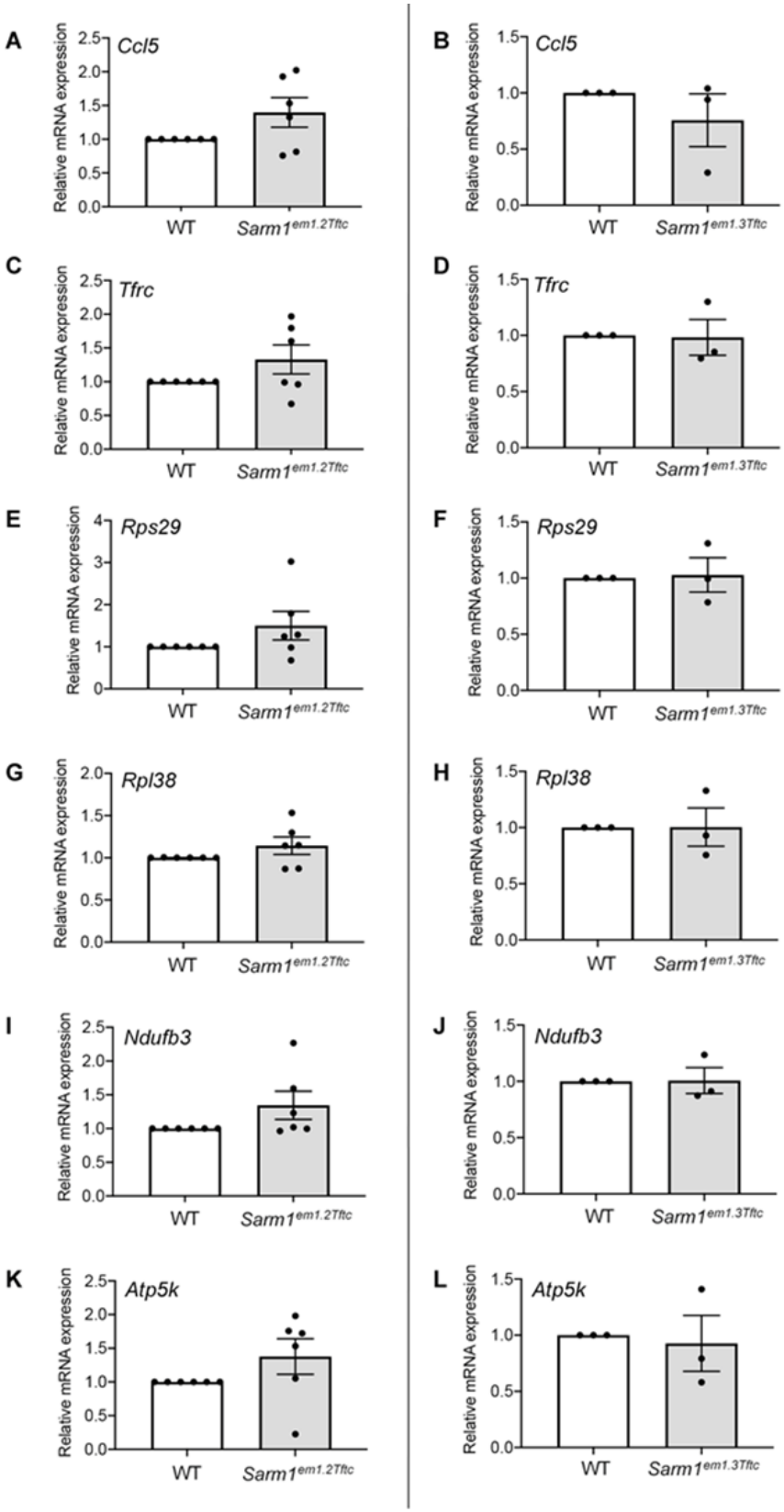

Figure 5.4 Transcription of selected genes is normal in the brainstem of *Sarm1*$^{em1.2Tftc}$ and *Sarm1*$^{em1.3Tftc}$ mice relative to WT

Expression of *Ccl5* (A, B), *Tfrc* (C, D), *Rps29* (E, F), *Rpl38* (G, H), *Ndufb3* (I, J), and *Atp5k* (K, L) in the brainstem of *Sarm1*$^{em1.2Tftc}$ and *Sarm1*$^{em1.3Tftc}$ mice respectively were measured by qRT-PCR, normalized to β-actin, and are presented relative to a littermate WT. Data are mean ± SEM for 6 *Sarm1*$^{em1.2Tftc}$ mice and 6 WT littermates, each performed in triplicate (A, C, E, G, I, K) and for 3 *Sarm1*$^{em1.2Tftc}$ mice and 3 WT littermates, each performed in triplicate (B, D, F, H, J, L). There were no significant differences determined by two-tailed Wilcoxon matched-pairs signed rank test.

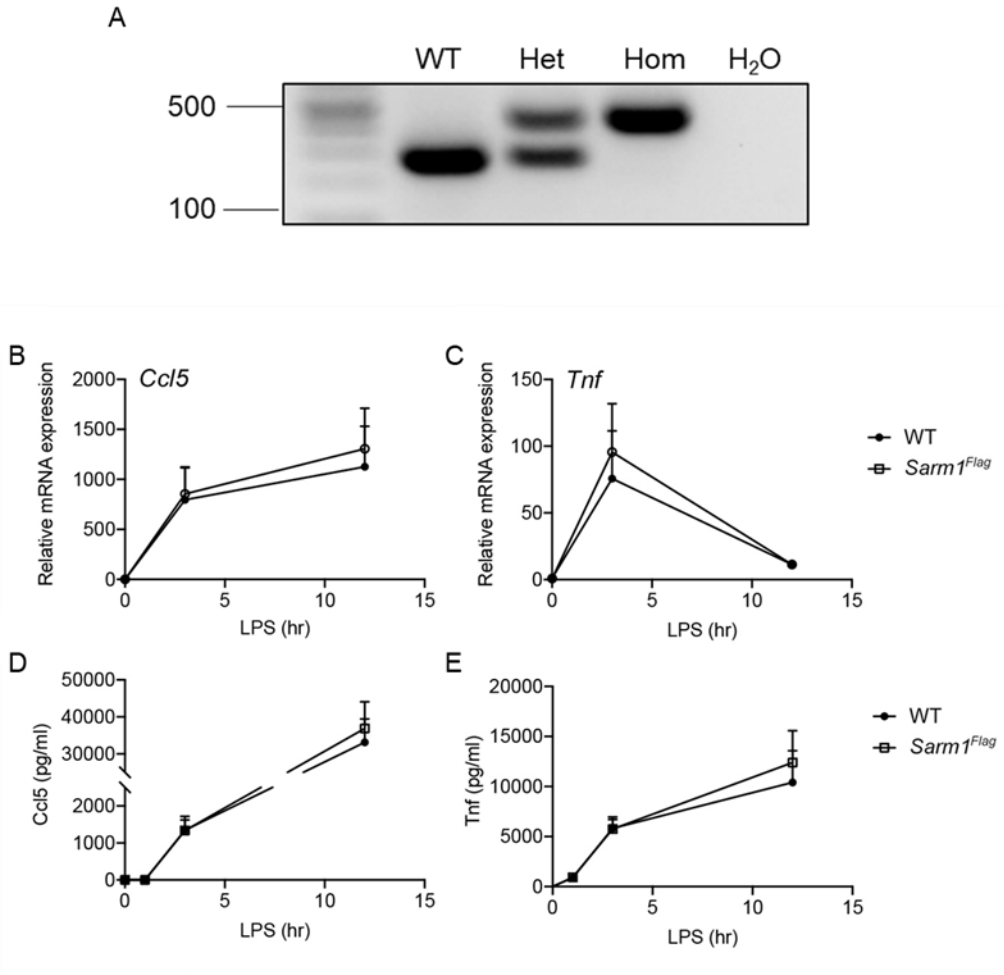

Figure 5.5 Genotyping and cytokine responses of a novel epitope-tagged SARM1 mouse generated using CRISPR/Cas9

(A) Genotyping results for *Sarm1*^{Flag} littermates. WT, wild type; het, heterozygote; hom, homozyote (B-E) WT and *Sarm1*^{Flag} BMDM were stimulated with 100 ng/ml LPS as indicated. Expression of *Ccl5* (B) and *Tnf* (C) mRNA were assayed by qRT-PCR, normalized to the housekeeping gene β-actin, and are presented relative to the untreated WT control. Supernatants were assayed for CCL5 (D) and TNF (E) protein by ELISA. Data are mean ±SEM from 3-4 mice per genotype, performed in triplicate. There were no significant differences determined by multiple Mann-Whitney tests with Holm-Šídák multiple comparisons test.

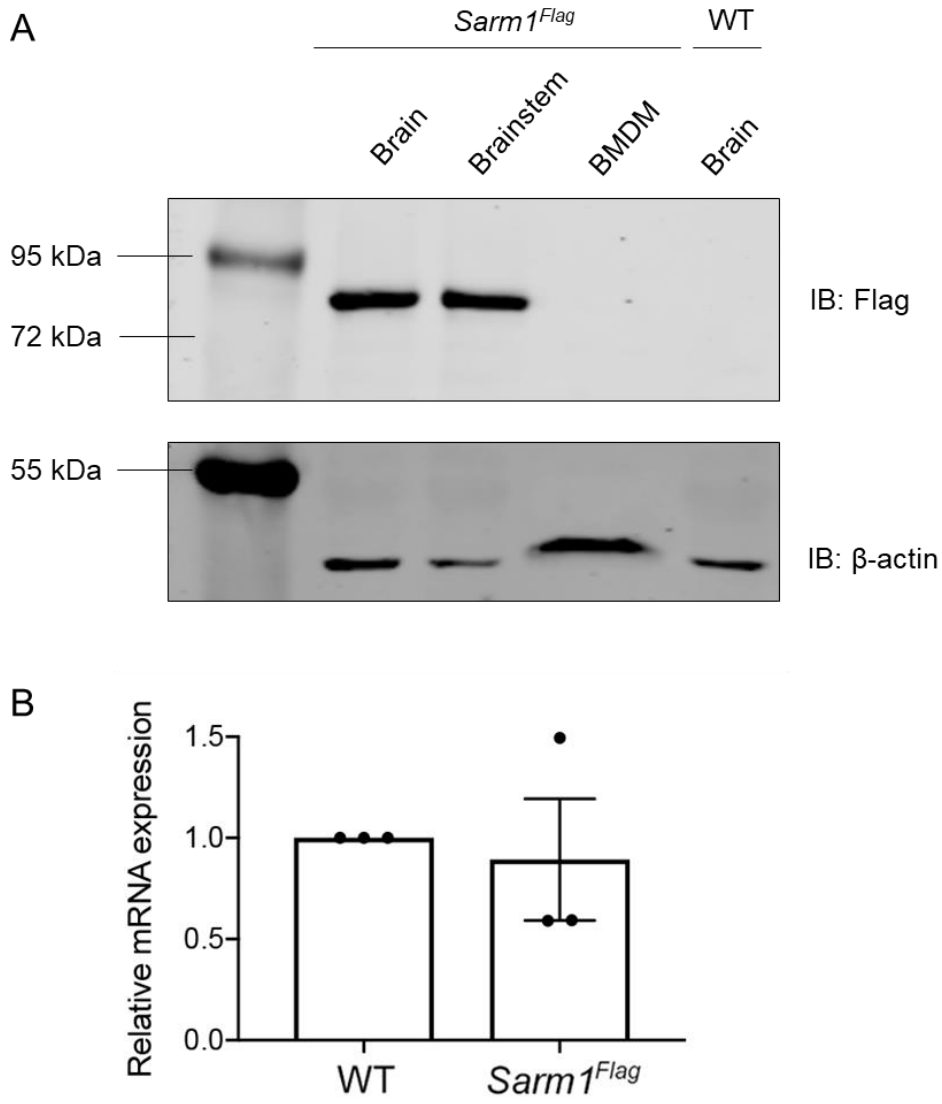

Figure 5.6 SARM1 is undetectable in pBMDMs from *Sarm1*^{Flag} mice by Western blot, despite detectable mRNA expression

(A) Immunoblot comparing expression of Flag-tagged SARM1 in brain, brainstem, and BMDM from *Sarm1*^{Flag} mice, with WT brain lysate acting as a negative control. 30 μg of protein was loaded per sample as determined by BCA assay. β-actin was used as a loading control. Blot is representative of four independent experiments.
(B) Expression of *Sarm1* mRNA in *Sarm1*^{Flag} BMDM as measured by qRT-PCR, normalized to the housekeeping gene β-actin, and presented relative to the WT control. Data are mean ±SEM from 3 mice per genotype, performed in triplicate.

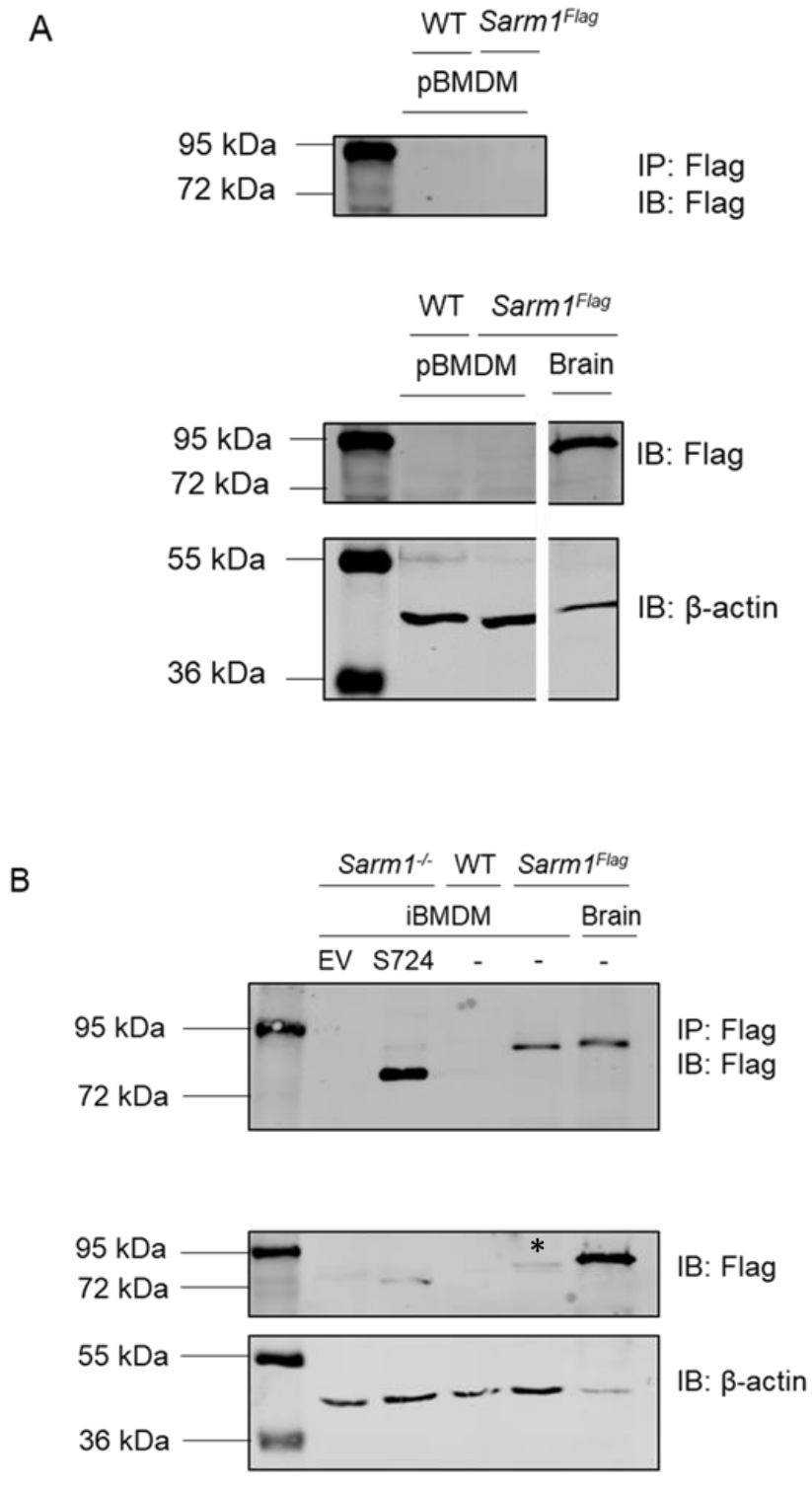

Figure 5.7 Immortalisation of *Sarm1*^{Flag} BMDMs reveals weak but detectable expression of SARM1 protein in macrophages

(A) SARM1 is undetectable in pBMDM from *Sarm1*^{Flag} mice following IP, while it is easily detectable in brains from *Sarm1*^{Flag} mice by immunoblot (IB).
(B) SARM1 is readily detectable in iBMDM by immunoprecipitation followed by immunoblotting, and weakly detectable by immunoblotting alone. Flag-tagged SARM1 was detected by immunoprecipitation in *Sarm1*$^{-/-}$ iBMDM stably overexpressing SARM1 (S724) or *Sarm1*^{Flag} iBMDM, and *Sarm1*^{Flag} brain. The asterisk indicates a faint band corresponding to epitope-tagged SARM1.
β-actin was used as a loading control for input. Representative of 3 independent experiments.

5.3 Discussion

Previous data from *Sarm1*^{em1Tftc} mice did not reveal any role for SARM1 in transcriptional regulation in macrophages (Chapter 4). However, the García-Sastre lab reported that a number of genes which encode components of the electron transport chain are differentially expressed in the brainstem of SARM1-deficient mice compared to WT [246]. Given that another lab member has observed that mitochondrial respiration is altered in *Sarm1*^{em1Tftc} BMDM, I wondered if electron transport chain components may also be differentially expressed in SARM1-deficient macrophages. Thus, the expression of *Tfrc*, *Rps29*, *Rpl38*, *Ndufb3*, and *Atp5k* was measured by qRT-PCR in BMDMs from *Sarm1*^{em1Tftc} mice and WT controls, both basally and following TLR4-stimulation. There were no significant differences in the expression of any of the measured genes at any time point. Similarly, with the exception of basal *Tfrc*, none of these genes were differentially expressed in pBMDMs from *Sarm1*^{E682A} mice compared to WT littermate controls. As *Tfrc* was not basally differentially expressed in *Sarm1*^{em1Tftc} pBMDMs relative to WT, it is unlikely that this differential expression was related to the absence of intact SARM1 NADase activity. Rather, it is likely artefactual. It is perhaps unsurprising that differential expression of these electron transport chain components was not observed in *Sarm1*^{emTftc} BMDMs given that RNA sequencing of B6 congenic *Sarm1*$^{-/-}$ BMDMs did not reveal any differences in expression of electron transport chain components (Section 3.2.5). Thus, the altered mitochondrial respiration observed in *Sarm1*^{em1Tftc} BMDMs does not result from differential gene expression in the absence of SARM1. This adds to the body of data in this thesis which does not support a role for SARM1 in regulating transcription in macrophages.

I also sought to investigate if the DEGs revealed by RNA sequencing in the brainstem of CRISPR/Cas9 SARM1 knockout mice by the García-Sastre lab [246] would be detectable in the brainstems of our three independent CRISPR/Cas9 SARM1-knockout mice. If these genes were SARM1-regulated, it would be critical to define if therapeutic modulation of SARM1 activity would have an impact on their expression levels. Thus, the expression of *Tfrc*, *Rps29*, *Rpl38*, *Ndufb3*, and *Atp5k* was assessed by qRT-PCR in the brainstem of *Sarm1*$^{em1.1Tftc}$ mice compared to WT littermate controls. In contrast to the García-Sastre lab's study, these genes were expressed at similar levels between the genotypes. To rule out the possibility that this is unique to *Sarm1*$^{em1.1Tftc}$, the expression of these genes was also measured in brainstems from *Sarm1*$^{em1.2Tftc}$ and *Sarm1*$^{em1.3Tftc}$ mice compared to their

WT littermates. Again, there were no significant differences in gene expression between the WT and SARM1-knockout mice. The reasons underlying the different phenotypes observed between our mice and those generated by the García-Sastre lab are not yet resolved. It is possible that I did not detect differential gene expression for technical reasons. Perhaps the sensitivity of qRT-PCR is insufficient to observe differential gene expression of that magnitude, which was detectable by RNA sequencing. It also may be related to differences between our three CRISPR/Cas9 SARM1 knockout mice and the mouse in which the RNA sequencing study was performed. Overall, based on the measurement of a number of genes by qRT-PCR, our new SARM1-knockout mice do not support a role for SARM1 in transcription in macrophages or in the brainstem.

Delineating the cells and tissues in which SARM1 is expressed would be helpful in determining its function. However, the lack of antibody capable of specifically and reliably detecting SARM1 outside of the nervous system has precluded conclusive determination of where SARM1 is expressed, and this has hindered studies into its functions. This has led to speculation that SARM1 expression and function may in fact be limited to the nervous system. To investigate if murine SARM1 is actually expressed in macrophages or confined to the nervous system, we generated a mouse which expressed epitope-tagged SARM1 using CRISPR/Cas9. SARM1 could be readily detected in the cerebrum and brainstem by immunoblotting, using an antibody directed against Flag. This is consistent with reports of abundant and easily detected SARM1 expression in the nervous system. SARM1 was not similarly detectable in primary BMDMs from *Sarm1*^{Flag} mice, despite detectable mRNA in this cell type. To discern if SARM1 expression in BMDMs is low or completely absent, Flag-immunoblotting was preceded by Flag-immunoprecipitation. SARM1 remained undetectable in primary BMDMs. However, SARM1 was detectable by Flag-immunoprecipitation followed by Flag-immunoblotting in iBMDMs, which were generated in order to overcome limitations in cell number associated with pBMDMs. This could indicate that immortalisation may cause SARM1 expression to increase in macrophages. However, it also remains possible that due to continued proliferation of iBMDMs and not pBMDMs after cells were seeded for experiments, the actual number of iBMDMs used could far exceed the number of pBMDMs. Nonetheless, caution should be exercised when interpreting results relating to SARM1 function derived from immortalised BMDMs, as they may not accurately represent primary macrophages. Importantly, these data indicate that SARM1 expression is not confined to the nervous system, and do not rule

out a role for SARM1 in macrophages. The *Sarm1*^{Flag} mouse was instrumental in defining that murine SARM1 expression is not limited to the nervous system. I confirmed that TLR4-induced transcription was normal in BMDMs from this mouse, and another lab member confirmed that the C-terminal tags did not affect the activation or activity of SARM1 in the context of vincristine-induced axon degeneration [195]. Therefore this mouse will be a useful tool for us and others in further studies into the locations and contexts in which SARM1 is expressed.

Overall in this chapter data from the *Sarm1*^{Flag} mouse, in which SARM1 is epitope-tagged, has clarified that murine SARM1 is not limited to the nervous system. SARM1 expression was detectable in BMDM from this mouse, albeit to a lower extent than in the brain and brainstem. However, data from the three CRISPR/Cas9 SARM1 knockout mice did not support a role for SARM1 in transcription in the brainstem or in BMDM, despite expression there. This chapter also emphasised the importance of exercising caution when interpreting results from iBMDM, as epitope-tagged SARM1 was detectable in *Sarm1*^{Flag} iBMDM and not pBMDM by Flag immunoprecipitation following by anti-Flag immunoblotting. This may have been due to enhanced expression of SARM1 in iBMDMs or due to continued proliferation of iBMDMs after cells were seeded for experiments.

Chapter 6 Final Discussion

In the last decade, our understanding of SARM1 structure and function expanded rapidly, with the majority of research studies focusing on the role of SARM1 as an executioner of axon degeneration. With the recent discovery of potent inhibitors and activators of SARM1 NADase activity, the prospect of modulating the axodegenerative activity of SARM1 as a therapeutic strategy grows ever closer to becoming a reality. With this in mind, it is important to consider the effect that targeted inhibition or activation of SARM1 may have on the less well-explored and well-characterised functions of SARM1 outside of the nervous system. Thus, further investigation is required into the non-neuronal roles for SARM1. Specifically, how and where SARM1 contributes to immune responses remains to be clarified. There are seemingly conflicting reports on the subcellular localisation of SARM1, and despite remarkable sequence similarity, disparate roles are reported to exist for human and murine SARM1. Our laboratory had previously published a study describing impaired *Ccl5* induction in response to both TLR and non-TLR stimuli in macrophages from *Sarm1*$^{-/-}$ mice, but otherwise normal induction of inflammatory genes in response to TLR stimulation in these cells [34]. In contrast, human SARM1 has a role in antagonising TLR signalling [36]. Therefore to contribute to our understanding of the immune roles for SARM1, I sought to elucidate the mechanism by which murine SARM1 regulates *Ccl5* induction.

In the initial stage of this project, I used BMDMs from conventional B6 congenic *Sarm1*$^{-/-}$ mice to determine if transcription was altered in the absence of SARM1 in macrophages. In agreement with previously published results from our lab, both pBMDMs and iBMDMs derived from the *Sarm1*$^{-/-}$ mice exhibited reduced *Ccl5* expression relative to their WT counterparts following TLR stimulation. Upon further examination of the TLR-mediated induction of inflammatory mediators in these cells, it emerged that phenotypes observed in the *Sarm1*$^{-/-}$ iBMDMs were absent in the pBMDMs from *Sarm1*$^{-/-}$ mice, namely elevated IL-6 production and reduced nitric oxide production relative to WT controls. The exact underlying cause for these phenotypic differences between pBMDMs and iBMDMs from *Sarm1*$^{-/-}$ mice is unclear, but there are many possible culprits. Perhaps the process of immortalisation using Cre-J2 retrovirus proceeds slightly differently in the absence of SARM1, and thereby have introduced subtle differences in *Sarm1*$^{-/-}$ iBMDMs but not WT

iBMDMs. As little is known about the manner in which these cells were generated, the aberrant phenotype may stem from age- or sex-mismatched mice being used as source material. It also may simply represent real biological variation between individual mice. In support of this, iBMDMs generated from a mouse of the *Sarm1*$^{em1.2Tftc}$ line and a sex-matched littermate control, using similar seeding density of bone marrow cells during differentiation, shared a similar phenotype to the corresponding pBMDMs, while an identically generated iBMDM line from the *Sarm1*$^{em1.3Tftc}$ line did not.

Regardless of the cause of the altered phenotype in *Sarm1*$^{-/-}$ iBMDMs, this highlights a number of caveats associated with iBMDMs in general, which ought to be considered both when generating and employing this cell type. Firstly, care must be taken at every stage of iBMDM generation to avoid the introduction of confounding variations. The mice from which iBMDMs are to be derived should be as well-matched as possible, to avoid age-related and sexual dimorphism in responses. The mice should have a similar genetic background, and ideally littermates should be used. Bone marrow cells should be seeded at equal densities during the process of differentiation, as seeding density can influence the level of inflammatory cytokine production in the resulting iBMDMs. Secondly, the provenance of each iBMDM line, including the sex, age, and relatedness of mice used and the method of differentiation, should be carefully recorded and made available to all users. Thirdly, caution should be exercised when interpreting and extrapolating results from a single line of iBMDMs. By their nature, iBMDMs represent only the single biological replicate from which they are derived. As a result, repeated experiments in this cell type cannot account for biological replication. Additionally, the process of immortalisation involves exposure to a retrovirus and expression of oncogenes, and this may have an impact on the cells' responses. In light of these issues, it bears considering if iBMDMs ought to be accepted as an appropriate cell type for studies in which the use of pBMDMs is tenable.

Examination of the subcellular localisation of overexpressed SARM1 in *Sarm1*$^{-/-}$ iBMDMs did not illuminate any potential mechanism of action: RNA sequencing was therefore performed on unstimulated and CL075-treated pBMDM from WT and B6 congenic *Sarm1*$^{-/-}$ mice, with the objectives of identifying additional genes which are SARM1-regulated and shedding light on potential mechanisms of transcriptional regulation. Differential gene expression analysis was applied to the sequencing data, and a list of genes which were differentially expressed in the pBMDMs from *Sarm1*$^{-/-}$ mice relative to WT

controls basally or following stimulation was compiled, using *Ccl5* as the positive control. It emerged that a disproportionate fraction of these differentially expressed genes reside on chromosome 11 in close proximity to the *Sarm1* and *Ccl5* loci. Strikingly, each of the eight DEGs present on chromosome 11 were within 5 cM of the *Sarm1* locus, and many contained sequences which deviated from the C57BL/6 reference sequence and matched known sequence variants in the 129 mouse strain. In fact, the probability of the region of 5 cM flanking either side of the target gene in a congenic mouse being of donor origin, in this case 129-derived, is ~46% [230]. This indicated that the DEGs on chromosome 11 in B6 congenic *Sarm1*$^{-/-}$ mice, including *Ccl5*, represent passenger genes introduced during the generation of the *Sarm1*$^{-/-}$ mouse by targeted gene disruption.

To conclusively delineate whether it is the presence of passenger genes or absence of SARM1 which is responsible for differential gene expression in pBMDMs from B6 congenic *Sarm1*$^{-/-}$ mice, our lab commissioned the generation of novel CRISPR/Cas9 SARM1-knockout mice. Compellingly, *Ccl5* induction was equivalent to WT littermate controls in pBMDMs from each of the three resulting SARM1-deficient mouse lines in response to TLR stimulation, as was the expression of a number of other DEGs discovered in the B6 congenic *Sarm1*$^{-/-}$ pBMDMs through RNA sequencing. Further, stable overexpression of SARM1 in *Sarm1*$^{-/-}$ iBMDM failed to rescue *Ccl5* induction. Cumulatively, these data show that the previously observed phenotype of impaired *Ccl5* induction in B6 congenic *Sarm1*$^{-/-}$ BMDMs was an artefact resulting from passenger mutations. During the course of this project, another study reported passenger genes as the cause of reduced *Ccl5* expression in *Sarm1*$^{-/-}$ macrophages [246], confirming the confounding effect of this 129-derived genetic material. Importantly, we therefore do not need to consider if therapeutic modulation of SARM1 will result in dysregulation of *Ccl5* expression in macrophages.

This project adds to a growing body of literature implicating passenger genes as a cause of phenotypes previously attributed to the targeted gene in transgenic mice. In one of the best recognised examples of this, the roles of caspase-11 in non-canonical inflammasome-induced cell death and endotoxic shock lethality were erroneously ascribed to caspase-1 [253]. This was because the congenic *Casp1*$^{-/-}$ mouse which previous studies relied upon carried the 129-associated *Casp11* passenger gene, which harbours a mutation that attenuates caspase-11 expression. As *Casp1* and *Casp11* are adjacent in the mouse genome,

separated by only ~1.5 Kb, they were not separated by recombination following generations of backcrossing of the *Casp1*$^{-/-}$ mouse to C57BL/6. Thus, the congenic *Casp1*$^{-/-}$ mouse was effectively a *Casp1*$^{-/-}$*Casp11*$^{-/-}$ double knockout mouse [253]. Similarly, the loci of several members of the matrix metalloproteinase (MMP) family members reside within a 5 cM interval of the *Casp11* locus. While congenic *Mmp7*$^{-/-}$, *Mmp8*$^{-/-}$, and *Mmp13*$^{-/-}$ mice are protected from LPS lethality, it was subsequently shown that congenic *Mmp13*$^{-/-}$ mice harbour the unexpressed 129-associated *Casp11* mutant sequence [254]. When the *Casp11* mutation was eliminated from the genome through extensive backcrossing to C57BL/6, the *Mmp13*$^{-/-}$ mice were no longer protected against a lethal LPS dose [254]. The 129 mouse strain also harbours a variant of *P2rx7*, which encodes the ATP-gated ion channel P2X7, that is expressed at much higher levels in T cells than the C57BL/6 *P2rx7* variant [255]. Congenic *P2rx4*$^{-/-}$ mice harbour this 129 mutant *P2rx7* gene, which influences the sensitivity of their T-cells to P2X7 activators and thus renders them more susceptible to NAD^+-induced cell death [255]. This phenotype is unrelated to the absence of P2X4, and confounds interpretation of functional assays [255]. Thus, the presence of passenger genes flanking the target gene in congenic mice can have a substantial impact on the phenotype. Passenger genes may also contribute to the observation that inconsistent phenotypes sometimes arise in congenic mice across different labs. The number of generations of backcrossing influences the extent to which passenger genes contaminate the congenic mouse genome. Thus, with extensive backcrossing to the desired background strain, the donor-derived segment of DNA flanking the target gene in the congenic mouse is diminished, and passenger genes may be replaced with those corresponding to the background strain, resulting in the loss or gain of phenotypes.

The issue of passenger genes in congenic mice likely has far-reaching effects. *In silico* analysis of over 5,000 congenic mouse strains derived from 129 embryonic stem cells found that a remarkable 97% of these mouse lines harbour at least 1 passenger gene within a 1 cM interval of the targeted gene, with approximately a quarter of these strains having > 20 passenger genes [254]. This suggests that almost all congenic mice possess confounding passenger genes. In recent years, the reliance on congenic mice is declining as CRISPR/Cas9-mediated genome editing becomes an increasingly accessible preferred option. In February 2022, MGI reported that within the available pool of genetically modified mice, ~23% are congenic and ~44% are isogenic. This represents a reversal in the ratio of congenic to isogenic mouse strains available in 2015, reported by Vanden Berghe

et al. as 46% and 29% respectively [254]. While CRISPR/Cas9 has superseded targeted gene disruption as the primary method of generating genetically engineered mice, in some instances there remains an overreliance on congenic mouse models as was the case with murine SARM1 studies until recently. Our study and that of the García-Sastre lab [246] remain the only peer-reviewed publications using isogenic rather than congenic SARM1-knockout mice to investigate SARM1 function. Thus, it is still unclear how many of the published phenotypes ascribed to SARM1 deletion are impacted by the passenger genes which contaminate congenic mice.

This is reflective of a wider general issue in studies using genome-edited animals. Use of animals possessing passenger genes results in the misattribution of phenotypes to the targeted gene of interest, and these misattributed phenotypes may be incorrectly informing our current knowledge and thinking, particularly where they contribute to the establishment of dogmas. Therefore it is critical that we acknowledge how the confounding effect of passenger genes in congenic mice may be misinforming current studies, even where newer mouse models are employed. One could argue that where an isogenic mouse exists, congenic mice should no longer be employed in studies. It seems sensible that phenotypes observed in congenic mice should be examined in the corresponding isogenic mice as soon as it is made available. The publication of repeated studies in isogenic mice is central to the purging of the literature of phenotypes discovered in congenic mice and incorrectly attributed to the targeted gene of interest. While there is often reluctance to publish negative results in the scientific community, it is essential in order to correct misinformation and to allow us to re-evaluate and recontextualise previous findings.

In addition to identifying genes which were expressed to different levels, RNA sequencing also revealed alternative transcripts expressed of some chromosome 11 genes in B6 congenic *Sarm1*$^{-/-}$ BMDMs relative to WT. Among the most interesting of these is *Xaf1*, the transcript of which was found to possess an extended 3' UTR in these *Sarm1*$^{-/-}$ pBMDMs relative to the WT controls and the C57BL/6 reference sequence, which could affect the transcript stability. Interrogation of the RNA sequence at the *Xaf1* locus in *Sarm1*$^{-/-}$ pBMDM revealed a multitude of sequence deviations, which corresponded to known 129-associated variants, which were absent in WT controls. Notably, one of these mutations results in a premature stop codon, truncating a number of C-terminal amino acids. This truncation was also observed by Uccellini *et al.* in RNA from B6 congenic

Sarm1$^{-/-}$ mice [246]. The C-terminus of XAF1 is known to be required for binding to XIAP and antagonising its anti-apoptotic effects [232], and it is therefore possible that this small truncation may interfere with XAF1 pro-apoptotic activity. It is reasonable to speculate that the copious mutations observed in the *Xaf1* locus in B6 congenic *Sarm1*$^{-/-}$ mice may interfere with the pro-cell death functions of XAF1, which include the release of cytochrome c [210] and binding of XIAP [209]. Thus, the presence of the *Xaf1* passenger gene in B6 congenic *Sarm1*$^{-/-}$ mice may have influenced the cell death phenotype in these mice. Indeed, the protection from pyroptotic death observed in pBMDMs from B6 congenic *Sarm1*$^{-/-}$ mice [25] was not recapitulated in pBMDMs from each of our three novel CRISPR/Cas9 SARM1-knockout mice (K. Shanahan, personal communication), though whether this is related to differences in XAF1 expression between 129 and C57BL/6 strains is unclear. The presence of the 129-associated *Xaf1* passenger gene is also likely to have contributed to the phenotype of accelerated prion disease observed in B6 congenic *Sarm1*$^{-/-}$ mice [169], and this work bears repeating in the improved CRISPR/Cas9 SARM1-knockout mouse models which are now available.

Additionally, each of the three *Nlrp1* paralogues also showed different expression patterns in the B6 congenic *Sarm1*$^{-/-}$ BMDMs relative to WT BMDMs and the C57BL/6 reference sequence. The expression profiles of *Nlrp1a*, *Nlrp1b*, and *Nlrp1c-ps* in B6 congenic *Sarm1*$^{-/-}$ BMDMs resembles that of 129 mice rather than C57BL/6. The differential expression of the *Nlrp1* paralogue transcripts accounts for the response of different mouse strain to *B. anthracis*, with C57BL/6 mice being resistant and 129 mice being sensitive [234]. Thus, there are likely functional consequences to the expression of alternative transcripts of the *Nlrp1* paralogues in the B6 congenic *Sarm1*$^{-/-}$ mouse, rendering it unsuitable as a model in which to study the effects of certain pathogens.

This work in B6 congenic *Sarm1*$^{-/-}$ mice is a striking example of how passenger genes can jeopardise studies by contributing to an observed phenotype in congenic mice. This ought to be considered when interpreting results from any study carried out in congenic mice. However, it is important to note that the presence of passenger genes and absence of SARM1 were not the sole differences between the B6 congenic *Sarm1*$^{-/-}$ and WT mice employed in this project. The *Sarm1*$^{-/-}$ mice were generated by homozygous breeding pairs, and WT mice were acquired from the TBSI animal facility. While age-matched and sex-matched animals were used, the mice are not littermates and are not co-housed. Thus

the mice of different genotype experience different environments and will not have similar microbiomes. In addition, aside from passenger genes, the genomes of the WT and *Sarm1*$^{-/-}$ mice will vary due to genetic drift. These factors may also have contributed to differential phenotypes between WT and B6 congenic *Sarm1*$^{-/-}$ mice. The newly generated CRISPR/Cas9 mouse lines were maintained through heterozygous breeding pairs, which eliminates these variables in addition to passenger genes.

The CRISPR/Cas9 SARM1-knockout mice present an improved model in which to examine the effects of SARM1 deletion compared to the B6 congenic *Sarm1*$^{-/-}$ mice, and already our collaborator Professor Jose Bengoechea has used this model to confirm a deleterious role for murine SARM1 in the context of *K. pneumoniae* infection [248], which the group had observed in the B6 congenic *Sarm1*$^{-/-}$ mouse. This was associated with enhanced inflammatory cytokine expression in the *Sarm1*$^{-/-}$ mouse lung and in iBMDMs [248]. Concerningly however, despite following a near-identical protocol and infecting with bacteria kindly gifted by the Bengoechea lab, I did not observe any differences in *K. pneumoniae*-induced gene induction between pBMDMs from WT and *Sarm1*^{em1Tftc} mice. It is implausible that passenger genes could account for the enhanced cytokine secretion observed by the Bengoechea lab, as I observed normal or slightly reduced gene induction in pBMDMs from B6 congenic *Sarm1*$^{-/-}$ mice. Consistent with the results observed following stimulation of isolated TLRs, I observed reduced *Ccl5* induction in B6 congenic *Sarm1*$^{-/-}$ pBMDMs compared to WT, but not CRISPR/Cas9 SARM1-knockout pBMDMs upon stimulation with *K. pneumoniae.* Additionally, the Bengoechea lab observed a common phenotype of enhanced inflammatory cytokine secretion in iBMDMs from both B6 congenic and CRISPR/Cas9 SARM1-knockout mice [248]. Technical differences, such as inadvertent deviations from the intended MOI due to differences in bacterial preparation or the use of difference cell culture plates may have contributed to the difference in phenotype observed between labs. Other inter-institutional differences which could feasibly influence the phenotype of the BMDMs include the cell culture room environment, variations in the density at which BMDMs were differentiated, and different batches of L929-conditioned supernatants used to differentiate BMDMs. It is also possible that the iBMDMs do not faithfully represent pBMDMs, and that the *in vivo* phenotype observed by the Bengoechea lab of improved bacterial clearance in SARM1-deficient mice was unrelated to the altered transcriptional responses that were observed in iBMDMs [248]. Once again, this reinforces that caution ought to be exercised when interpreting results from

iBMDMs. Regardless of the underlying reason, it is concerning that the results observed by our collaborators cannot be repeated in our lab using similar mice and bacteria.

Data from the three CRISPR/Cas9 SARM1-knockout mice did not support a role for SARM1 in transcription in macrophages, however there are examples of murine SARM1 regulating transcription in the nervous system. Of particular relevance, Uccellini *et al.* in the García-Sastre lab reported differential expression of a number of genes in the brainstem of CRISPR/Cas9 SARM1-knockout mice which they had generated [246]. In this study, RNA sequencing of uninfected brainstems revealed differential expression of a number of genes which encode components of the electron transport chain [246], and this is of interest as recent data from our lab suggests that mitochondrial respiration is altered in BMDMs from CRISPR/Cas9 SARM1-knockout mice (K.Shanahan, personal communication). I therefore measured the expression of the genes in question in BMDMs from our three CRISPR/Cas9 SARM1-knockout mice by qRT-PCR, but found no significant differences. Additionally, I observed no significant differences in expression of these genes between the brainstem of WT and CRISPR/Cas9 SARM1-deficient mice, in contrast to the results published by Uccellini *et al*. The reasons underlying the different phenotypes observed between our mice and those generated by the García-Sastre lab are not yet resolved. Perhaps RNA sequencing is sufficiently sensitive to detect subtly altered expression of these genes in the SARM1-deficient brainstem compared to WT, which are below the limit of detection by qRT-PCR. It also remains possible that the primers I designed to detect the mRNA of these genes could not amplify certain transcripts which are differentially expressed in the presence and absence of SARM1. Finally, the differential gene expression observed by the García-Sastre lab may be unique to the mice used in their RNA sequencing experiment. Both we and the Uccellini lab could confirm functional loss of SARM1 by showing ablated axon degeneration in neurons from our respective CRISPR/Cas9 SARM1-knockout mice, thus it is not the case that any of the mice are not legitimately SARM1-deficient.

In addition to generating a SARM1-deficient mouse, the TBSI transgenics facility used CRISPR/Cas9 genome editing to generate a mouse in which SARM1 lacked NADase activity, named $Sarm1^{E682A}$. This mouse was intended for use as a tool to delineate which roles for SARM1 required intact enzymatic activity, and which were NADase-independent. This would be useful in determining which functions of SARM1 could be dysregulated by therapeutic inhibition or activation of SARM1 NADase activity. Transcription in BMDMs

from these mice was similar to WT in response to TLR4 stimulation and *K. pneumoniae* infection, mirroring the phenotype observed in *Sarm1*^{em1Tftc} mice. However, while *Sarm1* transcription in this mouse could be detected by qRT-PCR, SARM1 protein could not be detected by Western blot (R. Sugisawa, personal communication), even in neurons where SARM1 is generally highly expressed. This could result from disruption of the epitope which is recognised by SARM1 antibodies or be due to a legitimate lack of SARM1 expression in this mouse, although resolving this matter is beyond the scope of this project. If this issue could be overcome, this mouse would be a useful tool in determining which functions of SARM1 require functional enzyme activity. Regardless, in the context of this project it provides additional confirmation of a lack of role for SARM1 overall in transcription.

This study did not support a role for murine SARM1 in transcription in BMDMs, and there has been some contention surrounding SARM1 expression in macrophages. It is difficult to detect SARM1 protein in macrophages by Western blot, and difficulty has been reported in confirming *Sarm1* mRNA expression by qRT-PCR [246]. This has led to some speculation that SARM1 expression and function may be confined to the nervous system. Indeed, much of what we know of the role of SARM1 in murine macrophages comes from studies relying on the B6 congenic *Sarm1*$^{-/-}$ mouse, which we know to be an unsuitable model, or using SARM1 overexpression, which is not guaranteed to faithfully recapitulate the function of endogenous SARM1. This uncertainty surrounding SARM1 expression in macrophages was addressed using the *Sarm1*^{Flag} mouse, which is to our knowledge, the first mouse expressing SARM1 which possesses an epitope tag, allowing for easy detection using an antibody directed against Flag. This tag does not interfere with SARM1 activity in neurons [195], and transcription was normal in BMDMs from this mouse. SARM1 could readily be detected in the brainstem and cerebrum of this mouse by Western blotting, but was not similarly detectable in pBMDMs despite detectable *Sarm1* mRNA in this cell type. SARM1 was detectable in iBMDMs derived from *Sarm1*^{Flag} mice by Flag-immunoprecipitation followed by Flag-immunoblotting. The *Sarm1*^{Flag} mouse was therefore instrumental in defining that murine SARM1 expression is not limited to the nervous system, and data from this mouse do not rule out a role for SARM1 in macrophages.

The principal objective of this project was to understand the role of murine SARM1 in regulating the expression of *Ccl5*. In investigating this I discovered that the genome of B6 congenic *Sarm1*$^{-/-}$ mice, which are heavily relied upon for murine SARM1 studies, is mired with passenger genes. This confounds the interpretation of results obtained in these mice, particularly when gene expression is the focal point. Using novel SARM1-deficient mice which were generated by CRISPR/Cas9 and therefore do not harbour passenger genes, I clarified that *Ccl5* expression is not SARM1-regulated in macrophages. Thus, therapeutic modulation of SARM1 activity would not dysregulate *Ccl5* expression. In fact, the data in this thesis do not support any transcriptional role for SARM1. This adds to a growing body of literature implicating passenger genes in B6 congenic mice as the legitimate causative agent of a phenotype previously ascribed to the gene which is edited in these mice. It serves as warning to ensure that genome-edited mice are appropriately matched to their respective WT controls. Multiple lines of evidence from this thesis suggest that iBMDMs should be used judiciously, and caution should be exercised when interpreting and extrapolating results derived from these cells. During the course of this project, a number of novel mice were generated which present improved models in which to investigate the effect of SARM1 deletion, the requirement for SARM1 NADase activity, and the contexts in which SARM1 is expressed (see Table 6.1). The *Sarm1*^{Flag} mouse allowed me to clarify that SARM1 is expressed in BMDMs, albeit to a lesser degree than in the brain. Overall, this work demonstrates that murine SARM1 does not have a broad transcriptional role in macrophages despite its expression in these cells, and describes important new animal models in which to further explore and re-evaluate SARM1 function.

Table 6.1 Characteristics of the mouse lines used in this study

Genotype	B6 congenic *Sarm1*$^{-/-}$	*Sarm1*^{em1Tftc}	*Sarm1*^{Flag}	*Sarm1*^{E682A}
Method of generation	Targeted gene disruption	CRISPR/Cas9	CRISPR/Cas9	CRISPR/Cas9
Background	> 99% C57BL/6 < 1% 129X1/SvJ	C57BL/6	C57BL/6	C57BL/6
Passenger genes	Present on chromosome 11	Absent	Absent	Absent
Ccl5 induction	Impaired	Normal	Normal	Normal
SARM1 detectable in BMDM?	No	No	Yes, following Flag immunoprecipitation	Only by qRT-PCR, not by Western blot
Potential uses	Not recommended, improved mouse models are now available.	Re-evaluation of phenotypes previously observed in congenic mice. Further research into the effect of SARM1 deletion.	Determination of where and when SARM1 is expressed. Identification or confirmation of SARM1 binding partners.	Defining the requirement for intact enzymatic activity for the various roles of SARM1.

Future Directions

This study illuminated the presence of passenger genes on chromosome 11 of the heavily relied upon B6 congenic *Sarm1*$^{-/-}$ mouse and, using novel CRISPR/Cas9-generated SARM1-deficient mice, demonstrated that these passenger genes were the *bona fide* cause for the altered expression of a number of genes previously observed in macrophages from B6 congenic *Sarm1*$^{-/-}$ mice. To conclusively define if the differential expression of any of other genes observed in BMDMs from congenic *Sarm1*$^{-/-}$ mice by RNA sequencing resulted from the absence of SARM1, BMDMs from CRISPR/Cas9 SARM1-knockout mice and littermate WT controls could be subjected to RNA sequencing using a similar protocol. The data from this would also provide useful background information for any researchers using these CRISPR/Cas9 SARM1-deficient mice in further studies.

Using the novel CRISPR/Cas9 SARM1-knockout mice I demonstrated that SARM1 does not regulate *Ccl5* expression in macrophages, clarifying that the diminished *Ccl5* expression previously reported by our lab in SARM1-deficient macrophages was caused by the presence of passenger genes in the B6 congenic *Sarm1*$^{-/-}$ mouse. However, it remains broadly unknown which of the roles reported for SARM1 from studies using B6 congenic *Sarm1*$^{-/-}$ mice are legitimate, and which are artefacts resulting from passenger genes. Thus the degree to which these passenger genes have confounded our collective understanding of murine SARM1 remains to be determined, and it is unclear how much of the literature on murine SARM1 is definitively correct. Given the substantial interest in developing therapeutics which target SARM1 to modulate axon degeneration, it is important that there is a clear and correct understanding of the non-degenerative functions of SARM1, and how these would be affected by its modulation. Therefore, all research previously performed in B6 congenic *Sarm1*$^{-/-}$ mice should be carefully re-examined. The novel SARM1-deficient mice generated in the course of this study are an appropriate model in which to interrogate the previously reported roles for murine SARM1 and delineate which are real, thus allowing us to re-evaluate our understanding of SARM1. The studies which most urgently ought to be repeated in the CRISPR/Cas9 SARM1-knockout mice are those which implicate the differential expression of genes proximal to the *Sarm1* locus in B6 congenic *Sarm1*$^{-/-}$ mice as the consequence of SARM1 loss that results in the manifestation of a phenotype. This includes the role of SARM1 in prion disease. The accelerated prion

pathogenesis reported in B6 congenic *Sarm1*$^{-/-}$ mice was attributed to increased expression of *Xaf1* [169], which we now appreciate is an artefact caused by passenger genes, thus casting uncertainty on the interpretation of this study. In addition to the repetition of previous studies, future studies should be carried out in the CRISPR/Cas9 SARM1-knockout mice rather than B6 congenic *Sarm1*$^{-/-}$ mice, to prevent any further unreliable results or misattributed phenotypes. Speaking more broadly, where possible the use of congenic mice in research should be discontinued in favour of isogenic mice, which are now increasingly available and accessible.

Further work is required to clarify the role for SARM1 in the response to *Klebsiella pneumoniae* infection in macrophages given that I could not repeat the results observed by our collaborators, the Bengoechea lab. While similar mice and bacteria were used in both of our studies, it is possible that the inconsistency in phenotype observed between our labs stem from inter-institutional differences, or from differences in how the individual researchers perform the experiment. Thus, if a researcher from each group were to swap locations and perform the experiment in the other lab group's facilities, the source of the discrepancy in phenotype may become more apparent.

Another useful tool generated in the course of this study is the *Sarm1*^{Flag} mouse, which expresses endogenous SARM1 with Flag and Strep tags to facilitate detection with antibodies. This epitope-tagged SARM1 was demonstrated to be functional in an axon degeneration assay [195], suggesting that the expression, localisation, folding, oligomerisation, and activation of SARM1 is unimpeded by the presence of the C-terminal tags. Thus, this new mouse can be used to determine the cell types and tissues in which SARM1 is expressed, simply using Western blot and immunoprecipitation, and to compare its relative expression levels. Expanding on this, the *Sarm1*^{Flag} mouse could be used to determine the conditions in which SARM1 expression is enhanced or diminished. For example, to determine if SARM1 expression is modulated in macrophages in response to *K. pneumoniae* infection, BMDMs from the *Sarm1*^{Flag} mouse could be infected with *K. pneumoniae* over a range of time-points then subjected to Western blot, and the relative levels of SARM1 compared. Understanding the contexts in which SARM1 is present or absent may provide clues as to its functions. Additionally, a cyclohexamide chase assay could be used in cells from the *Sarm1*^{Flag} mouse to determine the stability of the SARM1 protein. High SARM1 turnover could potentially be an additional layer of control of this

protein, which must be tightly controlled as its activity can cause catastrophic NAD^+ depletion. However, given that SARM1 exists as a preformed octamer in its inactive state, it may be very stable.

The subcellular localisation of SARM1 has been examined in a number of cell types using overexpressed epitope-tagged SARM1, however it is possible that the specific tags used or the non-endogenous expression level could cause altered localisation of SARM1 in these systems. Thus, the *Sarm1*^{Flag} mouse presents a new and appropriate model in which to define the subcellular localisation of endogenous murine SARM1. Overexpressed epitope-tagged SARM1 has also been used to determine the proteins with which SARM1 interacts, and it is unclear if this faithfully represents endogenous SARM1. Given that SARM1 exists as an octamer, it is difficult to understand how SARM1 could have so many interacting partners, including NLRP3, ATP synthase, NLRX, UXT1, UXT2, and TRIF among others. Co-immunoprecipitation using an antibody targeting Flag or Strep could be used on cells from the *Sarm1*^{Flag} mouse to clarify if these are true interacting partners of endogenous murine SARM1, and co-immunoprecipitation coupled to mass spectrometry could be used to elucidate the full interactome of SARM1.

It is unfortunate that SARM1 cannot be detected on the protein level in the *Sarm1*^{E682A} mouse, as this would be a useful tool to delineate which functions of SARM1 require intact NADase activity and could be affected by its therapeutic modulation. Further work is required to understand why SARM1 remains undetectable in this mouse, whether it is not recognised by the antibody or it is simply not expressed. This may not be possible until the first NADase-independent role for SARM1 is conclusively established. If this function proceeds as normal in WT and *Sarm1*^{E682A} mice, but not *Sarm1*^{em1Tftc} mice, this would indicate that NADase-inactive SARM1 is in fact expressed in the *Sarm1*^{E682A} mouse and that the problem lies in the detection.

Overall, the mice described in this thesis present novel and improved tools in which to explore and to re-examine the roles for murine SARM1.

References

1. Gallo, R.L., *Human Skin Is the Largest Epithelial Surface for Interaction with Microbes.* J Invest Dermatol, 2017. **137**(6): p. 1213-1214.
2. Helander, H.F. and L. Fändriks, *Surface area of the digestive tract - revisited.* Scand J Gastroenterol, 2014. **49**(6): p. 681-9.
3. Hasleton, P.S., *The internal surface area of the adult human lung.* J Anat, 1972. **112**(Pt 3): p. 391-400.
4. Janeway, C.A., *Pillars article: approaching the asymptote? Evolution and revolution in immunology. Cold spring harb symp quant biol. 1989. 54: 1-13.* J Immunol, 2013. **191**(9): p. 4475-87.
5. Janeway, C.A. and R. Medzhitov, *Innate immune recognition.* Annu Rev Immunol, 2002. **20**: p. 197-216.
6. Matzinger, P., *Tolerance, danger, and the extended family.* Annu Rev Immunol, 1994. **12**: p. 991-1045.
7. Medzhitov, R., *Toll-like receptors and innate immunity.* Nat Rev Immunol, 2001. **1**(2): p. 135-45.
8. O'Neill, L.A., K.A. Fitzgerald, and A.G. Bowie, *The Toll-IL-1 receptor adaptor family grows to five members.* Trends Immunol, 2003. **24**(6): p. 286-90.
9. Yamamoto, M., et al., *Role of adaptor TRIF in the MyD88-independent toll-like receptor signaling pathway.* Science, 2003. **301**(5633): p. 640-3.
10. Yamamoto, M., et al., *TRAM is specifically involved in the Toll-like receptor 4-mediated MyD88-independent signaling pathway.* Nat Immunol, 2003. **4**(11): p. 1144-50.
11. Ruscanu, S., et al., *The double-stranded RNA bluetongue virus induces type I interferon in plasmacytoid dendritic cells via a MYD88-dependent TLR7/8-independent signaling pathway.* J Virol, 2012. **86**(10): p. 5817-28.
12. Ní Cheallaigh, C., et al., *A Common Variant in the Adaptor Mal Regulates Interferon Gamma Signaling.* Immunity, 2016. **44**(2): p. 368-79.
13. O'Neill, L.A. and A.G. Bowie, *The family of five: TIR-domain-containing adaptors in Toll-like receptor signalling.* Nat Rev Immunol, 2007. **7**(5): p. 353-64.
14. Mink, M., et al., *A novel human gene (SARM) at chromosome 17q11 encodes a protein with a SAM motif and structural similarity to Armadillo/beta-catenin that is conserved in mouse, Drosophila, and Caenorhabditis elegans.* Genomics, 2001. **74**(2): p. 234-44.
15. Harris, T.W., et al., *WormBase: a modern Model Organism Information Resource.* Nucleic Acids Res, 2020. **48**(D1): p. D762-D767.
16. Couillault, C., et al., *TLR-independent control of innate immunity in Caenorhabditis elegans by the TIR domain adaptor protein TIR-1, an ortholog of human SARM.* Nat Immunol, 2004. **5**(5): p. 488-94.
17. Liberati, N.T., et al., *Requirement for a conserved Toll/interleukin-1 resistance domain protein in the Caenorhabditis elegans immune response.* Proc Natl Acad Sci U S A, 2004. **101**(17): p. 6593-8.
18. Kurz, C.L., et al., *Caenorhabditis elegans pgp-5 is involved in resistance to bacterial infection and heavy metal and its regulation requires TIR-1 and a p38 map kinase cascade.* Biochem Biophys Res Commun, 2007. **363**(2): p. 438-43.

19. Blum, E.S., et al., *Control of nonapoptotic developmental cell death in Caenorhabditis elegans by a polyglutamine-repeat protein.* Science, 2012. **335**(6071): p. 970-3.
20. Hayakawa, T., et al., *Regulation of anoxic death in Caenorhabditis elegans by mammalian apoptosis signal-regulating kinase (ASK) family proteins.* Genetics, 2011. **187**(3): p. 785-92.
21. Akhouayri, I., et al., *Toll-8/Tollo negatively regulates antimicrobial response in the Drosophila respiratory epithelium.* PLoS Pathog, 2011. **7**(10): p. e1002319.
22. Monsanto-Hearne, V., et al., *Drosophila miR-956 suppression modulates Ectoderm-expressed 4 and inhibits viral replication.* Virology, 2017. **502**: p. 20-27.
23. Meyer, S.N., et al., *An ancient defense system eliminates unfit cells from developing tissues during cell competition.* Science, 2014. **346**(6214): p. 1258236.
24. Panneerselvam, P., et al., *Targeting of pro-apoptotic TLR adaptor SARM to mitochondria: definition of the critical region and residues in the signal sequence.* Biochem J, 2012. **442**(2): p. 263-71.
25. Carty, M., et al., *Cell Survival and Cytokine Release after Inflammasome Activation Is Regulated by the Toll-IL-1R Protein SARM.* Immunity, 2019. **50**(6): p. 1412-1424.e6.
26. Kim, Y., et al., *MyD88-5 links mitochondria, microtubules, and JNK3 in neurons and regulates neuronal survival.* J Exp Med, 2007. **204**(9): p. 2063-74.
27. Murata, H., et al., *SARM1 and TRAF6 bind to and stabilize PINK1 on depolarized mitochondria.* Mol Biol Cell, 2013. **24**(18): p. 2772-84.
28. Killackey, S.A., et al., *The mitochondrial Nod-like receptor NLRX1 modifies apoptosis through SARM1.* Mol Cell Biochem, 2019. **453**(1-2): p. 187-196.
29. Osterloh, J.M., et al., *dSarm/Sarm1 is required for activation of an injury-induced axon death pathway.* Science, 2012. **337**(6093): p. 481-4.
30. Essuman, K., et al., *The SARM1 Toll/Interleukin-1 Receptor Domain Possesses Intrinsic NAD(+) Cleavage Activity that Promotes Pathological Axonal Degeneration.* Neuron, 2017. **93**(6): p. 1334-1343.e5.
31. Murata, H., et al., *c-Jun N-terminal kinase (JNK)-mediated phosphorylation of SARM1 regulates NAD(+) cleavage activity to inhibit mitochondrial respiration.* J Biol Chem, 2018. **293**(49): p. 18933-18943.
32. Essuman, K., et al., *TIR Domain Proteins Are an Ancient Family of NAD.* Curr Biol, 2018. **28**(3): p. 421-430.e4.
33. Summers, D.W., et al., *SARM1-specific motifs in the TIR domain enable NAD+ loss and regulate injury-induced SARM1 activation.* Proc Natl Acad Sci U S A, 2016. **113**(41): p. E6271-e6280.
34. Gürtler, C., et al., *SARM regulates CCL5 production in macrophages by promoting the recruitment of transcription factors and RNA polymerase II to the Ccl5 promoter.* J Immunol, 2014. **192**(10): p. 4821-32.
35. Panneerselvam, P., et al., *T-cell death following immune activation is mediated by mitochondria-localized SARM.* Cell Death Differ, 2013. **20**(3): p. 478-89.
36. Carty, M., et al., *The human adaptor SARM negatively regulates adaptor protein TRIF-dependent Toll-like receptor signaling.* Nat Immunol, 2006. **7**(10): p. 1074-81.
37. Peng, J., et al., *SARM inhibits both TRIF- and MyD88-mediated AP-1 activation.* Eur J Immunol, 2010. **40**(6): p. 1738-47.
38. Yuan, S., et al., *Amphioxus SARM involved in neural development may function as a suppressor of TLR signaling.* J Immunol, 2010. **184**(12): p. 6874-81.

39. Belinda, L.W., et al., *SARM: a novel Toll-like receptor adaptor, is functionally conserved from arthropod to human.* Mol Immunol, 2008. **45**(6): p. 1732-42.
40. Zhou, X., et al., *Molecular characterization of porcine SARM1 and its role in regulating TLRs signaling during highly pathogenic porcine reproductive and respiratory syndrome virus infection in vivo.* Dev Comp Immunol, 2013. **39**(1-2): p. 117-26.
41. Toshchakov, V.Y. and S.N. Vogel, *Cell-penetrating TIR BB loop decoy peptides a novel class of TLR signaling inhibitors and a tool to study topology of TIR-TIR interactions.* Expert Opin Biol Ther, 2007. **7**(7): p. 1035-50.
42. Nimma, S., et al., *Structural Evolution of TIR-Domain Signalosomes.* Front Immunol, 2021. **12**: p. 784484.
43. Carlsson, E., J.L. Ding, and B. Byrne, *SARM modulates MyD88-mediated TLR activation through BB-loop dependent TIR-TIR interactions.* Biochim Biophys Acta, 2016. **1863**(2): p. 244-53.
44. Szretter, K.J., et al., *The immune adaptor molecule SARM modulates tumor necrosis factor alpha production and microglia activation in the brainstem and restricts West Nile Virus pathogenesis.* J Virol, 2009. **83**(18): p. 9329-38.
45. Pudla, M., K. Limposuwan, and P. Utaisincharoen, *Burkholderia pseudomallei-induced expression of a negative regulator, sterile-alpha and Armadillo motif-containing protein, in mouse macrophages: a possible mechanism for suppression of the MyD88-independent pathway.* Infect Immun, 2011. **79**(7): p. 2921-7.
46. Peters, O.M., M. Ghasemi, and R.H. Brown, *Emerging mechanisms of molecular pathology in ALS.* J Clin Invest, 2015. **125**(6): p. 2548.
47. Burke, R.E. and K. O'Malley, *Axon degeneration in Parkinson's disease.* Exp Neurol, 2013. **246**: p. 72-83.
48. Fukuda, Y., Y. Li, and R.A. Segal, *A Mechanistic Understanding of Axon Degeneration in Chemotherapy-Induced Peripheral Neuropathy.* Front Neurosci, 2017. **11**: p. 481.
49. Feldman, E.L., et al., *Diabetic neuropathy.* Nat Rev Dis Primers, 2019. **5**(1): p. 41.
50. Waller, A., *Experiments on the Section of the Glosso-Pharyngeal and Hypoglossal Nerves of the Frog, and Observations of the Alterations Produced Thereby in the Structure of Their Primitive Fibres.* Edinb Med Surg J, 1851. **76**(189): p. 369-376.
51. George, E.B., J.D. Glass, and J.W. Griffin, *Axotomy-induced axonal degeneration is mediated by calcium influx through ion-specific channels.* J Neurosci, 1995. **15**(10): p. 6445-52.
52. Park, J.Y., et al., *Mitochondrial swelling and microtubule depolymerization are associated with energy depletion in axon degeneration.* Neuroscience, 2013. **238**: p. 258-69.
53. Lunn, E.R., et al., *Absence of Wallerian Degeneration does not Hinder Regeneration in Peripheral Nerve.* Eur J Neurosci, 1989. **1**(1): p. 27-33.
54. Wang, M.S., et al., *The WldS protein protects against axonal degeneration: a model of gene therapy for peripheral neuropathy.* Ann Neurol, 2001. **50**(6): p. 773-9.
55. Wang, M.S., et al., *WldS mice are resistant to paclitaxel (taxol) neuropathy.* Ann Neurol, 2002. **52**(4): p. 442-7.
56. Ferri, A., et al., *Inhibiting axon degeneration and synapse loss attenuates apoptosis and disease progression in a mouse model of motoneuron disease.* Curr Biol, 2003. **13**(8): p. 669-73.
57. Samsam, M., et al., *The Wlds mutation delays robust loss of motor and sensory axons in a genetic model for myelin-related axonopathy.* J Neurosci, 2003. **23**(7): p. 2833-9.

58. Mi, W., et al., *The slow Wallerian degeneration gene, WldS, inhibits axonal spheroid pathology in gracile axonal dystrophy mice.* Brain, 2005. **128**(Pt 2): p. 405-16.
59. Kerschensteiner, M., et al., *In vivo imaging of axonal degeneration and regeneration in the injured spinal cord.* Nat Med, 2005. **11**(5): p. 572-7.
60. Hoopfer, E.D., et al., *Wlds protection distinguishes axon degeneration following injury from naturally occurring developmental pruning.* Neuron, 2006. **50**(6): p. 883-95.
61. Mack, T.G., et al., *Wallerian degeneration of injured axons and synapses is delayed by a Ube4b/Nmnat chimeric gene.* Nat Neurosci, 2001. **4**(12): p. 1199-206.
62. Summers, D.W., A. DiAntonio, and J. Milbrandt, *Mitochondrial dysfunction induces Sarm1-dependent cell death in sensory neurons.* J Neurosci, 2014. **34**(28): p. 9338-50.
63. Sasaki, Y., et al., *cADPR is a gene dosage-sensitive biomarker of SARM1 activity in healthy, compromised, and degenerating axons.* Exp Neurol, 2020. **329**: p. 113252.
64. Turkiew, E., et al., *Deletion of Sarm1 gene is neuroprotective in two models of peripheral neuropathy.* J Peripher Nerv Syst, 2017. **22**(3): p. 162-171.
65. Geisler, S., et al., *Prevention of vincristine-induced peripheral neuropathy by genetic deletion of SARM1 in mice.* Brain, 2016. **139**(Pt 12): p. 3092-3108.
66. Geisler, S., et al., *Vincristine and bortezomib use distinct upstream mechanisms to activate a common SARM1-dependent axon degeneration program.* JCI Insight, 2019. **4**(17).
67. Coleman, M.P. and V.H. Perry, *Axon pathology in neurological disease: a neglected therapeutic target.* Trends Neurosci, 2002. **25**(10): p. 532-7.
68. Cavanagh, J.B., *The 'dying back' process. A common denominator in many naturally occurring and toxic neuropathies.* Arch Pathol Lab Med, 1979. **103**(13): p. 659-64.
69. Fogh, I., et al., *A genome-wide association meta-analysis identifies a novel locus at 17q11.2 associated with sporadic amyotrophic lateral sclerosis.* Hum Mol Genet, 2014. **23**(8): p. 2220-31.
70. van Rheenen, W., et al., *Genome-wide association analyses identify new risk variants and the genetic architecture of amyotrophic lateral sclerosis.* Nat Genet, 2016. **48**(9): p. 1043-8.
71. Peters, O.M., et al., *Loss of Sarm1 does not suppress motor neuron degeneration in the SOD1G93A mouse model of amyotrophic lateral sclerosis.* Hum Mol Genet, 2018. **27**(21): p. 3761-3771.
72. White, M.A., et al., *Sarm1 deletion suppresses TDP-43-linked motor neuron degeneration and cortical spine loss.* Acta Neuropathol Commun, 2019. **7**(1): p. 166.
73. Arai, T., et al., *TDP-43 is a component of ubiquitin-positive tau-negative inclusions in frontotemporal lobar degeneration and amyotrophic lateral sclerosis.* Biochem Biophys Res Commun, 2006. **351**(3): p. 602-11.
74. Peters, O.M., et al., *Genetic diversity of axon degenerative mechanisms in models of Parkinson's disease.* Neurobiol Dis, 2021. **155**: p. 105368.
75. Henninger, N., et al., *Attenuated traumatic axonal injury and improved functional outcome after traumatic brain injury in mice lacking Sarm1.* Brain, 2016. **139**(Pt 4): p. 1094-105.
76. Green, R.E., et al., *Scale and pattern of atrophy in the chronic stages of moderate-severe TBI.* Front Hum Neurosci, 2014. **8**: p. 67.

77. Bradshaw, D.V., et al., *Genetic inactivation of SARM1 axon degeneration pathway improves outcome trajectory after experimental traumatic brain injury based on pathological, radiological, and functional measures.* Acta Neuropathol Commun, 2021. **9**(1): p. 89.
78. Sun, Y., et al., *Sarm1-mediated neurodegeneration within the enteric nervous system protects against local inflammation of the colon.* Protein Cell, 2021.
79. Sundaramoorthy, V., et al., *Novel role of SARM1 mediated axonal degeneration in the pathogenesis of rabies.* PLoS Pathog, 2020. **16**(2): p. e1008343.
80. Araki, T., Y. Sasaki, and J. Milbrandt, *Increased nuclear NAD biosynthesis and SIRT1 activation prevent axonal degeneration.* Science, 2004. **305**(5686): p. 1010-3.
81. Berger, F., et al., *Subcellular compartmentation and differential catalytic properties of the three human nicotinamide mononucleotide adenylyltransferase isoforms.* J Biol Chem, 2005. **280**(43): p. 36334-41.
82. Gilley, J. and M.P. Coleman, *Endogenous Nmnat2 is an essential survival factor for maintenance of healthy axons.* PLoS Biol, 2010. **8**(1): p. e1000300.
83. Yahata, N., S. Yuasa, and T. Araki, *Nicotinamide mononucleotide adenylyltransferase expression in mitochondrial matrix delays Wallerian degeneration.* J Neurosci, 2009. **29**(19): p. 6276-84.
84. Sasaki, Y., et al., *Transgenic mice expressing the Nmnat1 protein manifest robust delay in axonal degeneration in vivo.* J Neurosci, 2009. **29**(20): p. 6526-34.
85. Conforti, L., et al., *NAD(+) and axon degeneration revisited: Nmnat1 cannot substitute for Wld(S) to delay Wallerian degeneration.* Cell Death Differ, 2007. **14**(1): p. 116-27.
86. Yan, T., et al., *Nmnat2 delays axon degeneration in superior cervical ganglia dependent on its NAD synthesis activity.* Neurochem Int, 2010. **56**(1): p. 101-6.
87. Wang, J., et al., *A local mechanism mediates NAD-dependent protection of axon degeneration.* J Cell Biol, 2005. **170**(3): p. 349-55.
88. Gerdts, J., et al., *SARM1 activation triggers axon degeneration locally via NAD^+ destruction.* Science, 2015. **348**(6233): p. 453-7.
89. Gerdts, J., et al., *Sarm1-mediated axon degeneration requires both SAM and TIR interactions.* J Neurosci, 2013. **33**(33): p. 13569-80.
90. Sasaki, Y., et al., *Nicotinamide mononucleotide adenylyl transferase-mediated axonal protection requires enzymatic activity but not increased levels of neuronal nicotinamide adenine dinucleotide.* J Neurosci, 2009. **29**(17): p. 5525-35.
91. Essuman, K., et al., *TIR Domain Proteins Are an Ancient Family of NAD^+-Consuming Enzymes.* Curr Biol, 2018. **28**(3): p. 421-430.e4.
92. Zhang, Q., et al., *TIR domain-containing adaptor SARM is a late addition to the ongoing microbe-host dialog.* Dev Comp Immunol, 2011. **35**(4): p. 461-8.
93. Hopkins, E.L., et al., *A Novel NAD Signaling Mechanism in Axon Degeneration and its Relationship to Innate Immunity.* Front Mol Biosci, 2021. **8**: p. 703532.
94. Burroughs, A.M., et al., *Comparative genomic analyses reveal a vast, novel network of nucleotide-centric systems in biological conflicts, immunity and signaling.* Nucleic Acids Res, 2015. **43**(22): p. 10633-54.
95. Sikowitz, M.D., et al., *Reversal of the substrate specificity of CMP N-glycosidase to dCMP.* Biochemistry, 2013. **52**(23): p. 4037-47.
96. Armstrong, S.R., et al., *Crystal structures of nucleoside 2-deoxyribosyltransferase in native and ligand-bound forms reveal architecture of the active site.* Structure, 1996. **4**(1): p. 97-107.

97. Ghosh, J., et al., *Characterization of Streptococcus pyogenes beta-NAD+ glycohydrolase: re-evaluation of enzymatic properties associated with pathogenesis.* J Biol Chem, 2010. **285**(8): p. 5683-94.
98. Gilley, J., et al., *Enrichment of SARM1 alleles encoding variants with constitutively hyperactive NADase in patients with ALS and other motor nerve disorders.* Elife, 2021. **10**.
99. Bloom, A.J., et al., *Constitutively active SARM1 variants that induce neuropathy are enriched in ALS patients.* Mol Neurodegener, 2022. **17**(1): p. 1.
100. Xue, T., et al., *Phosphorylation at S548 as a Functional Switch of Sterile Alpha and TIR Motif-Containing 1 in Cerebral Ischemia/Reperfusion Injury in Rats.* Mol Neurobiol, 2021. **58**(2): p. 453-469.
101. Kwong, A.K., et al., *Catalysis-based inhibitors of the calcium signaling function of CD38.* Biochemistry, 2012. **51**(1): p. 555-64.
102. Zhao, Z.Y., et al., *A Cell-Permeant Mimetic of NMN Activates SARM1 to Produce Cyclic ADP-Ribose and Induce Non-apoptotic Cell Death.* iScience, 2019. **15**: p. 452-466.
103. Horsefield, S., et al., *NAD^+ cleavage activity by animal and plant TIR domains in cell death pathways.* Science, 2019. **365**(6455): p. 793-799.
104. Wan, L., et al., *TIR domains of plant immune receptors are NAD.* Science, 2019. **365**(6455): p. 799-803.
105. Sporny, M., et al., *Structural Evidence for an Octameric Ring Arrangement of SARM1.* J Mol Biol, 2019. **431**(19): p. 3591-3605.
106. Bratkowski, M., et al., *Structural and Mechanistic Regulation of the Pro-degenerative NAD Hydrolase SARM1.* Cell Rep, 2020. **32**(5): p. 107999.
107. Jiang, Y., et al., *The NAD+ -mediated self-inhibition mechanism of pro-neurodegenerative SARM1.* Nature, 2020. **588**(7839): p. 658-663.
108. Shen, C., et al., *Multiple domain interfaces mediate SARM1 autoinhibition.* Proc Natl Acad Sci U S A, 2021. **118**(4).
109. Figley, M.D., et al., *SARM1 is a metabolic sensor activated by an increased NMN/NAD.* Neuron, 2021. **109**(7): p. 1118-1136.e11.
110. Liu, H.W., et al., *Pharmacological bypass of NAD^+ salvage pathway protects neurons from chemotherapy-induced degeneration.* Proc Natl Acad Sci U S A, 2018. **115**(42): p. 10654-10659.
111. Di Stefano, M., et al., *A rise in NAD precursor nicotinamide mononucleotide (NMN) after injury promotes axon degeneration.* Cell Death Differ, 2015. **22**(5): p. 731-42.
112. Loreto, A., et al., *Mitochondrial impairment activates the Wallerian pathway through depletion of NMNAT2 leading to SARM1-dependent axon degeneration.* Neurobiol Dis, 2020. **134**: p. 104678.
113. Hughes, R.O., et al., *Small Molecule SARM1 Inhibitors Recapitulate the $SARM1^{-/-}$ Phenotype and Allow Recovery of a Metastable Pool of Axons Fated to Degenerate.* Cell Rep, 2021. **34**(1): p. 108588.
114. Summers, D.W., et al., *DLK Activation Synergizes with Mitochondrial Dysfunction to Downregulate Axon Survival Factors and Promote SARM1-Dependent Axon Degeneration.* Mol Neurobiol, 2020. **57**(2): p. 1146-1158.
115. Ko, K.W., et al., *Live imaging reveals the cellular events downstream of SARM1 activation.* Elife, 2021. **10**.
116. Hsu, J.M., et al., *Injury-Induced Inhibition of Bystander Neurons Requires dSarm and Signaling from Glia.* Neuron, 2021. **109**(3): p. 473-487.e5.

117. Vargas, M.E., et al., *Live Imaging of Calcium Dynamics during Axon Degeneration Reveals Two Functionally Distinct Phases of Calcium Influx.* J Neurosci, 2015. **35**(45): p. 15026-38.
118. Loreto, A., et al., *Wallerian Degeneration Is Executed by an NMN-SARM1-Dependent Late Ca(2+) Influx but Only Modestly Influenced by Mitochondria.* Cell Rep, 2015. **13**(11): p. 2539-2552.
119. Mészáros, L.G., J. Bak, and A. Chu, *Cyclic ADP-ribose as an endogenous regulator of the non-skeletal type ryanodine receptor Ca2+ channel.* Nature, 1993. **364**(6432): p. 76-9.
120. Kolisek, M., et al., *Cyclic ADP-ribose and hydrogen peroxide synergize with ADP-ribose in the activation of TRPM2 channels.* Mol Cell, 2005. **18**(1): p. 61-9.
121. Li, Y., et al., *Sarm1 activation produces cADPR to increase intra-axonal Ca++ and promote axon degeneration in PIPN.* J Cell Biol, 2022. **221**(2).
122. Ma, M., et al., *Calpains mediate axonal cytoskeleton disintegration during Wallerian degeneration.* Neurobiol Dis, 2013. **56**: p. 34-46.
123. Yang, J., et al., *Regulation of axon degeneration after injury and in development by the endogenous calpain inhibitor calpastatin.* Neuron, 2013. **80**(5): p. 1175-89.
124. Yang, J., et al., *Pathological axonal death through a MAPK cascade that triggers a local energy deficit.* Cell, 2015. **160**(1-2): p. 161-76.
125. Walker, L.J., et al., *MAPK signaling promotes axonal degeneration by speeding the turnover of the axonal maintenance factor NMNAT2.* Elife, 2017. **6**.
126. Carty, M. and A.G. Bowie, *SARM: From immune regulator to cell executioner.* Biochem Pharmacol, 2019. **161**: p. 52-62.
127. Gould, S.A., et al., *Sarm1 haploinsufficiency or low expression levels after antisense oligonucleotides delay programmed axon degeneration.* Cell Rep, 2021. **37**(11): p. 110108.
128. Chen, Y.H., et al., *SARM1 is required in human derived sensory neurons for injury-induced and neurotoxic axon degeneration.* Exp Neurol, 2021. **339**: p. 113636.
129. Kuzmin, D.A., et al., *The clinical landscape for AAV gene therapies.* Nat Rev Drug Discov, 2021. **20**(3): p. 173-174.
130. Williams, P.R., et al., *A recoverable state of axon injury persists for hours after spinal cord contusion in vivo.* Nat Commun, 2014. **5**: p. 5683.
131. Nikić, I., et al., *A reversible form of axon damage in experimental autoimmune encephalomyelitis and multiple sclerosis.* Nat Med, 2011. **17**(4): p. 495-9.
132. Li, W.H., et al., *Permeant fluorescent probes visualize the activation of SARM1 and uncover an anti-neurodegenerative drug candidate.* Elife, 2021. **10**.
133. Bosanac, T., et al., *Pharmacological SARM1 inhibition protects axon structure and function in paclitaxel-induced peripheral neuropathy.* Brain, 2021. **144**(10): p. 3226-3238.
134. Loreto, A., et al., *Neurotoxin-mediated potent activation of the axon degeneration regulator SARM1.* Elife, 2021. **10**.
135. Wu, T., et al., *Neurotoxins subvert the allosteric activation mechanism of SARM1 to induce neuronal loss.* Cell Rep, 2021. **37**(3): p. 109872.
136. Zhao, Y.J., et al., *Acidic pH irreversibly activates the signaling enzyme SARM1.* FEBS J, 2021.
137. Kerr, J.F., A.H. Wyllie, and A.R. Currie, *Apoptosis: a basic biological phenomenon with wide-ranging implications in tissue kinetics.* Br J Cancer, 1972. **26**(4): p. 239-57.
138. Ketelut-Carneiro, N. and K.A. Fitzgerald, *Apoptosis, Pyroptosis, and Necroptosis-Oh My! The Many Ways a Cell Can Die.* J Mol Biol, 2021: p. 167378.

139. Chinnaiyan, A.M., *The apoptosome: heart and soul of the cell death machine.* Neoplasia, 1999. **1**(1): p. 5-15.
140. Kischkel, F.C., et al., *Cytotoxicity-dependent APO-1 (Fas/CD95)-associated proteins form a death-inducing signaling complex (DISC) with the receptor.* EMBO J, 1995. **14**(22): p. 5579-88.
141. Cohen, G.M., *Caspases: the executioners of apoptosis.* Biochem J, 1997. **326 (Pt 1)**: p. 1-16.
142. Bortner, C.D., N.B. Oldenburg, and J.A. Cidlowski, *The role of DNA fragmentation in apoptosis.* Trends Cell Biol, 1995. **5**(1): p. 21-6.
143. Nemes, Z., et al., *Expression and activation of tissue transglutaminase in apoptotic cells of involuting rodent mammary tissue.* Eur J Cell Biol, 1996. **70**(2): p. 125-33.
144. Cossarizza, A., et al., *Mitochondrial modifications during rat thymocyte apoptosis: a study at the single cell level.* Exp Cell Res, 1994. **214**(1): p. 323-30.
145. Bratton, D.L., et al., *Appearance of phosphatidylserine on apoptotic cells requires calcium-mediated nonspecific flip-flop and is enhanced by loss of the aminophospholipid translocase.* J Biol Chem, 1997. **272**(42): p. 26159-65.
146. Fadok, V.A., et al., *Loss of phospholipid asymmetry and surface exposure of phosphatidylserine is required for phagocytosis of apoptotic cells by macrophages and fibroblasts.* J Biol Chem, 2001. **276**(2): p. 1071-7.
147. Kurosaka, K., et al., *Silent cleanup of very early apoptotic cells by macrophages.* J Immunol, 2003. **171**(9): p. 4672-9.
148. Kourtzelis, I., G. Hajishengallis, and T. Chavakis, *Phagocytosis of Apoptotic Cells in Resolution of Inflammation.* Front Immunol, 2020. **11**: p. 553.
149. Boise, L.H. and C.M. Collins, *Salmonella-induced cell death: apoptosis, necrosis or programmed cell death?* Trends Microbiol, 2001. **9**(2): p. 64-7.
150. Huang, L.S., et al., *mtDNA Activates cGAS Signaling and Suppresses the YAP-Mediated Endothelial Cell Proliferation Program to Promote Inflammatory Injury.* Immunity, 2020. **52**(3): p. 475-486.e5.
151. de Torre-Minguela, C., et al., *Gasdermins mediate cellular release of mitochondrial DNA during pyroptosis and apoptosis.* FASEB J, 2021. **35**(8): p. e21757.
152. Broz, P. and V.M. Dixit, *Inflammasomes: mechanism of assembly, regulation and signalling.* Nat Rev Immunol, 2016. **16**(7): p. 407-20.
153. Kayagaki, N., et al., *Caspase-11 cleaves gasdermin D for non-canonical inflammasome signalling.* Nature, 2015. **526**(7575): p. 666-71.
154. Rivers-Auty, J. and D. Brough, *Potassium efflux fires the canon: Potassium efflux as a common trigger for canonical and noncanonical NLRP3 pathways.* Eur J Immunol, 2015. **45**(10): p. 2758-61.
155. Wang, Y., et al., *GSDME mediates caspase-3-dependent pyroptosis in gastric cancer.* Biochem Biophys Res Commun, 2018. **495**(1): p. 1418-1425.
156. Wang, Y., et al., *Chemotherapy drugs induce pyroptosis through caspase-3 cleavage of a gasdermin.* Nature, 2017. **547**(7661): p. 99-103.
157. Holler, N., et al., *Fas triggers an alternative, caspase-8-independent cell death pathway using the kinase RIP as effector molecule.* Nat Immunol, 2000. **1**(6): p. 489-95.
158. Zhang, D.W., et al., *RIP3, an energy metabolism regulator that switches TNF-induced cell death from apoptosis to necrosis.* Science, 2009. **325**(5938): p. 332-6.
159. Sun, L., et al., *Mixed lineage kinase domain-like protein mediates necrosis signaling downstream of RIP3 kinase.* Cell, 2012. **148**(1-2): p. 213-27.

160. Wang, H., et al., *Mixed lineage kinase domain-like protein MLKL causes necrotic membrane disruption upon phosphorylation by RIP3.* Mol Cell, 2014. **54**(1): p. 133-146.
161. Yan, B., et al., *Membrane Damage during Ferroptosis Is Caused by Oxidation of Phospholipids Catalyzed by the Oxidoreductases POR and CYB5R1.* Mol Cell, 2021. **81**(2): p. 355-369.e10.
162. Andrabi, S.A., T.M. Dawson, and V.L. Dawson, *Mitochondrial and nuclear cross talk in cell death: parthanatos.* Ann N Y Acad Sci, 2008. **1147**: p. 233-41.
163. Sarhan, J., et al., *Caspase-8 induces cleavage of gasdermin D to elicit pyroptosis during.* Proc Natl Acad Sci U S A, 2018. **115**(46): p. E10888-E10897.
164. Tsuchiya, K., et al., *Caspase-1 initiates apoptosis in the absence of gasdermin D.* Nat Commun, 2019. **10**(1): p. 2091.
165. Bedoui, S., M.J. Herold, and A. Strasser, *Emerging connectivity of programmed cell death pathways and its physiological implications.* Nat Rev Mol Cell Biol, 2020. **21**(11): p. 678-695.
166. Kuan, C.Y., et al., *A critical role of neural-specific JNK3 for ischemic apoptosis.* Proc Natl Acad Sci U S A, 2003. **100**(25): p. 15184-9.
167. Mukherjee, P., et al., *Activation of the innate signaling molecule MAVS by bunyavirus infection upregulates the adaptor protein SARM1, leading to neuronal death.* Immunity, 2013. **38**(4): p. 705-16.
168. Mukherjee, P., et al., *SARM1, Not MyD88, Mediates TLR7/TLR9-Induced Apoptosis in Neurons.* J Immunol, 2015. **195**(10): p. 4913-21.
169. Zhu, C., et al., *SARM1 deficiency up-regulates XAF1, promotes neuronal apoptosis, and accelerates prion disease.* J Exp Med, 2019. **216**(4): p. 743-756.
170. Weinreb, R.N., T. Aung, and F.A. Medeiros, *The pathophysiology and treatment of glaucoma: a review.* JAMA, 2014. **311**(18): p. 1901-11.
171. Saggu, S.K., et al., *Wallerian-like axonal degeneration in the optic nerve after excitotoxic retinal insult: an ultrastructural study.* BMC Neurosci, 2010. **11**: p. 97.
172. Massoll, C., W. Mando, and S.K. Chintala, *Excitotoxicity upregulates SARM1 protein expression and promotes Wallerian-like degeneration of retinal ganglion cells and their axons.* Invest Ophthalmol Vis Sci, 2013. **54**(4): p. 2771-80.
173. Hernández, D.E., et al., *Axonal degeneration induced by glutamate excitotoxicity is mediated by necroptosis.* J Cell Sci, 2018. **131**(22).
174. Ko, K.W., J. Milbrandt, and A. DiAntonio, *SARM1 acts downstream of neuroinflammatory and necroptotic signaling to induce axon degeneration.* J Cell Biol, 2020. **219**(8).
175. Ozaki, E., et al., *SARM1 deficiency promotes rod and cone photoreceptor cell survival in a model of retinal degeneration.* Life Sci Alliance, 2020. **3**(5).
176. Coppieters, F., et al., *Hidden Genetic Variation in LCA9-Associated Congenital Blindness Explained by 5'UTR Mutations and Copy-Number Variations of NMNAT1.* Hum Mutat, 2015. **36**(12): p. 1188-96.
177. Khan, A.O., et al., *Genome-wide linkage and sequence analysis challenge CCDC66 as a human retinal dystrophy candidate gene and support a distinct NMNAT1-related fundus phenotype.* Clin Genet, 2018. **93**(1): p. 149-154.
178. Sasaki, Y., et al., *SARM1 depletion rescues NMNAT1-dependent photoreceptor cell death and retinal degeneration.* Elife, 2020. **9**.
179. Ding, J., et al., *Pore-forming activity and structural autoinhibition of the gasdermin family.* Nature, 2016. **535**(7610): p. 111-6.
180. Aglietti, R.A., et al., *GsdmD p30 elicited by caspase-11 during pyroptosis forms pores in membranes.* Proc Natl Acad Sci U S A, 2016. **113**(28): p. 7858-63.

181. Zanoni, I., et al., *An endogenous caspase-11 ligand elicits interleukin-1 release from living dendritic cells.* Science, 2016. **352**(6290): p. 1232-6.
182. Wolf, A.J., et al., *Hexokinase Is an Innate Immune Receptor for the Detection of Bacterial Peptidoglycan.* Cell, 2016. **166**(3): p. 624-636.
183. Gaidt, M.M. and V. Hornung, *Alternative inflammasome activation enables IL-1β release from living cells.* Curr Opin Immunol, 2017. **44**: p. 7-13.
184. Evavold, C.L., et al., *The Pore-Forming Protein Gasdermin D Regulates Interleukin-1 Secretion from Living Macrophages.* Immunity, 2018. **48**(1): p. 35-44.e6.
185. Son, S., et al., *Neutrophils Facilitate Prolonged Inflammasome Response in the DAMP-Rich Inflammatory Milieu.* Front Immunol, 2021. **12**: p. 746032.
186. Bidère, N., H.C. Su, and M.J. Lenardo, *Genetic disorders of programmed cell death in the immune system.* Annu Rev Immunol, 2006. **24**: p. 321-52.
187. Chang, S.C. and J.L. Ding, *Ubiquitination by SAG regulates macrophage survival/death and immune response during infection.* Cell Death Differ, 2014. **21**(9): p. 1388-98.
188. Chang, S.C., et al., *SAG-UPS attenuates proapoptotic SARM and Noxa to confer survival advantage to early hepatocellular carcinoma.* Cell Death Discov, 2015. **1**: p. 15032.
189. Stokman, G., et al., *NLRX1 dampens oxidative stress and apoptosis in tissue injury via control of mitochondrial activity.* J Exp Med, 2017. **214**(8): p. 2405-2420.
190. Soares, F., et al., *The mitochondrial protein NLRX1 controls the balance between extrinsic and intrinsic apoptosis.* J Biol Chem, 2014. **289**(28): p. 19317-30.
191. Singh, K., et al., *NLRX1 acts as tumor suppressor by regulating TNF-α induced apoptosis and metabolism in cancer cells.* Biochim Biophys Acta, 2015. **1853**(5): p. 1073-86.
192. Sethurathinam, S., et al., *UXT plays dual opposing roles on SARM-induced apoptosis.* FEBS Lett, 2013. **587**(20): p. 3296-302.
193. Sethman, C.R. and J. Hawiger, *The innate immunity adaptor SARM translocates to the nucleus to stabilize lamins and prevent DNA fragmentation in response to pro-apoptotic signaling.* PLoS One, 2013. **8**(7): p. e70994.
194. Cirl, C., et al., *Subversion of Toll-like receptor signaling by a unique family of bacterial Toll/interleukin-1 receptor domain-containing proteins.* Nat Med, 2008. **14**(4): p. 399-406.
195. Doran, C.G., et al., *CRISPR/Cas9-mediated SARM1 knockout and epitope tagged mice reveal that SARM1 does not regulate nuclear transcription, but is expressed in macrophages.* J Biol Chem, 2021: p. 101417.
196. Beaudoin, G.M., et al., *Culturing pyramidal neurons from the early postnatal mouse hippocampus and cortex.* Nat Protoc, 2012. **7**(9): p. 1741-54.
197. Roberson, S.M. and W.S. Walker, *Immortalization of cloned mouse splenic macrophages with a retrovirus containing the v-raf/mil and v-myc oncogenes.* Cell Immunol, 1988. **116**(2): p. 341-51.
198. Meijering, E., et al., *Design and validation of a tool for neurite tracing and analysis in fluorescence microscopy images.* Cytometry A, 2004. **58**(2): p. 167-76.
199. Schindelin, J., et al., *Fiji: an open-source platform for biological-image analysis.* Nat Methods, 2012. **9**(7): p. 676-82.
200. Kim, D., et al., *Graph-based genome alignment and genotyping with HISAT2 and HISAT-genotype.* Nat Biotechnol, 2019. **37**(8): p. 907-915.
201. Bray, N.L., et al., *Near-optimal probabilistic RNA-seq quantification.* Nat Biotechnol, 2016. **34**(5): p. 525-7.

202. Love, M.I., W. Huber, and S. Anders, *Moderated estimation of fold change and dispersion for RNA-seq data with DESeq2.* Genome Biol, 2014. **15**(12): p. 550.
203. Gu, Z., R. Eils, and M. Schlesner, *Complex heatmaps reveal patterns and correlations in multidimensional genomic data.* Bioinformatics, 2016. **32**(18): p. 2847-9.
204. Li, H., *A statistical framework for SNP calling, mutation discovery, association mapping and population genetical parameter estimation from sequencing data.* Bioinformatics, 2011. **27**(21): p. 2987-93.
205. Quinlan, A.R. and I.M. Hall, *BEDTools: a flexible suite of utilities for comparing genomic features.* Bioinformatics, 2010. **26**(6): p. 841-2.
206. Robinson, J.T., et al., *Integrative genomics viewer.* Nat Biotechnol, 2011. **29**(1): p. 24-6.
207. Hou, Y.J., et al., *SARM is required for neuronal injury and cytokine production in response to central nervous system viral infection.* J Immunol, 2013. **191**(2): p. 875-83.
208. Wang, Q., et al., *Sarm1/Myd88-5 Regulates Neuronal Intrinsic Immune Response to Traumatic Axonal Injuries.* Cell Rep, 2018. **23**(3): p. 716-724.
209. Liston, P., et al., *Identification of XAF1 as an antagonist of XIAP anti-Caspase activity.* Nat Cell Biol, 2001. **3**(2): p. 128-33.
210. Xia, Y., et al., *Xaf1 can cooperate with TNFalpha in the induction of apoptosis, independently of interaction with XIAP.* Mol Cell Biochem, 2006. **286**(1-2): p. 67-76.
211. Perrelet, D., et al., *Motoneuron resistance to apoptotic cell death in vivo correlates with the ratio between X-linked inhibitor of apoptosis proteins (XIAPs) and its inhibitor, XIAP-associated factor 1.* J Neurosci, 2004. **24**(15): p. 3777-85.
212. Hao, S. and D. Baltimore, *RNA splicing regulates the temporal order of TNF-induced gene expression.* Proc Natl Acad Sci U S A, 2013. **110**(29): p. 11934-9.
213. Ghosh, S., et al., *NAD: a master regulator of transcription.* Biochim Biophys Acta, 2010. **1799**(10-12): p. 681-93.
214. Mendes, K.L., D.F. Lelis, and S.H.S. Santos, *Nuclear sirtuins and inflammatory signaling pathways.* Cytokine Growth Factor Rev, 2017. **38**: p. 98-105.
215. Kim, M.Y., et al., *NAD+-dependent modulation of chromatin structure and transcription by nucleosome binding properties of PARP-1.* Cell, 2004. **119**(6): p. 803-14.
216. Di Stefano, M. and L. Conforti, *Diversification of NAD biological role: the importance of location.* FEBS J, 2013. **280**(19): p. 4711-28.
217. Wang, P.H., et al., *Litopenaeus vannamei sterile-alpha and armadillo motif containing protein (LvSARM) is involved in regulation of Penaeidins and antilipopolysaccharide factors.* PLoS One, 2013. **8**(2): p. e52088.
218. Yan, N., et al., *Grass carp SARM1 and its two splice variants negatively regulate IFN-I response and promote cell death upon GCRV infection at different subcellular locations.* Dev Comp Immunol, 2015. **48**(1): p. 102-15.
219. Mills, C.D., *Macrophage arginine metabolism to ornithine/urea or nitric oxide/citrulline: a life or death issue.* Crit Rev Immunol, 2001. **21**(5): p. 399-425.
220. Mata-Haro, V., et al., *The vaccine adjuvant monophosphoryl lipid A as a TRIF-biased agonist of TLR4.* Science, 2007. **316**(5831): p. 1628-32.
221. Hernandez, A., et al., *The role of MyD88- and TRIF-dependent signaling in monophosphoryl lipid A-induced expansion and recruitment of innate immunocytes.* J Leukoc Biol, 2016. **100**(6): p. 1311-1322.

222. Kwon, A.T., et al., *oPOSSUM-3: advanced analysis of regulatory motif over-representation across genes or ChIP-Seq datasets.* G3 (Bethesda), 2012. **2**(9): p. 987-1002.
223. Richardson, J.E., R.M. Baldarelli, and C.J. Bult, *Multiple genome viewer (MGV): a new tool for visualization and comparison of multiple annotated genomes.* Mamm Genome, 2021.
224. Moore, T.C. and T.M. Petro, *IRF3 and ERK MAP-kinases control nitric oxide production from macrophages in response to poly-I:C.* FEBS Lett, 2013. **587**(18): p. 3014-20.
225. Moore, T.C., et al., *IRF3 helps control acute TMEV infection through IL-6 expression but contributes to acute hippocampus damage following TMEV infection.* Virus Res, 2013. **178**(2): p. 226-33.
226. Lee, C.M. and J. Hu, *Cell density during differentiation can alter the phenotype of bone marrow-derived macrophages.* Cell Biosci, 2013. **3**: p. 30.
227. Jaillon, S., K. Berthenet, and C. Garlanda, *Sexual Dimorphism in Innate Immunity.* Clin Rev Allergy Immunol, 2019. **56**(3): p. 308-321.
228. Kim, O.H., et al., *Impaired phagocytosis of apoptotic cells causes accumulation of bone marrow-derived macrophages in aged mice.* BMB Rep, 2017. **50**(1): p. 43-48.
229. Yachdav, G., et al., *PredictProtein--an open resource for online prediction of protein structural and functional features.* Nucleic Acids Res, 2014. **42**(Web Server issue): p. W337-43.
230. Lusis, A.J., J. Yu, and S.S. Wang, *The problem of passenger genes in transgenic mice.* Arterioscler Thromb Vasc Biol, 2007. **27**(10): p. 2100-3.
231. Mohanan, N.K., et al., *Alternative polyadenylation: An enigma of transcript length variation in health and disease.* Wiley Interdiscip Rev RNA, 2021: p. e1692.
232. Tse, M.K., et al., *Domain organization of XAF1 and the identification and characterization of XIAP(RING) -binding domain of XAF1.* Protein Sci, 2012. **21**(10): p. 1418-28.
233. Chui, A.J., et al., *N-terminal degradation activates the NLRP1B inflammasome.* Science, 2019. **364**(6435): p. 82-85.
234. Sastalla, I., et al., *Transcriptional analysis of the three Nlrp1 paralogs in mice.* BMC Genomics, 2013. **14**: p. 188.
235. Vogl, T., et al., *Mrp8 and Mrp14 are endogenous activators of Toll-like receptor 4, promoting lethal, endotoxin-induced shock.* Nat Med, 2007. **13**(9): p. 1042-9.
236. Yamasaki, K., et al., *NLRP3/cryopyrin is necessary for interleukin-1beta (IL-1beta) release in response to hyaluronan, an endogenous trigger of inflammation in response to injury.* J Biol Chem, 2009. **284**(19): p. 12762-71.
237. Dauth, S., et al., *Cathepsin K deficiency in mice induces structural and metabolic changes in the central nervous system that are associated with learning and memory deficits.* BMC Neurosci, 2011. **12**: p. 74.
238. Doudna, J.A. and E. Charpentier, *Genome editing. The new frontier of genome engineering with CRISPR-Cas9.* Science, 2014. **346**(6213): p. 1258096.
239. Mojica, F.J., et al., *Biological significance of a family of regularly spaced repeats in the genomes of Archaea, Bacteria and mitochondria.* Mol Microbiol, 2000. **36**(1): p. 244-6.
240. Barrangou, R., et al., *CRISPR provides acquired resistance against viruses in prokaryotes.* Science, 2007. **315**(5819): p. 1709-12.
241. Jinek, M., et al., *A programmable dual-RNA-guided DNA endonuclease in adaptive bacterial immunity.* Science, 2012. **337**(6096): p. 816-21.

242. Kim, S., et al., *Highly efficient RNA-guided genome editing in human cells via delivery of purified Cas9 ribonucleoproteins.* Genome Res, 2014. **24**(6): p. 1012-9.
243. Sternberg, S.H., et al., *DNA interrogation by the CRISPR RNA-guided endonuclease Cas9.* Nature, 2014. **507**(7490): p. 62-7.
244. Barman, A., B. Deb, and S. Chakraborty, *A glance at genome editing with CRISPR-Cas9 technology.* Curr Genet, 2020. **66**(3): p. 447-462.
245. Fu, Y., et al., *High-frequency off-target mutagenesis induced by CRISPR-Cas nucleases in human cells.* Nat Biotechnol, 2013. **31**(9): p. 822-6.
246. Uccellini, M.B., et al., *Passenger Mutations Confound Phenotypes of SARM1-Deficient Mice.* Cell Rep, 2020. **31**(1): p. 107498.
247. Robertson, S.J., et al., *Comparison of Co-housing and Littermate Methods for Microbiota Standardization in Mouse Models.* Cell Rep, 2019. **27**(6): p. 1910-1919.e2.
248. Feriotti, C., et al., *Klebsiella pneumoniae hijacks the Toll-IL-1R protein SARM1 in a type I IFN-dependent manner to antagonize host immunity*. 2021: bioRxiv.
249. Bhan, U., et al., *Cooperative interactions between TLR4 and TLR9 regulate interleukin 23 and 17 production in a murine model of gram negative bacterial pneumonia.* PLoS One, 2010. **5**(3): p. e9896.
250. Hunt, J.J., et al., *TLR4 contributes to the host response to Klebsiella intraocular infection.* Curr Eye Res, 2014. **39**(8): p. 790-802.
251. Wieland, C.W., et al., *Host defence during Klebsiella pneumonia relies on haematopoietic-expressed Toll-like receptors 4 and 2.* Eur Respir J, 2011. **37**(4): p. 848-57.
252. Burberry, A., et al., *C9orf72 suppresses systemic and neural inflammation induced by gut bacteria.* Nature, 2020. **582**(7810): p. 89-94.
253. Kayagaki, N., et al., *Non-canonical inflammasome activation targets caspase-11.* Nature, 2011. **479**(7371): p. 117-21.
254. Vanden Berghe, T., et al., *Passenger Mutations Confound Interpretation of All Genetically Modified Congenic Mice.* Immunity, 2015. **43**(1): p. 200-9.
255. Er-Lukowiak, M., et al., *A P2rx7 Passenger Mutation Affects the Vitality and Function of T cells in Congenic Mice.* iScience, 2020. **23**(12): p. 101870.